

**Spatial variability of human-  
biometeorological conditions related to  
heat stress in Berlin, Germany, with focus  
on air temperature and radiation**

vorgelegt von

M. Sc.

Britta Jänicke

geb. in Braunschweig

von der Fakultät VI - Planen Bauen Umwelt  
der Technischen Universität Berlin  
zur Erlangung des akademischen Grades

Doktor der Naturwissenschaften

- Dr. rer. nat. –

genehmigte Dissertation

Promotionsausschuss:

Vorsitzender: Prof. Dr. Martin Kaupenjohann

Gutachter: Prof. Dr. Dieter Scherer

Gutachter: Prof. Dr. Christoph Schneider

Tag der wissenschaftlichen Aussprache: 29. Juli 2016

Berlin 2016





## List of papers

This thesis is presented in a cumulative form and based on the following papers I-IV, which are attached in the *Appendix*.

- I. **Jänicke, B.**, Meier, F., Hoelscher, M.-T., Scherer, D., 2015. Evaluating the effects of façade greening on human bioclimate in a complex urban environment. *Advances in Meteorology*, Article ID 747259. <http://dx.doi.org/10.1155/2015/747259>
- II. Walikewitz, N., **Jänicke, B.**, Langner, M., Endlicher, W., 2015. Assessment of indoor heat stress variability in summer and during heat warnings: A case study using the UTCI in Berlin, Germany. *International Journal of Biometeorology*, 1–14. <http://dx.doi.org/10.1007/s00484-015-1066-y>
- III. **Jänicke, B.**, Meier, F., Lindberg, F., Schubert, S., Scherer, D., 2016. Towards city-wide, building-resolving analysis of mean radiant temperature. *Urban Climate*, 15, 83-98. <http://dx.doi.org/10.1016/j.uclim.2015.11.003>
- IV. **Jänicke, B.**, Meier, F., Fenner, D., Fehrenbach, U., Holtmann, A., Scherer, D., 2016. Urban-rural differences in near-surface air temperature as resolved by the Central Europe Refined analysis (CER): sensitivity to planetary boundary layer schemes and urban canopy models. *International Journal of Climatology*, 1-17. <http://dx.doi.org/10.1002/joc.4835>

The following papers are also related to the thesis but with minor contributions from myself.

- Walikewitz, N., **Jänicke, B.**, Langner, M., Meier, F., Endlicher, W., 2015. The difference between the mean radiant temperature and the air temperature within indoor environments: A case study during summer conditions. *Building and Environment*, 84, 151-161. <http://dx.doi.org/10.1016/j.buildenv.2014.11.004>
- Hölscher, M.-T., Nehls, T., **Jänicke, B.**, Wessolek, G., 2016. Quantifying cooling effects of façade greening: shading, transpiration and insulation. *Energy and Buildings*, 114, 283-290. <http://dx.doi.org/10.1016/j.enbuild.2015.06.047>
- Buchin, O., **Jänicke, B.**, Meier, F., Scherer, D., Ziegler, F., 2016. The role of building models in the evaluation of heat-related risks. *Natural Hazards and Earth System Sciences*, 16, 963-976. <http://dx.doi.org/10.5194/nhess-16-963-2016>



## Summary

Heat stress endangers the health and lives of people especially in cities, since air temperature is often higher there than in the surrounding countryside. Human-biometeorological conditions related to heat stress are spatially variable, also within a city. Processes from the meso- to the micro-scale, i.e., large-scale weather situations and individual streets, have to be considered to capture this spatial variability. Analyses of human-biometeorological conditions on different scales are essential to examine the spatial variability and to understand underlying processes. They also enable the identification of hotspots in the city, which is valuable for implementing adaptation measures. So far, however, high-resolution and city-wide analyses, which consider micro- and meso-scale processes, have been rare.

The aim of this work is to investigate spatial variability of human-biometeorological conditions related to heat stress in Berlin at different scales and to contribute to future multi-scale analyses. Models on meso- and micro-scales were tested in terms of deviations from observations of near-surface air temperature ( $T_2$ ) and mean radiant temperature ( $T_{mrt}$ ). These models were then applied together with measurements to assess spatial variability of human-biometeorological conditions in Berlin. Furthermore, the propagation of spatial patterns from one scale to the other was examined.

To study the meso-scale, the Central Europe Refined Analysis (CER) was developed and  $T_2$  was evaluated against weather stations. The CER is a new dataset based on dynamical downscaling of a global reanalysis using the Weather Research and Forecasting model (WRF). On the micro-scale, three widely-used models – ENVI-met, RayMan and SOLWEIG – were evaluated, with respect to  $T_{mrt}$ . SOLWEIG was selected for further use due to the smallest deviations from observations and fast computation. A new sub-version of SOLWEIG for automated workflows was developed, which allows city-wide simulations. Thus, the weather situation from a meso-scale model as well as the influence of micro-scale urban structures on  $T_{mrt}$  was considered. The spatial variability of human-biometeorological conditions in Berlin was examined with the meso-scale analysis CER and the coupled SOLWEIG model. An indoor/outdoor observation network was also used for assessing the spatial variability on the building-scale.

The results reveal a high degree of spatial variability at the meso-, micro-, city-, and building-scale for  $T_2$ ,  $T_{mrt}$ , and the Universal Thermal Climate Index (UTCI). At the meso-scale, a nocturnal urban heat island, and intra-urban

differences between built-up and green areas were established, reaching 1.3 K and 0.4 K as a monthly average, respectively. At the city-scale and with regard to  $T_{mrt}$ , the degree of spatial variability was higher. Around noon,  $T_{mrt}$  values varied between 30°C and 60°C; the highest  $T_{mrt}$  values were reached in open, unshaded areas. The effect of façade greening on spatial variability of  $T_{mrt}$  and  $UTCI$  on the micro-scale, however, was low. The spatial variability at building-scale was high, with differences in the  $UTCI$  between buildings of 3 K on average over the summer. Thus, in some buildings, on more than 50% of the summer days, moderate heat stress occurred ( $UTCI \geq 26^\circ\text{C}$ ).

Spatial patterns, however, were not directly propagated from one scale to the other. Different processes were relevant for different scales. The pattern of  $T_{mrt}$  at the city-scale was influenced by the meso-scale  $T_2$  pattern in the daytime, but the spatial variability was mainly a result of the shadows cast by buildings and trees. At the building-scale, the spatial patterns of the indoor  $UTCI$  were hardly affected by the spatial patterns of the outdoor  $UTCI$  in the immediate neighbourhood of the building. Other factors, such as ventilation and building characteristics, seem more important. Knowledge about propagation through the scales is particularly valuable for future multi-scale model development.

## Zusammenfassung

Hitzestress gefährdet die Gesundheit und das Leben von Menschen insbesondere in Städten, weil dort die Lufttemperatur häufig höher ist als im Umland. Zudem sind die für Hitzestress relevanten human-biometeorologischen Bedingungen innerhalb einer Stadt räumlich variabel. Um diese räumliche Variabilität zu erfassen, müssen Prozesse von der Meso- bis zur Mikroskala, also die großskalige Wettersituationen genauso wie einzelne Straßenzüge, berücksichtigt werden. Analysen human-biometeorologischer Bedingungen auf verschiedenen Skalen sind essenziell, um die räumliche Variabilität in Städten zu erfassen und zugrundeliegende Prozesse zu verstehen. Sie ermöglichen auch, Hotspots in der Stadt zu identifizieren, um dort Anpassungsmaßnahmen umzusetzen. Bisher sind hochaufgelöste und stadtweite Analysen, die mikro- und mesoskalige Prozesse berücksichtigen, jedoch kaum vorhanden.

Ziel dieser Arbeit ist es daher, die räumliche Variabilität von human-biometeorologischen Bedingungen in Berlin auf verschiedenen Skalen zu untersuchen und einen Beitrag für künftige multiskalige Analysen zu leisten. Dazu werden verschiedene Modelle auf der Meso- und Mikroskala bezogen auf Abweichung zu Messungen der mittleren Strahlungstemperatur ( $T_{mrt}$ ) und oberflächennaher Lufttemperatur ( $T_2$ ) getestet. Die Modelle wurden dann zusammen mit Messungen verwendet, um die räumliche Variabilität human-biometeorologischer Bedingungen in Berlin zu erfassen. Außerdem wurde die Übertragung der räumlichen Muster von der einen zur anderen Skala untersucht.

Zur Untersuchung der Mesoskala wurde die Central Europe Refined Analysis (CER) entwickelt und anhand von Messdaten bezogen auf  $T_2$  evaluiert. Die CER ist einen neuer Datensatz basierend auf dynamischem Downscaling einer globalen Reanalyse mit dem Weather Research and Forecasting model (WRF). Auf der Mikroskala wurden drei häufig verwendete Modelle, ENVI-met, RayMan und SOLWEIG, hinsichtlich der  $T_{mrt}$  evaluiert. Aufgrund der geringsten Abweichungen zu Messdaten und der kurzen Rechenzeit wurde SOLWEIG für die weitere Verwendung ausgewählt. Eine neuentwickelte Sub-Version von SOLWEIG mit einem automatisierten Arbeitsablauf ermöglicht es, stadtweite Simulationen durchzuführen. Dadurch werden sowohl die Wettersituation aus einem mesoskaligen Modell als auch der mikroskaligen Einfluss von Stadtstrukturen auf die  $T_{mrt}$  berücksichtigt. Anhand der mesoskaligen Analyse CER und des gekoppelten SOLWEIG Modells wurde die räumliche Variabilität human-biometeorologischer Größen in Berlin

untersucht. Ein Innen-/Außenraum-Klimamessnetz wurde verwendet, um die räumliche Variabilität auf der Gebäudeskala zu betrachten.

Die Ergebnisse zeigen eine hohe räumliche Variabilität der  $T_2$ ,  $T_{mrt}$  und des Universal Thermal Climate Index ( $UTCI$ ) auf der Meso-, Stadt- und Gebäudeskala.  $T_2$  wies auf der Mesoskala eine nächtliche städtische Wärmeinsel (1.3 K im Monatsmittel) und intra-urbane Differenzen zwischen bebauten Flächen und Grünflächen (0.7 K im Monatsmittel) auf. Auf der Stadtskala und in Bezug auf  $T_{mrt}$  war die räumliche Variabilität ausgeprägter. Zur Mittagszeit traten  $T_{mrt}$ -Werte zwischen 30°C und 60°C auf, wobei die höchsten Werte an offenen, nicht-beschatteten Flächen vorkamen. Die Wirkung von Fassadenbegrünung auf die räumliche Variabilität von  $T_{mrt}$  und  $UTCI$  in der Mikroskala war hingegen gering. Auf der Gebäudeskala war die Variabilität bezogen auf den  $UTCI$  mit bis zu 3 K im Sommermittel deutlich ausgeprägt, sodass in manchen Gebäuden an 50% der Sommertage moderater Hitzestress ( $UTCI \geq 26^\circ\text{C}$ ) auftrat.

Die räumlichen Muster übertrugen sich aber nicht direkt von der einen zur anderen Skala. Auf den jeweiligen Skalen waren unterschiedliche Prozesse relevant. Das Muster der  $T_{mrt}$  tagsüber auf der Stadtskala war zwar auch von der mesoskaligen Lufttemperaturverteilung beeinflusst, die räumliche Variabilität wurde allerdings hauptsächlich durch Schattenwürfe von Gebäuden und Bäumen verursacht. Auch auf der Gebäudeskala war das räumliche Muster von  $UTCI$  im Innenraum kaum von dem räumlichen Muster im Außenraum im direkten Umfeld der Gebäude beeinflusst. Dort scheinen andere Faktoren wie Belüftung und Gebäudeeigenschaften mehr Einfluss zu haben. Solche Kenntnisse über die Übertragung der Muster zwischen den Skalen sind besonders für künftige multiskalige Modellentwicklungen wichtig.

# Contents

1 Introduction	11
1.1 Heat stress and urban climate	11
1.2 Objectives	16
2 Materials and methods	19
2.1 Study area	19
2.2 Observations	20
2.3 Simulations	23
3 Results and Discussion	27
3.1 Model evaluation	27
3.1.1 Meso-scale models	27
3.1.2 Micro-scale models	30
3.2 Spatial variability of human-biometeorological conditions	31
3.2.1 Meso-scale variability	31
3.2.2 Micro-scale variability	32
3.2.3 Building-scale variability	37
3.3 Propagation of spatial variability through the scales	39
3.3.1 Propagation from meso- to city-scale	39
3.3.2 Propagation from city- to building-scale	40
4 Conclusions and perspectives	43
References	45
Abbreviations	57
Appendix	59
Paper I	61
Paper II	79
Paper III	94
Paper IV	112
Danksagung	132





# 1 Introduction

## 1.1 Heat stress and urban climate

Extreme heat events are one of the most dangerous natural disasters worldwide (Borden and Cutter, 2008; WHO, 2015). Moreover, heat stress threatens human health, particularly in cities, where air temperature ( $T_a$ ) and population density are often higher than in rural surroundings. As detected in many cities over the world, mortality and morbidity increase during extreme heat events (Guo et al., 2014; Kovats and Hajat, 2008). This also includes mid-latitude cities like Berlin, Germany (Gabriel and Endlicher, 2011; Scherer et al., 2013; Schuster et al., 2014). Extreme heat events or heat waves are infrequent events; they refer to multiple consecutive days with extraordinarily high  $T_a$  in a given region (cf. Meehl and Tebaldi, 2004; Perkins, 2015; Russo et al., 2014). Extreme heat events do not occur every year but lead to severe impacts if they do develop. For instance, the extreme heat event of August 2003 is associated with about 40,000 additional deaths in Europe (García-Herrera et al., 2010). Hot weather conditions, on the other hand, occur several times during an ordinary summer and also lead to heat-stress related mortality (Scherer et al., 2013). Owing to their frequent occurrence, and thus, frequent damages, hot weather conditions are also highly relevant in the context of heat stress.

In the future, global climate change and ongoing urbanisation are likely to aggravate heat stress in cities.  $T_a$  has already risen in the last few decades, and both the frequency and the intensity of extreme heat events have increased throughout Europe (IPCC, 2014). Heat-stress related mortality and morbidity have become amplified in the past several decades in Europe and are projected to increase further (Fallmann et al., 2015; IPCC, 2014). Ongoing urbanisation leads to a higher level of heat-stress vulnerability in densely populated cities. More than half of the world's population lives in cities; the percentage of urban population is even higher in certain regions, especially in the mid-latitude areas like Europe (73%) (UN, 2014).

The phenomenon of higher  $T_a$  in cities as compared to their rural surroundings is known as the urban heat island (UHI). Generally, UHIs establish under anticyclonic conditions, i.e. low wind speed and scant cloud

cover (Grimmond et al., 2010). UHIs often reach their highest intensities at night and are influenced by urban structures, topography, season, time of day and climate (Grimmond et al., 2010). The main causes of UHIs are a modified energy balance with an increased sensible heat flux due to the presence of more artificial surfaces and an increased surface area, as well as the decreased latent heat flux due to smaller vegetation cover (Grimmond et al., 2010). This is accompanied by a greater amount of thermal inertia and heat storage, caused by the higher heat capacity of artificial surfaces, complex processes of radiation due to shading and multiple reflections, and the changed emissivity of long-wave radiation and anthropogenic heat fluxes (Barlow, 2014; Zhao et al., 2014). At night, artificial surfaces release more heat than vegetated surfaces, which is a major reason for the creation of UHIs (Zhao et al., 2014). During the day, heat is dissipated less efficiently by convection in cities than in rural areas because of the higher aerodynamic resistance present in cities (Zhao et al., 2014). Previous studies have demonstrated that the intensity of UHIs and the underlying processes vary among cities (Arnfield, 2003; Baklanov et al., 2016; Barlow, 2014; Santamouris, 2015; Souch and Grimmond, 2006; Wienert and Kuttler, 2005; Zhao et al., 2014). Although the general causes of UHIs have been researched extensively, the quantification and understanding of the processes leading to spatial modifications remain incomplete (Grimmond et al., 2010).

In addition, considering indoor climate is also important in the context of heat stress, as people spend most of their time (over 90%) indoors in industrialised countries (Brasche and Bischof, 2005; Höppe and Martinac, 1998; Höppe, 2002). Indoor and outdoor climate exchange happens through building envelopes. Therefore, the outdoor climate has some influence on the indoor climate (Mills et al., 2010; Nguyen et al., 2014). A direct determination of indoor climate on the basis of outdoor climate, however, is difficult because there are many other influencing factors, such as building design, material, and cooling systems (Höppe and Martinac, 1998).

#### *Variables and indices for assessing human-biometeorological conditions*

Urban climate influences human-biometeorological conditions via different climate elements, namely short- and long-wave radiation,  $T_a$ , atmospheric moisture and wind speed. Heat stress occurs when the body is not able to effectively dissipate metabolic heat and thus increases its core temperature (Gosling et al., 2014). Under these circumstances, heat stress can cause adverse effects like reduced mental and physical abilities and increased morbidity and mortality (Gosling et al., 2014). More than 100 indices (approximately 40 have been reviewed by Blazejczyk et al. (2012) and Jendritzky et al. (2012)) have been developed for estimating human-

biometeorological conditions that combine different climate elements to generate a single value (van Hoof, 2008). The Universal Thermal Climate Index (*UTCI*) was recently developed to overcome some of the problems of the former indices (cf. Jendritzky et al., 2012). The *UTCI* is based on a human body model with a constant metabolic rate and on a clothing model (Bröde et al., 2012; Jendritzky et al., 2012). It offers a continuous scale based on equivalent temperatures (in °C), and an ordinal scale based on thermal stress categories (Bröde et al., 2012; Jendritzky et al., 2012). Like many other indices, the *UTCI* is calculated on the basis of mean radiant temperature,  $T_a$ , wind speed, and atmospheric humidity.

While such indices describe human-biometeorological conditions extensively, using individual climate elements can also be appropriate for certain issues. A simple approach for assessing human-biometeorological conditions is to use the near-surface air temperature ( $T_2$ : air temperature 2 m above ground level). The connection of  $T_2$  to heat stress has often been confirmed in studies that relate mortality to  $T_2$  (e.g. Barnett et al., 2010; Ha and Kim, 2013; Hajat and Kosatky, 2010; Scherer et al., 2013). Another advantage of using  $T_2$  is that it can easily be accessed at any weather station and additional complex measurements or simulations are not required. A different approach is to use the mean radiant temperature ( $T_{mrt}$ ). Under sunny conditions,  $T_{mrt}$  is the most important variable for describing human-biometeorological conditions (Kántor and Unger, 2011).  $T_{mrt}$  (or more precisely the mean radiant flux density, which is transferred through the Stefan-Boltzmann law to  $T_{mrt}$ ) summarises the long- and short-wave radiation fluxes reaching the human body (Höppe, 1992). Different methods exist to observe and simulate  $T_{mrt}$  (Kántor and Unger, 2011; Krüger et al., 2014; Thorsson et al., 2007) with different levels of uncertainty (Kántor and Unger, 2011; Weihs et al., 2012). Earlier research (e.g. Thorsson et al., 2014) solely used  $T_{mrt}$  for describing human-biometeorological conditions due to its high correlation with biometeorological indices under sunny conditions (Kántor and Unger, 2011; Kuttler, 1999; Provençal et al., 2016). Indoors, biometeorological indices that also include relative humidity are more appropriate than  $T_{mrt}$ . The scale and spatial resolution also influence the suitability of a variable. For example,  $T_{mrt}$  is more spatially variable than  $T_2$  because of its sensitivity to radiation and shadow patterns (Kántor and Unger, 2011; Lindberg et al., 2014; Shashua-Bar et al., 2012). Thus,  $T_2$  might be more appropriate for representing a larger area.

### *Challenges of assessing the spatial variability of human-biometeorological conditions related to heat stress*

Biometeorological conditions not only differ between a city and its rural surrounding but also vary spatially within a city. This intra-urban variability could lead to spatial variability in heat-stress risks (e.g. Guo et al., 2013; Kim et al., 2014; Scherber et al., 2014; Schuster et al., 2014). Thus, examining the spatial variability of biometeorological conditions city-wide and building-resolving is beneficial for understanding the causes behind spatial patterns, analysing heat-related risks, and identifying hotspots. Furthermore, such analyses could be used in climate-sensitive planning and conceptualisation of measures to reduce heat stress (e.g. Dütemeyer et al., 2013; Mills et al., 2010; Norton et al., 2015). Local modifications induced by trees or façade greening for example, can be used to reduce heat-stress hazards. Moreover, spatial variability is included in Mayer's (1989) definition of an ideal urban climate. According to him, an ideal urban climate has a high spatial variation of atmospheric conditions while avoiding extreme conditions.

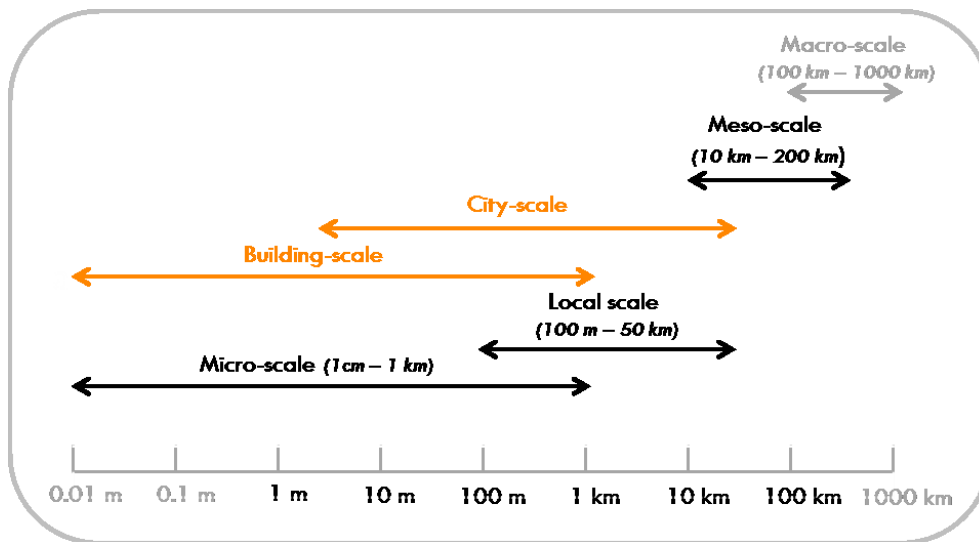


Figure 1: Overview of horizontal distance scales according to Oke (1987) (coloured in black and grey). Scales and distances that are less important here are coloured in grey. Building- and city-scale (orange) have been added to Oke's (1987) scale definition.

Examining the spatial variability of human-biometeorological conditions within cities, however, is challenging as heterogeneous city structures and processes need to be considered at different scales. Hence, studies that examine biometeorological conditions in Berlin and in many other cities at high-resolution and city-wide are rare at present. Individual elements (like street canyons or trees) at the micro-scale, the entire city at the meso-scale, and synoptic conditions at the macro-scale interact with each other and influence the urban climate (Gosling et al., 2014; Oke, 1987) (Figure 1). Here,

the micro-scale is further split into the city-scale and the building-scale (Figure 1). City-scale refers to a combination of city-wide and micro-scale at the same time (Muller et al., 2013); it considers the entire city area while resolving buildings explicitly. The building-scale deals with distances similar to the micro-scale (Figure 1) but is concerned with processes within buildings and the exchanges between buildings and the external surroundings.

For studying the urban climate and human-biometeorological conditions, many individual methods are available that address one of these scales. Methods can be divided into observations and modelling; both are essential for the spatial analysis of the urban climate (e.g. for observations: Barlow, 2014; Grimmond, 2006; Muller et al., 2013, and for models: Chen et al., 2011; Martilli, 2007). Ground-based observations are spatially constrained and numerical climate models yield output with unknown accuracy. Thus, numerical models are often used in combination with evaluations against observations. Generating patterns of land surface temperature through remote sensing is also possible (Tomlinson et al., 2011; Voogt and Oke, 2003). In this thesis, however, remote sensing is not considered because land surface temperature is not directly related to human-biometeorological conditions (e.g.  $T_2$ ) (Azevedo et al., 2016; Keramitsoglou et al., 2012). For example, remote-sensed land surface temperature takes into account a combination of roof, wall and ground surface (Voogt and Oke, 2003), whereas mainly the ground and lower wall surfaces would be relevant for pedestrian thermal sensation. Moreover, surface temperature has a loose relation with human-biometeorological conditions, since in many indices (like  $UTCI$ ) it is only considered within  $T_{mrt}$  as long-wave emitted radiation.

At the meso-scale, numerical weather prediction (NWP) models simulate weather or climate conditions. They cover the entire area of a city, but the grid spacing is generally coarse (0.5 km to 10 km). The NWP models used in this thesis include the Weather Research and Forecast (WRF) model (Skamarock and Klemp, 2008) and the COSMO-CLM (CCLM) (Rockel et al., 2008). Among NWP models, urban canopy models (UCMs) parametrise sub-scale urban processes (Chen et al., 2011). Three different types of UCMs can be distinguished. The simplest slab models within land surface models (LSM) do not resolve the three-dimensional structure of cities because they depict the urban land cover with the same equations as any other land cover category. In single-layer urban canopy models (SLUCM), urban structures are described as infinitely long street canyons separated by walls, roofs, and façades. Multi-layer UCMs have the most sophisticated approaches; they account for direct exchanges of energy and moisture between the urban roughness sub-layer and the planetary boundary layer (Chen et al., 2011). All three types are

frequently applied, although some issues remain unresolved, such as uncertainties about the required level of complexity in UCMs or their spatial resolution (Chen et al., 2011; Ching, 2013; Grimmond et al., 2010; Grimmond et al., 2011; Martilli, 2007; Masson, 2005; Prein, 2015; Rummukainen, 2010).

Micro-scale models resolve urban structures explicitly, but the domain size is often limited to a few hundred metres due to high computational demands. Micro-climate models such as ENVI-met (Bruse and Fleer, 1998), SOLWEIG (Lindberg et al., 2008) and RayMan (Matzarakis et al., 2010) are frequently used for studying individual streets, neighbourhoods, or districts. Furthermore, they yield biometeorological indices or  $T_{mrt}$  as output. Comparisons between different models for the purpose of sound model selection have rarely been done (Chen et al., 2014).

Models that bridge the meso- and micro-scale are needed for analysing human-biometeorological conditions with high spatial resolution across the city. At present, there is no model that can handle all the scales simultaneously. Bridges between the meso- and micro-scale have become possible in numerical simulations only recently, due to an increase in computational capacity (Barlow, 2014). Thus, some studies have already combined meso-scale and micro-scale models to simulate small sections of interest, often focusing on transport and dispersion modelling (e.g. Prusa et al., 2008; Tewari et al., 2010). WRF has also been used to dynamically downscale a global circulation model (Conry et al., 2015). Subsequently, these results were used as input for the micro-scale model ENVI-met for a specific neighbourhood (Conry et al., 2015). Creating city-wide and building-resolving analyses remains a challenge. More research on multi-scale analyses and ways to deal with these scale gaps is necessary (Chen et al., 2012).

## 1.2 Objectives

This thesis aims to depict and understand the spatial variability of outdoor and indoor human-biometeorological conditions related to heat stress by using Berlin as an exemplary mid-latitude city. Therefore, I have explored approaches for urban climate analyses at different scales, and intended to identify processes causing spatial variability (Figure 2). This thesis has been developed in the Research Unit 1736 'Urban climate and heat stress in mid-latitude cities in view of climate change' (UCaHS) by the *Deutsche Forschungsgemeinschaft* (DFG) (translation: German Research Foundation), which deals with multi- and interdisciplinary topics related to urban climate and heat stress (cf. <http://ucahs.org/>).

Lacking a universal model for addressing human-biometeorological conditions at different scales, the first objective (Section 3.1 *Model evaluation*) is to explore accuracies and constraints of urban climate models at meso- and micro-scale. Results of the evaluations constitute the basis for the development of a coupled city-scale model and for the analyses of spatial variability (cf., second objective). At the meso-scale, a new dataset using WRF to describe past weather and climate conditions has been developed and evaluated. Section 3.1 also evaluates an existing simulation with the meso-scale model CCLM. CCLM serves as the input for city-scale analysis due to its finer grid spacing. At the micro-scale, three models – ENVI-met, RayMan and SOLWEIG – are evaluated, before the last is selected for use in the coupled city-scale approach.

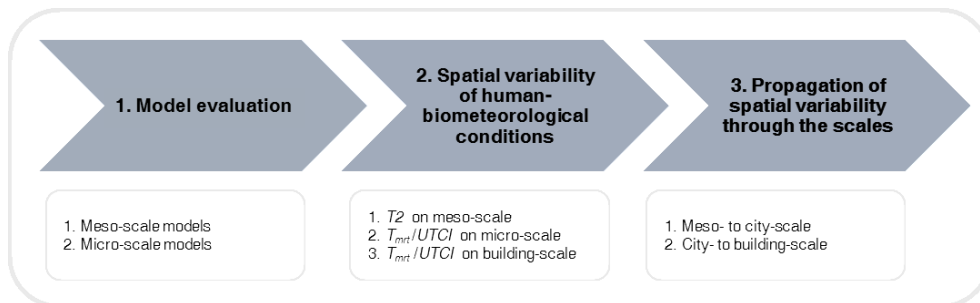


Figure 2: Overview of objectives and structure of the thesis.

The second objective is to analyse the spatial variability of human-biometeorological conditions related to heat stress in Berlin (Section 3.2 *Spatial variability of human-biometeorological conditions*). Meso-, city-, micro- and building-scale analyses from simulations and observations serve to examine the spatial variability of  $T_2$ ,  $T_{mrt}$ , and  $UTCI$ . In this way, spatial patterns of heat-stress hazards have been investigated and the possible influencing factors have been discussed. Furthermore, the effect of façade greening on outdoor human-biometeorological conditions has been assessed.

The third objective is to explore whether the spatial variability of human-biometeorological conditions is propagated from one scale to the other (Section 3.3 *Propagation of spatial variability through the scales*). For this purpose, spatial patterns between the meso- and city-scale and between the city- and building-scale have been compared and implications for future multi-scale modelling approaches have been discussed.

The overall structure of this thesis is based on the three main research objectives. First, the thesis briefly summarises the used methods and settings in the simulations (Section 2 *Materials and methods*). Second, the results of the respective objectives are presented and discussed (Section 3 *Results and*

*Discussion*). Finally, conclusions and future research directions are provided (Section 4 *Conclusions and perspectives*). The thesis is based on four peer-reviewed papers, all of which have been reprinted in the *Appendix*.



## 2 Materials and methods

The applied methods and workflows are summarised in Figure 3 and briefly described in the following. The observations and simulations have been applied for different periods in the summer – for one day, one month, or the whole season. The respective dates are given in Section 3 *Results and Discussion*.

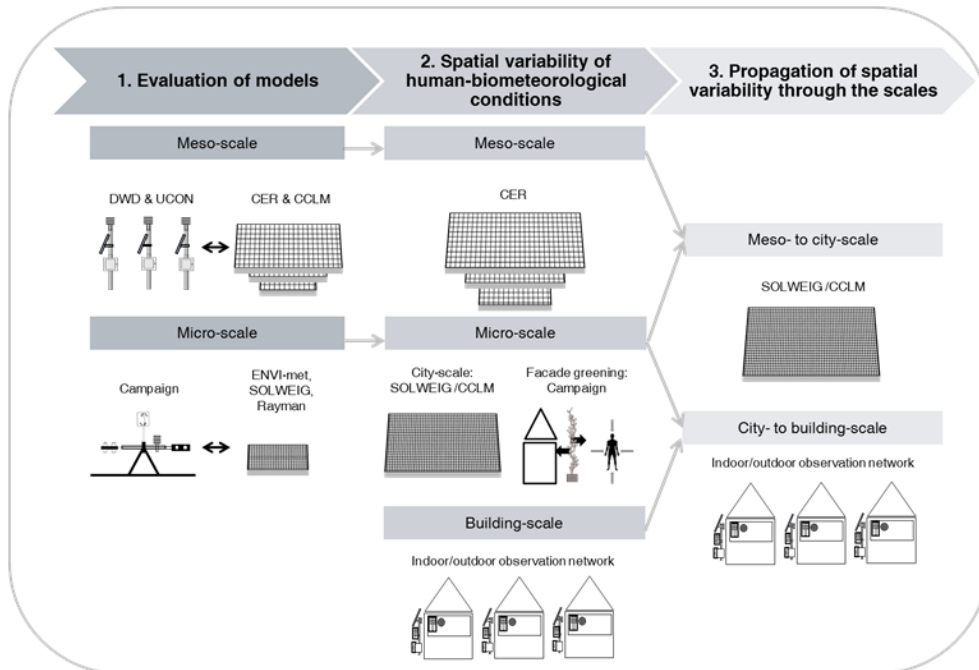


Figure 3: Overview of the applied methods for the respective research objectives.

### 2.1 Study area

Berlin is chosen as the study area because heat stress is highly relevant there. Earlier studies based on Berlin showed that heat stress can be a serious threat to human health (Gabriel and Endlicher, 2011; Scherber et al., 2014; Scherer et al., 2013). Furthermore, many people are affected in Berlin since, with 3.5 million inhabitants, it is the largest city in Germany.

The city also has suitable preconditions for analysing urban climate. Berlin offers a location without the direct influences of mountains or seas, which might interfere with the formation of urban climate. Moreover, Berlin has a long and continued tradition of urban climate research, as summarised by Endlicher and Lanfer (2003) and Kratzer (1957). Such research, in its initial stages, started with the ‘The Academy of Sciences’ in the 18<sup>th</sup> century and involved several investigations into  $T_a$ , precipitation and radiation differences between the city and its surroundings. In the 1970s/80s, the research continued intensely with various analyses, as summarised by Horbert (2000) as well as Hupfer and Chmielewski (1990). Since 1995, the Berlin Senate Department for Urban Development and the Environment (SenStadt) has been carrying out urban climate analyses for planning purposes within the Urban and Environmental Information System (‘Umweltatlas’). The grid spacing of the underlying simulations has been continuously reduced with improvements in the applied FITNAH model (SenStadt, 2015). The simulation results of different variables and biometeorological indices, including the *UTCI*, using 10-m grid spacing, were made available for the entire city, with the latest update in November 2015. The simulations, however, are based on ideal cases with moderate  $T_a$  and no geostrophic wind (SenStadt, 2015). While this assumption is considered as reasonable for planning approaches, it does not enable research on real-case heat-stress situations. Besides simulations, Berlin also offers pre-existing observation networks as well as available input and boundary data for models.

## 2.2 Observations

As already mentioned, observations are essential for analysing human-biometeorological conditions. Depending on the location of the site and the measurement heights, the data from observations might be representative of the micro-, local-, or meso-scale (Muller et al., 2013; WMO, 2008). Hence, when using observations for model evaluation, the scale of the measurements must fit the scale of the used model (Chen et al., 2012). In particular, the comparison of observations with simulation results may not be like-with-like in nature for meso-scale models; ‘representation errors’ can occur, especially in complex areas (Argüeso et al., 2011). Several methods to overcome such representation errors have been discussed by Argüeso et al. (2011). This thesis accounts for this problem by considering the land cover around stations (cf. Papers III and IV). Additionally, different observations and networks have been used for the different scales: weather station networks for the meso-scale, a campaign in a complex environment for the micro-scale, and an indoor/outdoor network for the building-scale. Figure 4 summarises the different observation sites and networks described in the following section.

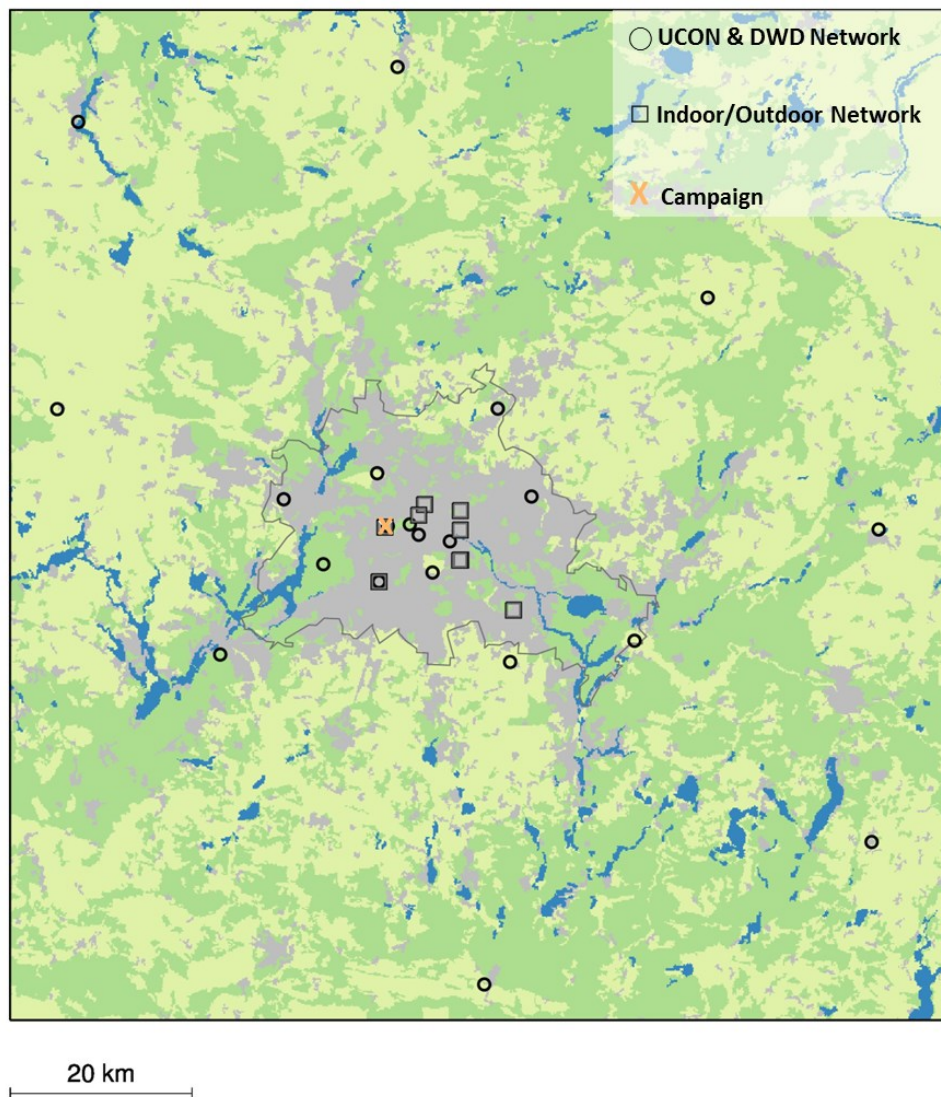


Figure 4: The locations of observational sites of the different networks and the campaign. Land cover is visualised based on CORINE (EEA, 2010) with aggregated classes: water (blue), agriculture, grassland, airports (light green), forests, urban green (dark green), built-up (grey). For detailed descriptions of the respective observations, refer to Papers I, II, III, and IV.

#### *UCON and DWD network*

Two pre-existing measurement networks have been used in this thesis – the Measurement and Observation Network of the German National Meteorological Service (DWD) and the Urban Climate Observation Network (UCON) of the Technische Universität Berlin (TUB). These two networks have provided the time series data for  $T_2$  used for evaluating CCLM and WRF (Papers III and IV).

The DWD network measures  $T_a$  at a height of 2 m according to WMO guidelines, thus reducing local effects as far as possible<sup>1</sup>. Data from different sites in Berlin and its surrounding areas has been used in Papers III and IV (Figure 4). UCON sites fall within Berlin's administrative boundary and are located in built-up and vegetated areas (Fenner et al., 2014).<sup>2</sup> In general, the UCON aims to describe urban alterations from regional climate and is thus more influenced by local conditions as compared to synoptic DWD stations. Networks describing local climate, like the UCON, are needed for analysing heat stress and examining the urban climate, but are only available in a few cities. For instance, Schaeffer et al. (2016) recommend using such weather stations because synoptic weather stations do not sufficiently reflect the intra-urban variability.

For evaluations, the time series of  $T_2$  observed by the UCON and DWD networks have been compared with the  $T_2$  data simulated by the meso-scale models at the nearest grid point with a land cover category similar to the close surroundings of the respective weather stations (Papers III and IV). In this thesis and in Paper IV, weather stations have been grouped according to their surrounding land cover and location into the following categories: rural sites (outside Berlin's administrative border), urban greened sites (parks, forests or other green spaces within Berlin) and built-up sites (predominantly built-up surroundings).

### *Indoor/outdoor network*

Paper II presents a new measurement network for analysing human-biometeorological conditions at the building-scale, consisting of eight sites in and around buildings<sup>3</sup>. The network aims to cover the most common building types in Berlin constructed in different years. They include two private flats, two retirement homes, two offices, a school, and a hospital. At most of the sites, several rooms were equipped with sensors to measure  $T_a$ , relative humidity, wind speed, and globe temperature. The indoor observations are accompanied by  $T_a$  and relative humidity observations collected from sensors mounted on the outdoor façade of the buildings or erected directly next to the building (details in Paper II). In Paper II, my co-authors and I have used  $T_a$ , relative humidity and  $T_{mrt}$  to calculate the indoor  $UTCI$ .  $T_{mrt}$  could not be observed indoors at some sites and has been assumed to be equal to  $T_a$ . This is a reasonable approximation, according to Walikewitz et al. (2014). An additional assumption has been made by increasing indoor wind speed to

---

<sup>1</sup> [ftp://ftp-cdc.dwd.de/pub/CDC/observations\\_germany/climate/hourly/air\\_temperature/](ftp://ftp-cdc.dwd.de/pub/CDC/observations_germany/climate/hourly/air_temperature/)

<sup>2</sup> [http://www.klima.tu-berlin.de/index.php?show=forschung\\_dch\\_messnetz&lan=en](http://www.klima.tu-berlin.de/index.php?show=forschung_dch_messnetz&lan=en)

<sup>3</sup> <http://www.ucahs.org/index.php?page=observations&lan=en>

0.3 m/s in order to calculate the indoor *UTCI*, as discussed in Paper II. Outdoors, the observed values of  $T_a$  and relative humidity from the buildings have been used together with global radiation from an off-site station in order to simulate  $T_{mrt}$  with the SOLWEIG model and calculate the *UTCI*. The outdoor *UTCI* and  $T_{mrt}$  values, therefore, aim to represent the conditions around the buildings.

### *Campaign*

In order to evaluate the micro-climate models and assess the effect of façade greening, in Paper I my co-authors and I have performed a measurement campaign on a cloud-free summer day (23 August 2013) in front of a building wall. The building wall is half-greened with Virginia creepers (*Parthenocissus tricuspidata*) while the other half is bare. The building is located in the TUB campus in a compact midrise local climate zone (cf., Stewart and Oke, 2012) (Figure 4). The campaign includes integral radiation measurements of  $T_{mrt}$  as well as measurements of wind speed, relative humidity,  $T_a$ , surface temperature ( $T_s$ ), and several other variables (described in Paper I and Hoelscher et al., 2015). Integral radiation measurements with angular factors are the most accurate methods for observing  $T_{mrt}$  (Johansson et al., 2014).  $T_{mrt}$  has been measured in front of the greened and the bare wall surface by moving a mobile measurement station between the sites.  $T_s$  has been observed using thermocouples attached to the building walls either behind the façade greening or on the portion of the wall without greening.

## 2.3 Simulations

Various widely-used models (WRF, CCLM, ENVI-met, RayMan and SOLWEIG) were applied to assess the spatial variability of human-biometeorological conditions in Berlin and its surrounding areas (Figure 5).

### *Meso-scale models*

In Paper IV, my co-authors and I have developed the Central Europe Refined analysis (CER) a gridded meteorological dataset at high spatial and high temporal resolutions that provides past atmospheric conditions suitable for urban climate studies for Berlin. For this purpose, WRF (version WRF-ARW 3.6.1) has been used to dynamically downscale the global reanalysis data ERA-interim (Dee et al., 2011). Series of short-term integrations have been performed using a daily re-initialisation strategy, which has also been successfully applied by Maussion et al. (2014). The CER follows a two-way nesting approach (30 km, 10 km, and 2 km). The smallest domain (2 km) covers Berlin and the federal state of Brandenburg, the areas on which this thesis is focused (Figure 5).

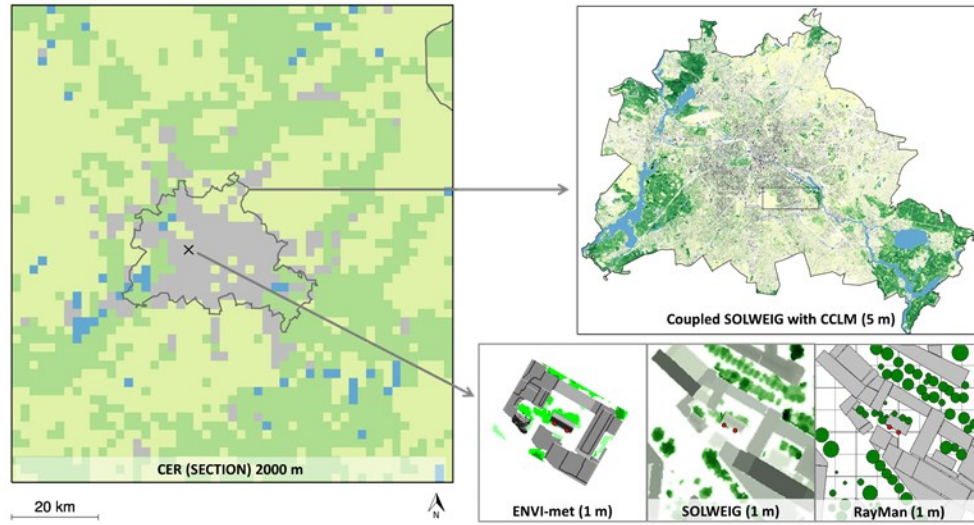


Figure 5: Model domains of the different models with grid spacing in brackets (figures are adapted from Papers I and III).

The three different types of UCMs tested within the CER differ in their complexity: the slab model within the Noah LSM (Chen and Dudhia, 2001), the SLUCM (Kusaka et al., 2001) and the Building Effect Parameterisation (BEP) (Martilli et al., 2002), which is a multi-layer UCM. In Paper IV, we have also tested two different planetary boundary layer schemes. Here, only the simulations with the Bougeault-Lacarrère (BOU) scheme (Bougeault and Lacarrère, 1989) have been considered because BOU has produced lower deviations from observations compared to the other scheme (MYJ). Furthermore, this thesis presents simulations using the mosaic approach (Li et al., 2013) to account for land cover heterogeneity at the sub-grid scale. This approach has been selected here due to lower deviations in  $T_2$  to observations as compared to the dominant approach (cf. Paper IV).

Additionally, CCLM coupled with the Double-Canyon Effect Parametrization scheme (DCEP) (CCLM+DCEP) has been used to derive spatially-gridded input data for SOLWEIG. In Paper III, my co-authors and I have used the already available simulation by Schubert & Grossman-Clarke (2013) because of its finer grid spacing (1 km) as compared to the CER (2 km). DCEP (Schubert et al., 2012) is a multi-layer UCM based on the BEP.

### *Micro-scale models*

Three well-known models (ENVI-met, SOLWEIG, and RayMan) have been evaluated to find a suitable model for coupling with a meso-scale model and for simulation of  $T_{mrt}$  at the selected sites (Paper I).

While ENVI-met (Version 3.1 Beta 5 and Version 4.0 Preview) (Bruse and Fleer, 1998; Bruse, 1999; Huttner, 2012) is a CFD-model that considers surface-plant-air interactions, SOLWEIG (2013a and sub-version) (Lindberg and Grimmond, 2011a; Lindberg et al., 2008) and RayMan (RayManPro) (Matzarakis et al., 2007) only simulate modifications of radiation fluxes. ENVI-met has high computational demands of a personal computer. Its domain size is limited to several hundred metres, depending on the selected grid spacing (maximum 250×250 grid points). RayMan calculates  $T_{mrt}$  and several biometeorological indices using vector data of buildings and trees at the point of interest. SOLWEIG simulates radiation fluxes and  $T_{mrt}$  based on rastered surface models of buildings and trees. In SOLWEIG and RayMan, land cover is only differentiated in terms of vegetation and non-vegetation, while albedo and emissivity are not spatially variable.

All three models require initial (ENVI-met) or input (SOLWEIG and RayMan) data of several meteorological variables, acquired from on- and off-site observations (Papers I and II) and meso-scale simulations (Paper III). Furthermore, environmental parameters such as albedo, emissivity, and transmissivity have been specified. Building and vegetation height data have been provided by SenStadt<sup>4</sup>.

### *Coupling of the models*

A coupled model (SOLWEIG/CCLM+DCEP) has been applied in Paper III after the meso- and micro-scale models were individually tested. The coupled model has been used to investigate the spatial variability of  $T_{mrt}$  at the city-scale (Section 3.2.2 *Micro-scale variability*), and to study the propagation of the meso-scale spatial variability of  $T_2$  to city-scale  $T_{mrt}$  variability (Section 3.3.1 *Propagation from meso- to city-scale*). For this purpose, my co-authors and I have developed a new sub-version of the SOLWEIG 2013a model (Lindberg et al. 2011) in Paper III, which can use gridded meteorological input data to include meso-scale variability induced by weather or urban climate.

### *Evaluation thresholds*

For assessing the deviations of  $T_2$ , the thresholds for attaining a desirable accuracy suggested by Schlünzen and Sokhi (2008) have been applied, which are 2 K for the Root Mean Square Deviation (*RMSD*) and ±0.5 K for the Mean Deviation (*MD*). For the CER, additionally the representation of spatial variability has been evaluated by comparing urban-rural differences ( $\Delta\text{UBU-RUR}$ ) and intra-urban differences ( $\Delta\text{UBU-UGR}$ ) between simulations and observations.

---

<sup>4</sup> <http://www.stadtentwicklung.berlin.de/umwelt/umweltatlas/el610.htm>

$T_{mrt}$  observations from the measurement campaign have been used as references for evaluating the micro-scale models (Paper I). Deviations of  $T_{mrt}$  between simulations and observations were compared for the different models and with former studies.



## 3 Results and Discussion

### 3.1 Model evaluation

The following section presents a synthesis, of deviations of  $T_2$  and  $T_{mrt}$  between the observations and the outputs of the applied models, ranging from the meso- to micro-scale. Uncertainty ranges and deficits, which are relevant for interpreting model outputs, are derived.

#### 3.1.1 Meso-scale models

##### *Absolute deviations from observations*

The  $T_2$  simulated by CCLM+DCEP for 5 August 2003 and its adjacent days reveals low deviations as compared to the weather stations in the DWD and UCON networks (Figure 6). In Figure 6, the deviations from 12 weather stations have been visualised separated into the categories built-up and all sites (Paper III). Deviations are mostly below the thresholds of  $\pm 0.5$  K for  $MD$  and 2 K for  $RMSD$  (Figure 6). A similar high accordance between the CCLM+DCEP and the observations has also been found in earlier studies on Berlin and Basel (Schubert and Grossman-Clarke, 2014, 2013; Schubert et al., 2012).

The CER also shows small deviations in  $T_2$  as compared to observations made in July 2015 (Figure 6) (Paper IV). Within the CER, my co-authors and I have additionally tested, in Paper IV, the sensitivity of  $T_2$  to different UCMs. We have not, however, detected an improvement in model performance with the increase in complexity of the UCMs; the simplest UCM (slab) shows the best overall performance (Figure 6). Thus, within the applied setting and grid spacing, using complex UCMs is not necessary. While some previous studies (Fallmann et al., 2014; Shaffer et al., 2014) also reveal no improvements with increasing complexity of the UCMs, other studies (Kim et al., 2013; Kusaka et al., 2012a; Li and Bou-Zeid, 2014) conclude that more complex schemes (SLUCMs or multi-layer UCMs) perform better than slab models.

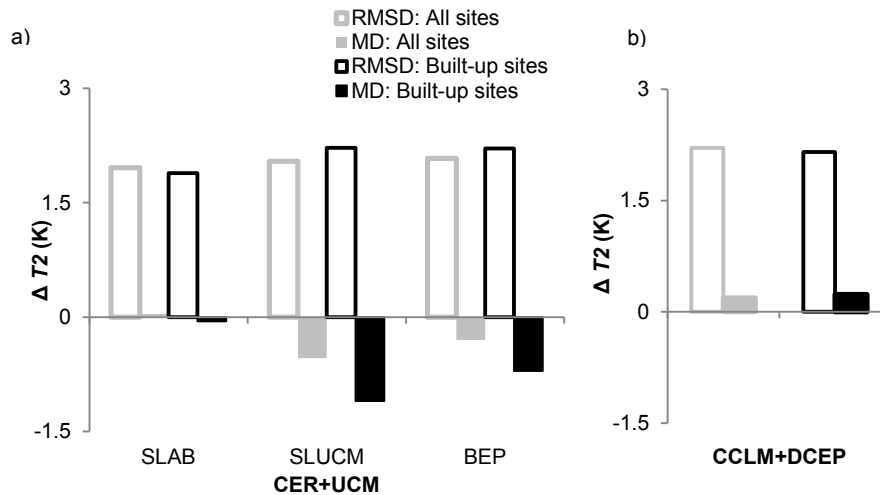


Figure 6: Evaluation of the CER with different UCMs for July 2015 (a) and of CCLM+DCEP for 3 August to 18 August 2003 (b). Averaged deviations in air temperature ( $T_2$ ) in terms of Root Mean Square Deviation ( $RMSD$ ) and Mean Deviation ( $MD$ ) are presented based on hourly data. Grey bars are values averaged over all sites; black bars are values averaged over sites located in built-up areas (figures are adapted from tables in Papers III and IV).

Deviations in the CER and the CCLM+DCEP are in a range similar to other studies that have used NWP (e.g. Dasari *et al.*, 2014; Flagg and Taylor, 2011; Kim *et al.*, 2013; Kusaka *et al.*, 2012b; Liao *et al.*, 2014; Zhang and Zheng, 2004). It is important to remember that CCLM+DCEP and CER results are not directly comparable because they are based on different simulated periods.

Deviations in  $T_2$  could be attributed to representation errors. The CER and CCLM+DCEP simulate conditions for the centre of each grid cell of  $2 \text{ km} \times 2 \text{ km}$  or  $1 \text{ km} \times 1 \text{ km}$ , but measurements could be influenced by the local climate in close surroundings. Therefore, some minor deviations between observations and simulations are expected to result from different footprints. Particularly in heterogeneous environments such as cities, it is crucial to establish representative pairs of weather stations and grid points (Argüeso *et al.*, 2011; Muller *et al.*, 2013; WMO, 2008).

#### Urban-rural and intra-urban differences

NWPs are mostly evaluated on the basis of absolute values. For urban climate studies, however, the representation of urban-rural and intra-urban differences is equally important. The CER (using BOU, slab and mosaicking) reproduces urban-rural and intra-urban differences with characteristics similar to the ones found in observations (Table 1). The CER and observations show a nocturnal UHI and minor differences between the city and its surrounding areas during the day. Intra-urban differences between urban greened and built-up sites, however, have been underestimated by the CER.

Table 1: Cross-table of urban-rural differences ( $\Delta$  Urban built-up – Rural,  $\Delta$  Urban greened – Rural) and intra-urban variability ( $\Delta$  Urban built-up – Urban greened) from observations and the CER (using BOU, slab and mosaicking) during the day (10-15 UTC) and night (22-03 UTC) in July 2015 (table is adapted from Paper IV).

$\Delta T2$ (K)			
Observation	Rural	Urban greened	Urban built-up
Night			
Rural		0.3	1.8
Urban greened	0.3		1.5
Urban built-up	0.5	0.3	
Day			
CER	Rural	Urban greened	Urban built-up
Night			
Rural		0.6	1.3
Urban greened	0.4		0.7
Urban built-up	0.8	0.5	
Day			

Some of the few studies exploring the representation of intra-urban variability in meso-scale models (Salamanca et al., 2012; Trusilova et al., 2015, 2013) have also detected such underestimations of urban-rural differences. Detailed analyses of energy and radiation fluxes can help understand the underlying reasons for these discrepancies. Also, land surface temperatures derived from satellite remote sensing (e.g. MODIS) could be used to evaluate the CER (cf. Hu et al., 2014).

Despite some deviations and discrepancies, the meso-scale models have reproduced  $T2$  sufficiently well and therefore provide reliable city-wide meteorological data for Berlin. Furthermore, the CER evaluation has demonstrated that the CER can reproduce the spatiotemporal patterns of  $T2$  with small deviations from observations and that the daily re-initialisation strategy used by Maussion et al. (2014) can be transferred to other regions and even to an urban context. Until now, the CER has only been evaluated in the context of  $T2$ . Hence, statements about skills with regard to any other variable cannot be made, since small errors in  $T2$  might be accompanied by larger errors in other variables (cf. Kim et al., 2013; Liao et al., 2014). Evaluations in the future can be extended by considering other variables. For this thesis, however, this limitation is of minor relevance since only  $T2$  is used here.

### 3.1.2 Micro-scale models

In Paper I, my co-authors and I evaluated micro-scale models regarding  $T_{mrt}$  as a complement to meso-scale models and for usage in the coupled SOLWEIG/CCLM+DCEP model.

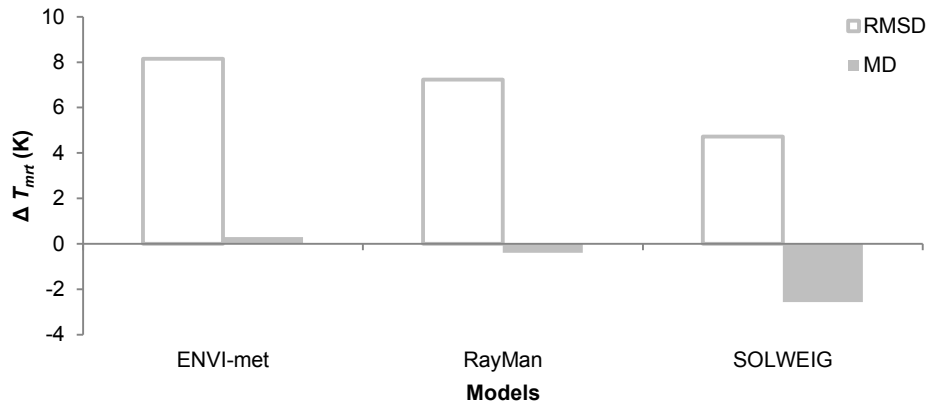


Figure 7: Evaluation of ENVI-met, RayMan and SOLWEIG regarding mean radiant temperature ( $T_{mrt}$ ) on 23 July 2013 using Root Mean Square Deviation ( $RMSD$ ) and Mean Deviation ( $MD$ ) (figure is adapted from Paper I).

All the tested micro-scale models have simulated  $T_{mrt}$  to a reasonable extent in terms of  $RMSD$  and  $MD$  (Paper I) (Figure 7).  $MD$ s are lowest in ENVI-met and RayMan, since positive and negative errors cancel each other out (Figure 7). Overall, however, SOLWEIG shows the lowest  $RMSD$  values. The range of deviation is similar to the results of previous studies, with average values of  $MD \pm 2-8$  K and  $RMSD$  2-15 K (Chen et al., 2014; Huttner, 2012; Hwang et al., 2011; Krüger et al., 2014; Lin et al., 2010; Lindberg and Grimmond, 2011b; Lindberg et al., 2008; Thorsson et al., 2007). Evaluation of different models for the same setting also reduces the lack of model comparisons. So far RayMan, SOLWEIG and ENVI-met have been compared to each other by Chen et al. (2014), and ENVI-met and RayMan have been compared very recently by Lee and Mayer (2016).

It is important to note that deviations between simulations and observations vary over the diurnal cycle and reveal larger errors at night. During the night,  $T_{mrt}$  has been underestimated in all experiments due to the underestimation of long-wave upward radiation (see Paper I). Yang et al. (2011) discuss these shortcomings in ENVI-met 3 and reveal that night-time  $T_s$  was also underestimated. In SOLWEIG, Lindberg et al. (2016) also detect nocturnal underestimated  $T_{mrt}$  and mentioned possible improvements in follow-up versions.

In summary, the low  $RMSD$  in SOLWEIG is remarkable given the simple calculation approach in SOLWEIG as compared to the more elaborate ENVI-met model. ENVI-met, however, offers more opportunities for other issues and provides more options for tuning and modifications by the users. Deviations in RayMan are midway between SOLWEIG and ENVI-met. RayMan's fast computation is a major advantage, but the restriction to a single point of interest impedes its usage in the analysis of spatial variability. SOLWEIG has been selected to simulate  $T_{mrt}$  city-wide and building-resolving in Section 3.2.2 *Micro-scale variability* because of the low  $RMSD$  and the fast computation.

## 3.2 Spatial variability of human-biometeorological conditions

This section describes the spatial variability of different climate elements related to heat stress based on the evaluated models and measurements.

### 3.2.1 Meso-scale variability

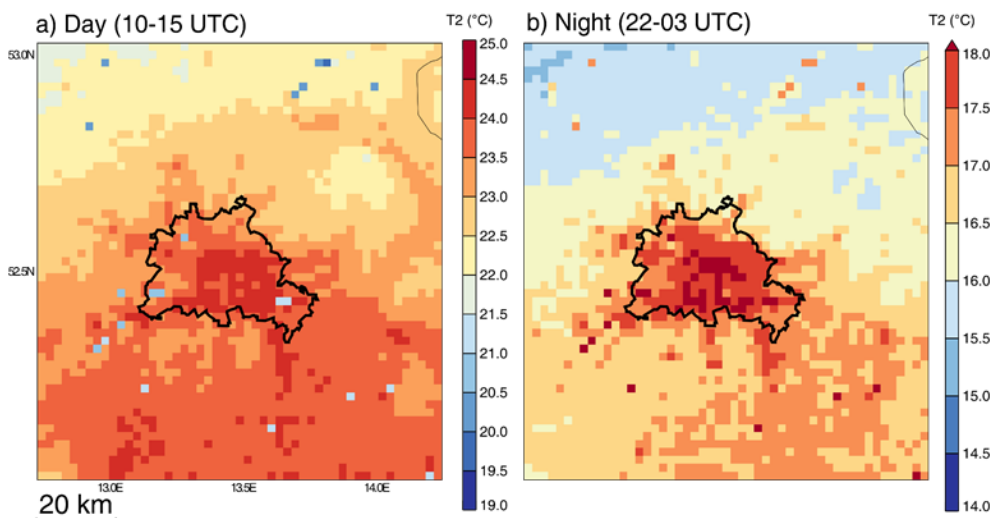


Figure 8: Mean  $T_2$  in July 2015 as resolved by the CER (using BOU, slab, and mosaicking) during the day (10-15 UTC) and night (22-03 UTC). Colour bars vary between day and night. Shape marks Berlin's administrative border (figures are taken from Paper IV).

The spatial variability of  $T_2$  as resolved by the CER was larger during the night than during the day. Nocturnal urban-rural differences are typical for Berlin (Endlicher and Lanfer, 2003; Fenner et al., 2014; Hupfer and Chmielewski, 1990; Trusilova et al., 2015). While Paper IV and Trusilova et al. (2015) focus on average urban-rural differences for Berlin, Fenner et al. (2014) observe through analysis on hourly basis that urban-rural differences may rise up to 10 K during the night. In the CER, Berlin remains warmer than the countryside on average throughout the day. This has also been detected by Fenner et al. (2014) and Trusilova et al. (2015) for Berlin. Fenner et al. (2014) also reveal

that an urban cool island is established for some hours during the day using observational data. For other cities, both the higher mean intensity of the UHIs and urban cool islands during the day have been reported (e.g. Erell and Williamson, 2007; Santamouris, 2015).

In the CER, the spatial variability of  $T_2$  is also visible in the form of intra-urban differences between built-up and urban greened sites (Figure 8 and Table 1). In particular, urban greened sites are cooler at night-time than built-up sites. This intra-urban variability also indicates that urban green can reduce the intensity of UHIs and might contribute to the reduction of heat stress in Berlin. The cooling effects of greened areas have frequently been investigated for other cities (e.g. reviews by Bowler et al. (2010) and Jamei et al. (2016)). Bowler et al. (2010), for instance, reveal that the average cooling effect of parks is 0.9 K at day and 1.2 K at night. In contrast, some studies report a higher  $T_2$  for certain hours in urban green spaces or neighbourhoods with high green fractions as compared to their built-up surroundings (Cohen et al., 2012; Grimmond et al., 1996; Potchter et al., 2006; Skoulika et al., 2014; Yu and Hien, 2006). Thus, even though the effects of urban green on human-biometeorological conditions have frequently been examined, it remains difficult to estimate the cooling effects for a specific location in advance. City-specific analyses like this study are needed for quantifying the effects of parks.

Furthermore, Figure 8 and Table 1 show that urban greened sites are warmer than rural sites during the day (0.4 K) and night (0.6 K). This can be interpreted as a meso-scale footprint of the city, which is not as local as the effect that leads to differences between urban built-up and urban greened sites. This meso-scale effect is smaller during both night and day compared to the local and land cover-related differences.

Future studies may extend the simulation period to a decade. This would allow investigations into other issues, for example whether the UHI intensity is stronger during extreme heat events in Berlin as several recent studies have detected for other cities (Li et al., 2015; Ramamurthy et al., 2015; Schatz and Kucharik, 2015).

### 3.2.2 Micro-scale variability

The following section examines the spatial variability of biometeorological conditions across the city based on the coupled SOLWEIG/CCLM+DCEP model and also for a smaller area with a focus on the effects of façade greening.

### City-scale variability

The spatial variability of  $T_{mrt}$  and  $UTCI$  was high on the selected cloud-free day (5 August 2003) during an extreme heat event with regard to the results of the newly-developed coupled SOLWEIG approach (Paper III) (Figure 9). The night-time situation is not shown because the  $T_{mrt}$  simulated by SOLWEIG reveals more uncertainties during the night, as already discussed (Section 3.1.2 *Micro-scale models*).

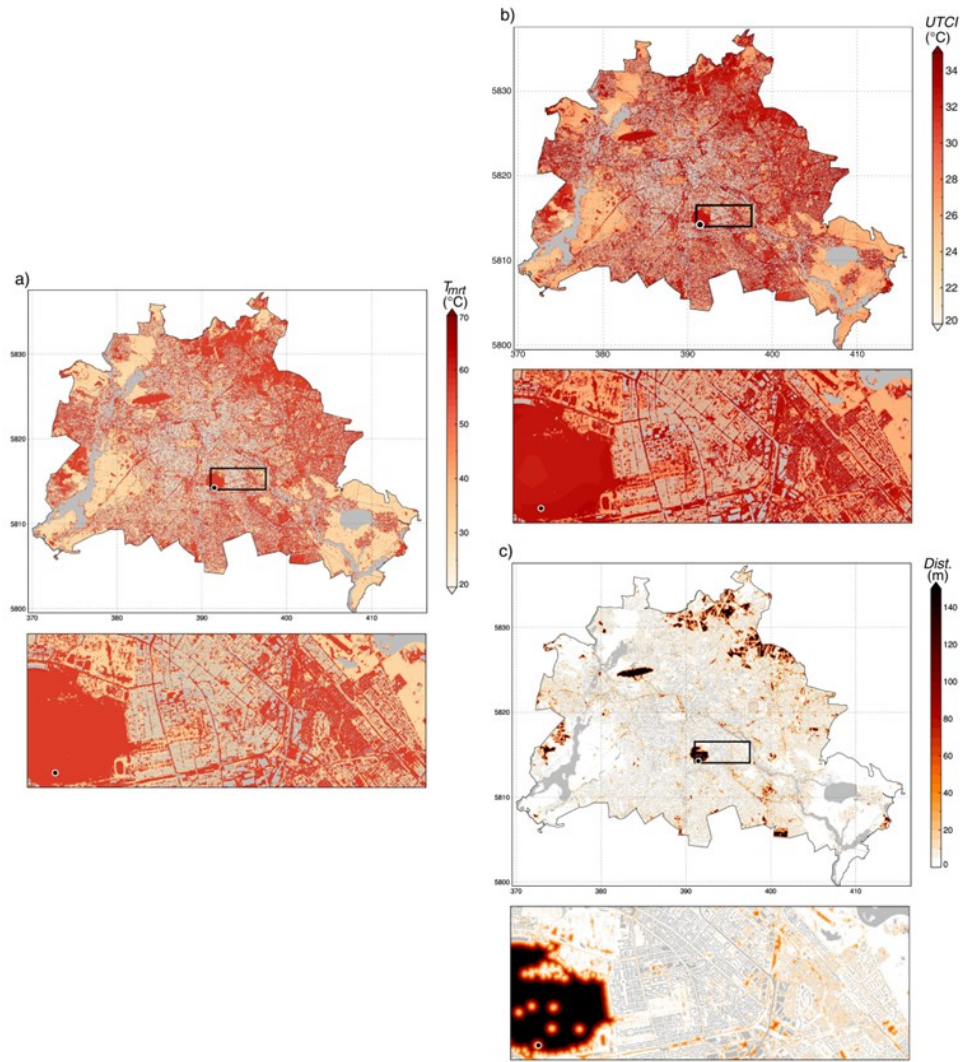


Figure 9: Spatial variability of  $T_{mrt}$  (°C) (a) and  $UTCI$  (°C) (b), and distance (Dist.) (m) to sites with  $T_{mrt}$  lower than the threshold of 55.5°C at midday (12 CET) on 5 August 2003. The circle indicates the position of the weather station at a former airport (Tempelhof). The zoomed area shows details for the weather station and for a variety of urban structures. Water surfaces and roof areas have been excluded and coloured in grey (figures are taken or adapted from Paper III).

The patterns of  $T_{mrt}$  and  $UTCI$  are similar because, under sunny conditions,  $T_{mrt}$  is the most important factor influencing biometeorological indices (Kuttler, 1999). My approach for estimating  $UTCI$ , however, is oversimplified and should be interpreted with caution. For rough estimation, I have used the other variables ( $T_2$ , relative humidity and wind speed) required for calculating  $UTCI$  from the meso-scale model with a much coarser grid spacing than  $T_{mrt}$  ( $1\text{ km} \times 1\text{ km}$  in comparison to  $5\text{ m} \times 5\text{ m}$ ). Therefore, I have concentrated on  $T_{mrt}$  in the following, which is also described in Paper III. In the future, simple diagnostic wind models (cf. Wellens et al., 1994) or a geostatistical model based on CFD-simulation and high-resolution digital surface models as examined by Johansson et al. (2016) might be tested to overcome this shortcoming.

The spatial differences of  $T_{mrt}$  have been found to reach up to 30 K at midday (Figure 9 a). The high spatial variability of  $T_{mrt}$  can be associated with two causes: First, higher spatial resolution leads to higher variability as compared to the meso-scale models. Second,  $T_{mrt}$  is, in general, more variable than  $T_2$  due to its stronger dependence on short-wave radiation patterns. The large influence of shading patterns on  $T_{mrt}$  can also be seen by grouping into sunlit and shaded areas with high and low values respectively (Figure 9 a). As a consequence,  $T_{mrt}$  is lower in shaded than in sunlit areas during the day. Open inner-city areas (e.g. airports) as well as sparsely built-up areas in the outskirts show the highest  $T_{mrt}$  values. The results of high spatial variability match those reported in previous studies for smaller areas in summer and under clear-sky conditions (Lau et al., 2015; Lindberg et al., 2014; SenStadt, 2015; Thorsson et al., 2011).

The distance map visualises hotspots in Figure 9 c. Distance maps emphasise areas with long distance to  $T_{mrt}$  values lower than a given threshold. Here, a threshold of  $55.5^\circ\text{C}$  has been used, which has found to increase heat-stress related mortality in Gothenburg, Sweden by 5% according to Thorsson et al. (2014). Note that the findings from Gothenburg are not directly transferable to Berlin; this threshold is used only to demonstrate the application. The idea of distance maps is that if a person only needs to change the side of a street to reduce heat-stress hazards, countermeasures may not be required. If one has to walk for a longer distance to find cooler conditions countermeasures seem to be more important.

In general, patterns are similar to the original  $T_{mrt}$  map but hotspots are more distinctly visible in the distance map (Figure 9 c). Inner-city airports (north-west and middle) and other open spaces with few or low trees, like allotments, emerge visibly with large distances. Additional areas with large distances to



walk are located at the edges of the city, particularly in the north-east. To reduce heat-stress hazards at such sites, planting trees to increase the shaded area, for example, could be effective as already discussed here and in a number of studies (Bowler et al., 2010; Lindberg and Grimmond, 2011b; Thorsson et al., 2011). Paper III also implies that dense building structures can reduce daytime heat-stress hazards as also reviewed by Jamei et al. (2016). During night, however, dense building structures tend to increase  $T_a$  (Jamei et al., 2016).

The coupled SOLWEIG approach has some advantages, such as fast computation, which make city-wide calculations foremost feasible. Nevertheless, this approach is limited to radiation fluxes and does not include processes related to different land cover types or other variables. Recently, Lindberg et al. (2016) have introduced spatially-variable ground surface characteristics in SOLWEIG. They detected that the influence of spatially-resolved surface characteristics on  $T_{mrt}$  is smaller than the one from shading patterns. Consequently, different ground surface characteristics might be negligible. Furthermore, local climate effects like thermal circulation systems, which are at sub-scale in meso-scale models and not reproduced in SOLWEIG, remain unconsidered in our approach. Follow-up studies may use meteorological input with higher grid spacing than 1 km to avoid some of these problems.

Other methods to derive high-resolution and city-wide  $T_{mrt}$  are possible as well: approaches based on geostatistical regression models (with observations, and topographic and land cover data, for example) have also been used (Buttstädt and Schneider, 2014; Ketterer and Matzarakis, 2015; Yi et al., 2015). Such empirical models, however, are temporally limited to the availability of observation data, and may not explicitly include effects of buildings (such as shading). Another approach for examining human-biometeorological conditions at high spatial resolutions involves using statistical-dynamical downscaling to calculate perceived temperature and  $T_{mrt}$  and has been carried out by Schoetter et al. (2013). Schoetter et al. (2013), however, used a much coarser grid spacing of 250 m. Recently, SenStadt (2015) have also published new simulations results of  $UTCI$  and other variables with 10 m grid spacing based on the model FITNAH for ideal summer weather conditions. These different approaches have various unresolved issues related to either grid spacing or temporal extent, but they highlight the interest in high-resolution simulations of biometeorological conditions and the need for further research.

### Micro-scale effects of façade greening

The coupled SOLWEIG model approach is limited to modifications of radiation fluxes while other variables influencing human biometeorology, such as atmospheric moisture or wind speed, are not considered. For instance, façade greening could also lead to spatial variability of human-biometeorological conditions through transpiration and modified radiation fluxes, and is discussed as a countermeasure to reduce heat stress (e.g. Hunter et al., 2014; Köhler, 2008). In Paper I, my co-authors and I have tested whether current micro-scale models (ENVI-met, RayMan and SOLWEIG) are able to reproduce observed effects of façade greening, but these models show poor skills in this aspect. Thus, observations are used to examine whether façade greening can reduce heat-stress hazards and influence the spatial variability of human-biometeorological conditions.

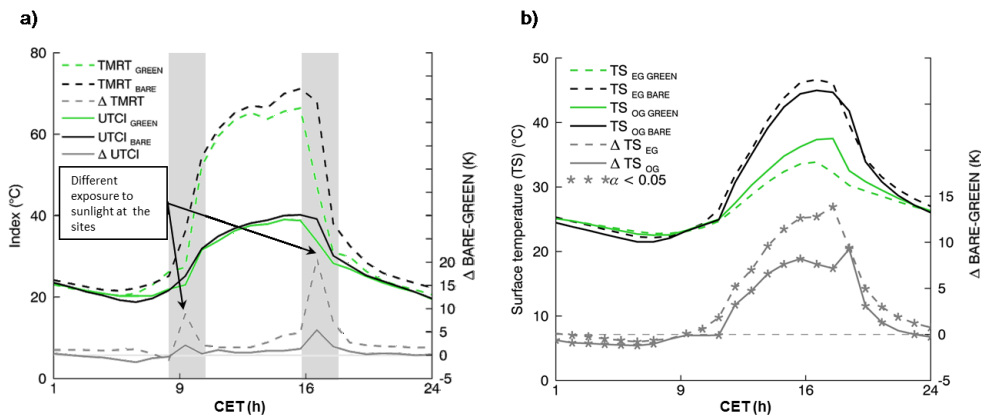


Figure 10:  $T_{mrt}$  and  $UTCI$  (23 July 2013) (a) surface temperature ( $T_s$ ) in the first (EG) and in the second (OG) floor (averaged over 21 to 24 July 2013) (b) observed at the bare and the greened site in front of the building. In part b) asterisks (\*) represent significant differences ( $\alpha < 0.05$ ) according to the Mann-Whitney U test (figure a is adapted from Paper I).

$T_{mrt}$  and  $UTCI$  show only a slight decrease in front of the greened façade as compared to the bare one (10-16 CET, 23 August 2013) (Figure 10). The observed difference of 2 K in  $T_{mrt}$  is distinct but lower than the measurement accuracy of about 4 K and thus not robust. In one of the few studies that investigate  $T_{mrt}$  reduction due to façade greening, larger differences of 2 to 13 K have been found in a tropical environment (Tan et al., 2014). Other studies observe that the effects of façade greening on exterior  $T_a$  are small (1.5 K) to negligible (Berry et al., 2013; Djedjig et al., 2013; Gross, 2012; Pérez et al., 2011). Figure 10 a also visualises slight differences in the shadow patterns between the two sites at sunrise and sunset (peaks around 9 and 16 CET) reflecting drawbacks in the study design. Optimal study sites for

assessing façade greening are difficult to find, as pointed out by Hunter et al. (2014), especially in complex urban environments.

Figure 10 b shows differences in  $T_s$  between the green and the bare site.  $T_s$  is less meaningful for outdoor human-biometeorological conditions, but influences indoor biometeorological conditions through the building envelope. A clear reduction of  $T_s$  of building walls behind the façade greening is visible in Figure 10 b and also shown in a related investigation by Hoelscher et al. (2015). Hoelscher et al. (2015) detect reductions in exterior and interior wall surface temperature as well as an insulation effect of façade greening. Reductions in  $T_s$  have been discovered before with values varying in the range of 2-20 K depending on plant type, time of day and type of façade greening (Cameron et al., 2015; Chen et al., 2013; Pérez et al., 2011; Wong et al., 2010). Moreover, Chen et al. (2013) and Eumorfopoulou and Kontoleon (2009) revealed a reduction of 0.4 to 1.5 K in indoor  $T_a$  due to façade greening.

Overall, our investigations show only a negligible effect of façade greening on outdoor  $T_{mrt}$ . For reducing outdoor heat stress at daytime, other actions might be more effective, such as shadowing with trees, which directly reduces  $T_{mrt}$  as shown earlier. Our results, however, do not necessarily imply that façade greening has no potentials for reducing heat stress, because indoor biometeorological conditions might be improved in poorly insulated buildings.

### 3.2.3 Building-scale variability

*UTCI* is applied for examining spatial variability at building-scale, because short-wave radiation is less important indoors and thus,  $T_{mrt}$  alone cannot describe indoor human-biometeorological conditions adequately.

*UTCI* calculations from the indoor/outdoor observation network in Paper II reveal that intra-urban variability also exists indoors. Mean *UTCI* values differed between buildings within a range of 3 K in the summer of 2014 (Figure 11 a). Furthermore, the numbers of days with heat stress, here defined as  $UTCI \geq 26^\circ\text{C}$ , were unequally distributed between the different study sites (Figure 11 b). In some buildings, heat stress occurred on more than 50% of all summer days in 2014. The variability in the number of days with heat stress was even higher indoors than outdoor. Earlier studies also report a high spatial variability in indoor climates in other cities (Mavrogianni et al., 2012; Oikonomou et al., 2012; White-Newsome et al., 2012). For instance, Oikonomou et al. (2012) detect higher spatial  $T_a$  differences indoors than produced by UHI outdoors in London. Most of the previous studies, however, have used  $T_a$  and not *UTCI* or other indices.

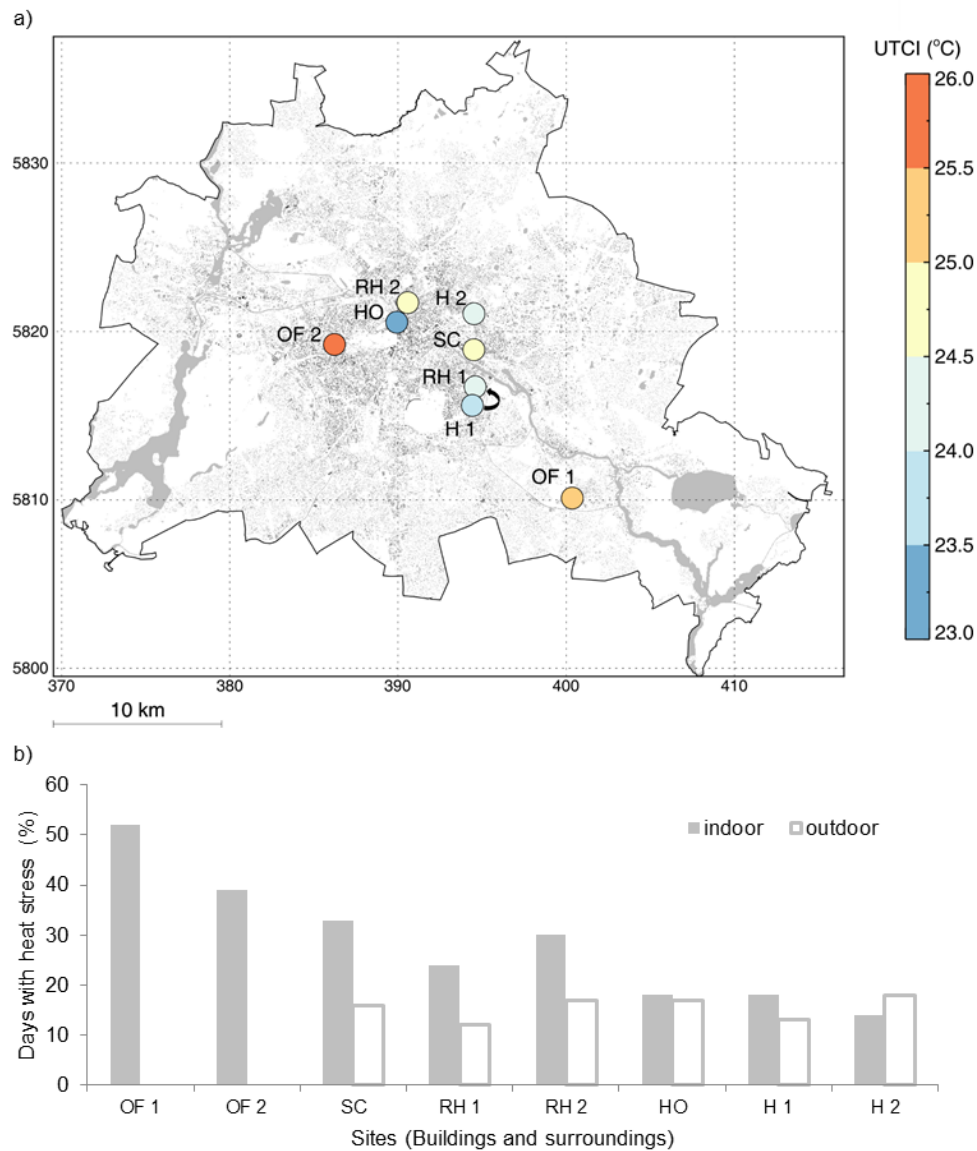


Figure 11: a) Mean indoor *UTCI* (June, July, and August 2014) based on observations from the indoor/outdoor network and simulations of *UTCI* by RayMan. The arrow indicates that site H1 is close to site RH1. b) Percentage of days (d) with mean indoor/outdoor *UTCI*  $\geq 26^{\circ}\text{C}$  (moderate heat-stress level) per study site in (June, July, and August 2014) in percentage of days (%) (figures are adapted from Paper II).

Taken together, the analysis reveals a high spatial variability at building-scale and shows that indoor heat stress exists on many summer days in some buildings, not only during official heat warnings, which were only nine days in 2014.

### 3.3 Propagation of spatial variability through the scales

#### 3.3.1 Propagation from meso- to city-scale

In Paper III, my co-authors and I have investigated the propagation of the spatial patterns of human-biometeorological conditions from meso- to city-scale by testing the sensitivity of  $T_{mrt}$  to spatially-resolved  $T_2$ . Furthermore, the results help to evaluate whether the effort of coupling a meso-scale model with a micro-scale model is worthwhile and necessary for future multi-scale approaches.

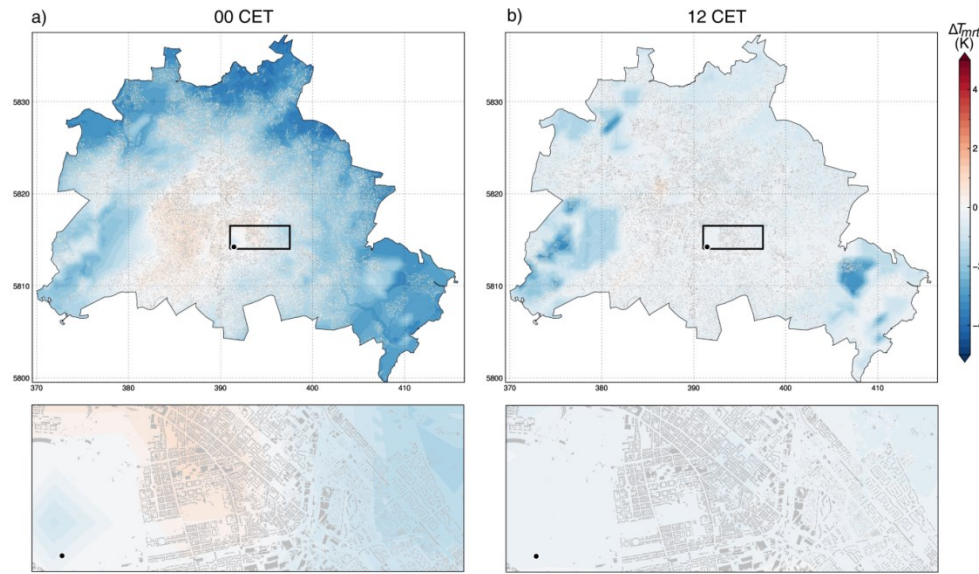


Figure 12: Differences in  $T_{mrt}$  (K) ( $\Delta T_{mrt} = \text{GRD\_ta} - \text{STD}$ ) between the experiments without (STD) and with gridded  $T_a$  (GRD\_ta) at midnight (00 CET) (a) and midday (12 CET) (b) on 5 August 2003. The circle indicates the position of the weather station (Tempelhof). The zoomed area shows details for Tempelhof and for a variety of urban structures (figures are taken from Paper III).

Using the gridded  $T_2$  as input for SOLWEIG produces slightly different results in  $T_{mrt}$  as compared to the standard version with meteorological input from just one reference point (Figure 12). During night, the patterns of  $T_{mrt}$  differences can be traced back to an UHI. During the day, differences are found only around water surfaces. In principle,  $T_2$  strongly influences  $T_{mrt}$  in SOLWEIG, since  $T_2$  is used to estimate long-wave radiation fluxes (Lindberg et al., 2008; Onomura et al., 2015). Onomura et al. (2015) detect a nearly linear relationship between  $T_2$  and  $T_{mrt}$ , where a difference of 1 K in  $T_2$  leads to a change of 0.84 K in  $T_{mrt}$ . In our case, however, the low  $T_2$  variability produces only small alterations in  $T_{mrt}$ . In other cities with larger  $T_2$  gradients, e.g. due to varying altitude, the influence of the  $T_2$  pattern on the  $T_{mrt}$  pattern might be stronger.

Additionally, my co-authors and I have tested in Paper III the sensitivity of  $T_{mrt}$  to gridded relative humidity and short-wave radiation, but we detected only negligible effects. The reason for the low sensitivity to gridded relative humidity is that relative humidity in SOLWEIG is only used for estimating the emissivity of the sky to simulate incoming long-wave radiation and to estimate the partitioning of direct and diffuse short-wave radiation (Lindberg et al., 2008). The low sensitivity to short-wave radiation can be attributed to low spatial variability on the selected cloud-free day.  $T_{mrt}$  is, in general, highly sensitive to short-wave radiation and thus, under cloudy weather situations special attention needs to be paid to the spatial variability of short-wave radiation.

Overall, the spatial variability of  $T_2$  has been propagated from the meso- to the city-scale. City-scale spatial variability of  $T_{mrt}$ , however, is more influenced by urban structures than by the  $T_2$  variability. This implies that considering both spatial variability at the meso-scale and directly resolved urban structures is necessary for analysing city-wide  $T_{mrt}$ .

### 3.3.2 Propagation from city- to building-scale

This section investigates whether outdoor patterns are propagated into indoor environments by using the indoor/outdoor observation network.

Table 2 shows that indoor  $UTCI$  and  $T_a$  are highly correlated with outdoor  $UTCI$  and  $T_a$ . This result agrees with earlier studies (Mills et al., 2010; Nguyen et al., 2014) that also reveal this relationship. Furthermore, Buchin et al., (2016a, 2016b) and Wright et al. (2005) relate indoor  $T_a$  with heat-stress related mortality. They recommend using indoor  $T_a$  instead of outdoor  $T_a$  for analysing heat-stress related mortality because the most vulnerable groups (elderly and ill people) remain indoors and the frequently detected lag times in mortality can partly be explained by the inertia of building envelopes.

Table 2: Correlation coefficients between indoor  $UTCI/T_a$  and outdoor  $UTCI/T_a$  from on-site (indoor/outdoor network) and off-site (reference site, Rothenburgstrasse) measurements (table is taken from Paper II).

Site	$UTCI$		$T_a$	
	Indoor vs. Outdoor on-site	Indoor vs. Outdoor off-site	Indoor vs. Outdoor on-site	Indoor vs. Outdoor off-site
SC	0.76	0.83	0.82	0.84
RH1	0.86	0.89	0.87	0.88
RH2	0.83	0.90	0.91	0.92
HO	0.88	0.88	0.93	0.93
H1	0.76	0.85	0.83	0.84
H2	0.79	0.82	0.84	0.84

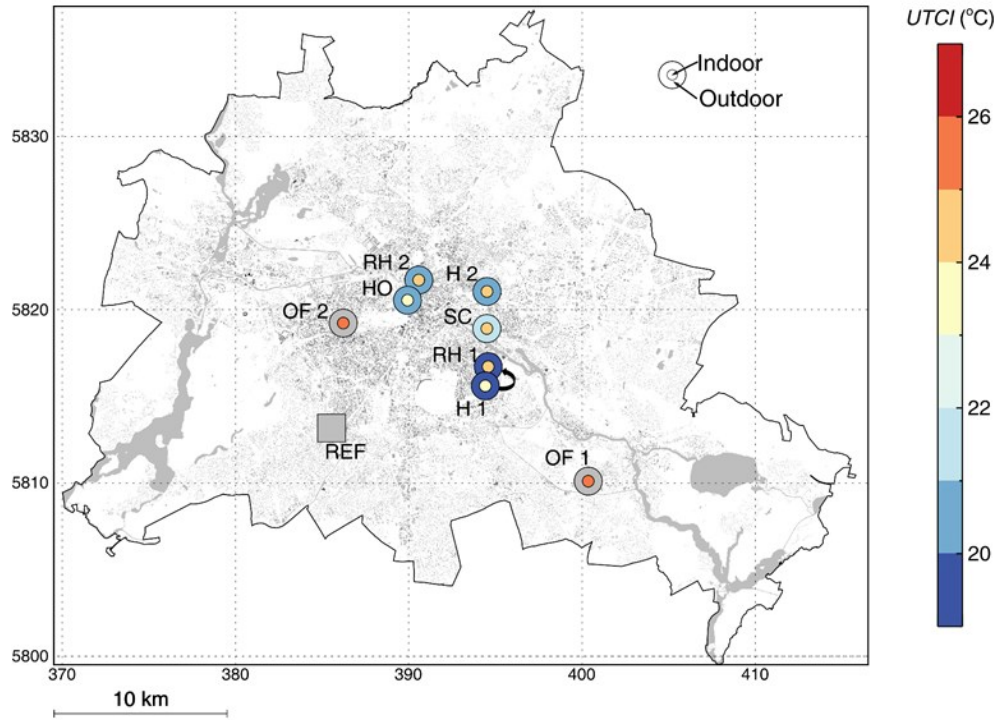


Figure 13: Mean indoor and outdoor  $UTCI$  values (20 July to 31 August 2014) based on observations from indoor/outdoor network and simulations using SOLWEIG and RayMan. The arrow indicates that site H1 is close to site RH1. REF (Rothenburgstrasse) is the off-site station as used in Table 2. Grey circles indicate missing data (figure is adapted from Paper II).

In Paper II, my co-authors and I have further analysed whether indoor conditions are also influenced by local outdoor conditions of the building surroundings. Thereby, we assessed whether spatial patterns of outdoor variability are propagated indoors. For this assessment, correlation coefficients of outdoor off-site observations (from one reference weather station) of  $T_a$  and simulated  $UTCI$  are compared with on-site observations (from the indoor/outdoor observation network) (Table 2). Correlation coefficients have not been found to increase on using on-site data.

Figure 13 visualises average indoor and outdoor  $UTCI$  values for summer 2014, as used in the correlation. Again, no clear relation between patterns of outdoor and indoor  $UTCI$  is visible. Thus, consideration of the direct building surrounding with on-site  $T_a$  observations or  $T_{mrt}$  simulations has shown no benefits in our study. Time-stratified analyses or more diverse urban surroundings at the sites might change these results. In contrast to our findings, Franck et al. (2013) detect an indoor pattern corresponding to outdoor structures in Leipzig, Germany.

Since the variability of indoor conditions is apparently not produced by the intra-urban variability of outdoor biometeorological conditions, other causes such as building characteristics might be more important for the detected indoor variability. In Paper II, my co-authors and I have also examined the relationships of indoor *UTCI* with window size and construction age, but we have not been able to reveal clear connections. For Berlin, Langner et al. (2014) observe increased *UTCI* with floor level, as also detected by Franck et al. (2013) using  $T_a$ . Other factors that have been found to influence indoor human-biometeorological conditions in earlier studies include building type, exposition, insulation and the behaviour of inhabitants (Mavrogianni et al., 2012; Nguyen et al., 2014; Wright et al., 2005). These drivers, however, are not fully understood (Nguyen et al., 2014) and it is difficult to obtain information for multiple sites.



## 4 Conclusions and perspectives

For the first objective, I have explored different model-based methods and have detected that micro- and meso-scale models produce overall small deviations from observations and are thus viable for analysing spatial variability at the respective scale. Moreover, a new dataset for analysing spatio-temporal variability at meso-scale (CER) has been developed. Testing different model settings such as different UCMs has helped to find a reasonable setup with low deviations from observation in  $T_2$ . The comparison has shown that moderately complex UCM (SLUCM) and the complex UCM (BEP) do not represent intra-urban and urban-rural differences more accurate than the simple slab scheme. With the CER, simulations spanning more than a decade (2001-2016) are possible and will be finalised in the near future. The results from the newly-developed coupled SOLWEIG model provide a framework for exploring spatial variability of building-resolving and city-wide  $T_{mrt}$  in Berlin and act as a meaningful complement to meso-scale analyses. Both methods – the CER and the coupled SOLWEIG model – can be easily applied to other cities.

My second objective was to investigate spatial variability of human-biometeorological conditions in Berlin. The most relevant finding for this objective is that high spatial variability occurs at the meso-, city-, and building-scale. Simulations and observations show spatial variability of  $T_a$ ,  $T_{mrt}$  and  $UTCI$  and have determined different patterns depending on the considered scale and variable. In future, the analysed periods of the CER and the coupled SOLWEIG model may be extended for more robustness for different weather conditions. This would also offer possibilities to analyse heat events at city-scale for various years when the CER serve as input for the coupled SOLWEIG model. Overall, the high spatial variability found at each scale implies that taking different scales into account is likely to be beneficial for other cities as well.

Addressing the third objective, I have revealed that the spatial patterns of human-biometeorological conditions related to heat stress in Berlin are not directly propagated from the meso- to micro-scale or from the micro- to building-scale. Other factors, such as urban structures, were the main cause

for the detected spatial variability at city-scale outdoor  $T_{mrt}$ . Indoors, spatial variability of  $UTCI$  was barely influenced by the outdoor spatial variability of  $UTCI$ . Hence, for analysing biometeorological conditions indoors, outdoor conditions at high spatial resolution, e.g. derived from the coupled SOLWEIG model, might not be necessary; one time series from a weather station or from a meso-scale NWP seems to be enough. More information, such as user behaviour or detailed building data, is required to account for the multiple factors influencing human-biometeorological conditions indoors.

Some issues, however, remain unresolved in this thesis and need to be addressed in future research. Depending on the focus of investigations, the CER also might be evaluated in terms of variables other than  $T_2$ . In micro-scale models, I have detected an underestimation of nocturnal  $T_{mrt}$  that should be sorted out before investigating night-time results. Moreover, the inclusion of wind and relative humidity in city-scale models is an open issue which is already reflected in future research programmes such as the research project 'Stadtklima im Wandel' (translation: urban climate under change) starting in summer 2016.

Only heat-stress hazard is considered in the scope of this study. However, if people actually live or spend time in areas with high heat-stress hazards (exposure), and if damage to human health occurs (risks) remains unknown. In follow-up studies, exposure to heat stress might be included by information about population density, population structure and land use. Heat-stress risks can be included through data of mortality and morbidity. Building-resolving and city-wide analyses might also be valuable for planning purposes or other applications, as they can help identify hotspots in cities or suitable locations for various countermeasures.

## References

- Argüeso, D., Hidalgo-Muñoz, J.M., Gámiz-Fortis, S.R., Esteban-Parra, M.J., Dudhia, J., Castro-Díez, Y., 2011. Evaluation of WRF parameterizations for climate studies over southern Spain using a multistep regionalization. *J. Clim.* 24, 5633–5651. doi:10.1175/JCLI-D-11-00073.1
- Arnfield, A.J., 2003. Two decades of urban climate research: a review of turbulence, exchanges of energy and water, and the urban heat island. *Int. J. Climatol.* 23, 1–26. doi:10.1002/joc.859
- Azevedo, J., Chapman, L., Muller, C., 2016. Quantifying the Daytime and Night-Time Urban Heat Island in Birmingham, UK: A Comparison of Satellite Derived Land Surface Temperature and High Resolution Air Temperature Observations. *Remote Sens.* 8, 153. doi:10.3390/rs8020153
- Baklanov, A., Molina, L.T., Gauss, M., 2016. Megacities, air quality and climate. *Atmos. Environ.* 126, 235–249. doi:10.1016/j.atmosenv.2015.11.059
- Barlow, J.F., 2014. Progress in observing and modelling the urban boundary layer. *Urban Clim.* 10, 216–240. doi:10.1016/j.uclim.2014.03.011
- Barnett, A.G., Tong, S., Clements, A.C.A., 2010. What measure of temperature is the best predictor of mortality? *Environ. Res.* 110, 604–611. doi:10.1016/j.envres.2010.05.006
- Berry, R., Livesley, S.J., Aye, L., 2013. Tree canopy shade impacts on solar irradiance received by building walls and their surface temperature. *Build. Environ.* 69, 91–100. doi:10.1016/j.buildenv.2013.07.009
- Blazejczyk, K., Epstein, Y., Jendritzky, G., Staiger, H., Tinz, B., 2012. Comparison of UTCI to selected thermal indices. *Int. J. Biometeorol.* 56, 515–35. doi:10.1007/s00484-011-0453-2
- Borden, K.A., Cutter, S.L., 2008. Spatial patterns of natural hazards mortality in the United States. *Int. J. Health Geogr.* 7, 64. doi:10.1186/1476-072X-7-64
- Bougeault, P., Lacarrère, P., 1989. Parameterization of orography-induced turbulence in a mesobeta-scale model. *Mon. Weather Rev.* 117, 1872–1890.
- Bowler, D.E., Buyung-Ali, L., Knight, T.M., Pullin, A.S., 2010. Urban greening to cool towns and cities: A systematic review of the empirical evidence. *Landsc. Urban Plan.* 97, 147–155. doi:10.1016/j.landurbplan.2010.05.006
- Brasche, S., Bischof, W., 2005. Daily time spent indoors in German homes - Baseline data for the assessment of indoor exposure of German occupants. *Int. J. Hyg. Environ. Health* 208, 247–253. doi:10.1016/j.ijheh.2005.03.003
- Bröde, P., Fiala, D., Błażejczyk, K., Holmér, I., Jendritzky, G., Kampmann, B., Tinz, B., Havenith, G., 2012. Deriving the operational procedure for the Universal Thermal Climate Index (UTCI). *Int. J. Biometeorol.* 56, 481–94. doi:10.1007/s00484-011-0454-1
- Bruse, M., 1999. Die Auswirkungen kleinskaliger Umweltgestaltung auf das Mikroklima. Dissertation Fakultät für Geowissenschaften der Ruhr-

Universität Bochum.

- Bruse, M., Flerer, H., 1998. Simulating surface-plant-air interactions inside urban environments with a three dimensional numerical model. *Environ. Model. Softw.* 13, 373–384. doi:10.1016/S1364-8152(98)00042-5
- Buchin, O., Hoelscher, M.-T., Meier, F., Nehls, T., Ziegler, F., 2016a. Evaluation of the health-risk reduction potential of countermeasures to urban heat islands. *Energy Build.* 114, 27–37. doi:10.1016/j.enbuild.2015.06.038
- Buchin, O., Jänicke, B., Meier, F., Scherer, D., Ziegler, F., 2016b. The role of building models in the evaluation of heat-related risks. *Nat. Hazards Earth Syst. Sci.* 16, 963–976. doi:10.5194/nhess-16-963-2016
- Buttstädt, M., Schneider, C., 2014. Thermal load in a medium-sized European city using the example of Aachen, Germany. *Erdkunde* 68, 71–83. doi:10.3112/erdkunde.2014.02.01
- Cameron, R.W.F., Taylor, J., Emmett, M., 2015. A Hedera green façade – Energy performance and saving under different maritime-temperate, winter weather conditions. *Build. Environ.* 92, 111–121. doi:10.1016/j.buildenv.2015.04.011
- Chen, F., Dudhia, J., 2001. Coupling an Advanced Land Surface-Hydrology Model with the Penn State-NCAR MM5 Modeling System. Part I: Model Implementation and Sensitivity. *Mon. Weather Rev.* 129, 569–585. doi:10.1175/1520-0493(2001)129<0569:CAALSH>2.0.CO;2
- Chen, F., Kusaka, H., Bornstein, R., Ching, J., Grimmond, C.S.B., Grossman-Clarke, S., Loridan, T., Manning, K.W., Martilli, A., Miao, S., Sailor, D., Salamanca, F.P., Taha, H., Tewari, M., Wang, X., Wyszogrodzki, A. a., Zhang, C., 2011. The integrated WRF/urban modelling system: development, evaluation, and applications to urban environmental problems. *Int. J. Climatol.* 31, 273–288. doi:10.1002/joc.2158
- Chen, Q., Li, B., Liu, X., 2013. An experimental evaluation of the living wall system in hot and humid climate. *Energy Build.* 61, 298–307. doi:10.1016/j.enbuild.2013.02.030
- Chen, Y.-C., Lin, T.-P., Matzarakis, A., 2014. Comparison of mean radiant temperature from field experiment and modelling: a case study in Freiburg, Germany. *Theor. Appl. Climatol.* 118, 535–551. doi:10.1007/s00704-013-1081-z
- Ching, J.K.S., 2013. A perspective on urban canopy layer modeling for weather, climate and air quality applications. *Urban Clim.* 3, 13–39. doi:10.1016/j.uclim.2013.02.001
- Cohen, P., Potchter, O., Matzarakis, A., 2012. Daily and seasonal climatic conditions of green urban open spaces in the Mediterranean climate and their impact on human comfort. *Build. Environ.* 51, 285–295. doi:10.1016/j.buildenv.2011.11.020
- Conry, P., Sharma, A., Potosnak, M.J., Leo, L.S., Bensman, E., Hellmann, J.J., Fernando, H.J.S., 2015. Chicago's heat island and climate change: Bridging the scales via dynamical downscaling. *J. Appl. Meteorol. Climatol.* 150312130123006. doi:10.1175/JAMC-D-14-0241.1
- Dasari, H.P., Salgado, R., Perdigao, J., Challa, V.S., 2014. A regional climate simulation study using WRF-ARW model over Europe and evaluation for extreme temperature weather events. *Int. J. Atmos. Sci.* 2014, 22.

doi:<http://dx.doi.org/10.1155/2014/704079>

- Dee, D.P., Uppala, S.M., Simmons, A.J., Berrisford, P., Poli, P., Kobayashi, S., Andrae, U., Balmaseda, M.A., Balsamo, G., Bauer, P., Bechtold, P., Beljaars, A.C.M., van de Berg, L., Bidlot, J., Bormann, N., Delsol, C., Dragani, R., Fuentes, M., Geer, A.J., Haimberger, L., Healy, S.B., Hersbach, H., Hólm, E. V., Isaksen, I., Kållberg, P., Köhler, M., Matricardi, M., McNally, A.P., Monge-Sanz, B.M., Morcrette, J.-J., Park, B.-K., Peubey, C., de Rosnay, P., Tavolato, C., Thépaut, J.-N., Vitart, F., 2011. The ERA-Interim reanalysis: configuration and performance of the data assimilation system. *Q. J. R. Meteorol. Soc.* 137, 553–597. doi:10.1002/qj.828
- Djedjig, R., Bozonnet, E., Belarbi, R., 2013. Experimental study of the urban microclimate mitigation potential of green roofs and green walls in street canyons. *Int. J. Low-Carbon Technol.* 1–11. doi:10.1093/ijlct/ctt019
- Dütemeyer, D., Barlag, A.B., Kuttler, W., Axt-Kittner, U., 2013. Measures against heat stress in the city of Gelsenkirchen, Germany. *DIE ERDE – J. Geogr. Soc. Berlin* 144, 181–201. doi:10.12854/erde-144-14
- EEA, 2010. Corine Land Cover 2006 raster data [WWW Document]. <http://www.eea.europa.eu/data-and-maps/data/corine-land-cover-2006-raster>.
- Endlicher, W., Lanfer, N., 2003. Meso- and micro-climatic aspects of Berlin's urban climate. *DIE ERDE – J. Geogr. Soc. Berlin* 134, 277–293.
- Erell, E., Williamson, T., 2007. Intra-urban differences in canopy layer air temperature at a mid-latitude city. *Int. J. Climatol.* 28, 1243–1255. doi:10.1002/joc.1469
- Eumorfopoulou, E. a., Kontoleon, K.J., 2009. Experimental approach to the contribution of plant-covered walls to the thermal behaviour of building envelopes. *Build. Environ.* 44, 1024–1038. doi:10.1016/j.buildenv.2008.07.004
- Fallmann, J., Emeis, S., Suppan, P., 2014. Mitigation of urban heat stress – a modelling case study for the area of Stuttgart. *DIE ERDE – J. Geogr. Soc. Berlin* 144, 202–216. doi:10.12854/erde-144-15
- Fallmann, J., Wagner, S., Emeis, S., 2015. High resolution climate projections to assess the future vulnerability of European urban areas to climatological extreme events. *Theor. Appl. Climatol.* 1–17. doi:10.1007/s00704-015-1658-9
- Fenner, D., Meier, F., Scherer, D., Polze, A., 2014. Spatial and temporal air temperature variability in Berlin, Germany, during the years 2001–2010. *Urban Clim.* 10, 308–331. doi:10.1016/j.uclim.2014.02.004
- Flagg, D.D., Taylor, P. a., 2011. Sensitivity of mesoscale model urban boundary layer meteorology to the scale of urban representation. *Atmos. Chem. Phys.* 11, 2951–2972. doi:10.5194/acp-11-2951-2011
- Franck, U., Krüger, M., Schwarz, N., Grossmann, K., Röder, S., Schlink, U., 2013. Heat stress in urban areas: Indoor and outdoor temperatures in different urban structure types and subjectively reported well-being during a heat wave in the city of Leipzig. *Meteorol. Zeitschrift* 22, 167–177. doi:10.1127/0941-2948/2013/0384
- Gabriel, K.M.A., Endlicher, W.R., 2011. Urban and rural mortality rates during heat waves in Berlin and Brandenburg, Germany. *Environ. Pollut.* 159,

2044–2050. doi:10.1016/j.envpol.2011.01.016

- García-Herrera, R., Díaz, J., Trigo, R.M., Luterbacher, J., Fischer, E.M., 2010. A review of the European summer heat wave of 2003. *Crit. Rev. Environ. Sci. Technol.* 40, 267–306. doi:10.1080/10643380802238137
- Gosling, S.N., Bryce, E.K., Dixon, P.G., Gabriel, K.M. a, Gosling, E.Y., Hanes, J.M., Hondula, D.M., Liang, L., Bustos Mac Lean, P.A., Muthers, S., Nascimento, S.T., Petralli, M., Vanos, J.K., Wanka, E.R., 2014. A glossary for biometeorology. *Int. J. Biometeorol.* 58, 277–308. doi:10.1007/s00484-013-0729-9
- Grimmond, C.S.B., 2006. Progress in measuring and observing the urban atmosphere. *Theor. Appl. Climatol.* 84, 3–22. doi:10.1007/s00704-005-0140-5
- Grimmond, C.S.B., Blackett, M., Best, M.J., Baik, J.-J., Belcher, S.E., Beringer, J., Bohnenstengel, S.I., Calmet, I., Chen, F., Coutts, A., Dandou, A., Fortuniak, K., Gouvea, M.L., Hamdi, R., Hendry, M., Kanda, M., Kawai, T., Kawamoto, Y., Kondo, H., Krayenhoff, E.S., Lee, S.-H., Loridan, T., Martilli, A., Masson, V., Miao, S., Oleson, K., Ooka, R., Pigeon, G., Porson, A., Ryu, Y.-H., Salamanca, F., Steeneveld, G.J., Tombrou, M., Voogt, J., Young, D.T., Zhang, N., 2011. Initial results from Phase 2 of the international urban energy balance model comparison. *Int. J. Climatol.* 31, 244–272. doi:10.1002/joc.2227
- Grimmond, C.S.B., Blackett, M., Best, M.J., Barlow, J., Baik, J.-J., Belcher, S.E., Bohnenstengel, S.I., Calmet, I., Chen, F., Dandou, A., Fortuniak, K., Gouvea, M.L., Hamdi, R., Hendry, M., Kawai, T., Kawamoto, Y., Kondo, H., Krayenhoff, E.S., Lee, S.-H., Loridan, T., Martilli, A., Masson, V., Miao, S., Oleson, K., Pigeon, G., Porson, A., Ryu, Y.-H., Salamanca, F., Shashua-Bar, L., Steeneveld, G.-J., Tombrou, M., Voogt, J., Young, D., Zhang, N., 2010a. The international urban energy balance models comparison project: first results from phase 1. *J. Appl. Meteorol. Climatol.* 49, 1268–1292. doi:10.1175/2010JAMC2354.1
- Grimmond, C.S.B., Roth, M., Oke, T.R., Au, Y.C., Best, M., Betts, R., Carmichael, G., Cleugh, H., Dabberdt, W., Emmanuel, R., Freitas, E., Fortuniak, K., Hanna, S., Klein, P., Kalkstein, L.S., Liu, C.H., Nickson, A., Pearlmutter, D., Sailor, D., Voogt, J., 2010b. Climate and more sustainable cities: Climate information for improved planning and management of cities (Producers/Capabilities Perspective). *Procedia Environ. Sci.* 1, 247–274. doi:10.1016/j.proenv.2010.09.016
- Grimmond, C.S.B., Souch, C., Hubble, M.D., 1996. Influence of tree cover on summertime surface energy balance fluxes, San Gabriel Valley, Los Angeles. *Clim. Res.* 6, 45–57. doi:10.3354/cr006045
- Gross, G., 2012. Effects of different vegetation on temperature in an urban building environment. Micro-scale numerical experiments. *Meteorol. Zeitschrift* 21, 399–412. doi:10.1127/0941-2948/2012/0363
- Guo, Y., Barnett, A.G., Tong, S., 2013. Spatiotemporal model or time series model for assessing city-wide temperature effects on mortality? *Environ. Res.* 120, 55–62. doi:10.1016/j.envres.2012.09.001
- Guo, Y., Gasparrini, A., Armstrong, B., Li, S., Tobias, A., Lavigne, E., Sousa, M. De, Stagliorio, Z., 2014. Global variation in the effects of ambient temperature

- on mortality: a systematic evaluation. *Epidemiology* 25, 781–789. doi:10.1097/EDE.0000000000000165
- Ha, J., Kim, H., 2013. Changes in the association between summer temperature and mortality in Seoul, South Korea. *Int. J. Biometeorol.* 57, 535–44. doi:10.1007/s00484-012-0580-4
- Hajat, S., Kosatky, T., 2010. Heat-related mortality: a review and exploration of heterogeneity. *J. Epidemiol. Community Health* 64, 753–60. doi:10.1136/jech.2009.087999
- Hoelscher, M.-T., Nehls, T., Jänicke, B., Wessolek, G., 2016. Quantifying cooling effects of facade greening: Shading, transpiration and insulation. *Energy Build.* 114, 283–290. doi:10.1016/j.enbuild.2015.06.047
- Höppe, P., 2002. Different aspects of assessing indoor and outdoor thermal comfort. *Energy Build.* 34, 661–665. doi:10.1016/S0378-7788(02)00017-8
- Höppe, P., 1992. A new procedure to determine the mean radiant temperature outdoors. *Wetter und Leb.* 44, 147–151.
- Höppe, P., Martinac, I., 1998. Indoor climate and air quality. Review of current and future topics in the field of ISB study group 10. *Int. J. Biometeorol.* 42, 1–7.
- Horbert, M., 2000. *Klimatologische Aspekte der Stadt- und Landschaftsplanung. Landschaftsentwicklung und Umweltforschung - Schriftenreihe im Fachbereich Umwelt und Gesellschaft Nr. 113.*
- Hu, L., Brunsell, N.A., Monaghan, A.J., Barlage, M., Wilhelmi, O. V., 2014. How can we use MODIS land surface temperature to validate long-term urban model simulations? *J. Geophys. Res. Atmos.* 119, 3185–3201. doi:10.1002/2013JD021101
- Hunter, A.M., Williams, N.S.G., Rayner, J.P., Aye, L., Hes, D., Livesley, S.J., 2014. Quantifying the thermal performance of green façades: A critical review. *Ecol. Eng.* 63, 102–113. doi:10.1016/j.ecoleng.2013.12.021
- Hupfer, P., Chmielewski, F.-M., 1990. *Das Klima von Berlin.* Akademie Verlag.
- Huttner, S., 2012. Further development and application of the 3D microclimate simulation ENVI-met. Dissertation, Johannes Gutenberg-Universität in Mainz.
- Hwang, R.-L., Lin, T.-P., Matzarakis, A., 2011. Seasonal effects of urban street shading on long-term outdoor thermal comfort. *Build. Environ.* 46, 863–870. doi:10.1016/j.buildenv.2010.10.017
- IPCC, 2014. Synthesis Report. Contribution of Working Groups I, II and III to the Fifth Assessment Report of the Intergovernmental Panel on Climate Change.
- Jamei, E., Rajagopalan, P., Seyedmahmoudian, M., Jamei, Y., 2016. Review on the impact of urban geometry and pedestrian level greening on outdoor thermal comfort. *Renew. Sustain. Energy Rev.* 54, 1002–1017. doi:10.1016/j.rser.2015.10.104
- Jendritzky, G., de Dear, R., Havenith, G., 2012. UTCI-why another thermal index? *Int. J. Biometeorol.* 56, 421–8. doi:10.1007/s00484-011-0513-7
- Johansson, E., Thorsson, S., Emmanuel, R., Krüger, E., 2014. Instruments and methods in outdoor thermal comfort studies – The need for standardization. *Urban Clim.* 10, 346–366.

doi:10.1016/j.uclim.2013.12.002

- Johansson, L., Onomura, S., Lindberg, F., Seaquist, J., 2016. Towards the modelling of pedestrian wind speed using high-resolution digital surface models and statistical methods. *Theor. Appl. Climatol.* 124, 189–203. doi:10.1007/s00704-015-1405-2
- Kántor, N., Unger, J., 2011. The most problematic variable in the course of human-biometeorological comfort assessment - the mean radiant temperature. *Cent. Eur. J. Geosci.* 3, 90–100. doi:10.2478/s13533-011-0010-x
- Keramitsoglou, I., Daglis, I.A., Amiridis, V., Chrysoulakis, N., Ceriola, G., Manunta, P., Maiheu, B., De Ridder, K., Lauwaet, D., Paganini, M., 2012. Evaluation of satellite-derived products for the characterization of the urban thermal environment. *J. Appl. Remote Sens.* 6, 061704. doi:10.1117/1.JRS.6.061704
- Ketterer, C., Matzarakis, A., 2015. Comparison of different methods for the assessment of the urban heat island in Stuttgart, Germany. *Int. J. Biometeorol.* 59, 1299–1309. doi:10.1007/s00484-014-0940-3
- Kim, K.R., Yi, C., Lee, J.-S., Meier, F., Jänicke, B., Fehrenbach, U., Scherer, D., 2014. BioCAS: Biometeorological Climate impact Assessment System for building-scale impact assessment of heat-stress related mortality. *DIE ERDE – J. Geogr. Soc. Berlin* 145, 62–79. doi:10.12854/erde-145-6
- Kim, Y., Sartelet, K., Raut, J.-C., Chazette, P., 2013. Evaluation of the weather research and forecast/urban model over greater Paris. *Boundary-Layer Meteorol.* 149, 105–132. doi:10.1007/s10546-013-9838-6
- Köhler, M., 2008. Green facades—a view back and some visions. *Urban Ecosyst.* 11, 423–436. doi:10.1007/s11252-008-0063-x
- Kovats, R.S., Hajat, S., 2008. Heat stress and public health: a critical review. *Annu. Rev. Public Health* 29, 41–55. doi:10.1146/annurev.publhealth.29.020907.090843
- Kratzer, A., 1957. *The climate of cities*. Vieweg & Sohn, Braunschweig.
- Krüger, E.L., Minella, F.O., Matzarakis, A., 2014. Comparison of different methods of estimating the mean radiant temperature in outdoor thermal comfort studies. *Int. J. Biometeorol.* 58, 1727–1737. doi:10.1007/s00484-013-0777-1
- Kusaka, H., Chen, F., Tewari, M., Dudhia, J., Gill, D.O., Duda, M.G., Wang, W., Miya, Y., 2012a. Numerical simulation of urban heat island effect by the WRF model with 4-km Grid increment: An inter-Comparison study between the urban canopy model and slab model. *J. Meteorol. Soc. Japan. Ser. II* 90B, 33–45. doi:10.2151/jmsj.2012-B03
- Kusaka, H., Hara, M., Takane, Y., 2012b. Urban climate projection by the WRF Model at 3-km horizontal grid increment: Dynamical downscaling and predicting heat stress in the 2070's August for Tokyo, Osaka, and Nagoya Metropolis. *J. Meteorol. Soc. Japan. Ser. II* 90B, 47–63. doi:10.2151/jmsj.2012-B04
- Kusaka, H., Kondo, H., Kikegawa, Y., Kimura, F., 2001. A simple single-layer urban canopy model for atmospheric models: Comparison with multi-layer and slab models. *Boundary-Layer Meteorol.* 101, 329–358. doi:10.1023/A:1019207923078



- Kuttler, W., 1999. Human-biometeorologische Bewertung stadtklimatologischer Erkenntnisse für die Planungspraxis. Wissenschaftliche Mitteilungen aus dem Inst. für Meteorol. und dem Inst. für Troposphärenforsch. der Univ. Leipzig 13, 100–117.
- Langner, M., Scherber, K., Endlicher, W.R., 2013. Indoor heat stress: An assessment of human bioclimate using the UTCI in different buildings in Berlin. *DIE ERDE – J. Geogr. Soc. Berlin* 144, 260–273. doi:10.12854/erde-144-18
- Lau, K.K.-L., Ren, C., Ho, J., Ng, E., 2015. Numerical modelling of mean radiant temperature in high-density sub-tropical urban environment. *Energy Build.* 114, 80–86. doi:10.1016/j.enbuild.2015.06.035
- Lee, H., Mayer, H., 2016. Validation of the mean radiant temperature simulated by the RayMan software in urban environments. *Int. J. Biometeorol.* 1–11. doi:10.1007/s00484-016-1166-3
- Li, D., Bou-Zeid, E., 2014. Quality and sensitivity of high-resolution numerical simulation of urban heat islands. *Environ. Res. Lett.* 9, 55001. doi:10.1088/1748-9326/9/5/055001
- Li, D., Bou-Zeid, E., Barlage, M., Chen, F., Smith, J. a., 2013. Development and evaluation of a mosaic approach in the WRF-Noah framework. *J. Geophys. Res. Atmos.* 118, 11918–11935. doi:10.1002/2013JD020657
- Li, D., Sun, T., Liu, M., Yang, L., Wang, L., Gao, Z., 2015. Contrasting responses of urban and rural surface energy budgets to heat waves explain synergies between urban heat islands and heat waves. *Environ. Res. Lett.* 10, 054009. doi:10.1088/1748-9326/10/5/054009
- Liao, J., Wang, T., Wang, X., Xie, M., Jiang, Z., Huang, X., Zhu, J., 2014. Impacts of different urban canopy schemes in WRF/Chem on regional climate and air quality in Yangtze River Delta, China. *Atmos. Res.* 145–146, 226–243. doi:10.1016/j.atmosres.2014.04.005
- Lin, T.-P., Matzarakis, A., Hwang, R.-L., 2010. Shading effect on long-term outdoor thermal comfort. *Build. Environ.* 45, 213–221. doi:10.1016/j.buildenv.2009.06.002
- Lindberg, F., Grimmond, C.S.B., 2011a. The influence of vegetation and building morphology on shadow patterns and mean radiant temperatures in urban areas: model development and evaluation. *Theor. Appl. Climatol.* 105, 311–323. doi:10.1007/s00704-010-0382-8
- Lindberg, F., Grimmond, C.S.B., 2011b. Nature of vegetation and building morphology characteristics across a city: Influence on shadow patterns and mean radiant temperatures in London. *Urban Ecosyst.* 14, 617–634. doi:10.1007/s11252-011-0184-5
- Lindberg, F., Holmer, B., Thorsson, S., 2008. SOLWEIG 1.0 - modelling spatial variations of 3D radiant fluxes and mean radiant temperature in complex urban settings. *Int. J. Biometeorol.* 52, 697–713. doi:10.1007/s00484-008-0162-7
- Lindberg, F., Holmer, B., Thorsson, S., Rayner, D., 2014. Characteristics of the mean radiant temperature in high latitude cities-implications for sensitive climate planning applications. *Int. J. Biometeorol.* 58, 613–27. doi:10.1007/s00484-013-0638-y
- Lindberg, F., Onomura, S., Grimmond, C.S.B., 2016. Influence of ground surface

- characteristics on the mean radiant temperature in urban areas. *Int. J. Biometeorol.* 1–14. doi:10.1007/s00484-016-1135-x
- Martilli, A., 2007. Current research and future challenges in urban mesoscale modelling. *Int. J. Climatol.* 27, 1909–1918. doi:10.1002/joc.1620
- Martilli, A., Clappier, A., Rotach, M.W., 2002. An urban surface exchange parameterisation for mesoscale models. *Boundary-Layer Meteorol.* 104, 261–304. doi:10.1023/A:1016099921195
- Masson, V., 2005. Urban surface modeling and the meso-scale impact of cities. *Theor. Appl. Climatol.* 84, 35–45. doi:10.1007/s00704-005-0142-3
- Matzarakis, A., Rutz, F., Mayer, H., 2010. Modelling radiation fluxes in simple and complex environments: basics of the RayMan model. *Int. J. Biometeorol.* 54, 131–9. doi:10.1007/s00484-009-0261-0
- Matzarakis, A., Rutz, F., Mayer, H., 2007. Modelling radiation fluxes in simple and complex environments - application of the RayMan model. *Int. J. Biometeorol.* 51, 323–34. doi:10.1007/s00484-006-0061-8
- Maussion, F., Scherer, D., Mölg, T., Collier, E., Curio, J., Finkelnburg, R., 2014. Precipitation seasonality and variability over the Tibetan Plateau as resolved by the high Asia reanalysis. *J. Clim.* 27, 1910–1927. doi:10.1175/JCLI-D-13-00282.1
- Mavrogianni, A., Wilkinson, P., Davies, M., Biddulph, P., Oikonomou, E., 2012. Building characteristics as determinants of propensity to high indoor summer temperatures in London dwellings. *Build. Environ.* 55, 117–130. doi:10.1016/j.buildenv.2011.12.003
- Mayer, H., 1989. Workshop „Ideales Stadtklima“ am 26. Oktober 1988 in München. *DMG Mitteilungen* 3/89, 52–54.
- Meehl, G.A., Tebaldi, C., 2004. More intense, more frequent, and longer lasting heat waves in the 21st century. *Science* 305, 994–997. doi:10.1126/science.1098704
- Mills, G., Cleugh, H., Emmanuel, R., Endlicher, W., Ereil, E., McGranahan, G., Ng, E., Nickson, A., Rosenthal, J., Steemer, K., 2010. Climate information for improved planning and management of mega cities (needs perspective). *Procedia Environ. Sci.* 1, 228–246. doi:10.1016/j.proenv.2010.09.015
- Muller, C.L., Chapman, L., Grimmond, C.S.B., Young, D.T., Cai, X., 2013. Sensors and the city: a review of urban meteorological networks. *Int. J. Climatol.* 33, 1585–1600. doi:10.1002/joc.3678
- Nguyen, J.L., Schwartz, J., Dockery, D.W., 2014. The relationship between indoor and outdoor temperature, apparent temperature, relative humidity, and absolute humidity. *Indoor Air* 24, 103–112. doi:10.1111/ina.12052
- Norton, B. a., Coutts, A.M., Livesley, S.J., Harris, R.J., Hunter, A.M., Williams, N.S.G., 2015. Planning for cooler cities: A framework to prioritise green infrastructure to mitigate high temperatures in urban landscapes. *Landsc. Urban Plan.* 134, 127–138. doi:10.1016/j.landurbplan.2014.10.018
- Oikonomou, E., Davies, M., Mavrogianni, A., Biddulph, P., Wilkinson, P., Kolokotroni, M., 2012. Modelling the relative importance of the urban heat island and the thermal quality of dwellings for overheating in London. *Build. Environ.* 57, 223–238.

doi:10.1016/j.buildenv.2012.04.002

- Oke, T.R., 1987. *Boundary layer climates*, 2nd ed. Cambridge University Press, London.
- Onomura, S., Grimmond, C.S.B., Lindberg, F., Holmer, B., Thorsson, S., 2015. Meteorological forcing data for urban outdoor thermal comfort models from a coupled convective boundary layer and surface energy balance scheme. *Urban Clim.* 11, 1–23. doi:10.1016/j.uclim.2014.11.001
- Pérez, G., Rincón, L., Vila, A., González, J.M., Cabeza, L.F., 2011. Green vertical systems for buildings as passive systems for energy savings. *Appl. Energy* 88, 4854–4859. doi:10.1016/j.apenergy.2011.06.032
- Perkins, S.E., 2015. A review on the scientific understanding of heatwaves—Their measurement, driving mechanisms, and changes at the global scale. *Atmos. Res.* 164–165, 242–267. doi:10.1016/j.atmosres.2015.05.014
- Potchter, O., Cohen, P., Bitan, A., 2006. Climatic behavior of various urban parks during hot and humid summer in the Mediterranean city of Tel Aviv, Israel. *Int. J. C* 26, 1695–1711. doi:10.1002/joc.1330
- Prein, A.F., Langhans, W., Fossier, G., Ferrone, A., Ban, N., Goergen, K., Keller, M., Tölle, M., Gutjahr, O., Feser, F., Brisson, E., Kollet, S., Schmidli, J., van Lipzig, N.P.M., Leung, R., 2015. A review on regional convection-permitting climate modeling: Demonstrations, prospects, and challenges. *Rev. Geophys.* 53, 323–361. doi:10.1002/2014RG000475
- Provençal, S., Bergeron, O., Leduc, R., Barrette, N., 2016. Thermal comfort in Quebec City, Canada: sensitivity analysis of the UTCI and other popular thermal comfort indices in a mid-latitude continental city. *Int. J. Biometeorol.* 60, 591–603. doi:10.1007/s00484-015-1054-2
- Prusa, J.M., Smolarkiewicz, P.K., Wyszogrodzki, A. a., 2008. EULAG, a computational model for multiscale flows. *Comput. Fluids* 37, 1193–1207. doi:10.1016/j.jcp.2012.11.008
- Ramamurthy, P., Li, D., Bou-Zeid, E., 2015. High-resolution simulation of heatwave events in New York City. *Theor. Appl. Climatol.* 1–14. doi:10.1007/s00704-015-1703-8
- Rockel, B., Will, A., Hense, A., 2008. The Regional Climate Model COSMO-CLM (CCLM). *Meteorol. Zeitschrift* 17, 347–348. doi:10.1127/0941-2948/2008/0309
- Rummukainen, M., 2010. State-of-the-art with regional climate models. *Wiley Interdiscip. Rev. Chang.* 1, 82–96. doi:10.1002/wcc.008
- Russo, S., Dosio, A., Barbosa, P., Vogt, J., 2014. Extreme heat waves in present climate and their projection in a warming Mediterranean region. *J. Geophys. Res. Atmos.* 16, 2014. doi:10.1002/2014JD022098
- Salamanca, F., Martilli, A., Yagüe, C., 2012. A numerical study of the urban heat island over Madrid during the DESIREX (2008) campaign with WRF and an evaluation of simple mitigation strategies. *Int. J. Climatol.* 32, 2372–2386. doi:10.1002/joc.3398
- Santamouris, M., 2015. Analyzing the heat island magnitude and characteristics in one hundred Asian and Australian cities and regions. *Sci. Total Environ.* 512–513, 582–598. doi:10.1016/j.scitotenv.2015.01.060
- Schaeffer, L., de Crouy-Chanel, P., Wagner, V., Desplat, J., Pascal, M., 2016. How

- to estimate exposure when studying the temperature-mortality relationship? A case study of the Paris area. *Int. J. Biometeorol.* 60, 73–83. doi:10.1007/s00484-015-1006-x
- Schatz, J., Kucharik, C.J., 2015. Urban climate effects on extreme temperatures in Madison, Wisconsin, USA. *Environ. Res. Lett.* 10, 094024. doi:10.1088/1748-9326/10/9/094024
- Scherber, K., Langner, M., Endlicher, W., 2014. Spatial analysis of hospital admissions for respiratory diseases during summer months in Berlin taking bioclimatic and socio-economic aspects into account. *DIE ERDE – J. Geogr. Soc. Berlin* 144, 217–237. doi:10.12854/erde-144-16
- Scherer, D., Fehrenbach, U., Lakes, T., Lauf, S., Meier, F., Schuster, C., 2013. Quantification of heat-stress related mortality hazard, vulnerability and risk in Berlin, Germany. *DIE ERDE – J. Geogr. Soc. Berlin* 144, 238–259. doi:10.12854/erde-144-17
- Schlünzen, K.H., Sokhi, R.S., 2008. Overview of tools and methods for meteorological and air pollution mesoscale model evaluation and user training. WMO Jt. Rep. COST Action 728 GURME.
- Schoetter, R., Grawe, D., Hoffmann, P., Kirschner, P., Grätz, A., Schlünzen, K.H., 2013. Impact of local adaptation measures and regional climate change on perceived temperature. *Meteorol. Zeitschrift* 22, 117–130. doi:10.1127/0941-2948/2013/0381
- Schubert, S., Grossman-Clarke, S., 2014. Evaluation of the coupled COSMO-CLM/DCEP model with observations from BUBBLE. *Q. J. R. Meteorol. Soc.* 140, 2465–2483. doi:10.1002/qj.2311
- Schubert, S., Grossman-Clarke, S., 2013. The Influence of green areas and roof albedos on air temperatures during extreme heat events in Berlin, Germany. *Meteorol. Zeitschrift* 22, 131–143. doi:10.1127/0941-2948/2013/0393
- Schubert, S., Grossman-Clarke, S., Martilli, A., 2012. A double-canyon radiation scheme for multi-layer urban canopy models. *Boundary-Layer Meteorol.* 145, 439–468. doi:10.1007/s10546-012-9728-3
- Schuster, C., Burkart, K., Lakes, T., 2014. Heat mortality in Berlin – Spatial variability at the neighborhood scale. *Urban Clim.* 10, 134–147. doi:10.1016/j.uclim.2014.10.008
- SenStadt, 2015. EFRE Projekt 027 Stadtklima Abschlussbericht. Berlin.
- Shaffer, S.R., Chow, W.T.L., Georgescu, M., Hyde, P., Jenerette, G.D., Mahalov, A., Moustauoui, A., Ruddell, B.L., 2014. Multiscale modeling and evaluation of urban surface energy balance in the Phoenix metropolitan area. *J. Appl. Meteorol. Climatol.* 54, 322–338. doi:10.1175/JAMC-D-14-0051.1
- Shashua-Bar, L., Tsiros, I.X., Hoffman, M., 2012. Passive cooling design options to ameliorate thermal comfort in urban streets of a Mediterranean climate (Athens) under hot summer conditions. *Build. Environ.* 57, 110–119. doi:10.1016/j.buildenv.2012.04.019
- Skamarock, W.C., Klemp, J.B., 2008. A time-split nonhydrostatic atmospheric model for weather research and forecasting applications. *J. Comput. Phys.* 227, 3465–3485. doi:10.1016/j.jcp.2007.01.037
- Skoulika, F., Santamouris, M., Kolokotsa, D., Boemi, N., 2014. On the thermal characteristics and the mitigation potential of a medium size urban park

- in Athens, Greece. *Landsc. Urban Plan.* 123, 73–86. doi:10.1016/j.landurbplan.2013.11.002
- Souch, C., Grimmond, S., 2006. Applied climatology: urban climate. *Prog. Phys. Geogr.* 30, 270–279. doi:10.1191/0309133306pp484pr
- Stewart, I.D., Oke, T.R., 2012. Local climate zones for urban temperature studies. *Bull. Am. Meteorol. Soc.* 93, 1879–1900. doi:10.1175/BAMS-D-11-00019.1
- Tan, C.L., Wong, N.H., Jusuf, S.K., 2014. Effects of vertical greenery on mean radiant temperature in the tropical urban environment. *Landsc. Urban Plan.* 127, 52–64. doi:10.1016/j.landurbplan.2014.04.005
- Tewari, M., Kusaka, H., Chen, F., Coirier, W.J., Kim, S., Wyszogrodzki, A. a., Warner, T.T., 2010. Impact of coupling a microscale computational fluid dynamics model with a mesoscale model on urban scale contaminant transport and dispersion. *Atmos. Res.* 96, 656–664. doi:10.1016/j.atmosres.2010.01.006
- Thorsson, S., Lindberg, F., Björklund, J., Holmer, B., Rayner, D., 2011. Potential changes in outdoor thermal comfort conditions in Gothenburg, Sweden due to climate change: the influence of urban geometry. *Int. J. Climatol.* 31, 324–335. doi:10.1002/joc.2231
- Thorsson, S., Lindberg, F., Eliasson, I., Holmer, B., 2007. Different methods for estimating the mean radiant temperature in an outdoor urban setting. *Int. J. Climatol.* 27, 1983–1993. doi:10.1002/joc
- Thorsson, S., Rocklöv, J., Konarska, J., Lindberg, F., Holmer, B., Dousset, B., Rayner, D., 2014. Mean radiant temperature – A predictor of heat related mortality. *Urban Clim.* 10, 332–345. doi:10.1016/j.uclim.2014.01.004
- Tomlinson, C.J., Chapman, L., Thornes, J.E., Baker, C., 2011. Remote sensing land surface temperature for meteorology and climatology: A review. *Meteorol. Appl.* 18, 296–306. doi:10.1002/met.287
- Trusilova, K., Früh, B., Brienens, S., Walter, A., Masson, V., Pigeon, G., Becker, P., 2013. Implementation of an urban parameterization scheme into the regional climate model COSMO-CLM. *J. Appl. Meteorol. Climatol.* 52, 2296–2311. doi:10.1175/JAMC-D-12-0209.1
- Trusilova, K., Schubert, S., Wouters, H., Früh, B., Demuzere, M., Becker, P., 2015. The urban land use in the COSMO-CLM model: a comparison of three parameterizations for Berlin. *Meteorol. Zeitschrift.* doi:10.1127/metz/2015/0587
- UN, 2014. World urbanization prospects, World urbanization prospects: The 2014 revision, highlights (ST/ESA/SER.A/352). doi:10.4054/DemRes.2005.12.9
- van Hoof, J., 2008. Forty years of Fanger’s model of thermal comfort: comfort for all? *Indoor Air* 18, 182–201. doi:10.1111/j.1600-0668.2007.00516.x
- Voogt, J.A., Oke, T.R., 2003. Thermal remote sensing of urban climates. *Remote Sens. Environ.* 86, 370–384. doi:10.1016/S0034-4257(03)00079-8
- Walikewitz, N., Jänicke, B., Langner, M., Meier, F., Endlicher, W., 2014. The difference between the mean radiant temperature and the air temperature within indoor environments: A case study during summer conditions. *Build. Environ.* 84, 151–161. doi:10.1016/j.buildenv.2014.11.004

- Weihs, P., Staiger, H., Tinz, B., Batchvarova, E., Rieder, H., Vuilleumier, L., Maturilli, M., Jendritzky, G., 2012. The uncertainty of UTCI due to uncertainties in the determination of radiation fluxes derived from measured and observed meteorological data. *Int. J. Biometeorol.* 56, 537–55. doi:10.1007/s00484-011-0416-7
- Wellens, A., Moussiopoulos, N., Sahm, P., 1994. Comparison of a diagnostic model and the MEMO prognostic model to calculate wind fields in Mexico City. *Trans. Ecol. Environ.* 3, 14328–14336.
- White-Newsome, J.L., Sánchez, B.N., Jolliet, O., Zhang, Z., Parker, E.A., Timothy Dvonch, J., O'Neill, M.S., 2012. Climate change and health: Indoor heat exposure in vulnerable populations. *Environ. Res.* 112, 20–27. doi:10.1016/j.envres.2011.10.008
- WHO, 2015. Heatwaves and health: Guidance on warning-system development. WMO-No. 1142.
- Wienert, U., Kuttler, W., 2005. The dependence of the urban heat island intensity on latitude - A statistical approach. *Meteorol. Zeitschrift* 14, 677–686. doi:10.1127/0941-2948/2005/0069
- WMO, 2008. Guide to meteorological instruments and methods of observation. WMO-No. 8.
- Wong, N.H., Kwang Tan, A.Y., Chen, Y., Sekar, K., Tan, P.Y., Chan, D., Chiang, K., Wong, N.C., 2010. Thermal evaluation of vertical greenery systems for building walls. *Build. Environ.* 45, 663–672. doi:10.1016/j.buildenv.2009.08.005
- Wright, A., Young, A., Natarajan, S., 2005. Dwelling temperatures and comfort during the August 2003 heat wave. *Build. Serv. Eng. Res. Technol.* 26, 285–300. doi:10.1191/0143624405bt136oa
- Yang, F., Lau, S.S.Y., Qian, F., 2011. Thermal comfort effects of urban design strategies in high-rise urban environments in a sub-tropical climate. *Archit. Sci. Rev.* 54, 285–304. doi:10.1080/00038628.2011.613646
- Yi, C., Kim, K.R., An, S.M., Choi, Y.-J., Holtmann, A., Jänicke, B., Fehrenbach, U., Scherer, D., 2015. Estimating spatial patterns of air temperature at building-resolving spatial resolution in Seoul, Korea. *Int. J. Climatol.* 36, 533–549. doi:10.1002/joc.4363
- Yu, C., Hien, W.N., 2006. Thermal benefits of city parks. *Energy Build.* 38, 105–120. doi:10.1016/j.enbuild.2005.04.003
- Zhang, D.-L., Zheng, W.-Z., 2004. Diurnal cycles of surface winds and temperatures as simulated by five boundary layer parameterizations. *J. Appl. Meteorol.* 43, 157–169. doi:10.1175/1520-0450(2004)043<0157:DCOSWA>2.0.CO;2
- Zhao, L., Lee, X., Smith, R.B., Oleson, K., 2014. Strong contributions of local background climate to urban heat islands. *Nature* 511, 216–219. doi:10.1038/nature13462

## Abbreviations

BEP	Building Effect Parametrization
BOU	Bougeault-Lacarrère (planetary boundary layer) scheme
CCLM	CONsortium for Small-scale MOdeling (COSMO)-CLM Model
CER	Central Europe Refined analysis
CET	Central European Time (UTC+1)
CFD	Computational Fluid Dynamics
DCEP	Double-Canyon Effect Parametrization scheme
DFG	Deutsche Forschungsgemeinschaft
DWD	Deutscher Wetterdienst
EEA	European Environment Agency
ENVI-met	ENVIronmental METeorology (model)
IPCC	Intergovernmental Panel on Climate Change
LSM	Land Surface Model
<i>MD</i>	Mean Deviation
NWP	Numerical Weather Prediction (model)
RayMan	Radiation on the human body (model)
<i>RMSD</i>	Root Mean Square Deviation
SenStadt	Senatsverwaltung für Stadtentwicklung und Umwelt Berlin
SLUCM	Single-Layer Urban Canopy Model
SOLWEIG	Solar and Long Wave Environmental Irradiance Geometry
<i>T<sub>2</sub></i>	Air temperature at 2 m (°C)
<i>T<sub>a</sub></i>	Air temperature at other heights than 2 m (°C)
<i>T<sub>mrt</sub></i>	Mean radiant temperature (°C)
<i>T<sub>s</sub></i>	Surface temperature (°C)
TUB	Technische Universität Berlin
UCaHS	Urban Climate and Heat stress (DFG Research Unit 1736)
UCM	Urban Canopy Model
UCON	Urban Climate Observation Network
UHI	Urban heat island
UN	United Nations
UTC	Coordinated Universal Time
<i>UTCI</i>	Universal Thermal Climate Index
WHO	World Health Organization
WMO	World Meteorological Organization
WRF	Weather Research and Forecasting Model





## Appendix



## Paper I

# Evaluating the effects of façade greening on human bioclimate in a complex urban environment

Jänicke, B., Meier, F., Hoelscher, M., Scherer, D. (2015): *Evaluating the effects of façade Greening on human bioclimate in a complex urban environment*. Advances in Meteorology, Article ID 747259.  
<http://dx.doi.org/10.1155/2015/747259>

**Status:** Published (since 19 December 2014)

**Copyright:** (CC), 2015, Authors, Creative Commons Attribution 3.0 License

### Own contributions:

- Refining the research ideas and research design
- Search, review, and summary of literature
- Calculation of statistical metrics, setting up the micro-scale simulations, evaluation of models
- $T_{mrt}$  and radiation measurements
- Performing the analyses
- Interpretation of statistical analyses
- Creating graphics and tables
- Writing the manuscript, visualising results, and drafting



## Research Article

# Evaluating the Effects of Façade Greening on Human Bioclimate in a Complex Urban Environment

Britta Jänicke,<sup>1</sup> Fred Meier,<sup>1</sup> Marie-Therese Hoelscher,<sup>2</sup> and Dieter Scherer<sup>1</sup>

<sup>1</sup>Chair of Climatology, Department of Ecology, Berlin Institute of Technology, Rothenburgstraße 12, 12165 Berlin, Germany

<sup>2</sup>Chair of Soil Conservation, Department of Ecology, Berlin Institute of Technology, Ernst-Reuter-Platz 1, 10587 Berlin, Germany

Correspondence should be addressed to Britta Jänicke; britta.jaenicke@tu-berlin.de

Received 26 September 2014; Revised 19 December 2014; Accepted 19 December 2014

Academic Editor: Tzu-Ping Lin

Copyright © Britta Jänicke et al. This is an open access article distributed under the Creative Commons Attribution License, which permits unrestricted use, distribution, and reproduction in any medium, provided the original work is properly cited.

The evaluation of the effectiveness of countermeasures for a reduction of urban heat stress, such as façade greening, is challenging due to lacking transferability of results from one location to another. Furthermore, complex variables such as the mean radiant temperature ( $T_{\text{mrt}}$ ) are necessary to assess outdoor human bioclimate. We observed  $T_{\text{mrt}}$  in front of a building façade in Berlin, Germany, which is half-greened while the other part is bare.  $T_{\text{mrt}}$  was reduced (mean 2 K) in front of the greened compared to the bare façade. To overcome observational shortcomings, we applied the microscale models ENVI-met, RayMan, and SOLWEIG. We evaluated these models based on observations. Our results show that  $T_{\text{mrt}}$  (MD = -1.93 K) and downward short-wave radiation (MD = 14.39 W/m<sup>2</sup>) were sufficiently simulated in contrast to upward short-wave and long-wave radiation. Finally, we compare the simulated reduction of  $T_{\text{mrt}}$  with the observed one in front of the façade greening, showing that the models were not able to simulate the effects of façade greening with the applied settings. Our results reveal that façade greening contributes only slightly to a reduction of heat stress in front of building façades.

## 1. Introduction

Heat stress risk in cities threatens human health [1] and effective countermeasures are not clearly identified. Even though many measures to reduce outdoor urban heat stress are proposed from various disciplines and at different spatial scales [2], their effectiveness is still disputed. Assessing the effectiveness of countermeasures is challenging for many reasons. For example, the transferability of results from one location to another is limited due to the complexity of the urban system and various climates [3]. Moreover, the impact of a countermeasure on outdoor human bioclimate cannot be described sufficiently by simple climate elements, such as surface or air temperature. The mean radiant temperature ( $T_{\text{mrt}}$ ) is an important variable for the assessment of human bioclimate in urban environments because it includes long-wave and short-wave radiation that reaches the human body [4, 5].

Façade greening is a promising countermeasure to reduce urban heat. It can be attached to a large area in cities [6] and features several cobenefits, such as insulating buildings [7–9]

or serving as habitat for wildlife [6]. The knowledge about the effectiveness of façade greening to reduce outdoor heat stress risks, however, is still incomplete due to limits in transferring of results to other sites [10]. The cooling effects of façade greening regarding surface and air temperature depend on solar irradiance, vegetation properties, and the particular greening system [11–13]. Also, the mechanisms of cooling (e.g., through shadowing or transpiration) vary between different plant species [13]. The effects of façade greening on air temperature were found to be small to negligible [7, 11, 14]. Wall temperatures decreased more strongly [14, 15] as well as the emitted long-wave radiation [16].  $T_{\text{mrt}}$  was reduced by 2 K to 13 K in the tropics [15], but the effects for other locations are unknown. Studies that quantify the influence of façade greening on  $T_{\text{mrt}}$  are rare [15] because so far architecture and engineering disciplines are dominant with a focus on air and surface temperature and its influence on the building [10].

Microclimate models can be applied to expand the knowledge of the effects of façade greening on human bioclimate. Microclimate models, such as ENVI-met, RayMan, or

SOLWEIG, are often used in different disciplines. Particularly over the last few years, the number of studies applying ENVI-met and RayMan has grown rapidly. This is an encouraging trend as it may present an increasing awareness of the topic of human bioclimate in cities and may accelerate the implementation of countermeasures. Nevertheless, the reliability and the uncertainty of the results from studies solely based on simulations may vary appreciably. The deviations between observations and simulations have sparsely been evaluated in a comprehensive way. Thus, the inaccuracies in simulating countermeasures or real case situations are insufficiently known even apart from the special case of façade greening. A comparison of  $T_{\text{mrt}}$  simulated by ENVI-met, RayMan, and SOLWEIG under the same conditions was so far performed by Chen et al. [17]. Other variables, such as short-wave and long-wave radiation, did not undergo an intercomparison [36].

So far the models have not been applied to simulate façade greening and we are not aware of other models that are able to simulate façade greening with regard to outdoor human bioclimate. ENVI-met, RayMan, and SOLWEIG include plants, but specific vegetation types, such as façade greening, are not explicitly declared to be supported. Nevertheless, all of the models should be able to consider some aspects of façade greening. RayMan supports different trees with a specific emissivity and albedo as well as changes due to vegetation in the sky view factor (SVF). Thus, albedo and emissivity are modified due to façade greening. SOLWEIG considers vegetation in SVF and reduction of short-wave radiation through transmissivity and sets sunlit leaf temperatures to air temperature. Hence, especially long-wave radiation is expected to alternate in front of a building with façade greening. ENVI-met moreover simulates evapotranspiration. Thus, several effects of façade greening are expected to be reproduced, such as changes in SVF, increased water-vapor fluxes, decreased long-wave radiation, or modified short-wave radiation.

In order to study the effects of façade greening on outdoor human bioclimate, we will firstly use observational data to answer the following question: (1) How large is the reduction of  $T_{\text{mrt}}$  in front of a greened façade compared to a bare one at a study site? Afterwards, we will apply the models ENVI-met, RayMan, and SOLWEIG to the same site in order to (2) evaluate the general performance of the models in simulating  $T_{\text{mrt}}$  and other variables relevant to assess human bioclimate. Thereby, we will contribute to the intercomparison and evaluation of these models in a complex urban environment. Finally, we investigate (3) if the models are able to simulate the observed alteration of  $T_{\text{mrt}}$  in front of the façade greening. In a wider sense the last question addresses if microclimate models are able to represent specific types of urban vegetation such as façade greening.

## 2. Material and Methods

**2.1. Study Site.** In order to observe and simulate the effects of façade greening on  $T_{\text{mrt}}$ , we chose a south-southwest oriented building facade, which is half-covered with *Parthenocissus*

*tricuspidata* while the other part is bare. The façade is located at the campus of the Berlin Institute of Technology, Germany, Hardenbergstraße 38 (52.5112N, 13.3241E, 31–35 m above sea level), in a compact midrise zone (Local Climate Zone 2) [37]. *Parthenocissus tricuspidata* covers the building wall from the bottom to the top (9 m) and nearly half of the building width (11 m). The plants are attaching themselves to the façade without technical climbing support. They rooted in a raised bed on the west oriented side of the building (unsealed area about 6 m<sup>2</sup>). The substrate consists of loamy sand. The plants are irrigated in irregular intervals, but we irrigated the cavity before the measurement campaign to guarantee sufficient water supply. The albedo (calculated from observations on 7, 23, 2013, 1000–1600 Central European Time, CET) is 0.36 in front of the bare building wall, 0.28 in front of the façade greening, and 0.18 for the ground surface. The mean depth of the vegetation layer is  $0.27 \pm 0.08$  m (Table 1). The average leaf area density (LAD) of the façade greening is 1.85 m<sup>2</sup>/m<sup>3</sup> according to our measurements at one vertical transect of 1 m × 9 m. On 8, 19, 2013, we harvested all leaves at this vertical transect and measured the depth of the vegetation layer and the size of all leaves with an area meter (Model 3100, LI-COR, Inc.).

**2.2. Observation.** We measured on 7, 23, 2013 (00–23 CET), in front of the building façade. This day was characterized by clear sky conditions and high air temperatures (Figure 1). The measurements comprised mobile integral radiation measurements as well as wind speed, relative humidity, air temperature, and several other variables to initialize ENVI-met, such as soil and indoor temperature (Figure 2).

The mobile measurements quantified  $T_{\text{mrt}}$  using integral radiation measurements based on three ventilated net radiometers (CNR4, Kipp & Zonen Corp., accuracy  $\pm 10\%$  for daily totals) and the calculation of angular factors with the formula by Thorsson et al. [4] ((1) and (2)). Equation (1) summarizes the long- and short-wave radiations from the bottom, the top, and the four cardinal points. The variables were weighted according to the angular factors in order to estimate the shape of a standing person. Afterward  $T_{\text{mrt}}$  was calculated from mean radiant flux density ( $S_{\text{str}}$ ) with the Stefan-Boltzmann law (2). The net radiometers were oriented along the façade, which means towards north-northeast (NNE) and not towards the main cardinal points:

$$S_{\text{str}} = \alpha_k \int_{i=1}^6 K_i F_i + \epsilon_p \int_{i=1}^6 L_i F_i, \quad (1)$$

$$T_{\text{mrt}} = \sqrt[4]{\frac{S_{\text{str}}}{(\epsilon_p \sigma)}} - 273.15, \quad (2)$$

where  $F_i$  = angular factors for weighting the radiation fluxes (0.06 for up- and downward and 0.22 for the cardinal points),  $K_i$  = short-wave radiation (W/m<sup>2</sup>),  $L_i$  = long-wave radiation (W/m<sup>2</sup>),  $\alpha_k$  = absorption coefficient of short-wave radiation (0.07),  $\epsilon_p$  = the emissivity of the human body (0.97), and  $\sigma$  = the Stefan-Boltzmann constant ( $5.67 \cdot 10^{-8}$  W/m<sup>2</sup> K<sup>-4</sup>).

TABLE 1: Leaf area density (LAD) and depth of the façade greening based on a vertical transect of (1 m × 9 m).

Height (m)	0-1	1-2	2-3	3-4	4-5	5-6	6-7	7-8	8-9	Mean
LAD (m <sup>2</sup> /m <sup>3</sup> )	1.91	2.52	2.02	1.90	1.88	1.81	1.77	1.51	1.32	<b>1.85</b>
Depth (m)	0.34	0.36	0.30	0.26	0.30	0.34	0.22	0.18	0.13	<b>0.27</b>

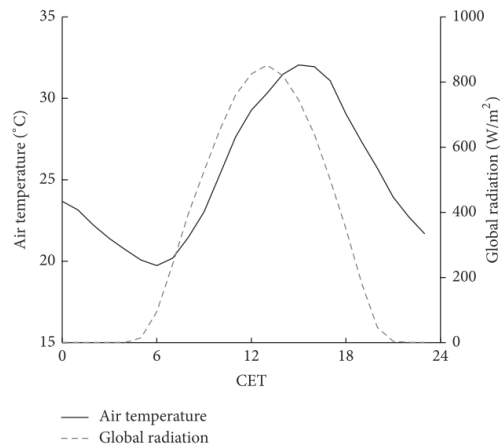


FIGURE 1: Air temperature in front of the façade and global radiation during the measurement campaign (7, 23, 2013).

The mobile station also included a ventilated temperature and relative humidity sensor (CS215, Campbell Scientific Inc., accuracy  $\pm 0.4^\circ\text{C}$  for  $+5$  to  $+40^\circ\text{C}$  and  $\pm 4\%$  for 0 to 100%). The station was set up at a distance of 1.2 m to the building. The measurement height was 1.1 m. We moved the station every 15 min between the greened and the bare site and aggregated the observed data afterwards from a minutely to an hourly resolution for each site (Figure 2).

Additional measurements especially for initializing ENVI-met comprised soil temperatures at a depth of 0.3 m, 0.2 m, and 0.1 m (analog mercury-thermometers), soil humidity (TDR probes) with a resolution of 10 min, and indoor air temperatures averaged over four rooms (Testo 174H, Testo AG, accuracy  $\pm 0.5^\circ\text{C}$  for  $-20$  to  $+70^\circ\text{C}$ ) with a 5 min resolution. Furthermore, short-wave transmissivity through the leaves was measured at two heights, each with two pyranometers, one behind and the other one in front of the greening (SP 110, Apogee). Mean transmissivity was 0.28. Off-site observations of global radiation and wind speed were carried out above roof level at the department of ecology (52.4572N, 13.3158E) with a distance of about 6 km to the study site.

**2.3. Models and Simulation.** For the same day (7, 23, 2013, 00–23 CET), we applied the microclimate models: ENVI-met Version 3.1 Beta 5, ENVI-met Version 4.0 Preview [18, 38], SOLWEIG 2013a [24, 25], and RayManPro [22, 23].

The façade greening was introduced into the models as a flat plant in front of the building with leaves from ground to top. Furthermore, we specified plant parameters (albedo, transmissivity, LAD, etc.) to represent the façade greening as later described for the different models.

In order to analyze the influence of predefined meteorological data from observations and to compare it to the calculations by the models, we performed seven experiments (Table 2). The current version of ENVI-met 3 (E0a) does not support forcing of air temperature and relative humidity and thus additionally the unreleased version 4.0 Preview was applied (E0 unforced and E1 forced). The new version has already been used in other publications [33, 34, 39]. SOLWEIG and RayMan require predefined values of air temperature and relative humidity. Both models can calculate short-wave downward radiation internally, which is the maximum short-wave downward radiation that can be derived at the specific date and location without clouds. These estimated values are used as global radiation to create experiments (R0 and S0) without measurement data of global radiation.

Building data for the input files was generated from the 3D city model of Berlin, which is available in the CityGML data format (<http://www.citygml.org>). We derived the spatial distribution and the height of vegetation from the Urban and Environmental Information System by the Senate Department for Urban Development and the Environment, Berlin. Terrain is neglected in all simulations because ENVI-met 3 does not support it. Furthermore, we assume its effects to be negligible due to the flat terrain at the study site. Meteorological data for the simulation were derived from on-site observations averaged between the greened and the bare sites in front of the façade for all variables with the exceptions of wind speed, wind direction, and global radiation. To initialize ENVI-met, daily mean values were applied.

**2.3.1. ENVI-met.** ENVI-met is a CFD model for simulating surface-plant-air interactions from micro- to local scale with a focus on urban environments [18, 38, 40]. It requires intensive computational resources of a personal computer as each of the experiments lasted over 10 days. ENVI-met is, in contrast to RayMan and SOLWEIG, able to simulate the physiological processes of vegetation and to describe vegetation not only as a porous obstacle.

The domain in ENVI-met had a spatial resolution of  $1\text{ m} \times 1\text{ m}$  and consisted of  $110 \times 80$  grid points after removing 30 nesting grid points at each border. The domain size in ENVI-met was limited. Thus, the model domain is smaller than in SOLWEIG and RayMan. We used telescoping grids (factor 15%) starting at 2 m to include the highest building (43 m) because vertical grids were limited to 30 layers. In ENVI-met the wind field and turbulent heat flux were simulated as well. Therefore, the model domain needed to be



TABLE 2: Overview of the input parameters and model settings in the seven experiments. “X” represents input of times series of meteorological data.

Input parameter	Name Model	E0a ENVI-met 3	E0 ENVI-met 4	E1	R0 RayMan	R1	S0 SOLWEIG	S1
<i>Meteorological data: initial</i>		Unit						
Wind speed (10 m)	m/s	2.3	2.3	2.3	—	—	—	—
Wind direction (10 m)	deg	57.0	57.0	57.0	—	—	—	—
Potential air temperature (2500 m)	°C	24.85	24.85	24.85	—	—	—	—
Specific humidity (2500 m)	g/kg	8.56	8.56	8.56	—	—	—	—
Relative humidity (2 m)	%	45.8	45.8	—	—	—	—	—
<i>Meteorological data</i>								
Air temperature (1.1 m)	°C	—	—	X	X	X	X	X
Relative humidity (1.1 m)	%	—	—	X	X	X	X	X
Global radiation	W/m <sup>2</sup>	—	—	—	—	X	—	X
<i>Soil data</i>								
Initial soil temperature (0–50 cm)	°C	23.10–25.71	23.10–25.71	23.10–25.71	—	—	—	—
Relative soil humidity (0–50 cm)	%	25.00	25.00	25.00	—	—	—	—
<i>Environmental parameter</i>								
Albedo surroundings	—	—	—	—	0.30	0.30	0.36	0.36
Albedo (wall)	—	0.36	0.36	0.36	—	—	—	—
Albedo (roof)	—	0.20	0.20	0.20	—	—	—	—
Albedo (plant)	—	0.28	0.28	0.28	0.28	0.28	—	—
Transmissivity of vegetation	—	—	—	—	—	—	0.28	0.28
Emissivity (ground)	—	—	—	—	—	—	0.95	0.95
Emissivity (walls)	—	—	—	—	—	—	0.90	0.90
Bowen ratio	—	—	—	—	1.00	1.00	—	—
Solar adjustment factor	—	0.85	0.85	0.85	—	—	—	—



FIGURE 2: Measurement arrangement and study site in Berlin, Germany.

rotated by 30° to avoid unrealistic roughness at the edges of the building walls (Figure 3). With the high resolution vegetation data, we introduced new vegetation classes based on the default plant database of ENVI-met to account for vegetation heights with a resolution of 1 m. The façade greening was also introduced as a new class with the measured LAD values

(Table 1). We interpolated the 9 measured levels to 10 relative height levels to adapt to the structure of ENVI-met’s plant database (see Table 3). According to on-site experiences, soils beneath vegetation were classified as loamy sand, streets as asphalt, areas beneath buildings as pavement, and nonstreet areas as light brick roads.



TABLE 3: Measured leaf area density (LAD) profile of façade greening (bold) and assumed parameter for the plant database in ENVI-met.

Plant	Type	Albedo	Height (m)	Root zone (m)	Leaf area density (LAD) at level										Root area density, all levels
					1	2	3	4	5	6	7	8	9	10	
Trees	Deciduous trees	0.28	6–31	2	0	0	0	0.2	0.7	2.2	2.2	2.0	1.7	0.4	0.1
Façade greening	Deciduous trees	0.28	9	1	<b>1.9</b>	<b>2.5</b>	<b>2.1</b>	<b>1.9</b>	<b>1.9</b>	<b>1.9</b>	<b>1.8</b>	<b>1.7</b>	<b>1.5</b>	<b>1.3</b>	0.1

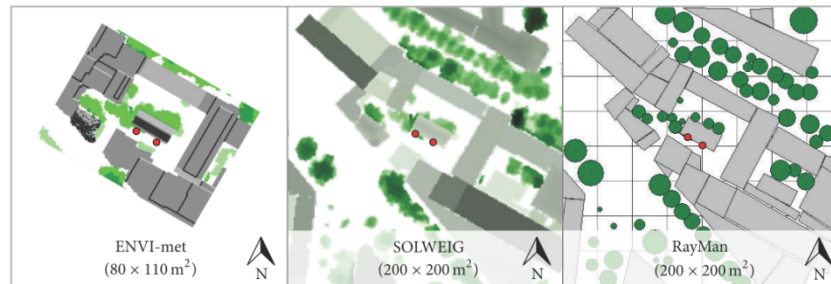


FIGURE 3: Model domains of the different models. In the domain of SOLWEIG, dark colors represent taller buildings and vegetation compared to pale colors. Red circles indicate the greened and the bare site of observation and analyses.

**2.3.2. SOLWEIG.** SOLWEIG simulates radiation fluxes and  $T_{\text{mrt}}$  based on digital surface models [24, 25]. In contrast to ENVI-met and RayMan, SOLWEIG calculates shadow patterns and consequently  $T_{\text{mrt}}$  for the middle of an hour; thus meteorological input was averaged accordingly. Vegetation and building data were also compiled with a resolution of 1 m. SOLWEIG uses trunk zones to calculate shadow patterns of vegetation, which were about 30% of the vegetation height at the study site. The façade greening was represented as a flat plant without a trunk characterized by the observed values of albedo and transmissivity. In order to generate a SOLWEIG run (S0) without measurement data of global radiation, SOLWEIGID was used. SOLWEIGID calculates the maximum global radiation for the geographical location, which SOLWEIG2013a is not able to do.

**2.3.3. RayMan.** Matzarakis et al. [22] developed the model RayMan (RayMan Pro 2.2) to calculate  $T_{\text{mrt}}$  and biometeorological indices in complex environments. The building and vegetation data were created manually with the supplied editor on the basis of the digital surface models. Due to this approach, buildings had a flat roof in RayMan. In contrast to SOLWEIG and ENVI-met, RayMan calculates fluxes only for one point of interest. Thus, two obstacle files were used with different center points. Similar to SOLWEIG, RayMan can calculate global radiation itself. Consequently, we did experiments with calculated (R0) and measured global radiation (R1). The façade greening was represented as series of plants in front of the building with a diameter of 1 m, a trunk length of 0 m, and an albedo of 0.28.

**2.4. Analyses.** The analyses of the simulation results refer to two points in front of the façade in each model domain,

the greened site and the bare site (Figure 3). For the model evaluation (Section 3.2), time series plots are only presented for the greened site, but the statistical analysis includes both sites.

The models that did not calculate a specific climate element (e.g., air temperature) were excluded for the section. Long-wave radiation from RayMan and ENVI-met was calculated from surface temperatures using the Stefan-Boltzmann law (with an emissivity of 0.95).

The selected statistical measures for the model evaluation are a combination of generally recommended ones [41, 42] and the ones mostly found in former studies (e.g., coefficient of determination ( $r^2$ )). Root-mean-square deviation (RMSD), mean deviation (MD), and mean absolute deviation (MAD) were calculated as described by Schlünzen and Sokhi [42]. For all statistical analyses we used IDL 8.2.2 (2007–2012 Exelis Visual Information Solutions, Inc.) and the library “Coyote” (1996–2014 Fanning Software Consulting, Inc.).

### 3. Results

**3.1. Measuring the Effects of Façade Greening on  $T_{\text{mrt}}$ .**  $T_{\text{mrt}}$  decreased by 2.13 K (1000–1600 CET, 7, 23, 2014) in front of the greened façade compared to the bare one (Figure 4). The components for calculating  $T_{\text{mrt}}$  varied slightly between both sites and not only the short-wave radiation reflected and the long-wave radiation emitted from the façade from NNE (Figure 5). Thus, the sums of short-wave and long-wave radiation downward, upward, and from the cardinal points differed between the bare and the greened site (Table 4). Nevertheless, long-wave radiation emitted from the greened site is clearly lower compared to the bare one.

TABLE 4: Sum (00–23 CET) of long- and short-wave radiation at the greened and the bare site up- and downward (up, down) and from the cardinal points (west-northwest (WNW), east-southeast (ESE), south-southwest (SSW), and north-northwest (NNE) (direction from the façades)) on 7, 23, 2013.  $F_i$  is the angular factor used in calculation of mean radiant temperature (0.06 for up- and downward radiation and 0.22 for radiation from the cardinal points).

Direction	Sum of short-wave radiations ( $\text{MJ d}^{-1}$ )				Sum of long-wave radiations ( $\text{MJ d}^{-1}$ )			
	Bare	Greened	$\Delta_{\text{Bare-greened}}$	$\Delta_{\text{Bare-greened}} \times F_i$	Bare	Greened	$\Delta_{\text{Bare-greened}}$	$\Delta_{\text{Bare-greened}} \times F_i$
Down	22.36	20.12	2.24	0.13	36.20	35.88	0.31	0.02
Up	4.35	3.57	0.78	0.05	43.02	42.04	0.99	0.06
WNW	8.67	6.11	2.56	0.56	39.92	39.60	0.33	0.07
ESE	10.93	10.39	0.54	0.12	40.49	39.62	0.87	0.19
SSW	14.27	13.44	0.83	0.18	39.36	38.81	0.55	0.12
NNE	5.03	3.54	1.49	0.33	42.29	39.92	2.37	0.52

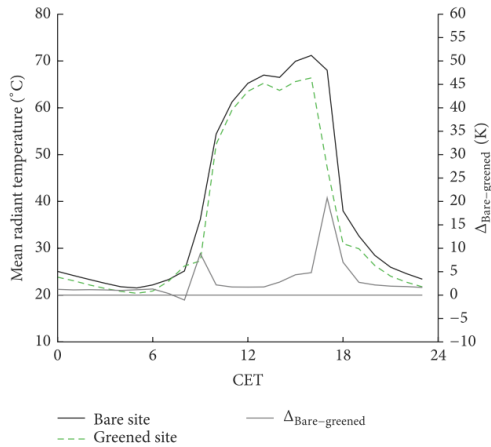


FIGURE 4: Mean radiant temperature observed at the bare and the greened site in front of the building on 7, 23, 2013.

### 3.2. Evaluation of ENVI-met, RayMan, and SOLWEIG

**3.2.1. Mean Radiant Temperature.** The models simulated  $T_{\text{mrt}}$  reasonably well in pattern and amplitude compared to the observations (Figures 6(a) and 6(b)). Experiments with SOLWEIG showed the lowest normalized standard deviation (Figure 6(b)) and high  $r^2$  (Table 5). Despite high absolute errors in RMSD and MAD, experiments with ENVI-met produced the lowest MD (Table 5).

**3.2.2. Long- and Short-Wave Radiation.** Short-wave downward radiation in front of the greened and the bare site was simulated with high  $r^2$  and low MD. RMSD showed larger deviation, especially in experiments with ENVI-met. Larger deviation also occurred in the morning and in the evening, which are the transition times between direct sun and shadow (Figure 7(a), Table 6). Simulated short-wave upward radiation differed much more from observations than short-wave

TABLE 5: Overview of the performance of the experiments (EXP) in simulating mean radiant temperature on 7, 23, 2013, regarding root-mean-square deviation (RMSD), mean deviation (MD), mean absolute deviation (MAD), and coefficient of determination ( $r^2$ ).

EXP	Mean radiant temperature (K)				$r^2$
	RMSD	MD	MAD		
E0a	7.98	-1.26	6.72		0.95
E0	8.30	0.99	6.90		0.94
E1	8.18	1.16	6.87		0.95
R0	7.11	-3.35	5.85		0.90
R1	7.35	-5.53	6.17		0.94
S0	4.63	-2.40	3.40		0.96
S1	4.81	-3.13	3.48		0.96
Mean	6.91	-1.93	5.63		0.94

downward radiation (Figure 7(b), Table 6). ENVI-met and SOLWEIG are able to compute short-wave upward radiation in contrast to RayMan. ENVI-met produced the amplitude more precisely than SOLWEIG, but SOLWEIG simulated the duration of intensive short-wave downward radiation closer to the observations (Figure 7(a)).

Concerning the long-wave downward radiation, SOLWEIG (S0 and S1) was the closest to the observations (Figures 7(c) and 7(d)). Long-wave upward radiation was underestimated during the night in all models. During the day, the differences between the simulations and observations decreased (Figure 7(c)).

**3.2.3. Air Temperature and Specific Humidity.** Simulations with RayMan and SOLWEIG are based on predefined air temperatures and specific humidity; only ENVI-met computes these variables itself. ENVI-met captured the diurnal cycle of air temperature, but specific humidity was reproduced with low deviations from observations only in the forced run (E1) (Figures 8(a) and 8(b)). E1 showed lower deviations than E0a and E0 in simulating air temperatures especially in the early morning (Figure 8(a), Table 7). E1 was the closest to the observation for specific humidity as well (Figure 8(b) and Table 7). The unforced experiments E0a and E0 overestimated specific humidity by 1.5 g/kg (RMSD).

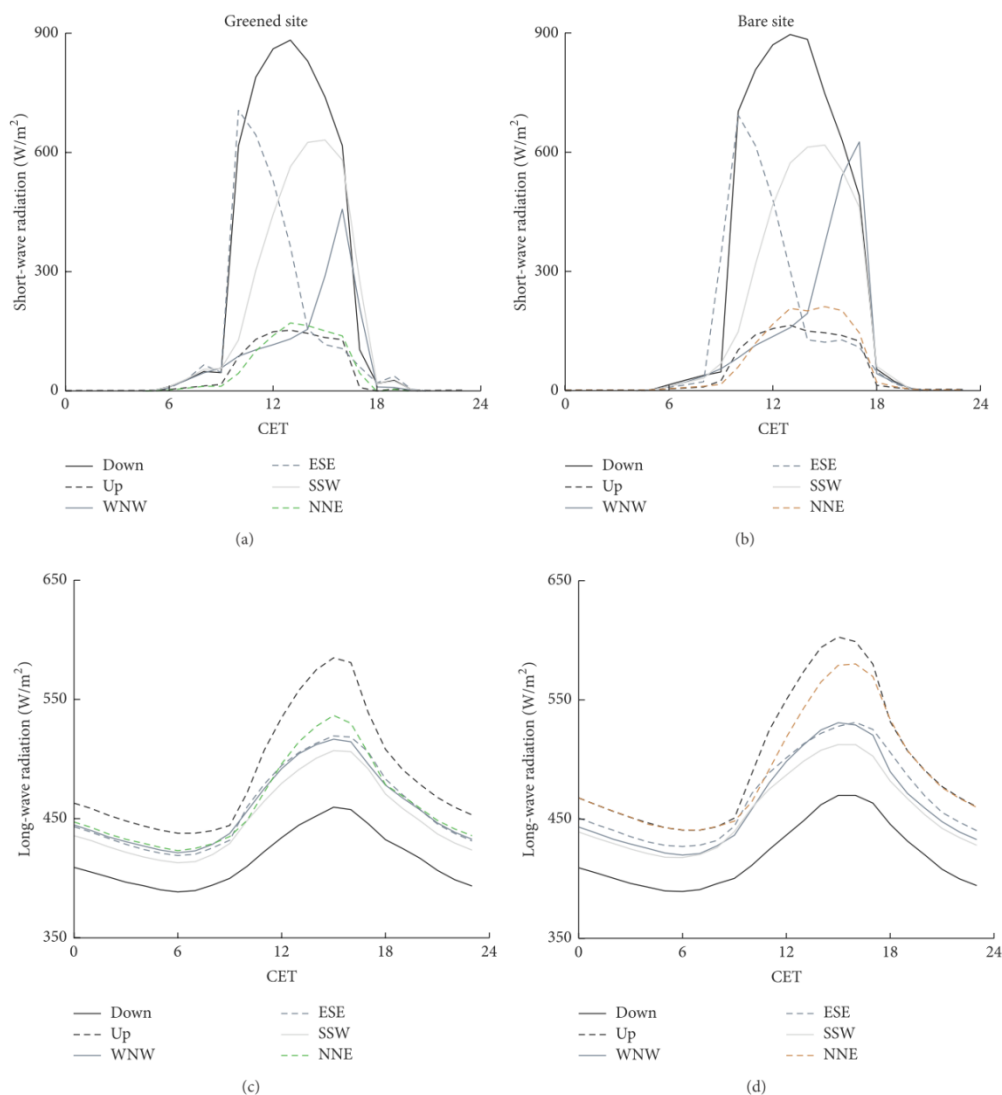


FIGURE 5: Short-wave radiation at the greened (a) and the bare (b) site and long-wave radiation at the greened (c) and the bare (d) site on 7, 23, 2013. All components used to calculate mean radiant temperature are represented, which are up- and downward radiation (up, down) and radiation from the cardinal points (west-northwest (WNW), east-southeast (ESE), south-southwest (SSW), and north-northwest (NNE) (direction from the façades)).

**3.3. Comparison of the Observed and Simulated Effects of Façade Greening.** The observed differences between the bare and the greened site were not well reproduced by the models (Figure 9 and Table 8). The peaks in the transition times were simulated in all models to different extent. The cooling

effect of façade greening, however, was only simulated by S0 and S1, although too small. The experiments with ENVI-met showed a higher  $T_{\text{mrt}}$  in front of the greened site than in front of the bare site, while R0 and R1 produced no differences between the sites (Table 8). Emitted long-wave radiation from

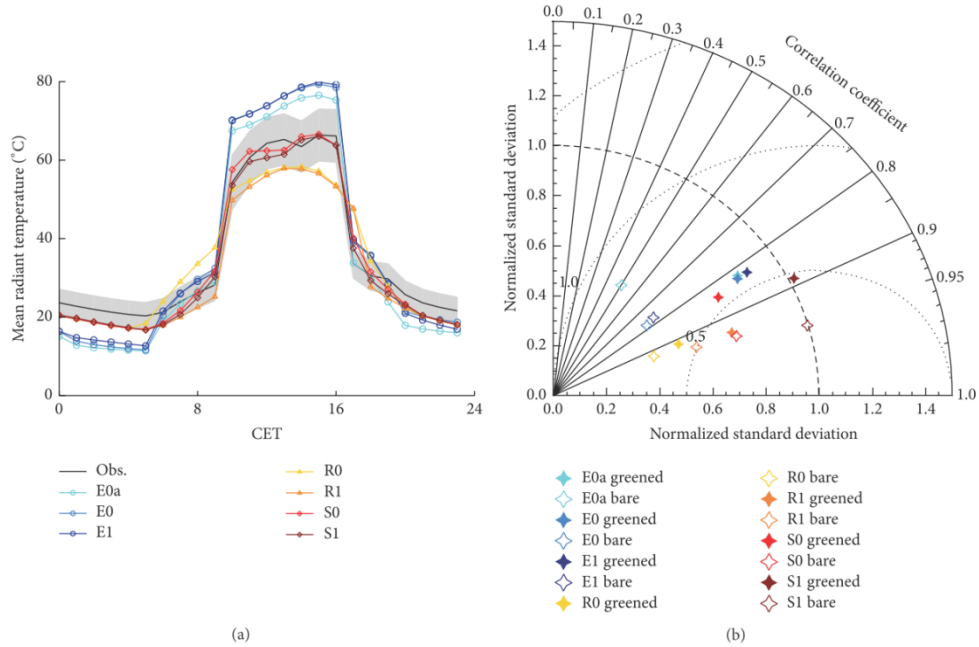


FIGURE 6: Mean radiant temperature on 7, 23, 2013, as observed and simulated (a) at the greened site and (b) Taylor-Diagram for the experiments with ENVI-met 3 (E0a), unforced (E0) and forced ENVI-met 4 (E1), RayMan without (R0) and with global radiation from observation (R1), and SOLWEIG without (S0) and with global radiation from observation (S1). The gray area indicates the accuracy range of the observations.

the greened site was reduced in the experiments with ENVI-met and SOLWEIG (Figure 10(a)), but to a smaller extent (Figure 10(b)).

#### 4. Discussion

**4.1. Measuring the Effects of Façade Greening on  $T_{mrt}$ .** The observed differences in  $T_{mrt}$  of 2 K were distinct but lower than the measurement accuracy of about 4 K. Tan et al. [15] detected larger differences of 2 to 13 K between sites with and without façade greening in a tropical environment. They only detected a reduction of  $T_{mrt}$  when the façade greening was opposed to direct sunlight and not shaded [15]. In addition, the reduction depended on the distance to the façade and was mainly limited to 1 m. Thus, the small observed differences in this study can be partly explained with the larger distance of the measurement to the façade of 1.2 m. Furthermore, the effects of façade greening on air temperature were found to be small (1.5 K, Djedjig et al. [11], 1 K, Berry et al. [16], 0.25 K, Gross [14], and negligible, Pérez et al. [7]). In this case study façade greening was only attached to one façade wall. Hence, the impact on modified long- and short-wave radiation from the greened façade accounts to only 22% in calculating  $T_{mrt}(1)$ . Therefore, the impact on  $T_{mrt}$  was limited, even though emitted long-wave radiation was clearly reduced

in front of the greened façade. The albedo also interferes with  $T_{mrt}$  because the light bare wall with its higher albedo reflected more short-wave radiation than the darker greened façade.

Furthermore, the differences in  $T_{mrt}$  cannot be reduced to the effects of façade greening exclusively. Boundary conditions were different between both sites regarding times of shadowing (Table 4). The opposing building structure is higher in front of the bare site than in front of the greened site (Figure 3), which leads to different shadowing times. In the evenings, at around 1700 CET, the greened façade was completely shadowed while the bare site still received direct sunlight for another half an hour. In the morning, at around 0900 CET, when the sunlight appeared at the façade, some differences existed as well. Furthermore, the opposing building might also have an influence regarding the reflection of short-wave radiation. With respect to short-wave and long-wave radiation, the greened site received less energy from all directions than the bare one. Consequently, the cooling effect of  $T_{mrt}$  was overestimated in the observations. This demonstrates shortcomings in the case study as both sites were not identical regarding the radiation characteristics, which introduces uncertainties when interpreting deviations between the sites. The problem of comparability and usability of case studies to observe the effects of façade greening

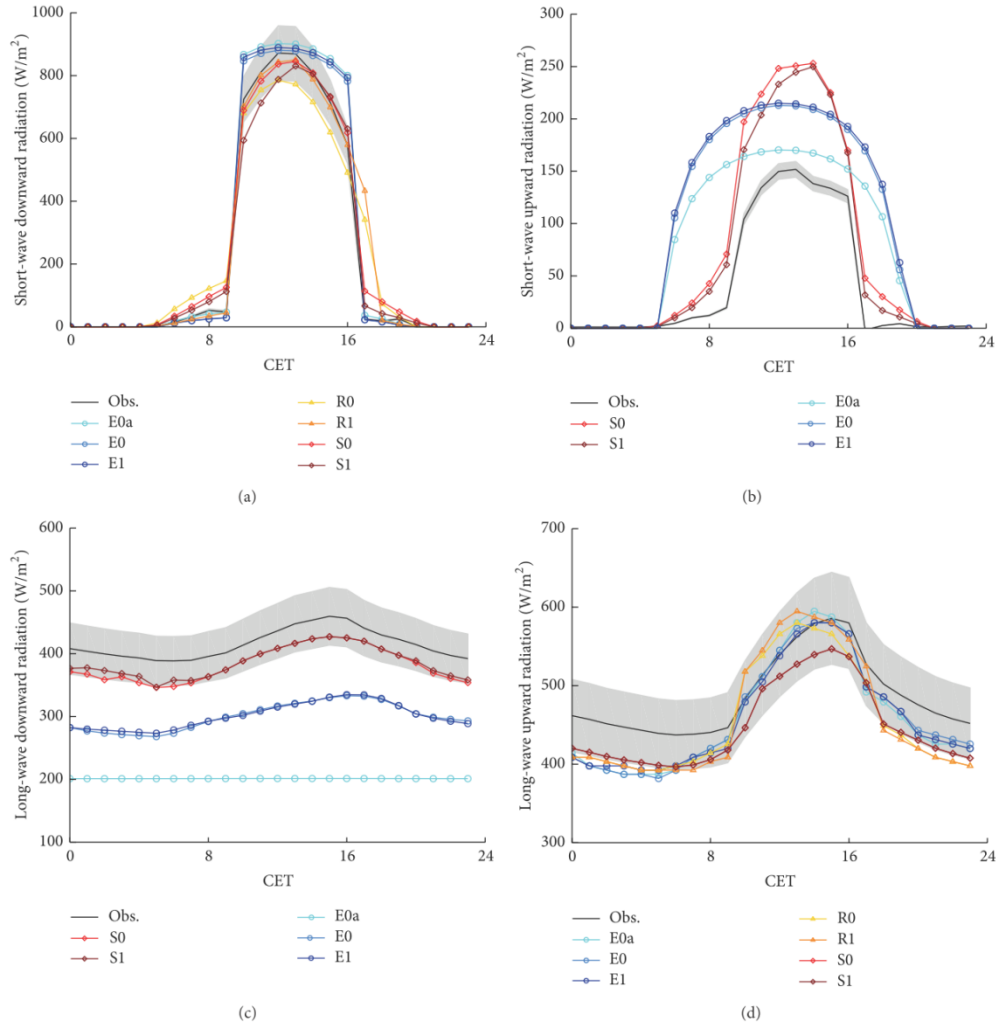


FIGURE 7: Comparison of simulated and observed (a) short-wave downward radiation, (b) short-wave upward radiation, (c) long-wave downward radiation, and (d) long-wave upward radiation on 7, 23, 2013, for the greened site in front of the façade simulated with ENVI-met 3 (E0a), unforced (E0) and forced ENVI-met 4 (E1), RayMan without (R0) and with global radiation from observation (R1), and SOLWEIG without (S0) and with global radiation from observation (S1). The gray areas indicate the accuracy range of the observations.

occurs often as criticized by Hunter et al. [10]. Specifically in complex urban environments optimal study sites are difficult to find. Elaborated assessments (e.g., integral radiation measurements) can reveal such problems in contrast to simple single-variable measurements (e.g., air temperature). Our findings further support the need of reliable model tools in combination with observations to study the effects of façade greening for specific sites and climates.

#### 4.2. Evaluation of ENVI-met, RayMan, and SOLWEIG

**4.2.1. Mean Radiant Temperature.** Simulated  $T_{\text{mrt}}$  deviated about 7 K (mean RMSD) from the observation in this and about MD 2–8 K and 2–15 K RMSD in former studies (Table 9). This uncertainty range is reasonable compared to the average accuracy in measurements of about 4 K. The uncertainty, however, varies largely depending on



TABLE 6: Overview of the performance in simulating downward (a) and upward (b) short-wave and long-wave radiation on 7, 23, 2013. For further explanations refer to Table 5.

(a)				
Short-wave downward radiation ( $\text{W/m}^2$ )				
EXP	RMSD	MD	MAD	$r^2$
E0a	130.46	46.31	50.33	0.91
E0	124.44	36.96	47.12	0.91
E1	128.17	40.46	49.70	0.91
R0	82.33	-6.15	54.06	0.96
R1	70.50	3.19	25.59	0.96
S0	54.65	-3.20	29.36	0.98
S1	65.86	-16.86	34.64	0.97
Mean	93.77	14.39	41.54	0.94
Long-wave downward radiation ( $\text{W/m}^2$ )				
EXP	RMSD	MD	MAD	$r^2$
E0a	209.60	-208.03	208.03	0.01
E0	116.32	-115.83	115.83	0.82
E1	115.27	-114.85	114.85	0.86
R0	—	—	—	—
R1	—	—	—	—
S0	34.89	-34.31	34.31	0.95
S1	31.66	-31.16	31.16	0.95
Mean	101.44	-100.71	100.71	0.71
(b)				
Short-wave upward radiation ( $\text{W/m}^2$ )				
EXP	RMSD	MD	MAD	$r^2$
E0a	61.86	38.34	39.84	0.60
E0	84.76	58.55	60.04	0.60
E1	87.12	60.50	62.00	0.60
R0	—	—	—	—
R1	—	—	—	—
S0	56.55	32.74	35.11	0.95
S1	51.36	27.94	30.57	0.95
Mean	68.33	43.61	45.51	0.74
Long-wave upward radiation ( $\text{W/m}^2$ )				
EXP	RMSD	MD	MAD	$r^2$
E0a	35.19	-26.89	30.96	0.91
E0	33.28	-23.81	27.62	0.92
E1	31.70	-24.88	27.19	0.93
R0	46.23	-35.65	42.69	0.83
R1	46.62	-33.10	43.46	0.86
S0	43.28	-42.09	42.09	0.97
S1	43.30	-42.12	42.12	0.97
Mean	39.94	-32.65	36.59	0.91

the selected model and study design (Table 9). Krüger et al. [20] concluded for RayMan that the uncertainty in calculating  $T_{\text{mrt}}$  depends on different factors, such as morphology, meteorological conditions, and surface properties. For example, correlation coefficients were much higher in this

TABLE 7: Overview of ENVI-met's performance in simulating air temperatures and specific humidity on 7, 23, 2013. For further explanations refer to Table 5.

EXP	RMSD	MD	MAD	$r^2$
Air temperature (K)				
E0a	1.39	0.00	1.13	0.87
E0	1.68	0.06	1.43	0.83
E1	0.96	0.40	0.86	0.98
Mean	1.35	0.16	1.14	0.89
Specific humidity (g/kg)				
E0a	1.44	1.17	1.31	0.10
E0	1.54	1.28	1.40	0.10
E1	0.35	-0.03	0.25	0.91
Mean	1.11	0.81	0.99	0.37

TABLE 8: Mean ( $\pm$ standard deviation), minimum and maximum difference in  $T_{\text{mrt}}$  between bare and greened site in observation (OBS) on 7, 23, 2013 (10–16 CET) and experiments (EXP) with ENVI-met 3 (E0a), ENVI-met 4 (E0 and E1), RayMan (R0 and R1) and SOLWEIG (S0 and S1).

EXP	$T_{\text{mrt}}$ (Bare – Greened) (K)		
	Mean	Minimum	Maximum
OBS	$2.13 \pm 1.81$	0.02	5.02
E0a	$-2.81 \pm 2.25$	-5.89	0.57
E0	$-4.14 \pm 1.41$	-5.56	-1.82
E1	$-4.32 \pm 1.44$	-5.42	-1.88
R0	$0.01 \pm 0.04$	0.00	0.10
R1	$-0.09 \pm 0.07$	-0.20	0.00
S0	$0.96 \pm 0.88$	-0.57	1.94
S1	$1.30 \pm 1.01$	-0.49	2.28

study compared to the investigations of Chen et al. [17]. Such deviations are caused by model specific parameterizations.

Other reasons for deviations in all applied models were discrepancies in building or plant shapes. All experiments produced larger deviations during the transition between shadow and direct radiation, which was also reported by Thorsson et al. [4] and Matzarakis et al. [23]. Such deviations are caused by inaccuracies in building shapes due to the spatial resolution of 1 m or by errors in the basic data of building shapes.

Simulated  $T_{\text{mrt}}$  differed hardly between the computed and predefined meteorological input data. Consequently, calculated global radiation by RayMan and SOLWEIG was sufficient for simulating  $T_{\text{mrt}}$ , and observations of global radiations did not enhance the model performance considerably, at least for this nearly cloud-free day. In ENVI-met, the forcing of air temperature and relative humidity showed only minor effects on simulating  $T_{\text{mrt}}$  as well.

In SOLWEIG, the transmissivity is of importance for calculating  $T_{\text{mrt}}$  beneath vegetation [25]. We applied an averaged value for the whole model domain because we measured transmissivity only at two points of the façade greening and SOLWEIG does not allow any spatial variations. Nevertheless, the range of deviations in this study is similar

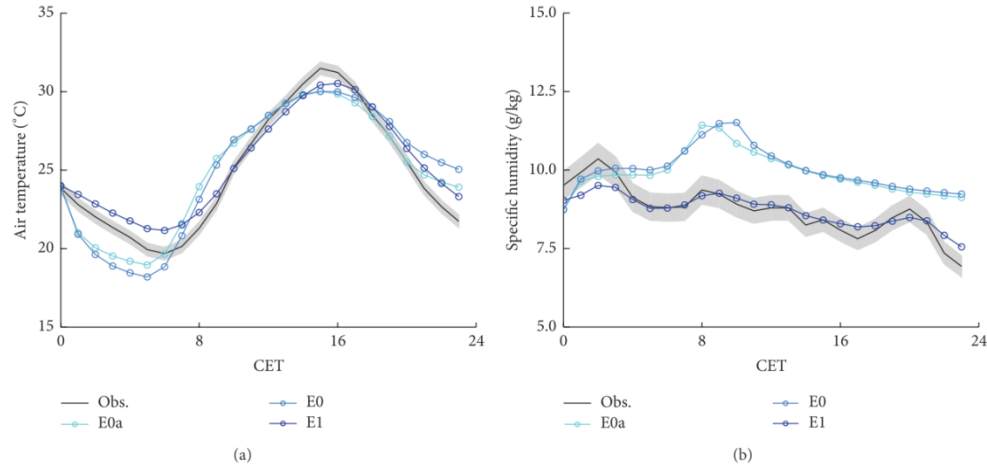


FIGURE 8: Comparison of simulated and observed (a) air temperatures and (b) specific humidity of the experiments with ENVI-met 3 (E0a) and unforced and forced ENVI-met 4 (E0 and E1) on 7, 23, 2013. The gray area indicates the accuracy range of the observations.

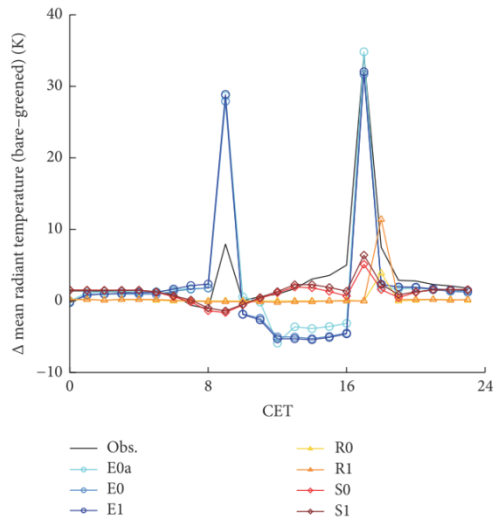


FIGURE 9: Differences between the bare and greened site in observation and simulations (7, 23, 2013) in experiments with ENVI-met 3 (E0a), unforced (E0) and forced ENVI-met 4 (E1), RayMan without (R0) and with global radiation from observation (R1), and SOLWEIG without (S0) and with global radiation from observation (S1).

to findings by Lindberg and Grimmond [25], who detected a RMSD of 3.1 K and a MAD of 2.74 K.

RayMan underestimated  $T_{mrt}$  in this study probably as a consequence of too low short-wave downward radiation. On

TABLE 9: Overview of deviations in mean radiant temperature between simulations and observations in other studies concerning root-mean-square deviation (RMSD), mean deviation (MD), mean absolute deviation (MAD), and coefficient of determination ( $r^2$ ). Standard deviations ( $\pm$ ) are stated, if more than one analysis is performed per study.

Reference	Mean radiant temperature (K)			
	RMSD	MD	MAD	$r^2$
ENVI-met				
[17]	—	—	—	$0.09 \pm 0.1$
[18]	$4.13 \pm 0.4$	—	—	—
E1	8.18	1.16	6.87	0.95
RayMan				
[17]	—	—	—	$0.82 \pm 0.0$
[19]	—	—	—	0.88
[20]	$14.93 \pm 3.5$	—	$12.88 \pm 3.5$	$0.37 \pm 0.2$
[21]	—	—	—	0.85
[4]	—	$8.45 \pm 1.7$	—	—
[22]	—	—	—	0.77
[23]	$1.7 \pm 0.5$	—	—	$0.96 \pm 0.5$
Mean	$8.32 \pm 2.0$	$8.45 \pm 1.7$	$12.88 \pm 3.5$	$0.74 \pm 0.23$
R1	7.35	-5.53	6.17	0.94
SOLWEIG				
[17]	—	—	—	0.32
[24]	4.8	$2.00 \pm 0.3$	—	0.94
[25]	3.1	—	2.74	0.91
Mean	3.95	$2.00 \pm 0.3$	2.74	0.72
S1	4.81	-3.13	3.48	0.96

the contrary, Krüger et al. [20] examined an overestimation for various cloudiness conditions (RMSD 14.93 K, MAD

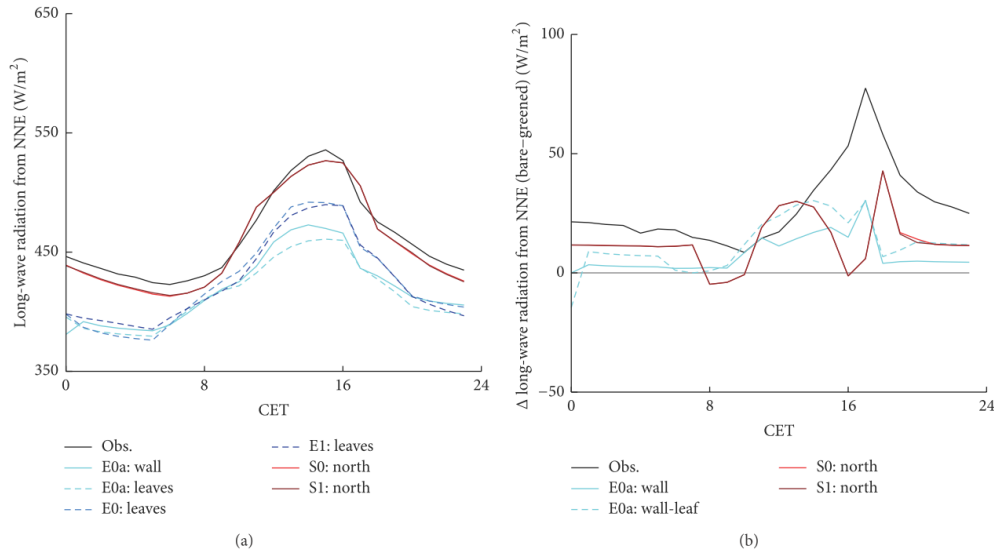


FIGURE 10: Simulated long-wave radiation (a) emitted from the greened site (wall or leaves) and (b) differences between bare and greened façade in simulations and observation for the experiments with ENVI-met 3 (E0a), unforced (E0) and forced ENVI-met 4 (E1), and SOLWEIG without (S0) and with global radiation from observation (S1) (7, 23, 2014).

12.88 K). Additionally, they detected a higher agreement with observations on clear sunny days compared to cloudy ones [20]. During sunny days the accuracy of SVF has a high influence on the uncertainty in simulating  $T_{\text{mrt}}$  [20]. Hence, inaccuracies in the building and vegetation shape had a large impact in this study. The deviation in RayMan varies remarkably in this study and other ones [4, 19, 22] (Table 9).

The uncertainty also differs strongly between different studies with ENVI-met. Ali-Toudert [43] detected an underestimation of  $T_{\text{mrt}}$  during the day and an overestimation during the night. In this study, however, the overestimation of short-wave radiation led to an overestimation of  $T_{\text{mrt}}$ . Yang et al. [44] also detected an overestimation in ENVI-met due to an overestimation of short-wave downward radiation (without statistical values).

Overall, SOLWEIG simulated  $T_{\text{mrt}}$  closest to the observation both in this study and in former ones (Table 9). ENVI-met showed the largest deviations in this study. Furthermore, shortcomings in the evaluation of all three models become visible regarding the amount of studies and in comparability due to different statistics to evaluate models uncertainty.

**4.2.2. Long- and Short-Wave Radiation.** Short-wave downward radiation showed less deviations compared to other radiation components. ENVI-met did not capture the amplitude of global radiation well, partly because only water vapor alternates short-wave radiation [44]. Additionally, Ali-Toudert [43] detected problems in simulating global radiation with ENVI-met and consequently a radiation adjustment

factor was introduced to ENVI-met. Here, short-wave downward radiation in ENVI-met was reduced in advance by 25% to match the amplitude of observations (Table 2). Additional deviations in short-wave downward radiation were produced by the resolution of grid points and by inaccuracies of the input data of buildings and vegetation as discussed for  $T_{\text{mrt}}$ . The small deviation in short-wave downward radiation was a main driver for the sufficient simulation of  $T_{\text{mrt}}$ .

Short-wave upward radiation has less impact on  $T_{\text{mrt}}$  due to the generally smaller energy flux density and low  $F_g$  in the calculation of  $T_{\text{mrt}}$ . Thus, the overestimation in all experiments was less decisive for simulating  $T_{\text{mrt}}$ . ENVI-met overestimated the duration of intense short-wave upward radiation because shadowing effects of the surface are neglected. SOLWEIG captured the duration but overestimated the amplitude of short-wave upward radiation due to a higher albedo. SOLWEIG cannot consider different albedo values of ground surfaces and walls. In future, this problem might be fixed because Lindberg and Grimmond [25] proposed for the next SOLWEIG version the possibility to specify albedo and emissivity spatially.

Long-wave downward radiation was underestimated. The overestimations of short-wave upward radiation and long-wave downward radiation compensate each other and thus the total impact of the inaccuracies on  $T_{\text{mrt}}$  was reduced. ENVI-met 3 (E0a) failed to simulate the diurnal variation of long-wave downward radiation as it uses averaged emissivity values and surface temperatures to calculate it.

Long-wave upward is underestimated during the night because the models do not consider heat storage of



the buildings sufficiently (ENVI-met 4) or not at all (ENVI-met 3, SOLWEIG, and RayMan). Hwang et al. [19] and Lin et al. [21] discussed these shortcomings in ENVI-met 3 and detected the fact that daytime surface temperature was overestimated and nighttime surface temperature was underestimated. ENVI-met 4 should be able to consider these effects in principle but failed in this case study. Possibly, the heat storage was insufficiently parameterized or the spin-up time was too short. Follow-up studies might acquire a more suitable description of heat storage in the walls. During the night, the underestimation of emitted long-wave radiation also led to undervalued  $T_{\text{mrt}}$  in all experiments.

Overall, the individual terms of the radiation balance were, with the exception of short-wave downward radiation, not plausibly simulated by all models. Short-wave downward radiation may also show much higher inaccuracies under cloudy conditions as Krüger et al. [20] detected for RayMan. Furthermore, the lack of model evaluation is more apparent for the individual terms of the radiation balance than for  $T_{\text{mrt}}$  as we detected only three other studies (Table 10), which leads to a high uncertainty regarding the reliability in simulating these variables.

**4.2.3. Air Temperature and Specific Humidity.** ENVI-met reproduced air temperature close to the observations with a RMSD between 0.9 and 1.6 K and MD between 0.0 and 0.4 K in this case study and with a mean RMSD of 1.9 K and MD  $-0.65$  K in former studies (Table 11). During the day, ENVI-met tended to underestimate air temperature but overestimated it during the night [21, 43]. Berkovic et al. [45], who compared simulations and observations qualitatively, found larger differences during the evenings for air temperatures and relative humidity (about 3 K, 15%). Forcing in E1 clearly decreased the uncertainty compared to E0 especially during the day but showed only minor effects on  $T_{\text{mrt}}$ .

The uncertainty in simulating air temperature with ENVI-met varies between different studies remarkably (Table 11). A high agreement was achieved by Skelhorn et al. [35] and Srivani and Hokao [26] after optimization and calibration efforts of different parameters and with a longer spin-up time. Air temperature has been evaluated in several studies. Thus, the simulation seems to be reliable, with an uncertainty of about 1.88 K (RMSD).

Specific humidity was evaluated by Chen et al. [17] with a RMSD of 0.82 g/kg, which is higher than in this study (RMSD = 0.35 g/kg). Forcing (E1) improved the simulation of specific humidity compared to the unforced runs (E0a, E0).

**4.3. Comparison of the Observed and Simulated Effects of Façade Greening.** The applied models were not able to reproduce the observed effects of façade greening. SOLWEIG was the only model that simulated at least a small reduction of  $T_{\text{mrt}}$ . The reductions cannot be related to transpirative effects of the plants because such effects are not considered in SOLWEIG. Thus, the decrease in  $T_{\text{mrt}}$  was produced by radiation changes. Simulated long-wave radiation emitted from the wall was clearly reduced in front of the façade greening (S0, S1).

TABLE 10: Overview of deviations in short-wave downward radiation between simulation and observation in other studies. For further explanation refer to Table 9.

Reference	Short-wave downward radiation ( $\text{W/m}^2$ )			
	RMSD	MD	MAD	$r^2$
ENVI-met				
[26]	—	$-289.15 \pm 8.8$	—	—
E1	128.17	40.46	49.70	0.91
SOLWEIG				
[24]	42.1	—	—	0.97
[25]	43.3	—	—	0.97
Mean	42.2	—	—	0.97
S1	65.86	$-16.86$	34.64	0.97

TABLE 11: Overview of deviations in air temperature and specific humidity between simulation and observation in other studies. For further explanations refer to Table 9.

Reference	Air temperature (K)			
	RMSD	MD	MAD	$r^2$
[27]	$2.79 \pm 0.0$	$0.66 \pm 0.1$	$2.40 \pm 0.1$	$0.70 \pm 0.0$
[28]	$1.45 \pm 0.1$	$-1.29 \pm 0.0$	$1.29 \pm 0.0$	—
[29]	$1.95 \pm 0.4$	—	—	—
[30]	$2.91 \pm 0.9$	$-0.62 \pm 1.3$	$2.45 \pm 0.7$	$0.90 \pm 0.1$
[18]	$1.37 \pm 0.4$	—	—	—
[31]	$1.74 \pm 0.3$	—	—	—
[32]	—	—	—	0.97
[33]	—	—	—	$0.70 \pm 0.1$
[34]	—	$-3.50 \pm 0.5$	—	$0.95 \pm 0.0$
[35]	—	$0.64 \pm 0.3$	—	0.94
[26]	—	$-0.56 \pm 0.9$	—	—
[26]	—	0.10	—	—
[36]	$0.93 \pm 0.1$	—	—	$0.95 \pm 0.0$
Mean	$1.88 \pm 0.4$	$-0.65 \pm 0.53$	$2.05 \pm 0.3$	$0.87 \pm 0.4$
E1	0.96	0.40	0.86	0.98
Specific humidity (g/kg)				
[36]	$0.82 \pm 0.0$	—	—	$0.54 \pm 0.0$
E1	0.35	$-0.03$	0.25	0.91

ENVI-met, which is able to simulate transpiration, reproduced higher  $T_{\text{mrt}}$  in front of the greened site compared to the bare site. Emitted long-wave radiation was reduced in front of the greened façade, but the effect was not permeated to  $T_{\text{mrt}}$ . Increasing the spin-up time in ENVI-met might amplify the generation of effects of façade greening. Specifically in ENVI-met and RayMan, the inabilities in simulating a reduction of  $T_{\text{mrt}}$  in front of the greened façade could not be easily traced back because they do not return all relevant components for  $T_{\text{mrt}}$ .

To conclude, the models showed a limited applicability to façade greening in this study. The small alterations of long- and short-wave radiation due to façade greening were indistinct. Thus, specific types of urban green cannot be included

in these models without further adaptations. Restrictions must be made, however, regarding the complex real-case study site. Moreover, modification of model parameters and settings (e.g., spin-up time) especially for ENVI-met could lead to other results but would go beyond the scope of this study.

## 5. Conclusions

The effect of façade greening on outdoor human bioclimate was limited in this case study because only a small reduction  $T_{mrt}$  in front of the façade greening was detected. Hence, façade greening has only a minor effect in reducing outdoor heat stress. With a façade greening attached to more than one façade in a street canyon or court yard the effect on  $T_{mrt}$ , however, might be enlarged.

The general ability of ENVI-met, RayMan, and SOLWEIG to simulate  $T_{mrt}$  was reasonable as expected for well-established models. Nevertheless, the deviations from observations vary largely between different studies. Additionally, the deviations from observations for other variables (specific humidity, long-wave downward or short-wave upward radiation) were higher and might impede the models' ability in assessing heat stress. When considering the large differences in complexity and computational time, the good performance of the simple SOLWEIG and RayMan models contrary to the elaborate ENVI-met model is encouraging. ENVI-met, however, offers more opportunities for various issues, such as studies of plant-air interactions or effects of changes in albedo of individual surfaces. It also provides more options for tuning and modifications by the users, which were not completely exhausted in this study. Moreover, we recognized a lack of model evaluations regarding the amount of evaluation studies and the considered variables. An explicit statement of model uncertainties for interpreting the results should be included in every study and not only in rare exceptional cases.

The applied models are helpful for assessing human bioclimate in general due to the acceptable uncertainty in simulating  $T_{mrt}$ . In the specific case of façade greening in a complex urban environment, however, their usability is limited in the current set-up. Generic studies or simple environments combined with modified parameterizations might improve the usability. Specific types of vegetation besides trees should not be incorporated in these models without modifications and extensive evaluation. Therefore, new simulation tools or advancements in existing models are desirable to complement observational case studies. The combination of biometeorological microclimate models and observations is helpful in order to complement benefits of each method. More effort in bridging the gaps between case studies and large-scale applications of countermeasures is needed to detect an effective countermeasure against heat stress risks in cities.

## Conflict of Interests

The authors declare that there is no conflict of interests regarding the publication of this paper.

## Acknowledgments

The authors wish to thank their colleagues for the great support during the measurement campaign and the enriching discussions. The study is part of the Research Unit 1736 "Urban Climate and Heat Stress in Mid-Latitude Cities in View of Climate Change (UCaHS)" (<http://www.UCaHS.org>) funded by the Deutsche Forschungsgemeinschaft (DFG) under the codes SCHE 750/8-1, SCHE 750/9-1, and WE 1125/30-1.

## References

- [1] D. Scherer, U. Fehrenbach, T. Lakes, S. Lauf, F. Meier, and C. Schuster, "Quantification of heat-stress related mortality hazard, vulnerability and risk in Berlin, Germany," *Die Erde*, vol. 144, no. 3-4, pp. 238–259, 2013.
- [2] A. M. Rizwan, L. Y. C. Dennis, and C. Liu, "A review on the generation, determination and mitigation of Urban Heat Island," *Journal of Environmental Sciences*, vol. 20, no. 1, pp. 120–128, 2008.
- [3] M. Georgescu, P. E. Morefield, B. G. Bierwagen, and C. P. Weaver, "Urban adaptation can roll back warming of emerging megapolitan regions," *Proceedings of the National Academy of Sciences of the United States of America*, vol. 111, no. 8, pp. 2909–2914, 2014.
- [4] S. Thorsson, F. Lindberg, I. Eliasson, and B. Holmer, "Different methods for estimating the mean radiant temperature in an outdoor urban setting," *International Journal of Climatology*, vol. 27, no. 14, pp. 1983–1993, 2007.
- [5] N. Kántor and J. Unger, "Benefits and opportunities of adopting GIS in thermal comfort studies in resting places: an urban park as an example," *Landscape and Urban Planning*, vol. 98, no. 1, pp. 36–46, 2010.
- [6] M. Köhler, "Green facades—a view back and some visions," *Urban Ecosystems*, vol. 11, no. 4, pp. 423–436, 2008.
- [7] G. Pérez, L. Rincón, A. Vila, J. M. González, and L. F. Cabeza, "Green vertical systems for buildings as passive systems for energy savings," *Applied Energy*, vol. 88, no. 12, pp. 4854–4859, 2011.
- [8] E. A. Eumorfopoulou and K. J. Kontoleon, "Experimental approach to the contribution of plant-covered walls to the thermal behaviour of building envelopes," *Building and Environment*, vol. 44, no. 5, pp. 1024–1038, 2009.
- [9] R. M. Pulselli, F. M. Pulselli, U. Mazzali, F. Peron, and S. Bastianoni, "Emergy based evaluation of environmental performances of living wall and grass wall systems," *Energy and Buildings*, vol. 73, pp. 200–211, 2014.
- [10] A. M. Hunter, N. S. G. Williams, J. P. Rayner, L. Aye, D. Hes, and S. J. Livesley, "Quantifying the thermal performance of green façades: a critical review," *Ecological Engineering*, vol. 63, pp. 102–113, 2014.
- [11] R. Djedjig, E. Bozonnet, and R. Belarbi, "Experimental study of the urban microclimate mitigation potential of green roofs and green walls in street canyons," *International Journal of Low-Carbon Technologies*, 2013.
- [12] T. Koyama, M. Yoshinaga, H. Hayashi, K.-I. Maeda, and A. Yamauchi, "Identification of key plant traits contributing to the cooling effects of green façades using freestanding walls," *Building and Environment*, vol. 66, pp. 96–103, 2013.

- [13] R. W. F. Cameron, J. E. Taylor, and M. R. Emmett, "What's 'cool' in the world of green façades? How plant choice influences the cooling properties of green walls," *Building and Environment*, vol. 73, pp. 198–207, 2014.
- [14] G. Gross, "Effects of different vegetation on temperature in an urban building environment. Micro-scale numerical experiments," *Meteorologische Zeitschrift*, vol. 21, no. 4, pp. 399–412, 2012.
- [15] C. L. Tan, N. H. Wong, and S. K. Jusuf, "Effects of vertical greenery on mean radiant temperature in the tropical urban environment," *Landscape and Urban Planning*, vol. 127, pp. 52–64, 2014.
- [16] R. Berry, S. J. Livesley, and L. Aye, "Tree canopy shade impacts on solar irradiance received by building walls and their surface temperature," *Building and Environment*, vol. 69, pp. 91–100, 2013.
- [17] Y.-C. Chen, T.-P. Lin, and A. Matzarakis, "Comparison of mean radiant temperature from field experiment and modelling: a case study in Freiburg, Germany," *Theoretical and Applied Climatology*, vol. 118, no. 3, pp. 535–551, 2014.
- [18] S. Huttner, *Further development and application of the 3D microclimate simulation ENVI-met [Ph.D. thesis]*, Johannes Gutenberg-Universität Mainz, 2012.
- [19] R.-L. Hwang, T.-P. Lin, and A. Matzarakis, "Seasonal effects of urban street shading on long-term outdoor thermal comfort," *Building and Environment*, vol. 46, no. 4, pp. 863–870, 2011.
- [20] E. L. Krüger, F. O. Minella, and A. Matzarakis, "Comparison of different methods of estimating the mean radiant temperature in outdoor thermal comfort studies," *International Journal of Biometeorology*, vol. 58, no. 8, pp. 1727–1737, 2013.
- [21] T.-P. Lin, A. Matzarakis, and R.-L. Hwang, "Shading effect on long-term outdoor thermal comfort," *Building and Environment*, vol. 45, no. 1, pp. 213–221, 2010.
- [22] A. Matzarakis, F. Rutz, and H. Mayer, "Modelling radiation fluxes in simple and complex environments—application of the RayMan model," *International Journal of Biometeorology*, vol. 51, no. 4, pp. 323–334, 2007.
- [23] A. Matzarakis, F. Rutz, and H. Mayer, "Modelling radiation fluxes in simple and complex environments: basics of the RayMan model," *International Journal of Biometeorology*, vol. 54, no. 2, pp. 131–139, 2010.
- [24] F. Lindberg, B. Holmer, and S. Thorsson, "SOLWEIG 1.0—modelling spatial variations of 3D radiant fluxes and mean radiant temperature in complex urban settings," *International Journal of Biometeorology*, vol. 52, no. 7, pp. 697–713, 2008.
- [25] F. Lindberg and C. S. B. Grimmond, "The influence of vegetation and building morphology on shadow patterns and mean radiant temperatures in urban areas: model development and evaluation," *Theoretical and Applied Climatology*, vol. 105, no. 3–4, pp. 311–323, 2011.
- [26] M. Srivanit and K. Hokao, "Evaluating the cooling effects of greening for improving the outdoor thermal environment at an institutional campus in the summer," *Building and Environment*, vol. 66, pp. 158–172, 2013.
- [27] W. T. L. Chow and A. J. Brazel, "Assessing xeriscaping as a sustainable heat island mitigation approach for a desert city," *Building and Environment*, vol. 47, no. 1, pp. 170–181, 2012.
- [28] W. T. L. Chow, R. L. Pope, C. A. Martin, and A. J. Brazel, "Observing and modeling the nocturnal park cool island of an arid city: horizontal and vertical impacts," *Theoretical and Applied Climatology*, vol. 103, no. 1–2, pp. 197–211, 2011.
- [29] R. Emmanuel and H. J. S. Fernando, "Urban heat islands in humid and arid climates: role of urban form and thermal properties in Colombo, Sri Lanka and Phoenix, USA," *Climate Research*, vol. 34, no. 3, pp. 241–251, 2007.
- [30] B. C. Hedquist and A. J. Brazel, "Seasonal variability of temperatures and outdoor human comfort in Phoenix, Arizona, U.S.A.," *Building and Environment*, vol. 72, pp. 377–388, 2014.
- [31] A. Middel, K. Häb, A. J. Brazel, C. A. Martin, and S. Guhathakurta, "Impact of urban form and design on mid-afternoon microclimate in Phoenix Local Climate Zones," *Landscape and Urban Planning*, vol. 122, pp. 16–28, 2014.
- [32] N. Müller, W. Kuttler, and A.-B. Barlag, "Counteracting urban climate change: adaptation measures and their effect on thermal comfort," *Theoretical and Applied Climatology*, vol. 115, no. 1–2, pp. 243–257, 2014.
- [33] E. Ng, L. Chen, Y. Wang, and C. Yuan, "A study on the cooling effects of greening in a high-density city: an experience from Hong Kong," *Building and Environment*, vol. 47, no. 1, pp. 256–271, 2012.
- [34] L. L. H. Peng and C. Y. Jim, "Green-roof effects on neighborhood microclimate and human thermal sensation," *Energies*, vol. 6, no. 2, pp. 598–618, 2013.
- [35] C. Skelhorn, S. Lindley, and G. Levermore, "The impact of vegetation types on air and surface temperatures in a temperate city: a fine scale assessment in Manchester, UK," *Landscape and Urban Planning*, vol. 121, pp. 129–140, 2014.
- [36] X. Yang, L. Zhao, M. Bruse, and Q. Meng, "Evaluation of a microclimate model for predicting the thermal behavior of different ground surfaces," *Building and Environment*, vol. 60, pp. 93–104, 2013.
- [37] I. D. Stewart and T. R. Oke, "Local climate zones for urban temperature studies," *Bulletin of the American Meteorological Society*, vol. 93, no. 12, pp. 1879–1900, 2012.
- [38] M. Bruse and H. Fleer, "Simulating surface-plant-air interactions inside urban environments with a three dimensional numerical model," *Environmental Modelling and Software*, vol. 13, no. 3–4, pp. 373–384, 1998.
- [39] N. H. Wong, A. Y. Kwang Tan, Y. Chen et al., "Thermal evaluation of vertical greenery systems for building walls," *Building and Environment*, vol. 45, no. 3, pp. 663–672, 2010.
- [40] M. Bruse, *Die Auswirkungen kleinskaliger Umweltgestaltung auf das Mikroklima [Ph.D. thesis]*, Universität Bochum, 1999.
- [41] C. J. Willmott, S. G. Ackleson, R. E. Davis et al., "Statistics for the evaluation and comparison of models," *Journal of Geophysical Research*, vol. 90, no. 5, pp. 8995–9005, 1985.
- [42] K. H. Schlünzen and R. S. Sokhi, "Overview of tools and methods for meteorological and air pollution mesoscale model evaluation and user training," WMO Joint Report COST Action 728 GURME, 2008.
- [43] F. Ali-Toudert, *Dependence of outdoor thermal comfort on street design in hot and dry climate [Ph.D. thesis]*, Universität Freiburg, Freiburg im Breisgau, Germany, 2005.
- [44] F. Yang, S. S. Y. Lau, and F. Qian, "Thermal comfort effects of urban design strategies in high-rise urban environments in a sub-tropical climate," *Architectural Science Review*, vol. 54, no. 4, pp. 285–304, 2011.
- [45] S. Berkovic, A. Yezioro, and A. Bitan, "Study of thermal comfort in courtyards in a hot arid climate," *Solar Energy*, vol. 86, no. 5, pp. 1173–1186, 2012.



## Paper II

# Assessment of indoor heat stress variability in summer and during heat warnings: A case study using the UTCI in Berlin, Germany

Walikewitz, N., Jänicke, B., Langner, M. and W. Endlicher (2015): *Assessment of indoor heat stress variability in summer and during heat warnings: A case study using the UTCI in Berlin, Germany*. International Journal of Biometeorology, 1–14. <http://dx.doi.org/10.1007/s00484-015-1066-y>

**Status:** Published (30 September 2015)

**Copyright:** © 2015, International Journal of Biometeorology (ISB). The accepted manuscript is printed here with permission of Springer.

### Own contributions:

- Contribution to refining of research ideas and outdoor research design
- Simulation of outdoor  $T_{mrt}$
- Outdoor measurements and data processing
- Processing outdoor data for simulations
- Writing the section about outdoor analyses
- Contribution to revisions of manuscript and revised manuscript



# Assessment of indoor heat stress variability in summer and during heat warnings: A case study using the UTCI in Berlin, Germany

Nadine Walikewitz<sup>\*</sup><sub>1</sub>, Britta Jänicke<sub>2</sub>, Marcel Langner<sub>3</sub>, Wilfried Endlicher<sub>1</sub>

<sub>1</sub>Geography Department, Humboldt-Universität zu Berlin, Unter den Linden 6, 10099 Berlin, Germany

<sub>2</sub>Department of Ecology, Technische Universität Berlin, Rothenburgstraße 12, 12165 Berlin, Germany

<sub>3</sub>Federal Environment Agency (Umweltbundesamt), Wörlitzer Platz 1, 06844 Dessau-Roßlau, Germany

nadine.walikewitz@geo.hu-berlin.de, britta.jaenicke@tu-berlin.de, marcel.langner@uba.de, wilfried.endlicher@geo.hu-berlin.de

<sup>\*</sup>Corresponding author. Phone +49 30 2093 9380; Fax +49 30 2093 6844

## Abstract

Humans spend most of their time in confined spaces and are hence primarily exposed to the direct influence of indoor climate. The Universal Thermal Climate Index (UTCI) was obtained in 31 rooms (eight buildings) in Berlin, Germany during summer 2013 and 2014. The indoor UTCI was determined from measurements of both air temperature and relative humidity and from data of mean radiant temperature and air velocity, which were either measured or modeled. The associated outdoor UTCI was obtained through facade measurements of air temperature and relative humidity, simulation of mean radiant temperature and wind data from a central weather station. The results show that all rooms experienced heat stress according to UTCI levels, especially during heat waves.

Indoor UTCI varied up to 6.6 K within the city and up to 7 K within on building. Heat stress either during day or at night occurred on 35 % of all days. By comparing the day and night thermal loads we identified maximum values above the 32 °C threshold for strong heat stress during the nighttime. Outdoor UTCI based on facade measurements provided no better explanation of indoor UTCI variability than the central weather station. In contrast, we found a stronger relationship of outdoor air temperature and indoor air temperature. Building characteristics, such as the floor level or window area, influenced indoor heat stress ambiguously. We conclude that indoor heat stress is a major hazard, and more effort toward understanding the causes and creating effective countermeasures is needed.

Keywords: Indoor climate, heat stress, UTCI, indoor measurements

## 1. Introduction

Heat stress is a serious risk to humans, especially in cities where the global increase in air temperature ( $T_a$ ) is amplified by urban structures (Matzarakis and Endler 2010). A significant increase in mortality due to heat stress has been shown by Almeida et al. (2013); D'Ippoliti et al. (2010); Gabriel and Endlicher (2011); McMichael and Haines (1997); Michelozzi et al. (2009); Smoyer et al. (2000); Ye et al. (2012). Analyses regarding heat stress and morbidity (McGeehin and Mirabelli 2001; Monteiro et al. 2013; Scherber et al. 2013), as well as impacts on human well-being (Kjellstrom and McMichael 2013), have been conducted. Heat stress and work performance also have a strong interrelationship (Lundgren et al. 2013; Witterseh et al. 2004),

However, only a limited number of studies examined the role of indoor climates in hazardous atmospheric conditions (Pfafferott and Becker 2008). People in industrialized countries spend on average 90 % of the day in confined spaces; hence, the assessment of indoor heat stress is an

important issue. The influence of outdoor climate on indoor climate, especially during heat stress events, has been well investigated (Nguyen et al. 2014; Quinn et al. 2014). Indoor  $T_a$  is mainly influenced by outdoor  $T_a$ , but its diurnal course is inhibited due to the physical characteristics of the building (Höppe 1993). Furthermore, thermal radiative fluxes within enclosed environments have a higher importance than solar radiation. However, when direct solar radiation enters a room through the windows, the additional thermal load needs to be considered (La Gennusa et al. 2005). Studies by for example Höppe (1993) and Melikov et al. (2013) indicate that air velocity ( $v$ ) influences the convective heat transfer and therefore improves the thermal sensation, especially at high room temperatures and humidity levels. Based on these results and those of further studies, it is evident that for the assessment and description of indoor heat stress, the meteorological parameters  $T_a$ , relative humidity (RH),  $v$  and mean radiant temperature ( $T_{mrt}$ ) should be considered.

Thermal indices, such as the recently developed UTCI (Jendritzky et al. 2012) that is used in this study, achieve this requirement. The UTCI is based on a multi-node model



of human heat transfer and temperature regulation (Fiala et al. 2012). Furthermore, an up-to-date clothing model takes into account the typical dressing behaviors in different thermal conditions and it is further representative of European and North American urban populations in outdoor spaces (Havenith et al. 2012). Bröde et al. (2012) provided a detailed description of the operational procedure to calculate the UTCI.

Indoor thermal conditions in urban areas have been assessed by for example Mirzaei et al. (2012) and Beizaee et al. (2013) but they only focus on Ta as the describing or forcing variable of indoor thermal conditions. Furthermore, these studies and others (Nguyen et al. 2014; Quinn et al. 2014) used central weather stations or simulations to describe the outdoor conditions. Hence, the urban spatial variability is not considered in their studies. Fenner et al. (2014) found significant spatial and temporal differences in outdoor Ta during heat waves in Berlin, and it is therefore likely that indoor climate differs within the urban area. Langner et al. (2013) used the UTCI for the assessment of indoor climate but only measured Ta and RH and did further not consider the outdoor climate.

Our chief objective was to examine the spatial and temporal variability of indoor heat stress in different buildings in Berlin, Germany. Based on the data of a detailed measurement system of indoor and outdoor climate, distributed over the city during summer 2013 and 2014, we calculate the UTCI to consider the main meteorological parameters Ta, RH, Tmrt and v. Furthermore, we examined heat-warning periods to estimate the maximal thermal load during the day and night. In a second step, the main driving factors of outdoor climate and building characteristics are analyzed. For the outdoor conditions, we calculated the UTCI based on on-site data to consider local climate variations in urban areas. To evaluate the results, we also used data from a central weather station. The building characteristics of floor level, window size and year of construction are considered to estimate differences between and within the observed buildings.

## 2. Methodology

To assess the variability of indoor heat stress, measurements were executed in eight different buildings (Fig. 1, Table 1) within 31 rooms, and outdoor data were measured at six different sites. Most measurements began in June 2013 and are ongoing. For this study, the 2013 and 2014 summer periods from the 1<sup>st</sup> of June to the 31<sup>st</sup> of August (184 days) were used. Due to the heterogenic urban structure of Berlin, we aimed to cover the most prevailing building types, constructed in various years. Due to the innovations of the UTCI (Jendritzky et al. 2012) and the need for a standardized application to compare indoor and outdoor conditions, the results are presented using the UTCI, even though the index was originally developed for outdoor conditions. The UTCI calculations were conducted with the software program RayMan 1.2 (available from <http://www.mif.uni-freiburg.de/rayman/intro.htm>) using the input parameters Ta, RH, v and Tmrt, as well as geographical data of Berlin (Matzarakis et al. 2007;

Matzarakis et al. 2010). Measured levels of v were mainly below the range of validity of 0.5 m/s at a level of 10 m above ground for the use of the regression function to calculate UTCI (Bröde et al. 2012). Hence, values below this threshold, as well as v values in rooms where no measurements were conducted, were set to 0.3 m/s at the level of a person's body. Furthermore, a metabolic heat production of 135 W/m<sup>2</sup> was assumed for all UTCI calculations. The analysis was conducted using the software program R Version 2.15.1 (RCoreTeam 2012), and all measurements were registered in Central European Time (CET).

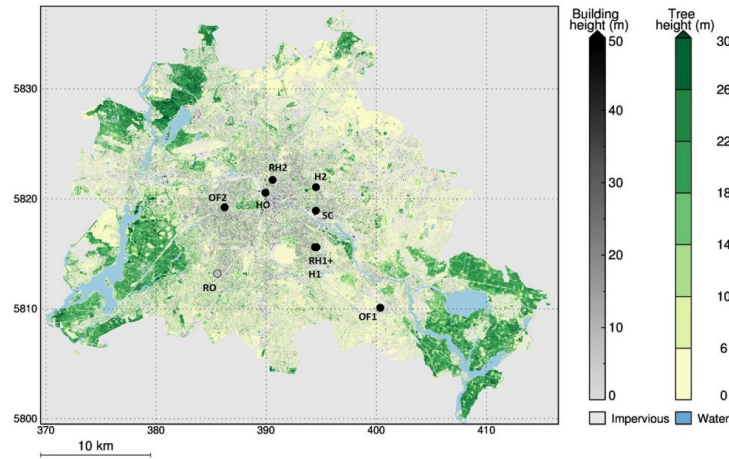
The analysis of the intra-urban and temporal variability of indoor heat stress is based on five study sites OF1, OF2, SC, RH1 and RH2 (Fig. 2). At the HO, H1 and H2 sites only two rooms were equipped with the measurement devices. Hence, no heat stress variability within the buildings can be described, and the sites are solely used for the indoor-outdoor comparison. Results relating indoor to outdoor climate are thus based on the study sites SC, RH1, RH2, HO, H1 and H2 due to data availability.

### 2.1 Indoor study design

The instrumental setup for the indoor measurements varies between the study sites (Table 1). In office 1 (OF1) and office 2 (OF2), as well as in the private flat 1 (H1), Ta, RH, v and Tmrt were measured. At the remaining sites (school (SC+SC\*), retirement home 1 (RH1) and retirement home 2 (RH2), hospital (HO) and the private flat 2 (H2)), only Ta and RH could be measured. At these study sites, the Tmrt was set to Ta, an assumption which was already used and explained in previous studies (Kántor and Unger 2011). To measure Ta and RH, each room was equipped with two Testo 174H loggers (accuracy of  $\pm 0.5$  °C and  $\pm 3$  %RH, respectively). V was derived by one PCE-009 hot wire anemometer per room (accuracy of  $\pm 0.5$  %), and Tmrt was measured by the use of one black globe thermometer (KIMO) per room (accuracy of  $\pm 0.5$  °C; 150 mm in diameter; 0.4 mm thickness). The use of a globe thermometer gives a good approximation of the detailed and extensive integral radiation measurement (Bedford and Warner 1934; Kuehn et al. 1970; Walikewitz et al. 2015). The sensors were fixed at a height of approximately 1.1 m above the ground, corresponding to the average height of the center of gravity for adults. The investigated rooms in each building are located at different floor levels but are equal in size and orientation of the windows (southwest). One room per side is northeast oriented to estimate the influence of direct solar radiation (indicated by N). Study site SC differs due to a lightweight construction extension of the building at the top floor with different window areas and orientation (indicated by \*) compared to the solid stone construction from 1909.

To estimate the average conditions per room, the placement of sensors at locations where they may be influenced by direct solar radiation or heating installations was avoided. All data were recorded at 5-minute intervals and then aggregated to mean hourly/daily values only when all data on a given hour/day were available.





**Fig. 1** Map of Berlin including the eight study sites (black) and the reference station RO (grey). Data source: <http://www.stadtentwicklung.berlin.de/umwelt/umweltatlas/ei610.htm>

**Table 1** Overview of the measurement sites as well as the indoor/outdoor data acquisition; air temperature (Ta), relative humidity (RH), air velocity (v), mean radiant temperature (Tmrt); in buildings where only Ta and RH was measured, Tmrt was set be equal to Ta and v was set to be 0.3 m/s; ✓ indicates for which part of the analysis the data are used; RO=reference station; \*partly enlarged in 2006; \*\* reconstructed in 1950 after the second world war; \*\*\* windows within a room have the same size

site	abbrevi- ation	year of constructio- n	overview			orientation of the rooms (windows)	floor levels	wall material	number of rooms/star- t	measured values	outdoor measured floor	data usage	
			geographic coordinates	total size of windows (m <sup>2</sup> ) per room	room size (m <sup>2</sup> )/volume (m <sup>3</sup> )							indoor	outdoor comparison
Office 1	OF1	2003	13.534373 52.432088	19.5	50.1/97	3 southwest 1 northeast	5	concrete	4 06/2013	Ta, RH, v, Tmrt	no measurements	✓	
Office 2	OF2	1962	13.323401 52.511305	8.4	19.4/62	4 southwest 1 northeast	10	concrete	5 06/2013	Ta, RH, v, Tmrt	no measurements	✓	
School	SC	1909 2006*	13.44554 52.510148	8.2/12.2*	52.2/208 70.6/211*	4 southwest 3 southeast*	4	brick concrete*	4/3* 06/2013	Ta, Tmrt=Ta RH, v=0.3 m/s	1st, 4th	✓	✓
Retireme- nt home 1	RH1	2004	13.447388 52.480398	5.3	17.7/44	4 southwest 1 northeast	5	concrete	5 06/2013	Ta, Tmrt=Ta RH, v=0.3 m/s	1st	✓	✓
Retireme- nt home 2	RH2	1993	13.386747 52.534539	3.3	21.5/55	3 southwest 1 northeast	5	concrete	4 06/2013	Ta, Tmrt=Ta RH, v=0.3 m/s	3rd, 5th	✓	✓
Hospital	HO	1900 1950**	13.377579 52.523924	3.4	31.8/111.3	1 southwest	5	brick	1 05/2014	Ta, Tmrt=Ta RH, v=0.3 m/s	3rd		✓
Private flat 1	H1	1910	13.445280 52.480403	3.2	24.6/73.8	1 southwest 1 northeast	5	brick	2 10/2013	Ta, RH, v, Tmrt	data from side RH1		✓
Private flat 2	H2	1920	13.444979 52.529375	3.3	35.2/112.6	1 southwest 1 northeast	5	brick	2 06/2014	Ta, RH, Tmrt, v=0.3 m/s	3rd floor		✓



**Fig. 2** Overview of the outdoor facades of the five study sites used for the indoor climate analysis

### 2.3 Outdoor study design

The outdoor observations consisted of Ta and RH sensors (DK390 HumiLog GP "rugged", EU-325  $\pm 0.3$  °C and RFT-325  $\pm 2$  %) at six sites (Table 1) that are ventilated when sunlit by means of solar panels. Wind speed and global radiation, which were used for the calculation of outdoor Tmrt and UTCI, were observed only at one reference station in Berlin, Rothenburgstraße (RO; 52.4572 N, 13.3158 E; 47m amsl) at roof level (20 m) with a cup anemometer and a star pyranometer (see Fenner et al. (2014)).

We simulated Tmrt for each site with the radiation model SOLWEIG 2014a (Lindberg et al. 2008) to obtain Tmrt values that should be representative of the outdoor conditions in the environment near the analyzed building sites. Therefore, we used digital surface models (DSM) of vegetation and buildings provided by Senate Department for Urban Development and the Environment, Berlin (2014). For each site, we defined a domain of 100 m  $\times$  100 m around the indoor station with a resolution of 5 m. Meteorological input was derived from on-site observations of relative humidity and air temperature together with off-site observations of wind speed and global radiation from RO. The simulated Tmrt of each domain was then averaged to a spatially median value for each hour, whereas roof areas were excluded. In the SOLWEIG simulation, we applied the following parameters: 0.25 as the fraction of the canopy DSM and 0.034 as the mean transmissivity according to Konarska et al. (2014), albedo=0.15, emissivity (walls)=0.9, emissivity (ground)=0.95, absorption (shortwave)=0.7, absorption (longwave)=0.9.

### 2.4 Heat waves

During the study period in 2013, three weather warning periods regarding outdoor heat stress were issued by the German weather service (DWD) and four in 2014. For a detailed description of the warning system of the DWD, see Koppe (2009). The first and the second period in 2013 lasted 3 days (18/06-20/06; 26/07-28/07), while the third one lasted 6 days (02/08-07/08). In 2014, the warning periods were shorter. The first one lasted three days (08/06-10/06), but the remaining three lasted only two days each (06/07-07/07; 19/07-20/07; 28/07-29/07). Heat warnings are divided into warning classes: Class 0 represents no heat warning, class 1 strong heat load and class 2 extreme heat load. All warning periods will be named heat waves (HW) in the following study and are numbered in ascending order based on their chronological appearance. The warning of one day is valid from 11am to 7pm. Heat stress levels regarding the UTCI are moderate heat stress ( $\geq 26$  °C UTCI) and strong heat stress ( $\geq 32$  °C UTCI).

## 3. Results

Table 2 presents the unequally distributed number of days with heat stress (UTCI  $\geq 26$  °C) at the different study sites in 2013 and 2014. In 2013, indoor heat stress occurred on 38.5 % of all days. The mean UTCI values of all rooms ranged from 23.1 $\pm$ 1.4 °C to 29.9 $\pm$ 3.3 °C. The maximum

UTCI calculations varied between 27.3 °C and 39.6 °C, and the minimum UTCI data from 18.6 °C to 23.6 °C. In 2014, heat stress was documented on 29.6 % of all days. The mean UTCI varied between 22.3 $\pm$ 1.3 °C and 27.9 $\pm$ 3.4 °C, whereas the maximum values ranged from 27.6 °C to 37.0 °C and minimum between 18.2 °C and 21.7 °C. On average, the UTCI values were lower in 2014, but the moderate heat stress threshold ( $\geq 26$  °C) was exceeded more frequently at some sites. All study sites experienced heat stress during the heat stress warning periods. The mean daily UTCI variability indoors (mean=0.56, max= 2.2, min= 0.3) was lower compared to outdoors (mean=9.78, max=17.5, min=4.3).

### 3.1 Description of the spatial and temporal variability of indoor heat stress

The spatial and temporal heat stress variability of indoor UTCI among the different sites is large in both years (Fig. 3). Statistical analysis of variance shows that there is a significant effect of the study site on UTCI (F(4,839)=50.6,  $p < 0.05$ ). The mean daily variability of indoor UTCI within the city was 4.87 K in 2013 and 3.93 K in 2014. The spatial variability of each day during the heat waves is presented in Table 3.

The highest indoor heat stress levels were calculated at OF1. For two days in 2013, the maximum UTCI values on the 5th floor exceeded the 38 °C threshold for very strong heat stress. On average, OF1 shows increasing heat stress levels with increasing floor level. RH1 showed the same pattern within the building but lower UTCI values (31.6 °C max). The thermal load at the RH2 was similar to RH1. However, the distribution within the building was the opposite, with decreasing UTCI with increasing floor level, as also observed at OF2, where the lowest floor (3<sup>rd</sup>) has the highest mean heat stress levels. The UTCI distributions at the school differed from the other sites. In addition to the rooms in the old building (SC), two rooms are located in the 2006 enlarged top floor (SC\*) with different window sizes and wall constructions. The mean UTCI in SC\* (25.0 °C) exceeded the value in SC (23.8 °C). The internal mean UTCI variation between the rooms at the school and at the two residential care homes for the elderly varied by approximately 1 K. The two office buildings in contrast showed noticeable differences of 4-7 K among the rooms. A time delay, the so-called lag effect after the beginning and the end of the heat waves, can be observed in all buildings, but it is unequally distributed.

Fig. 4 shows the UTCI distribution at the study sites during the different warning levels in 2013 and 2014. On average, UTCI values increased with increasing warning classes. Due to the big sample sizes, the UTCI threshold of 26 °C and even the 32 °C one are exceeded at some points during warning class 0. At three study sites, the upper quartile was above the 26 °C threshold of moderate heat stress. Furthermore, extreme values at four study sites exceeded the strong heat stress limit and at OF1 the 38 °C threshold when no heat stress warning was issued (class 0). The differences in sample size were mainly due to the varying number of rooms per study site (Table 1) and some data gaps.

**Table 2** Number of days (d) with mean indoor/outdoor UTCI  $\geq 26^\circ\text{C}$  (moderate heat stress level) per study side in 2013 and 2014; NA= missing daily data; percentage of days (%) of all measured data above  $26^\circ\text{C}$  (NA not included); n=92 per year

	2013 indoor			2014 indoor			2013 outdoor			2014 outdoor		
	d	%	NA	d	%	NA	d	%	NA	d	%	NA
OF 1	58	77.3	17	52	56.5	0	-	-	-	-	-	-
OF 2	29	40.3	20	39	42.4	0	-	-	-	-	-	-
SC	15	22.1	21	33	35.9	0	14	18.4	16	16	17.4	5
RH 1	27	34.2	13	24	26.1	0	-	-	-	12	13.8	5
RH 2	17	18.5	0	30	34.5	5	18	19.6	0	17	19.5	5
HO	-	-	-	18	20.9	6	-	-	-	17	21.5	13
H 1	-	-	-	18	19.6	0	-	-	-	13	14.9	5
H 2	-	-	-	14	17.3	11	-	-	-	18	24.7	19
mean	29.2	38.5	14.2	28.5	29.6	2.8	16.0	19.0	8.0	15.5	18.6	8.7

**Table 3** Mean UTCI variability (in K) for each day of the heat waves within the city

	day of the heat wave					
	1day	2day	3day	4day	5day	6day
1HW	6.62	3.52	2.24	-	-	-
2HW	5.14	5.08	5.85	-	-	-
3HW	4.95	4.95	5.36	5.20	4.88	4.66
4HW	2.24	2.32	2.01	-	-	-
5HW	2.62	2.23	-	-	-	-
6HW	3.92	4.06	-	-	-	-
7HW	2.25	2.36	-	-	-	-

**Table 4** Correlations between indoor UTCI (Ta) and outdoor UTCI (Ta) based on facade/station measurements

	UTCI-UTCI		Ta-Ta	
	indoor-facade	indoor-station	indoor-facade	indoor-station
SC	0.76	0.83	0.82	0.84
RH1	0.86	0.89	0.87	0.88
RH2	0.83	0.90	0.91	0.92
HO	0.88	0.88	0.93	0.93
H1	0.76	0.85	0.83	0.84
H2	0.79	0.82	0.84	0.84

Fig. 5 displays hourly indoor UTCI mean values for all days during the seven HWs divided into day (11am-7pm) and night (8pm-10am). Almost every day, the heat load exceeded the  $26^\circ\text{C}$  UTCI threshold for moderate heat stress at both times of the day. During the day at OF1, UTCI values exceed the  $32^\circ\text{C}$  limit (strong heat stress) during the 2<sup>nd</sup>, 3<sup>rd</sup> and 6<sup>th</sup> HWs. Despite the lower average UTCI values at night, the difference between day and night was low (mean= 0.6, min= -0.3, max= 2.7) and therefore the potential to recover from thermal stress is reduced. On some days, especially during HW4, the mean thermal load at night was even higher compared to the day.

### 3.2 Driving factors of the spatial and temporal variability of indoor heat stress

#### 3.2.1 Outdoor climate

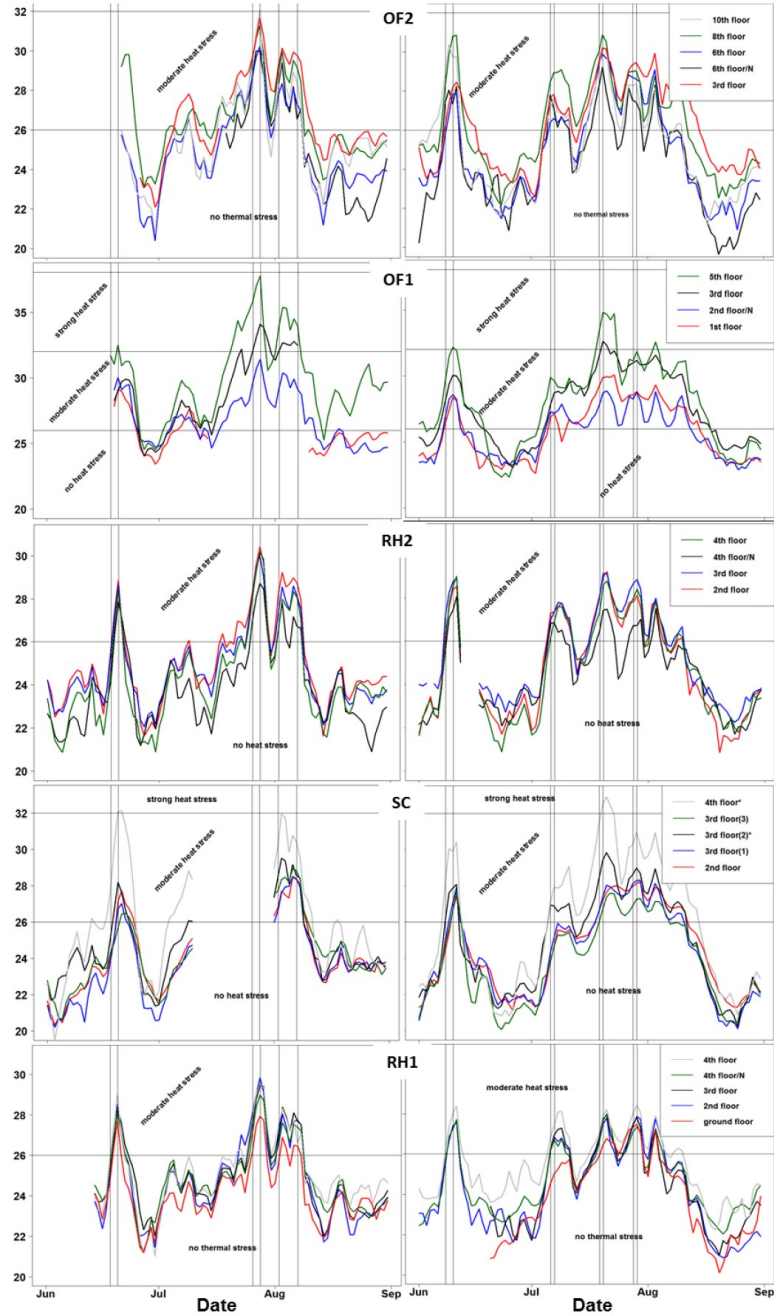
Previous studies show that outdoor climate is the main driving factor regarding indoor climate. This result is confirmed by the results of this study. The analysis of indoor and outdoor UTCI during summer 2013 and 2014 resulted in an  $r^2$  value of 0.6 ( $p < 0.01$ ), indicating that 60% of the variance of indoor UTCI can be explained by outdoor UTCI. The individual examination of each study site showed correlation coefficients between 0.76 and 0.88 and therefore strong correlations between indoor and outdoor UTCI with small differences between the study sites. To examine if on-site measurements are a better indicator for indoor climate,

we repeated the study with data from a central weather station. Table 4 summarizes the correlation results ( $p < 0.01$ ) between indoor UTCI/Ta and outdoor UTCI/Ta based on data from the on-site measurements and on data from the central weather station. The highest correlation was found between indoor Ta and outdoor Ta.

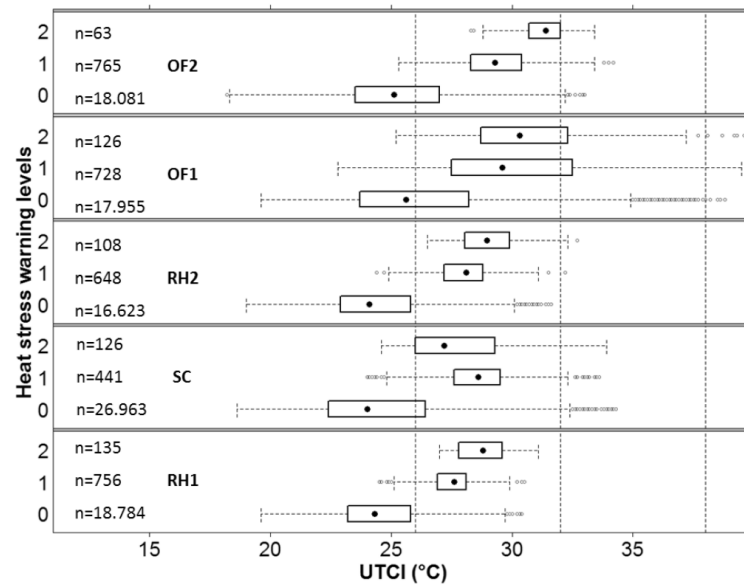
For comparing indoor UTCI with outdoor UTCI at different times of the day, we used the warning period 11am-7pm for daytime and 8pm- 10am for nighttime when no warnings are issued. Fig. 6 and Fig. 7 display the results for daytime and nighttime, respectively. During the day outdoor UTCI exceeds indoor UTCI of approximately  $5.6 \pm 3.9$  K (max 15.1 K; min -2.5 K). The second day of the 5<sup>th</sup> heat wave was the only day when mean indoor UTCI was higher than that outdoors at all study sites during the daytime. During night, the typical situation is the opposite. Indoor UTCI exceeds outdoor UTCI of approximately  $3.8 \pm 2.1$  K (max 8.4 K; min -1.9 K).

#### 3.2.2 Building characteristics

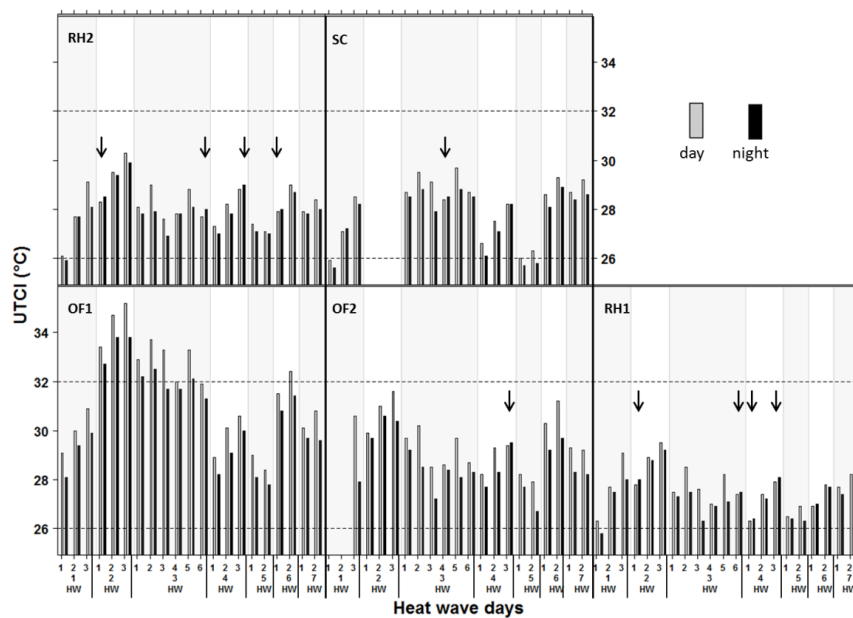
The description of the variability of heat stress in the first part of the results indicates that some building characteristics may influence the UTCI. The first physical parameter we analyzed was floor level to determine if the observable differences are significant. The correlation between floor levels and UTCI over all measurement sites showed a very weak but positive relationship ( $r = 0.21$ ,  $p = 0.01$ ). However, it is likely that the influence of floor level on one side is overlain by a small effect of another building.



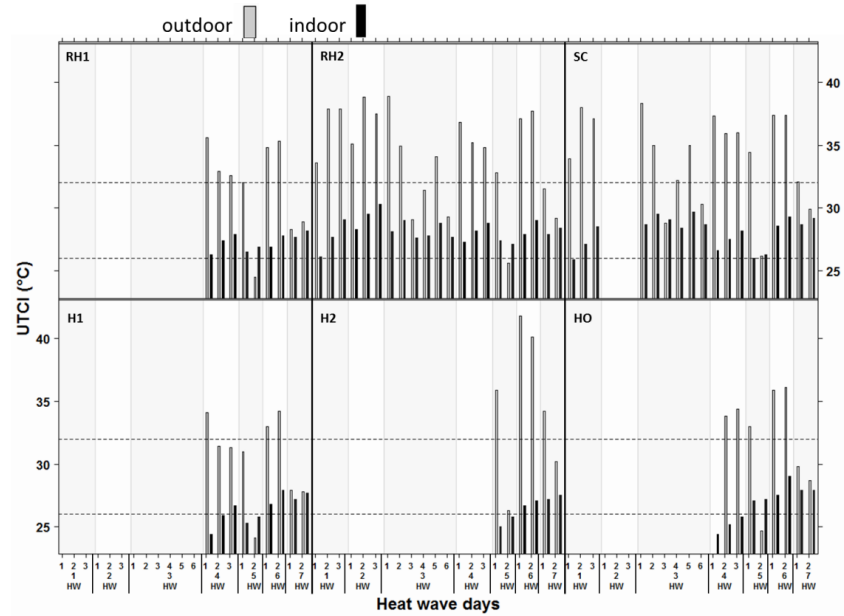
**Fig. 3** Mean daily indoor UTCI values presenting the spatial/temporal heat stress variability in all rooms at all study sites; left=2013 and right=2014; horizontal lines indicate 26 °C and 32 °C UTCI thresholds for moderate and strong heat stress levels; vertical lines show the beginning and end of each heat wave; due to readability only five of the seven rooms at study site SC are displayed, the first excluded is similar to the 3<sup>rd</sup> floor (2) in the new portion and the second one to the 2<sup>nd</sup> floor in the old portion



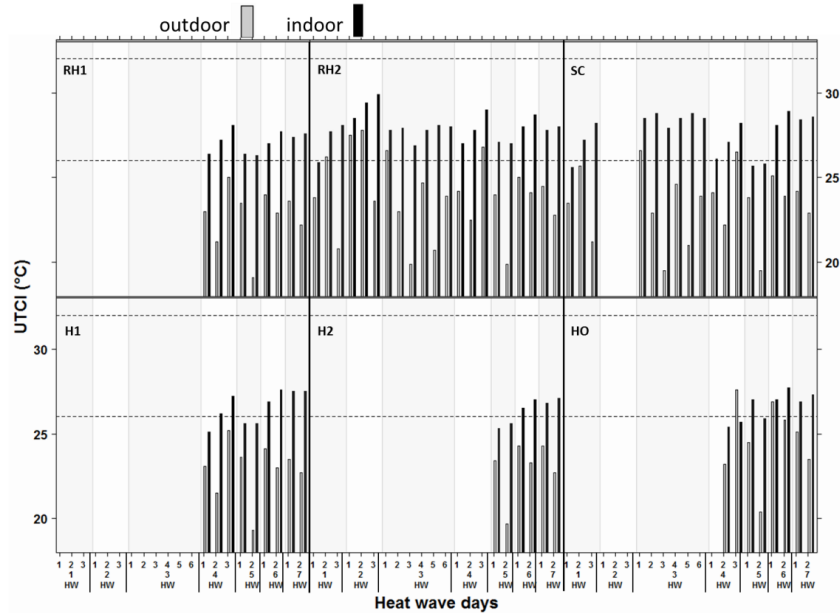
**Fig. 4** Hourly indoor UTCI values (°C) at different warning levels at all study sites during summer 2013 and 2014; warning levels: 0=no warning, 1=strong heat load, 2=extreme heat load; n=sample size; vertical lines indicate UTCI heat stress thresholds (26 °C moderate heat stress, 32 °C strong heat stress, 38 °C very strong heat stress)



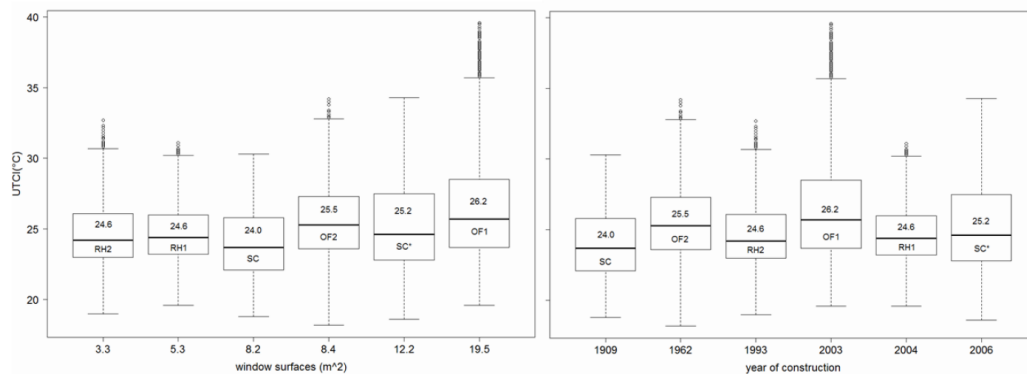
**Fig. 5** Mean hourly indoor UTCI values (°C) during the seven heat waves (1-7HW) in 2013 and 2014 divided into day (11am-7pm) and night (8pm-10am) at all study sites; horizontal lines indicate the 26 °C and 32 °C UTCI threshold lines for moderate and strong heat stress; vertical lines show the start and end of the heat waves; arrows indicate days with a higher heat load at night than that during the day



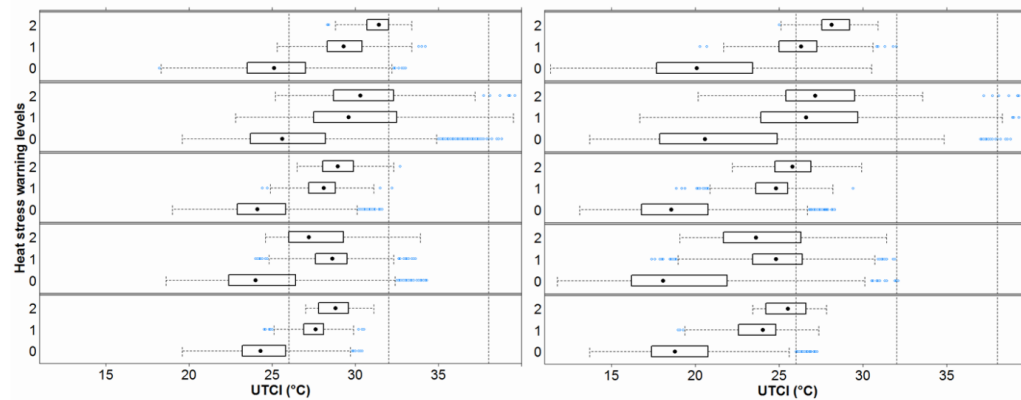
**Fig. 6** Mean hourly indoor (black) and outdoor (grey) UTCI values (°C) during the seven heat waves (1-7HW) in 2013 and 2014 at *daytime* (11am-7pm) at all study sites; horizontal lines indicate the 26 °C and 32 °C UTCI threshold lines for moderate and strong heat stress; vertical lines show the start and end of the heat waves



**Fig. 7** Mean hourly indoor (black) and outdoor (grey) UTCI values (°C) during the seven heat waves (1-7HW) in 2013 and 2014 at *night* (8pm-10am) at all study sites; horizontal lines indicate the 26°C and 32 °C UTCI threshold lines for moderate and strong heat stress; vertical lines show the start and end of the heat waves



**Fig. 8** Analysis of the influence of the building characteristics 'size of windows' ( $m^2$ ) (left panel) and 'year of construction' (right panel) on the UTCI (mean hourly values)



**Fig. 9** Indoor UTCI values at different warning levels at all study sites. 0=no heat load, 1=strong heat load, 2=extreme heat load; left=standard UTCI; right= UTCI with correction terms

Hence, the sites have been analyzed separately. Five of the six sites showed a very weak or no correlation ( $p = 0.01$ ) between floor level and UTCI (RH1  $r = 0.22$ , SC  $r = 0.0$ , SC  $r = 0.16$ , OF2  $r = -0.09$ , RH2  $r = -0.08$ ). The negative correlations at OF2 and RH2 can be seen in Fig. 3, where on average the highest UTCI values occurred at the lowest floor levels. OF1, in contrast, showed a positive correlation ( $r = 0.64$ ;  $p = 0.01$ ). Other building characteristics used in this study were year of construction and size of the window surfaces in each building (Fig. 8). The size of the window areas showed a very weak relationship with the UTCI ( $r = 0.18$ ;  $p = 0.01$ ), as well as the year of construction with the UTCI ( $r = 0.13$ ,  $p = 0.01$ ). We found no differences when repeating the analysis using only daytime or nighttime UTCI values.

#### 4. Discussion

##### 4.1 Indoor heat stress during warning periods

The analysis shows that indoor heat stress during summer 2013 and 2014 was unequally distributed regarding spatial and temporal variability, especially over the course of the

heat waves. The examination of indoor UTCI during the warning periods showed heat stress ( $>26^\circ\text{C}$ ) at all warning levels (Fig. 4), indicating the importance of this analysis. Specifically, the high values at warning level 0, when no warning is issued, are noticeable. It is likely that the high UTCI values during class 0 can be traced back to the time limitation of the warning period from 11am to 7pm. In indoor environments the thermal load lasts longer compared to outdoors due to the absorption of solar radiation during the day and the disposal of thermal radiation during the night. Therefore, UTCI values after 7pm were still high but are not included in the warning classes. These results are confirmed by the comparison of the day and night indoor UTCI values (Fig. 5). The differences were small and on some days the night showed higher values than the previous day. The comparison of outdoor UTCI with indoor UTCI supports this finding. The diurnal course of indoor UTCI was dampened due to the heat transfer resistance of the walls and their heat capacity. This led to an additional thermal load during night when the strain outdoors was mostly reduced (Fig. 7). In summary, people within the study



rooms are affected by heat stress not only during day but also during night. Hence, the ability to cope with heat stress after a disturbed recovery phase at night is likely to decrease due to a possible accumulation effect of heat stress (Parson 2003). Based on these results it is recommended to adapt the heat warnings to indoor environments and to expand the warning periods to 24h warnings. Especially during the recovery phase at night, it is important to recommend adequate adaptation strategies to reduce the heat stress risks.

When using the official heat warnings of the DWD, some limitations have to be considered. The warnings are based on the thermal index 'Gefühlte Temperatur' (index of the DWD) and not on the UTCI. Hence, the warning levels/thresholds are not fully concordant. We used the UTCI to provide results, which are comparable to other studies and can easily be reproduced. The aim of this part of the study is to show the thermal load during official warnings and not to revise the warning system itself. Hence, the differences between warning levels due to the use of different indices are negligible for the conclusions of this study. Furthermore, the detailed study by Blazejczyk et al. (2012) showed that indices using complex thermal exchange models (e.g. UTCI, 'Gefühlte Temperatur') are highly correlated.

## 4.2 Driving factors of indoor heat stress

### 4.2.1 Outdoor climate

The second part of the study was executed to identify the main driving factors for the differences in indoor heat stress. The fact that indoor climate is mainly governed by outdoor climate (Franck et al. 2013; Höppe 1993; Nguyen et al. 2014; Quinn et al. 2014) is confirmed by the results of this study. However, our second assumption that on-site measurements provide a better explanation for indoor climate cannot be confirmed. The correlation between indoor climate and the central weather station was higher, independent of the variables UTCI or  $T_a$  (Tab. 4). One possible explanation is the position of the facade station. The sensors were mounted on different floors as close to the indoor measurements as monumental protection and mounting options allowed.  $T_a$  showed on average higher values and bigger daily amplitudes compared to the standard reference weather station due to the additional influence of the thermal radiation of the building. Furthermore, we found a higher relationship between outdoor  $T_a$  and indoor UTCI. Outdoor RH and  $v$  are therefore not decisive regarding the development of indoor climate. This finding is confirmed by the highest correlation between indoor and outdoor  $T_a$ .

### 4.2.2 Building characteristics

The correlation between indoor UTCI and different building characteristics (Tab. 1) was very low suggesting that floor level, size of the window and year of construction are not good indicators for UTCI in indoor environments. However, at some study sites, indoor heat stress can be specified through the combination of more than one building characteristic. At OF1 where the highest heat stress levels were measured, floor level correlates with UTCI ( $r=0.64$ ) and the building has the largest window surfaces. This may

suggest that for modern buildings with large window areas and thus a big impact of direct sunlight on indoor climate, the position of a room within a building is an important consideration or at least the size of the windows. The influence of multiple variables can be further seen in the comparison of OF1 with RH1. OF1, constructed in 2003 with big window areas, experienced the highest heat stress levels whereas RH1, constructed in 2004 with relatively small window areas showed one of the lowest UTCI values in all buildings. The correlation of UTCI with all window sizes was very low. Nevertheless, a tendency to have higher UTCI values in rooms with a bigger window surface is observable. The two office buildings, as well as SC\*, had the highest maximum heat stress levels and concurrently the largest window surfaces (Fig. 8).

The study site SC is of a special interest due to two different window surfaces and two different years of construction combined in one building (Tab. 1). Built in 1909, SC consists of thick solid stone walls. This type of wall has a lower heat transmission coefficient ( $\sim 1.2 \text{ W/m}^2\text{K}$ ) compared to glass ( $2.8\text{-}5.9 \text{ W/m}^2\text{K}$ ) (Schulze 2004), and the rooms within this part of the building need more time to heat up and cool down, which can be seen in the pronounced lag effect and on average lower heat stress levels (Fig. 3). Rooms within the new part (SC\*) are of a lightweight construction and hence heat up more quickly. The UTCI values had higher pronounced daily cycles and higher peaks. Furthermore, the average UTCI values within SC (window size of  $8.2 \text{ m}^2$ ) were lower compared to the new part ( $12.2 \text{ m}^2$ ). In contrast, RH1 with a window area of  $5.3 \text{ m}^2$  experienced higher heat stress levels than SC ( $8.2 \text{ m}^2$ ). This deviation can be explained again by the construction of the building. In addition to the thick solid stone walls, the size of the room is bigger than the other study rooms. Hence, the higher amount of solar radiation entering the rooms was dampened due to the lower heat transmission coefficient of the wall and the bigger air capacity. These characteristics lead to a compensation of the bigger window surfaces. Nevertheless, to confirm these results, more study sites of the same types are needed.

### 4.2.3 User behavior

As a last possible driving factor of indoor heat stress, it is important to consider user behavior. We did not consider it within our study, but the results already indicate a possible influence. RH2 shows a reversed UTCI distribution with the highest values at the lowest floor and vice versa. This was very likely due to the behavior of the people within the rooms, i.e. room ventilation, shading of the room. At the highest floor, the person was aware of heat stress risks and took measures to reduce it, whereas the person at the lowest floor was bedridden. A further example is at OF2, where the lowest floor experienced the highest UTCI values. The room was the only one not in use. The influence of user behavior can also be found in the lag-effect at the study site SC. During the first heat wave, summer holidays started and no measures to reduce the heat stress could be taken. After the third event, the lag-effect is less pronounced due to influencing user behavior during school days. In summary, the consideration of user behavior is important, and studies regarding indoor heat stress should include this factor.



### 4.3 UTCI corrections

Using the UTCI in indoor environments requires some explanations. The UTCI was developed and evaluated for outdoor conditions and hence, is not applicable indoors. However, when describing indoor heat stress, it is important to consider the outdoor conditions. Furthermore, we built our study on all relevant meteorological parameters influencing human bioclimate and not just on  $T_a$ . It is therefore necessary to use a rational index with a thermal comfort model and further to consider the human physiology (Fiala et al. 2012), as well as the influence of clothes (Havenith et al. 2012).

Currently, the use of the UTCI in indoor environments has some limitations pertinent to this study. First,  $v$  is not within the range of validation for the UTCI calculation (see 2). This increase in  $v$  possibly leads to an underestimation of heat stress because within the UTCI calculation higher  $v$  levels reduce the thermal load. Second, the activity of a person is above the average indoor levels, where a sitting position ( $55 \text{ W/m}^2$ ) is the main activity. The determination leads likely to an overestimation of heat stress due to a higher internal heat production and hence a higher thermo-physiological model output. A first attempt to overcome some limitations regarding different activity levels and exposure times had been conducted by Bröde et al. (Leibnitz Institut; not published) for outdoor conditions. Based on their results, we used their UTCI correction terms considering activity at a resting level with a metabolic rate of heat production of 1.1 met (1 met =  $58.15 \text{ W/m}^2$ ) and exposure duration covering an 8-hour shift length in 30-min steps because they are similar to indoor conditions. The results are presented in Fig. 9 and show lower UTCI values on average at all sites. However, the results do not include a modification regarding  $v$ . Due to the incompleteness and missing evaluation of this UTCI adaptation for indoor environments, we do not consider the correction terms in the analysis but emphasize the need for further study regarding this area.

### 5. Conclusion

Heat stress occurred on 34 % of all days in summer 2013 and 2014 either during day or at night in Berlin. Indoor heat stress in mid-latitude cities is therefore a major hazard and may be amplified in the next decades due to the global increase in  $T_a$ . More effort in understanding the causes and creating effective countermeasures to reduce indoor heat stress is needed. The spatial variability within the city needs to be considered too, especially regarding local adaptation strategies. During heat waves, indoor heat stress at night is higher than that outdoors due to the thermal inertness of the buildings. As a consequence the recovery phase during night is disturbed, and it is likely that the ability to cope with heat stress during the next day will be decreased. Hence, the warning period of the official service during daytime is not enough for indoor environments. We recommend extending the warning periods and adapting the warning system to indoor environments.

Regarding the development of indoor heat stress, the study confirms that indoor climate is mainly governed by outdoor

climate. Furthermore, we found that on-site measurements of outdoor climate provide no better explanation of UTCI variability indoors, and therefore central weather station data can be applied for the assessment of indoor conditions. For a more detailed analysis of the interactions between indoor and outdoor climate, a building model has to be applied. The analyzed building characteristics are not good indicators for UTCI. However, we found some relationships between the sizes of the window areas and maximum UTCI values. We assume that real-case experimental studies complicate the analysis of influencing building characteristics, indicated also by the possible influence of user behavior. Moreover, more study sites of the same type should be used. For future studies, we also recommend to monitor user behavior during the measurements like opening and closing of windows to control ventilation or shading of windows to control radiation.

### Acknowledgements

We would like to thank the German research foundation (DFG) for funding Research Unit 1736 'Urban Climate and Heat stress in mid-latitude cities in view of climate change (UCaHS)' (EN138/21-1, SCHE 750/8-1 and SCHE 750/9-1) and Phillip Schuster for his support with data collection.

### References

- Almeida S, Casimiro E, Analitis A (2013) Short-Term Effects of Summer Temperatures on Mortality in Portugal: A Time-Series Analysis *J Toxicol Env Heal A* 76:422-428 doi:10.1080/15287394.2013.771550
- Bedford T, Warner CG (1934) The Globe Thermometer in Studies of Heating and Ventilation *Epidemiology & Infection* 34:458-473 doi:10.1017/S0022172400043242
- Beizaee A, Lomas KJ, Firth SK (2013) National survey of summertime temperatures and overheating risk in English homes *Building and Environment* 65:1-17 doi:10.1016/j.buildenv.2013.03.011
- Blazejczyk K, Epstein Y, Jendritzky G, Staiger H, Tinz B (2012) Comparison of UTCI to selected thermal indices *Int J Biometeorol* 56:515-535 doi:10.1007/s00484-011-0453-2
- Bröde P et al. (2012) Deriving the operational procedure for the UTCI *Int J Biometeorol* 56:481-494 doi:10.1007/s00484-011-0454-1
- D'Ippoliti D et al. (2010) The impact of heat waves on mortality in 9 European cities: results from the EuroHEAT project *Environmental Health* 9:37
- Fenner D, Meier F, Scherer D, Polze A (2014) Spatial and temporal air temperature variability in Berlin, Germany, during the years 2001–2010 *Urban Climate* 10, Part 2:308-331 doi:10.1016/j.uclim.2014.02.004
- Fiala D, Havenith G, Bröde P, Kampmann B, Jendritzky G (2012) UTCI-Fiala multi-node model of human heat transfer and temperature regulation *Int J Biometeorol* 56:429-441 doi:10.1007/s00484-011-0424-7
- Franck U, Krüger M, Schwarz N, Grossmann K, Röder S, Schlink U (2013) Heat stress in urban areas: Indoor and

- outdoor temperatures in different urban structure types and subjectively reported well-being during a heat wave in the city of Leipzig *Meteorologische Zeitschrift* 22:167-177 doi:10.1127/0941-2948/2013/0384
- Gabriel KMA, Endlicher WR (2011) Urban and rural mortality rates during heat waves in Berlin and Brandenburg, Germany *Environmental Pollution* 159:2044-2050 doi:<http://dx.doi.org/10.1016/j.envpol.2011.01.016>
- Havenith G et al. (2012) The UTCI-clothing model *Int J Biometeorol* 56:461-470 doi:10.1007/s00484-011-0451-4
- Höppe PR (1993) Indoor climate *Experientia* 49:775-779 doi:10.1007/BF01923547
- Jendritzky G, de Dear R, Havenith G (2012) UTCI-Why another thermal index? *Int J Biometeorol* 56:421-428 doi:DOI 10.1007/s00484-011-0513-7
- Kántor N, Unger J (2011) The most problematic variable in the course of human-biometeorological comfort assessment — the mean radiant temperature *centeurjgeo* 3:90-100 doi:10.2478/s13533-011-0010-x
- Kjellstrom T, McMichael AJ (2013) Climate change threats to population health and well-being: the imperative of protective solutions that will last *Global health action* 6:20816 doi:10.3402/gha.v6i0.20816
- Konarska J, Lindberg F, Larsson A, Thorsson S, Holmer B (2014) Transmissivity of solar radiation through crowns of single urban trees-application for outdoor thermal comfort modelling *Theor Appl Climatol* 117:363-376 doi:10.1007/s00704-013-1000-3
- Koppe C (2009) Das Hitzewarnsystem des Deutschen Wetterdienstes/The heat health warning system of the German Meteorological Service *Umwelt-Medizinischer Informations-Dienst-Klimawandel und Gesundheit* 3:39-43
- Kuehn LA, Stubbs RA, Weaver RS (1970) Theory of the globe thermometer *Journal of Applied Physiology* 29:750-757
- Langner M, Scherber K, Endlicher W (2013) Indoor heat stress: An assessment of human bioclimate using the UTCI in different buildings in Berlin *Die Erde* 144:260-273
- Lindberg F, Holmer B, Thorsson S (2008) SOLWEIG 1.0 – Modelling spatial variations of 3D radiant fluxes and mean radiant temperature in complex urban settings *Int J Biometeorol* 52:697-713 doi:10.1007/s00484-008-0162-7
- Lundgren K, Kuklane K, Gao CS, Holmer I (2013) Effects of Heat Stress on Working Populations when Facing Climate Change *Ind Health* 51:3-15
- Matzarakis A, Endler C (2010) Climate change and thermal bioclimate in cities: impacts and options for adaptation in Freiburg, Germany *Int J Biometeorol* 54:479-483 doi:10.1007/s00484-009-0296-2
- Matzarakis A, Rutz F, Mayer H (2007) Modelling radiation fluxes in simple and complex environments - application of the RayMan model *Int J Biometeorol* 51:323-334 doi:DOI 10.1007/s00484-006-0061-8
- Matzarakis A, Rutz F, Mayer H (2010) Modelling radiation fluxes in simple and complex environments: basics of the RayMan model *Int J Biometeorol* 54:131-139 doi:10.1007/s00484-009-0261-0
- McGeethin MA, Mirabelli M (2001) The potential impacts of climate variability and change on temperature-related morbidity and mortality in the United States *Environmental health perspectives* 109 Suppl 2:185-189
- McMichael AJ, Haines A (1997) Global climate change: the potential effects on health *Bmj* 315:805-809
- Melikov AK, Skwarczynski MA, Kaczmarczyk J, Zabecky J (2013) Use of personalized ventilation for improving health, comfort, and performance at high room temperature and humidity *Indoor Air* 23:250-263 doi:10.1111/ina.12012
- Michelozzi P, Accetta G, De Sario M (2009) High Temperature and Hospitalizations for Cardiovascular and Respiratory Causes in 12 European Cities *Am J Respir Crit Care Med* 179:383 - 389
- Mirzaei PA, Haghighat F, Nakhaie AA, Yagouti A, Giguere M, Keusseyan R, Coman A (2012) Indoor thermal condition in urban heat Island - Development of a predictive tool *Building and Environment* 57:7-17 doi:DOI 10.1016/j.buildenv.2012.03.018
- Monteiro A, Carvalho V, Oliveira T, Sousa C (2013) Excess mortality and morbidity during the July 2006 heat wave in Porto, Portugal *Int J Biometeorol* 57:155-167 doi:DOI 10.1007/s00484-012-0543-9
- Nguyen JL, Schwartz J, Dockery DW (2014) The relationship between indoor and outdoor temperature, apparent temperature, relative humidity, and absolute humidity *Indoor Air* 24:103-112 doi:10.1111/ina.12052
- Parson KC (2003) Human thermal environments: the effects of hot, moderate and cold environments on human health, comfort and performance. London, New York
- Pfaffertott J, Becker P (2008) Erweiterung des Hitzewarnsystems um die Vorhersage der Wärmebelastung in Innenräumen (Extension of the Heat Health Warning System by Indoor Heat Prediction) *Bauphysik* 30:237-243 doi:10.1002/bapi.200810031
- Quinn A, Tamerius JD, Perzanowski M, Jacobson JS, Goldstein I, Acosta L, Shaman J (2014) Predicting indoor heat exposure risk during extreme heat events *Science of The Total Environment* 490:686-693 doi:<http://dx.doi.org/10.1016/j.scitotenv.2014.05.039>
- Scherber K, Langner M, Endlicher W (2013) Spatial analysis of hospital admissions for respiratory diseases during summer months in Berlin taking bioclimatic and socio-economic aspects into account *Die Erde* 144:217-237
- Schulze J (2004) Sehr unterschiedliche Dämmwirkung an Altbauten/Different effectiveness of insulation in old buildings. *Bauhandwerk*
- Smoyer KE, Rainham DGC, Hewko JN (2000) Heat-stress-related mortality in five cities in Southern Ontario: 1980–1996 *Int J Biometeorol* 44:190-197 doi:10.1007/s004840000070
- Walikewitz N, Jänicke B, Langner M, Meier F, Endlicher W (2015) The difference between the mean radiant temperature and the air temperature within indoor environments: A case study during summer conditions *Building and Environment* 84:151-161 doi:<http://dx.doi.org/10.1016/j.buildenv.2014.11.004>
- Witterseh T, Wyon DP, Clausen G (2004) The effects of moderate heat stress and open-plan office noise distraction on SBS symptoms and on the performance of

office work Indoor Air 14:30-40 doi:10.1111/j.1600-0668.2004.00305.x

Ye X, Wolff R, Yu W, Vaneckova P, Pan X, Tong S (2012) Ambient temperature and morbidity: a review of epidemiological evidence Environmental health perspectives 120:19-28 doi:10.1289/ehp.1003198

### Paper III

## **Towards city-wide, building-resolving analysis of mean radiant temperature**

**Jänicke, B.**, Meier, F., Lindberg, F., Schubert, S., Scherer, D., 2016. Towards city-wide, building-resolving analysis of mean radiant temperature. *Urban Climate*, 15, 83-98. <http://dx.doi.org/10.1016/j.uclim.2015.11.003>

**Status:** Published (29 November 2015)

**Copyright:** © 2015 Elsevier B.V.

#### **Own contribution:**

- Refining research ideas and research design
- Search, review, and summary of literature
- Performing the simulations
- Performing the analyses
- Interpretation of statistical analyses
- Creating graphics and tables
- Writing the manuscript, visualising results, and drafting
- Revisions of manuscript





Contents lists available at ScienceDirect

## Urban Climate

journal homepage: [www.elsevier.com/locate/uclim](http://www.elsevier.com/locate/uclim)

## Towards city-wide, building-resolving analysis of mean radiant temperature

Britta Jänicke<sup>a,\*</sup>, Fred Meier<sup>a</sup>, Fredrik Lindberg<sup>b</sup>, Sebastian Schubert<sup>c</sup>, Dieter Scherer<sup>a</sup><sup>a</sup> Technische Universität Berlin, Institut für Ökologie, Fachgebiet Klimatologie, Rothenburgstr. 12, D-12165 Berlin, Germany<sup>b</sup> University of Gothenburg, Department of Earth Sciences, Urban Climate Group, Box 460, SE-405 30 Göteborg, Sweden<sup>c</sup> Potsdam-Institut für Klimafolgenforschung, Postfach 60 12 03, D-14412 Potsdam, Germany

## ARTICLE INFO

## Article history:

Received 16 July 2015

Revised 22 October 2015

Accepted 4 November 2015

## Keywords:

Heat stress

Human bioclimate

SOLWEIG

Berlin

Mean radiant temperature

## ABSTRACT

This study presents a method to simulate  $T_{mrt}$  building-resolving while considering both micro-scale urban structures and meso-scale atmospheric conditions. We extended the model SOLWEIG, one of the few methods to derive mean radiant temperature ( $T_{mrt}$ ) building-resolved and city-wide, to include spatial patterns of meteorological input. Based on a day within an extreme heat event (2003) in Berlin, Germany, we examined the effect of the new method on  $T_{mrt}$ , which uses gridded meteorological input data from a mesoscale weather model, compared to a standard set-up using ungridded data. Results indicated a considerable effect of spatially resolved air temperature (up to 3.2 K) during midnight. Furthermore, we detected high sensitivity of  $T_{mrt}$  to the partitioning of direct and diffuse short-wave radiation. The spatial pattern of  $T_{mrt}$  revealed that at midday the city centre exhibited low values compared to open areas. We conclude that considering meso-scale atmospheric conditions and urban structure for simulating  $T_{mrt}$  city-wide can lead to a more appropriate description of heat-stress hazards and might also be valuable for climate-sensitive urban planning.

© 2015 Elsevier B.V. All rights reserved.

## 1. Introduction

Heat-stress hazards are particularly high in cities due to effects of urban climate like Urban Heat Island (UHI) (Hajat and Kosatky, 2010; Mishra et al., 2015). During heat waves, mortality rates are also higher in cities such as Berlin, Germany compared to their rural surroundings (Gabriel and Endlicher, 2011). But, even within one city, intra-urban variability towards heat stress can be high (Scherber et al., 2014). To analyse intra-urban heat stress hazards, rational biometeorological indices or the mean radiant temperature ( $T_{mrt}$ ) are essential (Jendritzky et al., 2012; Ketterer and Matzarakis, 2014) since air and surface temperature are insufficient for assessing human bioclimate.  $T_{mrt}$  is the most important variable describing the human heat balance under sunny conditions, as it sums up long- and short-wave radiation that reaches the human body (Höppe, 1992; Kántor and Unger, 2011; Thorsson et al., 2014, 2007). Yet  $T_{mrt}$  is highly variable due to urban structures such as trees, bushes, street canyons and buildings (Lindberg et al., 2014). Moreover, weather and climate (e.g. air temperature and radiative fluxes) influence the spatial pattern of  $T_{mrt}$ , because the atmospheric conditions are heterogeneous in large urban areas (Endlicher and Lanfer, 2003; Fenner et al., 2014; Stewart et al., 2014).

\* Corresponding author.

E-mail addresses: [britta.jaenicke@tu-berlin.de](mailto:britta.jaenicke@tu-berlin.de) (B. Jänicke), [fred.meier@tu-berlin.de](mailto:fred.meier@tu-berlin.de) (F. Meier), [fredrik@gvc.gu.se](mailto:fredrik@gvc.gu.se) (F. Lindberg), [Sebastian.schubert@pik-potsdam.de](mailto:Sebastian.schubert@pik-potsdam.de) (S. Schubert), [dieter.scherer@tu-berlin.de](mailto:dieter.scherer@tu-berlin.de) (D. Scherer).<http://dx.doi.org/10.1016/j.uclim.2015.11.003>

2212-0955/© 2015 Elsevier B.V. All rights reserved.

High spatial resolution is as important as an appropriate hazard description to understand the effects of heat stress and to implement suitable adaptation measures. In this study, we use the term 'building-resolving' to describe a grid spacing that is capable to explicitly resolve buildings as well as the spaces between buildings. The spacing, needed for this purpose, varies between different cities due to different street and building width. Many previous studies concentrated on the variability of  $T_{mrt}$  at a building-resolving resolution for streets, neighbourhoods or districts (e.g. Bruse and Fleer, 1998; Chen et al., 2014; Ketterer and Matzarakis, 2014; Lindberg et al., 2008). In contrast, little attention has been paid to the combination of building-resolving along with city-wide analyses. This requirement is nevertheless inevitable for effective climate-sensitive urban planning, which requires high-resolution analysis for case-specific adaptation measures as well as a comprehensive overview to identify priority areas within a city (e.g. Düttemeyer et al., 2013; Mills et al., 2010; Norton et al., 2015). Such analyses can help to identify areas with high heat-stress hazards (potential 'priority areas') during heat waves and to develop reasonable actions to reduce heat stress.

Various methods are available for city-wide analyses on the one hand and building-resolving resolutions on the other hand. The combination of both methods offers new insights, however, its implementation is a big challenge. City-wide analyses are frequently carried out with atmospheric numerical models coupled with urban canopy scheme. These models are in general reliable and widely used, even if some issues remain unsolved (e.g. Ching, 2013; Grimmond et al., 2010; Martilli, 2007). These meso-scale models are not yet able to resolve explicitly micro-scale urban structures, such as buildings and vegetation. In contrast, building-resolving studies are often performed with models focusing on human bioclimate, such as ENVI-met, RayMan or SOLWEIG. These models perform well in the micro- to local-scale (Chen et al., 2014; Jänicke et al., 2015; Kántor and Unger, 2011). CFD models, such as ENVI-met, are not able to represent an entire city due to high computational demands (Bruse and Fleer, 1998). RayMan produces results only for one point (Matzarakis et al., 2007). SOLWEIG is in principle able to simulate  $T_{mrt}$  for large areas with a high spatial resolution (Lindberg and Grimmond, 2011; Lindberg et al., 2008), but the standard version applies meteorological input data, including air temperature, relative humidity and short-wave downward radiation, only based on one point for spatial-temporal calculations. Hence, meteorological conditions might become unrealistic when the model domain is very large. In summary, it is to our knowledge with existing models not possible to simulate  $T_{mrt}$  building-resolving for an entire city while considering both meso-scale weather situation and urban modifications.

The aim of this study is to introduce and analyse sensitivities of a method that closes this gap. We analysed  $T_{mrt}$  during one day (5 August 2003) of an extreme heat event in Berlin. We incorporated the meso-scale weather situation and urban modifications from results of a regional climate model (RCM) coupled with an urban canopy scheme (UCM), whereas we simulated the effects of micro-scale urban structures on  $T_{mrt}$  with a new subversion of the SOLWEIG model. In the new subversion, we applied gridded meteorological input data from the meso-scale model instead of only one-dimensional data. Firstly, we assess results from the coupled RCM/UCM against in-situ observations regarding variables required for calculating  $T_{mrt}$  (Section 3.1). Then, we study the sensitivity of the new SOLWEIG subversion to urban structures (Section 3.2), partitioning of direct and diffuse short-wave radiation (Section 3.3) and gridded meteorological input data (Section 3.4). As a step towards climate-sensitive urban planning, we finally analyse the spatial pattern of  $T_{mrt}$  in Berlin to discuss implications for identifying priority areas during an extreme heat event (Section 3.5).

## 2. Materials and methods

### 2.1. Study area and period

Berlin (52°31'N, 13°24'O) is the largest city in Germany, with 3.5 million inhabitants. We chose Berlin as a test bed for a large mid-latitude city, because its urban climate is not directly influenced by mountains or oceans, which can interfere with the formation of UHI. Furthermore, heat stress had already been identified as a serious threat there (Gabriel and Endlicher, 2011; Scherber et al., 2014; Scherer et al., 2014).

As exemplary weather situation, we selected one day (5 August 2003) during an extreme heat event (from 1 to 13 August, 2003) in Berlin (see Schubert and Grossman-Clarke (2013) for the definition of extreme heat events and thresholds). The heat wave of 2003 was one of the most disastrous extreme heat events in modern European history, with the highest temperature since the beginning of record in many regions and around 40,000 associated extra deaths across the continent (García-Herrera et al., 2010). In Berlin, the mortality rates also increased strongly during this extreme heat event (Gabriel and Endlicher, 2011). The 5th August 2003 was characterised by high air temperature, with an average of 22.0 °C and nearly cloud-free. Above Berlin and other parts of Germany a stable anticyclone existed that brought mixed subtropical air masses from Western Europe (Verein Berliner Wetterkarte, 2003). We chose this nearly cloud-free day to minimise uncertainty regarding cloud parameterization of the meso-scale model. Additionally, we used a longer period (3–18 August 2003) in Section 3.1 for evaluating the RCM/UCM.

### 2.2. Simulation approach

For simulating  $T_{mrt}$  building-resolving and city-wide, we combined two different models. The coupled RCM/UCM provided meteorological input data to be used in the micro-scale model SOLWEIG. SOLWEIG is then used to simulate micro-scale modifications of radiation fluxes due to urban geometry and hence estimate  $T_{mrt}$  at building-resolving resolution.



### 2.2.1. Incorporation of meso-scale atmospheric conditions

Different regional atmospheric models could provide spatially resolved atmospheric data as meteorological input for calculating  $T_{mrt}$ . We used results from a simulation by Schubert and Grossman-Clarke (2013) that has already been conducted and found as plausible in Berlin. The simulation of the urban atmosphere were conducted with the mesoscale atmospheric model COSMO-CLM coupled with the Double Effect Parameterization Scheme (DCEP) (Rockel et al., 2008; Schubert et al., 2012). DCEP (Schubert et al., 2012) is a multi-layer UCM based on the Building-Effect-Parameterization (BEP) scheme (Martilli et al., 2002). In COSMO-CLM/DCEP, the urban fraction of a meso-scale model grid cell covered by impervious surfaces is conceptualised as multiple series of identical street canyon elements. These elements are characterised by their building and street width as well as their building height and street direction distribution. As described in detail in Schubert and Grossman-Clarke (2013), these parameters and the urban fraction were derived for each  $1 \times 1 \text{ km}^2$  grid cell of Berlin from an extensive 3-D building data set of Berlin. Other urban surface parameters (emissivity, thermal diffusivity, roughness length) were the default values as proposed in Martilli et al. (2002). The albedo for roof and street surfaces, though, were based on hyperspectral measurements (Roessner et al., 2011). Furthermore, volumetric heat capacity was increased. The non-urban, natural surface fractions of a meso-scale grid cell were treated by the original land surface scheme of COSMO-CLM. Its parameters were taken from the pre-processor of COSMO-CLM (Smiatek et al., 2008). Where necessary, Schubert and Grossman-Clarke (2013) adjusted these parameters to represent the non-urban part of the grid cell only. The data set has a grid spacing of  $1 \times 1 \text{ km}^2$ . For the usage as input data in the micro-scale model SOLWEIG, the data set was interpolated between central grid points linearly to match the building-resolving grid spacing (5 m). Such a simplified method without considering land cover assumes that air temperature differences are low within an area of  $1 \text{ km}^2$ .

Air temperature at 2 m is interpolated between the average surface temperature and the air temperature of the lowest model level (at a height of approx. 10 m). Here, the average surface temperature is the weighted average of temperatures of the natural surfaces and the street surfaces. The atmospheric temperatures are assumed equal for both tiles of the grid cell. Due to the multi-layer approach of DCEP, the urban influence on the 2 m temperature represents conditions within the canopy, which is also required as input in SOLWEIG.

Since RCM/UCM forms the basis for simulating  $T_{mrt}$ , its quality is important in terms of variables relevant for  $T_{mrt}$ . A high accordance of air temperature and net radiation regarding observational sites in Berlin and Berlin's surrounding was detected by Schubert and Grossman-Clarke (2013), but we additionally examined the skills with Root Mean Square Deviation (RMSD) and Mean Deviation (MD) with reference to air temperature, specific humidity and short-wave radiation for the longer selected period in August 2003. We selected this longer period to include different weather situations for the evaluation. For assessing air temperature, we consulted model performance criteria of  $RMSD \leq 2 \text{ K}$  and  $|MD| \leq 0.5 \text{ K}$  as suggested by Chemel and Sokhi (2012) and Schlünzen and Sokhi (2008). Thresholds for specific humidity and global short-wave radiations were not given there.

We chose all available weather stations during the selected period in Berlin maintained by the German weather service (DWD) (<http://www.dwd.de/klimadaten>), which were also partly used for evaluating RCM/UCM in Schubert and Grossman-Clarke (2013), as well as stations maintained by the Berlin Institute of Technology (TUB) (see Fenner et al., 2014). All used stations by TUB measured air temperature and relative humidity with Vaisala HMP35A, only at the stations DESS and ROTH a PT100 1/3 DIN Class B was operated instead (Table 1). We checked the data quality of stations maintained by TUB by flagging outliers and unrealistic values as described in more detail in Fenner et al. (2014). Data from DWD were already quality-checked products. For each station, we identified corresponding nearest grid points by comparing site characteristics with the urban fraction RCM/UCM (Table 1). Observations of short-wave radiation in Berlin were only available at two sites in summer 2003: ROTH (CNR4 by Kipp & Zonen) and JAGE (star pyranometer by Lambrecht) (Table 1). As a reference site, we used site REF located at a former airport in Berlin, because in many cities weather stations are only available at airports.

**Table 1**

Overview of weather stations in Berlin used for evaluating RCM/UCM operated by the German Weather Service (DWD) or by the Berlin Institute of Technology (TUB). Site characteristics are averaged values based on digital surface models within a 500 m radius around the station. Building fraction includes only built-up surface fractions. Paved surface fraction is estimated as a residual ( $1 - \text{building fraction} - \text{vegetation fraction} - \text{water fraction}$ ).

Site (Operator)	Longitude	Latitude	Building fraction (%)	Vegetation fraction (%)	Water fraction (%)	Paved surface fraction (%)	Building height (m)	Vegetation height (m)	Local climate zone
REF (DWD)	13.4021	52.4674	6	66	0	28	10	1	Low plants
ADLR (TUB)	13.5314	52.4295	17	36	4	43	13	2	Open midrise
ALBR (TUB)	13.3486	52.4447	17	59	3	21	12	7	Sparsely built
DAHF (TUB)	13.2252	52.4777	0	98	0	2	0	15	Dense trees
DESS (TUB)	13.3783	52.5045	27	30	3	40	21	6	Open midrise
FUBE (DWD)	13.3101	52.4578	17	63	0	20	11	8	Sparsely built
JAGE (TUB)	13.2251	52.4732	0	96	0	4	0	15	Dense trees
KPNK (TUB)	13.6157	52.4330	0	87	12	1	7	14	Dense trees
ROTH (TUB)	13.3158	52.4572	24	50	0	26	15	8	Open midrise
SPAN (TUB)	13.1584	52.5364	16	39	0	45	6	2	Sparsely built
TEGL (DWD)	13.3088	52.5644	6	61	0	33	11	2	Bush, shrub
TIER (TUB)	13.3636	52.5145	2	82	6	10	13	13	Dense trees

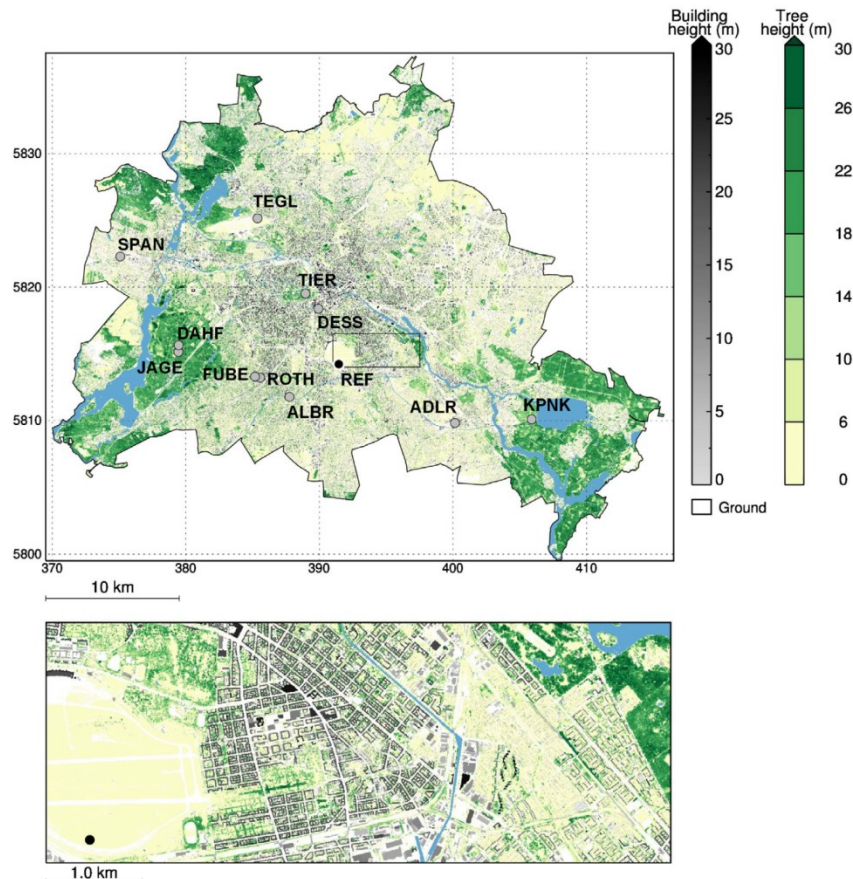


These twelve stations belong to different Local Climate Zones (LCZ) (Stewart and Oke, 2012) and thus represent some heterogeneity in Berlin (Table 1). Other LCZs, such as compact midrise, might also exist in Berlin, but are not covered by the weather stations. Note, for a rough estimation of LCZ, we included only building and vegetation fraction and height, and not all recommended factors (Stewart and Oke, 2012).

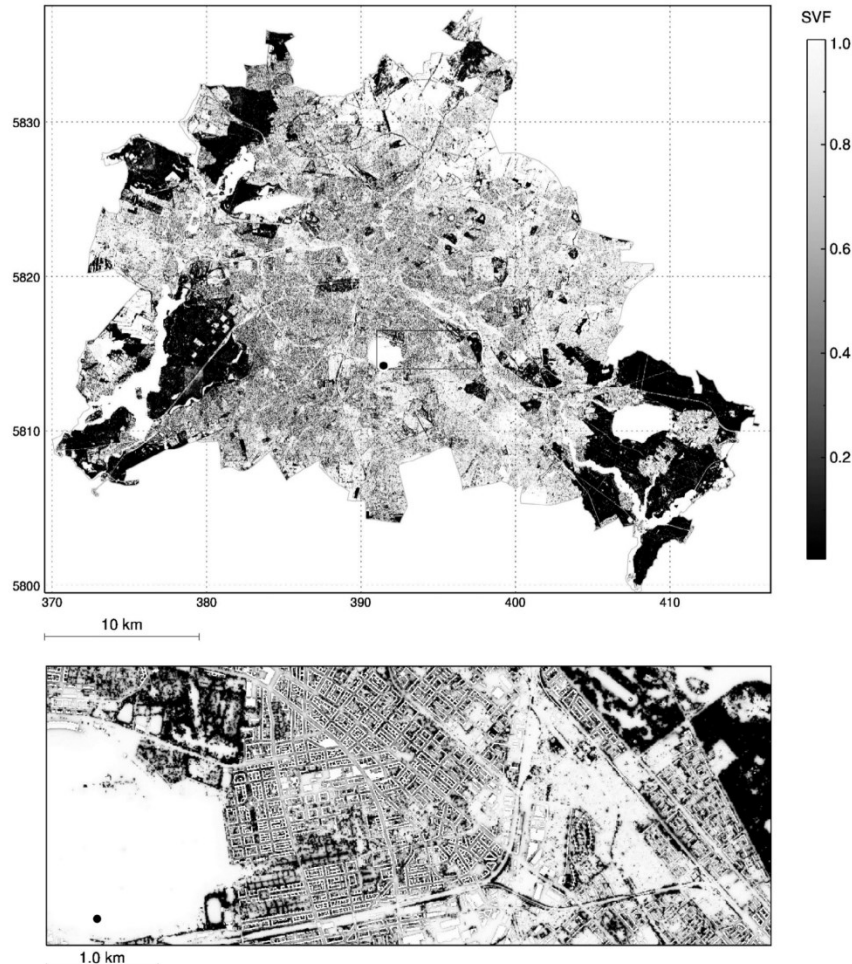
### 2.2.2. Incorporation of micro-scale urban structures

To simulate  $T_{mrt}$ , we applied the radiation model SOLWEIG, which estimates  $T_{mrt}$  and long- and short-wave radiation in six directions (upward, downward and the four cardinal points) (Lindberg and Grimmond, 2011a; Lindberg et al., 2008).  $T_{mrt}$  is simulated according to VDI (1994), but short-wave radiation components are estimated from short-wave downward radiation, and long-wave radiation components are estimated from air temperatures (Lindberg et al., 2008). For these simulations, meteorological input data of air temperature, relative humidity and global radiation or direct and diffuse short-wave radiation is required, as well as spatial information of building and vegetation heights represented by digital surface models (DSM) (Fig. 1). Furthermore, SOLWEIG calculates  $T_{mrt}$  by using view angles and sky view factors (SVF) (Fig. 2) together with shadowing patterns and empirical equations. SOLWEIG has been found to estimate  $T_{mrt}$  (average RMSD = 4.23 K) reliably in different cities including Berlin (e.g. as summarised by Jänicke et al., 2015).

For this study, we applied a new subversion of the SOLWEIG 2013a model (Lindberg et al., 2011) that is able to use gridded meteorological input data to represent weather situations and urban climates. DSMs of buildings and vegetation with a



**Fig. 1.** Model domain of SOLWEIG, with building and vegetation heights in Berlin (based on digital surface models with 5 m grid spacing) and used weather stations. Zoomed area shows details for the reference site and for a variety of urban structures. The exterior space indicates areas beyond the administrative area of Berlin for which DSMs were unavailable. Note, waters (coloured blue) and vegetation below 2 m were not included in SOLWEIG, but are also shown for clarity. (For interpretation of the references to colour in this figure legend, the reader is referred to the web version of this article.)



**Fig. 2.** Sky view factors (SVF) for vegetation and buildings as calculated by SOLWEIG for the model domain, average SVF = 0.60. The circle indicates the position of the weather station, REF. Zoomed area shows details for REF and for a variety of urban structures.





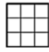












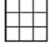
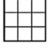

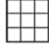
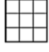
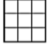
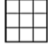
grid spacing of 5 m provide the heights of micro-scale urban structures (Senate Department for Urban Development and Environment Berlin, 2014) (<http://www.stadtentwicklung.berlin.de/umwelt/umweltatlas/el610.htm>) (Fig. 1). We excluded vegetation below 2 m, because these vegetation types hardly influence shadow pattern. To simulate the entire area of Berlin, we divided the city into  $47 \times 38$  tiles of  $1200 \text{ m} \times 1200 \text{ m}$ . These tiles overlap by 200 m at each edge, so that we could use  $1000 \text{ m} \times 1000 \text{ m}$  of each tile to avoid boundary effects due to higher SVF factors and artificially modified shadow patterns. We applied the following parameters: albedo (walls, ground and roof) = 0.20, transmissivity of short-wave radiation through vegetation = 0.05, wall emissivity = 0.9 and ground emissivity = 0.95. For all analyses, we excluded roof areas, because they are of minor relevance for outdoor human bioclimate.


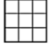
We performed six experiments (Table 2): The reference experiment (STD) used ungridded air temperature, relative humidity and direct and diffuse radiation based on the grid point of the RCM/UCM closest to weather station REF. We defined this ungridded experiment as the reference, because gridded meteorological data are usually unavailable with an appropriate resolution at a city-scale.

The next experiment (STD\_g) applied also only ungridded meteorological data, but received global radiation instead of direct and diffuse radiation as input data (Section 3.1). We performed this experiment to represent a case, which might occur often, where data of direct and diffuse radiation are unavailable. When only global radiation is used, SOLWEIG calculates

**Table 2**

Overview of performed experiments for analysing the sensitivity of  $T_{mrt}$  to global radiation ( $STD_g$ ) and to gridded meteorological data ( $GRD_{ta}$ ,  $GRD_{ta,rh}$  and  $GRD_{ta,rh,sw}$ ) as differences to standard approach ( $STD$ ).

Experiment	Urban structures	Air temperature (°C)	Relative humidity (%)	Direct & diffuse short-wave radiation ( $W/m^{-2}$ )	Global radiation ( $W/m^{-2}$ )
<i>Reference</i>					
<i>STD</i>					
<i>Sensitivity to global radiation instead of direct and diffuse radiation</i>					
<i>STD_g</i>					
<i>Sensitivity to one-point calculation (SOLWEIG1D)</i>					
<i>STD_1P</i>					
<i>Sensitivity to spatially distributed meteorological input</i>					
<i>GRD_ta</i>					
<i>GRD_ta,rh</i>					
<i>GRD_ta,rh,sw</i>					

 represents one-dimensional input from the associated grid point of the reference site.  
 represents gridded meteorological input of the variable.

direct and diffuse radiation internally. With  $STD_g$ , we assessed the difference in  $T_{mrt}$  between the approaches used in SOLWEIG and RCM/UCM for estimating the partitioning of direct and diffuse radiation from global radiation. In SOLWEIG, a relatively simple empirical method by Reindl et al. (1990) is applied. With the Reindl approach, the fraction of diffuse radiation is estimated based on clearness index, solar altitude, ambient temperature and relative humidity. This approach is well established, but simplified for applying with commonly available variables. In RCM/UCM, direct and diffuse radiation are simulated based on radiative transfer equations parameterised with the two-stream method (Ritter and Geleyn, 1992). Thereby, different atmospheric constituents such as aerosols, ozone, carbon dioxide and trace gases as well as vapour pressure are considered in every vertical layer. Hence, the approach applied in RCM/UCM is much more complex than the one used in SOLWEIG. Both approaches have been evaluated and found as plausible in other regions (Davin and Seneviratne, 2012; Jacovides et al., 2006; Kamali et al., 2005; Noorian et al., 2008; Schubert and Grossman-Clarke, 2014), but a direct comparison with observations in Berlin is so far not possible, because observations of direct and diffuse radiation are not available in Berlin.

The next four experiments focus on the influence of urban structures and the meso-scale weather situation. In order to assess the influence of micro-scale urban structures (vegetation and buildings), we performed an experiment ( $STD_{1P}$ ) for one point at sites REF with SOLWEIG1D. In this experiment, vegetation and building heights, and derived characteristics were parameterised by an averaged SVF of 0.6. Thus, we were able to compare a very simple, with the more elaborate and time-consuming approach ( $STD$ ) that includes the DSM of vegetation and buildings.

In the last three experiments gridded meteorological data of air temperature ( $GRD_{ta}$ ), relative humidity ( $GRD_{ta,rh}$ ) and direct and diffuse radiation ( $GRD_{ta,rh,sw}$ ) was incrementally considered to assess the sensitivity of  $T_{mrt}$  to these data (Section 3.2). In these experiments the sensitivity of  $T_{mrt}$  to meso-scale atmospheric conditions and urban modifications was evaluated. Long-wave radiation is not a meteorological input in SOLWEIG2013a and was therefore neglected in this study.



We examined the sensitivity of  $T_{mrt}$  in the experiments by analysing spatial patterns of deviations between the experiments during midday and midnight and by calculating two metrics: The mean deviation ( $\Delta_{MEAN}$ ) (K) assesses the average changes between  $T_{mrt}$  simulated by  $STD$  ( $T_{mrtSTD}$ ) and each of the other experiments ( $T_{mrtExp}$ ). We calculated the arithmetic mean of the difference of both experiments ( $\Delta_{MEAN} = (\overline{T_{mrtExp}} - \overline{T_{mrtSTD}})$ ). Maximum deviations ( $\Delta_{|MAX|}$ ) (K) were quantified with the 95th percentile ( $P_{95TH}$ ) of the absolute deviations ( $\Delta_{|MAX|} = P_{95TH}|\overline{T_{mrtExp}} - \overline{T_{mrtSTD}}|$ ).

### 3. Results and discussions

#### 3.1. Evaluation of city-wide meteorological input data for simulating $T_{mrt}$

We detected that RCM/UCM replicated variables relevant for simulating  $T_{mrt}$  with only few deviations from weather stations in Berlin, averaged during a period of 20 days (Table 3) as well as in terms of diurnal variation for the selected day (Fig. 3).

Air temperature exhibited low *RMSD* and *MD* for the longer period (from 30 July 2003 to 18 August 2003) (Table 3). *MD* was below the threshold of 0.5 K at most station and on average; *RMSD* was below or only slightly above the thresholds at some stations and on average. Larger deviations occurred regarding air temperature at some sites located within dense trees, namely *JAGE*, *DAHF*, *KPNK*, and within an open midrise local climate zone, namely *DESS* (Table 3). For air temperature larger deviations between the RCM/UCM and actual observations emerged during night-time than during daytime on the selected day (Fig. 3a).

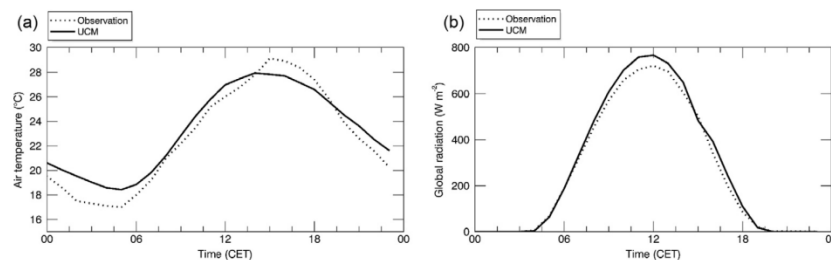
With respect to specific humidity, *RMSD* fluctuated around 2 g/kg and *MD* around 0.75 g/kg between the stations (Table 3). Deviations in global radiation between RCM/UCM and observations at *ROTH* and *JAGE* were also acceptable for the longer period (Table 3) and for the selected day (Fig. 3b).

For the longer period, deviations in global radiation could be caused by differences in cloud patterns between simulations and observations. For instance, small cloud banks might have not been reproduced by the RCM/UCM. Furthermore, on the selected day the RCM/UCM overestimated midday global radiation in this study, which was also detected (about  $50 \text{ W m}^{-2}$ ) in Basel, Switzerland by Schubert and Grossman-Clarke (2014). Regarding air temperature, findings by

**Table 3**

Evaluation of RCM/UCM against observations. Averaged deviation in terms of Root Mean Square Deviation (*RMSD*) and Mean Deviation (*MD*) are presented based on hourly data from 3 August 2003 to 18 August 2003.

Site	Air temperature (°C)		Specific humidity (g/kg)		Global radiation ( $\text{W m}^{-2}$ )	
	<i>RMSD</i>	<i>MD</i>	<i>RMSD</i>	<i>MD</i>	<i>RMSD</i>	<i>MD</i>
REF	1.76	0.00	1.83	0.63		
ADLR	2.19	0.39	1.85	0.87		
ALBR	2.50	−0.46	2.47	1.83		
DAHF	2.19	−0.34	1.79	0.93		
DESS	3.58	0.26	2.96	−0.86		
FUBE	1.59	0.57	2.01	1.63		
JAGE	2.43	0.72	2.27	−0.34	72.78	16.79
KPNK	2.22	−0.55	2.01	0.95		
ROTH	1.87	0.06	2.20	1.54	67.61	−8.01
SPAN	2.61	0.60	2.19	1.00		
TEGL	1.87	0.58	1.88	0.08		
TIER	1.71	0.41	1.79	0.68		
Average	2.21	[0.41]	2.11	[0.74]	70.20	[12.4]



**Fig. 3.** Comparison between RCM/UCM and observation of variables relevant for calculating  $T_{mrt}$  on 5 August 2003. Air temperature (at 2 m) is visualised at REF site (a) and global radiation (b) at ROTH site, which is the nearest site to REF with global radiation data.

Schubert et al. (2012) and this study are consistent with high degree of accuracy at day between the RCM/UCM and observations, and with overestimations at night. *RMSD* and *MD* also showed similar ranges (around 2 K) in this study and in results by Schubert and Grossman-Clarke (2013). The larger deviations in air temperature and specific humidity at some sites could be attributed to different reference points for the observations and RCM/UCM. Observations were conducted at a height of about 2 m and are influenced by micro-climate, whereas RCM/UCM simulates conditions for the centre of each grid cell. Thus, micro-scale influences on weather stations may not be captured with 1 km grid spacing.

In sum we hold that, despite some deviations and discrepancies, RCM/UCM reproduced variables relevant for simulating  $T_{mrt}$  sufficiently and therefore, does seem to provide reliable city-wide meteorological input for simulating  $T_{mrt}$  in Berlin. These conclusions, however, are limited to the considered weather stations and LCZs, which do not cover all characteristics in Berlin. Nevertheless, we believe that it is reasonable to assume a similar accuracy for other LCZs.

### 3.2. Sensitivity of $T_{mrt}$ to the partitioning of direct and diffuse radiation

Before the sensitivity of  $T_{mrt}$  to spatially gridded meteorological input is analysed, we present the sensitivity regarding separate consideration of direct and diffuse short-wave radiation. For this purpose, we examined the differences between the experiments *STD\_g* and *STD*.

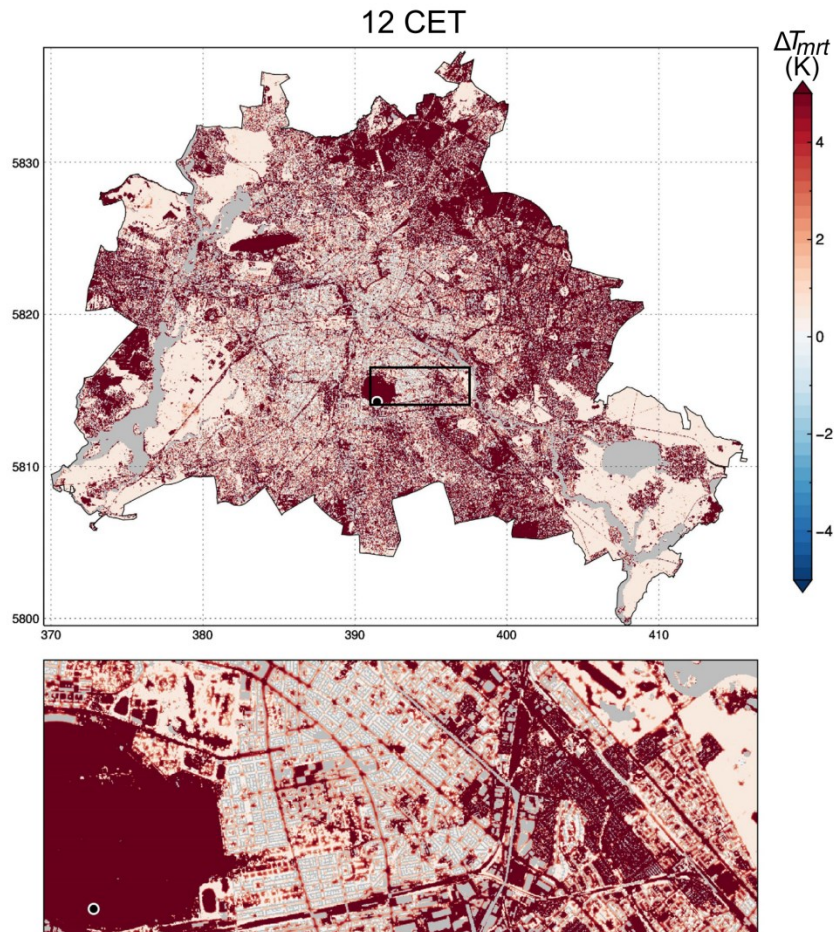
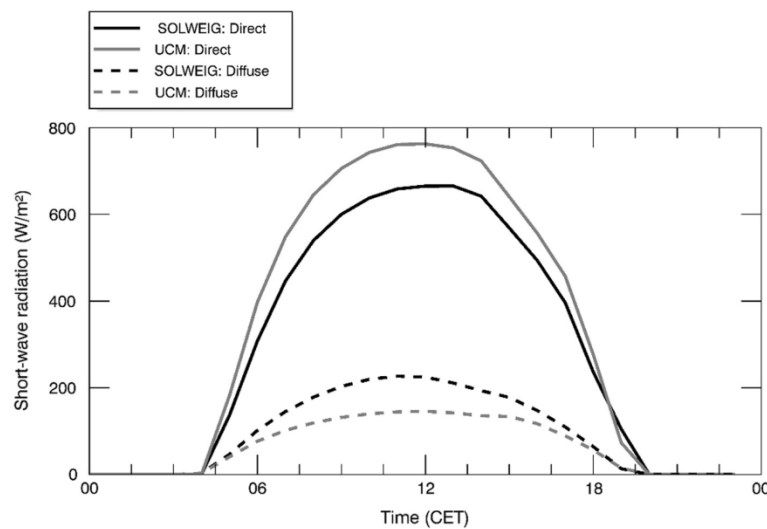


Fig. 4. Differences in  $T_{mrt}$  (K) between experiment *STD\_g* and *STD* ( $\Delta T_{mrt} = STD_g - STD$ ) at day (12 CET) on 5 August 2003. The circle indicates the position of the weather station *REF*. Zoomed area shows details for *REF* and for a variety of urban structures. Roof and water areas are excluded and colored in grey.

**Table 4**Daily mean ( $\Delta_{\text{MEAN}}$ ) and maximum absolute deviations ( $\Delta_{\text{MAX}}$ ) in  $T_{\text{mrt}}$  between the experiments *STD\_g* and *STD* on 5 August 2003.

CET (h)	$\Delta_{\text{MEAN}}$ (K)	$\Delta_{\text{MAX}}$ (K)
00–05	−0.48	1.08
06–11	0.19	7.76
12–17	0.24	7.36
18–23	−0.92	2.02
Mean	−0.24	4.56

**Fig. 5.** Comparison of direct and diffuse radiation simulated by SOLWEIG (experiment *STD\_g*) and by RCM/UCM (experiment *STD*) on 5 August 2003.

We determined that  $T_{\text{mrt}}$  simulated by SOLWEIG was highly sensitive to the usage of direct and diffuse radiation instead of global radiation during the day.  $T_{\text{mrt}}$  was higher in experiment *STD\_g* with global radiation than in *STD* with direct and diffuse radiation (Fig. 4). Particularly in large open areas  $T_{\text{mrt}}$  increased strongly, whereupon the areas within forests show the lowest alterations, such as the ones in southeast and southwest. The large sensitivity is also visible in terms of maximum difference ( $\Delta_{\text{MAX}}$ ) in Table 4.

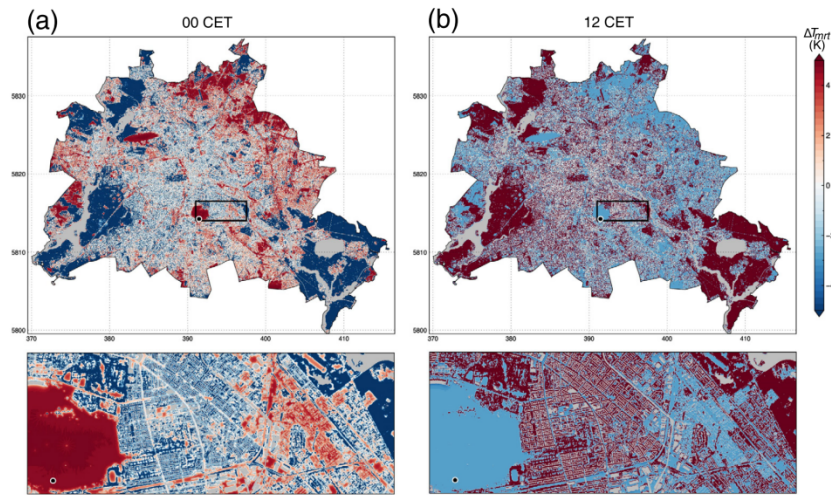
Main cause of these differences was the changed partitioning of direct and diffuse radiation in *STD\_g* compared to *STD* (Fig. 5). As explained in the method Section 2.2.2, the approaches for calculating direct and diffuse radiation differ clearly between SOLWEIG (*STD\_g*) and RCM/UCM (*STD*). The fraction of direct short-wave radiation was higher in *STD\_g* than in *STD* on the selected day (Fig. 5), which led to higher  $T_{\text{mrt}}$  particularly at open areas, where direct radiation was not blocked by urban structures. In other areas with more buildings or vegetation, the influence of the partitioning was smaller, because short-wave radiation is anyhow scattered and reduced due to urban obstacles. Moreover, Lindberg et al. (2014) tested the effect of reduced global radiation on  $T_{\text{mrt}}$  and thus recalculated direct and diffuse radiation in SOLWEIG. They also detected that the partitioning influences the pattern of  $T_{\text{mrt}}$ . The general reason for the high sensitivity of  $T_{\text{mrt}}$  to the partitioning of direct and diffuse radiation is, that short-wave radiation fluxes are the main quantities for simulating  $T_{\text{mrt}}$  under sunny conditions (Höppe, 1992; Kántor and Unger, 2011).

As a consequence of this high sensitivity, observation of direct and diffuse radiation, for instance with sunshine-pyranometers, could be beneficial to determine the actual partitioning in Berlin and to identify a suitable simulation approach. In the absence of observation for evaluation, we decided to use the more complex scheme of RCM/UCM in the following sections and thus *STD* as a basis. In summary, we confirmed that  $T_{\text{mrt}}$  was highly sensitive to the partitioning of direct and diffuse short-wave radiation. Therefore, we suggest that special attention to reliable data of direct and diffuse radiation should be paid for simulating  $T_{\text{mrt}}$ .

### 3.3. Sensitivity of $T_{\text{mrt}}$ to gridded urban structures

The purpose of this chapter is to assess the influence of urban structures, represented by DSM of building and vegetation, on  $T_{\text{mrt}}$  by comparing experiments *STD* and *STD\_1p*. The comparison of the two experiments revealed large differences at





**Fig. 6.** Differences in  $T_{mrt}$  (K) between experiment  $STD_{1p}$  and  $STD$  ( $\Delta T_{mrt} = STD_{1p} - STD$ ) at night (00 CET) (a) and day (12 CET) (b) at 5 August 2003. The circle indicates the position of the weather station, *REF*. Zoomed area shows details for *REF* and for a variety of urban structures. Roof and water areas are excluded and colored in grey.

**Table 5**  
Daily mean ( $\Delta_{MEAN}$ ) and maximum absolute deviations ( $\Delta_{MAX}$ ) in  $T_{mrt}$  between the experiments  $STD$  and  $STD_{1p}$  at 5 August 2003.

CET (h)	$\Delta_{MEAN}$ (K)	$\Delta_{MAX}$ (K)
00–05	–1.14	6.69
06–11	6.90	18.65
12–17	8.36	20.55
18–23	–0.72	6.78
Mean	3.35	13.17

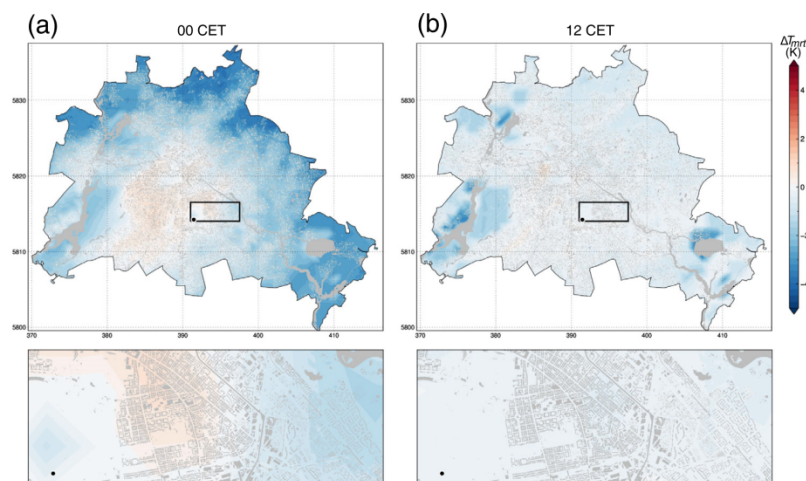
night and day (Fig. 6). At night,  $STD$  produced a large variability in  $T_{mrt}$ , whereas open areas exhibited lower temperatures, and densely built-up or vegetated areas exhibited higher temperatures compared to the simulation for the one point in experiment  $STD_{1p}$  (Fig. 6a). At day, this pattern reversed (Fig. 6b). High sensitivity of  $T_{mrt}$  to urban structures is also visible in terms of aggregated metrics (Table 5). Maximum differences ( $\Delta_{MAX}$ ) of up to 20 K occurred at daytime; mean differences ( $\Delta_{MEAN}$ ) were considerably lower (up to 8 K).

A possible explanation for the strong separation in areas with high and lower  $T_{mrt}$  could be the SVF. As  $STD_{1p}$  uses only one value for SVF (of 0.6), areas below and above this values performed contrary. Particularly at day, SVF and shadow pattern influence  $T_{mrt}$  leading to distinct differences (Lindberg et al., 2008). One unanticipated finding was that areas with few deviations only occurred at night, but at day most grids showed either over- or underestimations (Fig. 6). Furthermore, these over- and underestimations did not balance each other, but  $T_{mrt}$  was higher in  $STD_{1p}$  than in  $STD$  (Table 5).

The results implicated that including urban structures is important for assessing  $T_{mrt}$  and biometeorological indices. For example, considering the spatial variability of urban structures might enhance the understanding of intra-urban patterns of heat-stress related mortality. Studies that have analysed the statistical relation between mortality and PET or  $T_{mrt}$  based on simulations for one point or a small sample within the city (e.g. Nastos and Matzarakis, 2012; Thorsson et al., 2014), might gain further knowledge when considering urban structures and simulate  $T_{mrt}$  city-wide.

3.4. Sensitivity of  $T_{mrt}$  to spatially resolved meteorological data

For assessing the sensitivity to spatially gridded meteorological data, we again used the experiment  $STD$  as a reference. With this approach, we examined that  $T_{mrt}$  was especially sensitive to spatially distributed air temperature during night. Spatially distributed air temperature from RCM/UCM ( $GRD_{ta}$ ) exhibited clear modifications in  $T_{mrt}$  compared to  $STD$  with air temperature from site *REF*. At midday,  $T_{mrt}$  decreased slightly compared to  $STD$  around water surfaces in suburban areas



**Fig. 7.** Differences in  $T_{mrt}$  (K) ( $\Delta T_{mrt} = GRD\_ta - STD$ ) between the experiments *STD* and *GRD\_ta* at midnight (00 CET) (a) and midday (12 CET) (b) on 5 August 2003. The circle indicates the position of the weather station, *REF*. Zoomed area shows details for *REF* and for a variety of urban structures. Roof and water areas are excluded and colored in grey.

**Table 6**

Daily mean ( $\Delta_{MEAN}$ ) and maximum absolute ( $\Delta_{|MAX|}$ ) deviations of  $T_{mrt}$  between the experiments *STD* and *GRD\_ta*, *GRD\_ta,rh* and *GRD\_ta,rh,sw* on 5 August 2003.

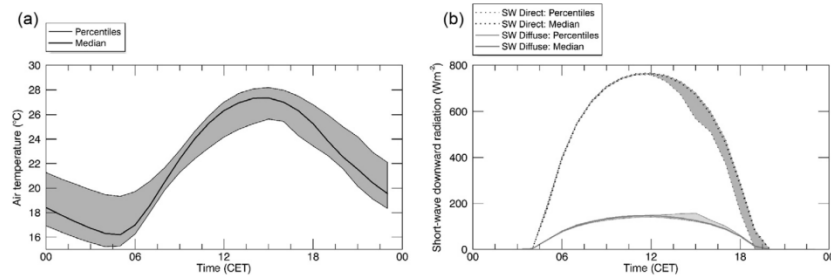
Experiment	CET (h)	$\Delta_{MEAN}$ (K)	$\Delta_{ MAX }$ (K)
<i>GRD_ta</i>	0–5	–1.61	3.23
	6–11	–0.57	1.35
	12–17	–0.59	1.84
	18–23	–1.38	2.86
	Mean	–1.04	2.32
<i>GRD_ta,rh</i>	0–5	–1.46	2.99
	6–11	–0.50	1.31
	12–17	–0.51	1.75
	18–23	–1.22	2.63
	Mean	–0.92	2.17
<i>GRD_ta,rh,sw</i>	0–5	–1.45	2.98
	6–11	–0.48	1.32
	12–17	–0.43	1.75
	18–23	–1.25	2.71
	Mean	–0.90	2.19

(Fig. 7), whereas at night a stronger alteration due to UHI was visible. As a result of the UHI, differences in  $T_{mrt}$  in *GRD\_ta* were positive in the built-up city-centre and negative in the suburban surrounding compared to *STD* (Fig. 7). The effect of spatially resolved air temperature was low on spatial average ( $\Delta_{MEAN}$ ), but high for individual grids ( $\Delta_{|MAX|}$ ) (Table 6).

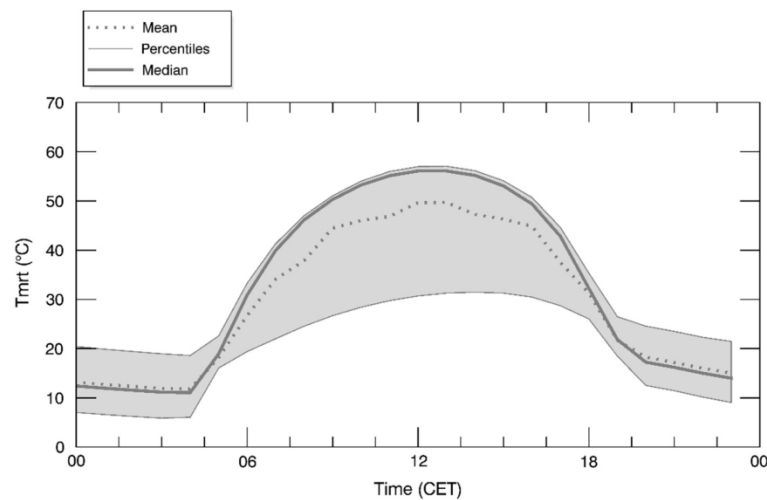
High sensitivity of  $T_{mrt}$  simulated by SOLWEIG to air temperature was also detected by Onomura et al. (2015), who found a nearly linear relationship between air temperature and  $T_{mrt}$ , where 1 K deviation in air temperature leads to 0.84 K changes in  $T_{mrt}$ . As explained earlier, air temperature is used in SOLWEIG for estimating long-wave radiation and has therefore a large influence on  $T_{mrt}$ . At day, however, air temperature simulated by RCM/UCM exhibited less variability (Fig. 8a) and less distinct patterns than at night, with exceptions of waters, which led to few deviations in  $T_{mrt}$ . At night, the range of air temperatures was larger probably due to UHI effects (Fig. 8a). Owing to the high sensitivity and intra-urban variability, we summarise that spatial distribution of air temperature should be considered when simulating  $T_{mrt}$  for an entire city, especially during the night. The intra-urban variability of air temperature might even be higher than simulated in RCM/UCM due to the rough grid spacing of 1 km (see Section 3.1). In addition, the influence of spatially distributed air temperature might be different and probably higher in other cities, because Berlin has no altitudinal gradient of air temperature due to its flat terrain, and thus, only relative, little variability of air temperature during the day.

Additionally spatially distributed input data on relative humidity (*GRD\_ta,rh*) did not produce any visible extra effects (therefore not shown) and only minor alteration in  $\Delta_{MEAN}$  and  $\Delta_{|MAX|}$  (Table 6). This result is consistent with findings by





**Fig. 8.** Spatial-temporal variability of meteorological input on 5 August 2003 used in the gridded experiments. Spatial variability is shown by the 5th and 95th percentiles and by the median for air temperature (a) as applied in *GRD\_ta*, *GRD\_ta,rh* and *GRD\_ta,rh,sw* and for direct and diffuse radiation (b) as applied in *GRD\_ta,rh,sw*.

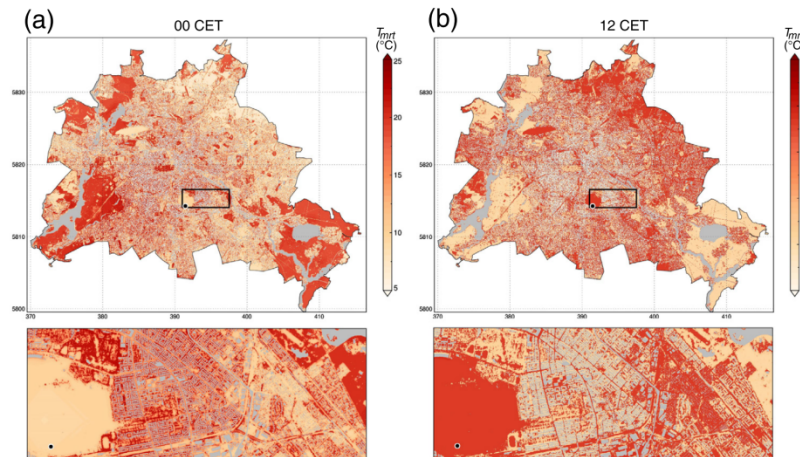


**Fig. 9.** Spatial-temporal variability of  $T_{mrt}$  on 5 August 2003. Spatial variability is shown by the 5th and 95th percentiles and by the median of *GRD\_ta,rh,sw*.

Onomura et al. (2015), who also detected that simulated  $T_{mrt}$  in SOLWEIG is less sensitive to relative humidity than to air temperature. Reason for the low effect is that in SOLWEIG relative humidity is only used for estimating the emissivity of the sky to simulate incoming long-wave radiation and in the Reindl approach (Lindberg et al., 2008).

Spatially distributed direct and diffuse short-wave radiation (*GRD\_ta,rh,sw*) also revealed negligible extra effects (Table 5) as spatial variability in short-wave radiation was low on the selected cloud-free day (Fig. 8b). In general, however, short-wave radiation strongly influences  $T_{mrt}$  as already discussed (Section 3.2). Thus, under cloudy weather situations, the sensitivity will be high and special attention needs to be paid regarding data quality.

Based on the results from the experiments with gridded meteorological input (*GRD\_ta*, *GRD\_ta,rh* and *GRD\_ta,rh,sw*), we recapitulate that for building-resolving and city-wide analyses of  $T_{mrt}$ , the used method of combining SOLWEIG with gridded atmospheric data has served well. Currently, drawbacks of this method are high demands on data storage and computational time, especially for longer periods. Other methods to derive building-resolving and city-wide  $T_{mrt}$  are possible as well: Regression models based on morphological parameters could also be used to estimate  $T_{mrt}$  based on reference stations. Yi et al. (2015) followed this approach to estimate air temperatures at building-resolving resolution. Regression models, however, such as most empirical models lack of transferability to other cities or weather conditions. Another option is in preparation by Lindberg et al. (2015), who simulated the fraction of sunlit facets directly within an UCM, which is applicable for parameterized simulation of  $T_{mrt}$ . To decrease the computing time for meteorological input data, a recently developed coupled model scheme by Onomura et al. (2015) is promising in that it combines a simple slab convective boundary layer model with an urban land surface model. Furthermore, they plan to directly couple this approach with SOLWEIG. In the one-way



**Fig. 10.** Spatial variability of  $T_{mrt}$  (°C) (experiment *GRD\_ta,rh,sw*) at midnight (00 CET) (a) midday (12 CET) (b) on 5 August 2003 simulated with *GRD\_ta,rh,sw*. The circle indicates the position of the weather station, *REF*. Zoomed area shows details for *REF* and for a variety of urban structures. Scaling of bars differs between a and b. Roof and water areas are excluded and colored in grey.

coupling approach we applied here, the spatially distributed meteorological data could also be provided by different types of regional and urban climate models and, thus, past as well as projected atmospheric conditions could be incorporated.

In essence, we demonstrated here the need of spatially distributed meteorological input data for simulating the  $T_{mrt}$  of an entire city to consider realistic weather conditions. From the three tested meteorological variables, relative humidity might not be required spatially resolved due to its low impact on  $T_{mrt}$ .

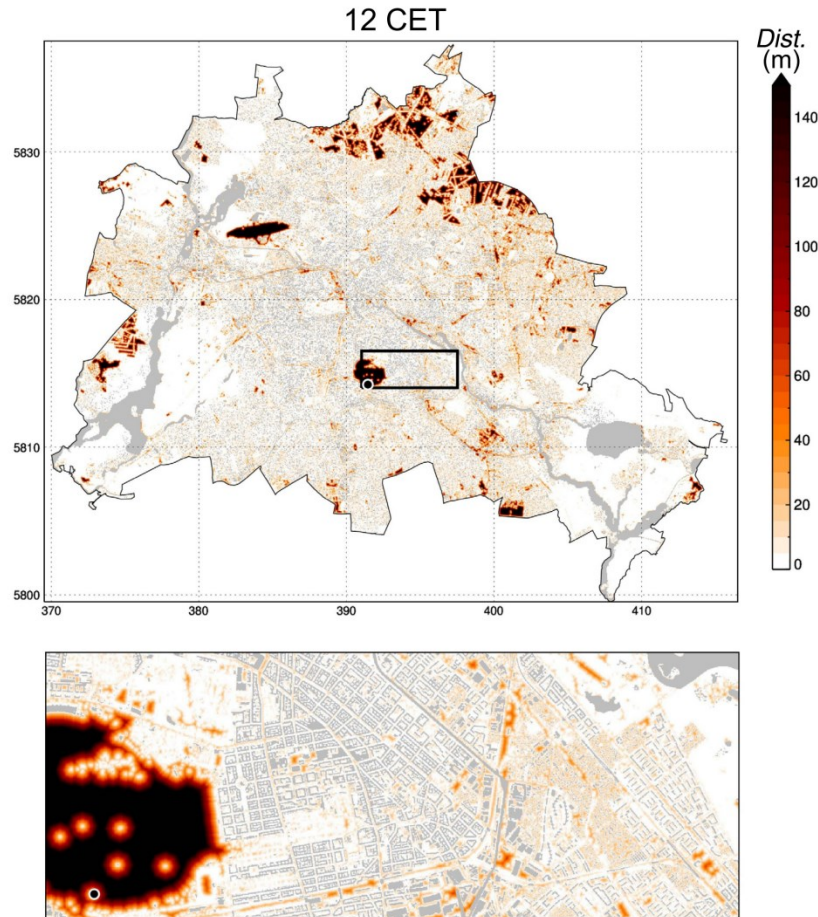
### 3.5. Spatial and temporal variability of $T_{mrt}$ in Berlin

We will now analyse spatial and temporal variability of  $T_{mrt}$  in Berlin, based on the experiment *GRD\_ta,rh,sw* with fully-gridded meteorological input data.

Spatial and temporal variability of  $T_{mrt}$  was high on 5 August 2003, with a large range of values and pronounced daily amplitudes (Fig. 9). The distribution of  $T_{mrt}$  was bimodal, which is also documented by clear differences between arithmetic mean and median (Fig. 9). These results of high spatial variability match those reported in previous studies in summer and under clear-sky conditions (e.g. Lindberg et al., 2014; Thorsson et al., 2011). Lindberg et al. (2014) also determined a bimodal distribution, caused by SVF and shadow patterns. Clustering in groups of shaded and sunlit areas can vanish, when clouds arise and the fraction of the diffuse short-wave radiation component increases (Lindberg et al., 2014).

At night (Fig. 10a), open areas exhibited the lowest  $T_{mrt}$  due to higher levels of emitted long-wave radiation. Patterns of  $T_{mrt}$  are mainly related to SVF (Fig. 2), hence the general patterns that open areas show lower  $T_{mrt}$  is explainable. Large wooded areas tended to have higher  $T_{mrt}$  than urban areas in the simulation, which seems implausible. Reasons for the higher  $T_{mrt}$  in wooded compared to built-up areas could be underestimations of heat storage released by built-up areas and impervious surfaces, and underestimations of nocturnal cooling of vegetated areas in the coupling of RCM/UCM and SOLWEIG. SOLWEIG underestimates nocturnal heat storage release, which leads to underestimated  $T_{mrt}$  during the night (Jänicke et al., 2015). SOLWEIG then estimates  $T_{mrt}$  only differentiated into vegetated and non-vegetated surfaces, without further surface characteristics, such as thermal conductance. RCM/UCM is also not able to represent such micro- to local scale effects within street canyons explicitly due to its 1 km grid spacing. Hence some effects, like local thermal circulation systems, which are at subscale in RCM/UCM and not considered in SOLWEIG, remain unconsidered in our approach. Therefore, the results need to be interpreted with caution as the actual intra-urban variability might be larger than simulated. Future studies may use meteorological input with higher grid spacing than 1 km to avoid some of these problems. This study was limited to assess relative changes between the experiments and discussing general pattern, but errors might also be evaluated based on observation of  $T_{mrt}$  in a follow-up study.

The pattern was reversed from night to day. Spatial pattern of  $T_{mrt}$  at day were divided in sunlit and shaded areas (Fig. 10b), with the cause of shadow (building or vegetation) being almost irrelevant. Thus, an urban cool island of  $T_{mrt}$  established during the day, with the highest values being in open inner-city areas (e.g. airports and water surfaces) as well as in sparsely built-up areas at the outskirts, which has also been mentioned by Lau et al. (2015). Furthermore, this pattern might correspond to findings by Schuster et al. (2014), who showed that heat-related deaths occurred not only in the inner-city



**Fig. 11.** Distance (Dist.) (m) to sites with  $T_{mrt}$  lower than the threshold of 55.5 °C of  $T_{mrt}$  on 5 August 2003 at midday (12 CET). The circle indicates the position of the weather station, REF. Zoomed area shows details for REF and for a variety of urban structures. Roof and water areas are excluded and colored in grey.

neighbour-hoods, but also in suburban areas. Relations between intra-urban variability of heat stress risks and  $T_{mrt}$ , however, are not yet performed in Berlin. Particularly in those open spaces with high  $T_{mrt}$  values, planting trees to increase shaded area could be effective to reduce heat stress, as already discussed in a number of studies (Bowler et al., 2010; Lindberg and Grimmond, 2011b; Thorsson et al., 2011).

In order to reduce  $T_{mrt}$ , and thus heat stress hazard, shadowing is very effective under sunny conditions. However, in mid-latitude cities shadowing the whole city is of course undesirable, because of the changed climate conditions in the other seasons. One possibility to identify priority areas for measures to reduce heat stress hazards are distance maps, which highlight areas with long distance to lower  $T_{mrt}$ . For example, if one just need to change the side of the street to reduce the heat stress hazard countermeasures may not be required; if one has to walk for a longer distance to find cooler conditions countermeasures seem to be more valuable.

Thus, we created a distance map to visualise the distance (in m) to reach a place with  $T_{mrt}$  below a certain threshold. As universal categories of  $T_{mrt}$  do not exist, we chose a threshold of 55.5 K, which was found to increase mortality risks in Gothenburg, Sweden by 5% according to Thorsson et al. (2014). Note that the findings from Gothenburg are not directly transferable to Germany, but we used this threshold just to demonstrate an application. Thereby, clear patterns became visible (Fig. 11). Inner-city airports (north-west and middle) and other open spaces with few or low trees like allotments emerged visibly with a large distance. Water surfaces were excluded in the distance map. Additional areas with large distances to walk were located at the edges of the city, particularly in the north-east, as already discussed. According to the



sensitivity studies in Section 3.3 and 3.4, the patterns are strongly related to urban structures and to a much smaller extend to intra-urban variability of meteorological conditions. Nevertheless, the maps (Figs. 10 and 11) only present a single day with its specific weather situations, which impede drawing robust conclusions for other periods. Future analyses of  $T_{mrt}$  may include several extreme heat events to advance this sensitivity and feasibility study. In addition, vulnerability to heat stress might be included in future studies with information about population density, population structure and land use (e.g. Dugord et al., 2012). For example, some areas at the edge of Berlin are inhabited by one of the largest fraction of elderly people, who are especially vulnerable to heat stress (Scherber et al., 2014), while other areas might have few relevance for assessing heat stress (e.g. inaccessible areas like airports).

#### 4. Conclusions

All in all, we showed that coupling SOLWEIG with spatially resolved meteorological data is feasible and useful for simulating  $T_{mrt}$  city-wide and building-resolving. We detected that the intra-urban variability of air temperature and short-wave radiation should be considered to incorporate micro- to local scale urban modifications and mesoscale weather conditions. Furthermore, the portioning of direct and diffuse radiation strongly influences  $T_{mrt}$  simulated by SOLWEIG, which indicate a need of model evaluation with observations. The large range of  $T_{mrt}$  values within the city demonstrated that analyses just based on one single point or small samples might not be able to represent the determined variability. This variability, caused by micro-scale urban geometry, local-scale effects of urban climate and meso-scale weather conditions, needs to be included to identify hazardous spaces during extreme heat events. Furthermore, we detected that city-wide pattern of  $T_{mrt}$  were characterised by the highest values at daytime at the edge of the city and open spaces.

Moreover, we hold that city-wide and building-resolving analyses (like the distance maps) can fulfil the criteria of comprehensive and spatially distributed information required for climate-sensitive urban planning (Mills et al., 2010; Norton et al., 2015).

#### Acknowledgements

We thank our colleagues, in particular Daniel Fenner, Hartmut Küster and Ingo Suchland, for support during analyses and observations. Furthermore, we are grateful for the helpful advices by the anonymous reviewers. For the provision of data, we thank the city of Berlin for supplying digital surface models of vegetation and buildings and the German Weather Service (DWD) for sharing meteorological observation data of sites in Berlin. The study is part of the Research Unit 1736 “Urban Climate and Heat Stress in Mid-Latitude Cities in View of Climate Change (UCaHS)” (<http://www.UCaHS.org>) funded by the Deutsche Forschungsgemeinschaft (DFG) under the codes SCHE 750/8-1, SCHE 750/9-1, and GE 1035/6-1.

#### References

- Bowler, D.E., Buyung-Ali, L., Knight, T.M., Pullin, A.S., 2010. Urban greening to cool towns and cities: a systematic review of the empirical evidence. *Landsc. Urban Plan.* 97, 147–155. <http://dx.doi.org/10.1016/j.landurbplan.2010.05.006>.
- Bruse, M., Fleer, H., 1998. Simulating surface-plant-air interactions inside urban environments with a three dimensional numerical model. *Environ. Model. Softw.* 13, 373–384. [http://dx.doi.org/10.1016/S1364-8152\(98\)00042-5](http://dx.doi.org/10.1016/S1364-8152(98)00042-5).
- Chemel, C., Sokhi, R.S., 2012. Response of London's urban heat island to a marine air intrusion in an easterly wind regime. *Bound.-Layer Meteorol.* 144, 65–81. <http://dx.doi.org/10.1007/s10546-012-9705-x>.
- Chen, Y.-C., Lin, T.-P., Matzarakis, A., 2014. Comparison of mean radiant temperature from field experiment and modelling: a case study in Freiburg, Germany. *Theor. Appl. Climatol.* <http://dx.doi.org/10.1007/s00704-013-1081-z>.
- Ching, J.K.S., 2013. A perspective on urban canopy layer modeling for weather, climate and air quality applications. *Urban Clim.* 3, 13–39. <http://dx.doi.org/10.1016/j.uclim.2013.02.001>.
- Davin, E.L., Seneviratne, S.I., 2012. Role of land surface processes and diffuse/direct radiation partitioning in simulating the European climate. *Biogeosciences* 9, 1695–1707. <http://dx.doi.org/10.5194/bg-9-1695-2012>.
- Dugord, P., Lauf, S., Schuster, C., Kleinschmit, B., 2012. Land use patterns, temperature distribution, and potential heat stress risk – the case study Berlin, Germany. *Comput. Environ. Urban Syst.* 48, 86–98. <http://dx.doi.org/10.1016/j.compenvurbysys.2014.07.005>.
- Dütemeyer, D., Barlag, A.B., Kuttler, W., Axt-Kittner, U., 2013. Measures against heat stress in the city of Gelsenkirchen, Germany. *Erde* 144, 181–201. <http://dx.doi.org/10.12854/erde-144-14>.
- Endlicher, W., Lanfer, N., 2003. Meso- and micro-climatic aspects of Berlin's urban climate. *Die Erde* 134, 277–293.
- Fenner, D., Meier, F., Scherer, D., Polze, A., 2014. Spatial and temporal air temperature variability in Berlin, Germany, during the years 2001–2010. *Urban Clim.* 10, 308–331. <http://dx.doi.org/10.1016/j.uclim.2014.02.004>.
- Gabriel, K.M., Endlicher, W.R., 2011. Urban and rural mortality rates during heat waves in Berlin and Brandenburg, Germany. *Environ. Pollut.* 159, 2044–2050. <http://dx.doi.org/10.1016/j.envpol.2011.01.016>.
- García-Herrera, R., Díaz, J., Trigo, R.M., Luterbacher, J., Fischer, E.M., 2010. A review of the European summer heat wave of 2003. *Crit. Rev. Environ. Sci. Technol.* 40, 267–306. <http://dx.doi.org/10.1080/10643380802238137>.
- Grimmond, C.S.B., Blackett, M., Best, M.J., Barlow, J., Baik, J.-J., Belcher, S.E., Bohnenstengel, S.I., Calmet, I., Chen, F., Dandou, A., Fortuniak, K., Gouvea, M.L., Hamdi, R., Hendry, M., Kawai, T., Kawamoto, Y., Kondo, H., Kravtsov, E.S., Lee, S.-H., Lorient, T., Martilli, A., Masson, V., Miao, S., Oleson, K., Pigeon, G., Porson, A., Ryu, Y.-H., Salamanca, F., Shashua-Bar, L., Steeneveld, G.-J., Tombrou, M., Voogt, J., Young, D., Zhang, N., 2010. The international urban energy balance models comparison project: first results from phase 1. *J. Appl. Meteorol. Climatol.* 49, 1268–1292. <http://dx.doi.org/10.1175/2010JAMC2354.1>.
- Hajat, S., Kosatky, T., 2010. Heat-related mortality: a review and exploration of heterogeneity. *J. Epidemiol. Community Health* 64, 753–760. <http://dx.doi.org/10.1136/jech.2009.087999>.
- Höppe, P., 1992. A new procedure to determine the mean radiant temperature outdoors. *Wetter und Leb.* 44, 147–151.
- Jacovides, C.P., Tymvios, F.S., Assimakopoulos, V.D., Kaltsounides, N.A., 2006. Comparative study of various correlations in estimating hourly diffuse fraction of global solar radiation. *Renew. Energy* 31, 2492–2504. <http://dx.doi.org/10.1016/j.renene.2005.11.009>.

- Jänicke, B., Meier, F., Hoelscher, M., Scherer, D., 2015. Evaluating the effects of façade greening on human bioclimate in a complex urban environment. *Adv. Meteorol.* 2015, 15. <http://dx.doi.org/10.1155/2015/747259>.
- Jendritzky, G., de Dear, R., Havenith, G., 2012. UTCI-why another thermal index? *Int. J. Biometeorol.* 56, 421–428. <http://dx.doi.org/10.1007/s00484-011-0513-7>.
- Kamali, G.A., Moradi, I., Khalili, A., 2005. Estimating solar radiation on tilted surfaces with various orientations: a study case in Karaj (Iran). *Theor. Appl. Climatol.* 84, 235–241. <http://dx.doi.org/10.1007/s00704-005-0171-y>.
- Kántor, N., Unger, J., 2011. The most problematic variable in the course of human-biometeorological comfort assessment - the mean radiant temperature. *Cent. Eur. J. Geosci.* 3, 90–100. <http://dx.doi.org/10.2478/s13533-011-0010-x>.
- Ketterer, C., Matzarakis, A., 2014. Human-biometeorological assessment of heat stress reduction by replanning measures in Stuttgart, Germany. *Landsc. Urban Plan.* 122, 78–88. <http://dx.doi.org/10.1016/j.landurbplan.2013.11.003>.
- Lau, K.K.-L., Lindberg, F., Rayner, D., Thorsson, S., 2015. The effect of urban geometry on mean radiant temperature under future climate change: a study of three European cities. *Int. J. Biometeorol.* 59, 799–814. <http://dx.doi.org/10.1007/s00484-014-0898-1>.
- Lindberg, F., Grimmond, C.S.B., 2011a. The influence of vegetation and building morphology on shadow patterns and mean radiant temperatures in urban areas: model development and evaluation. *Theor. Appl. Climatol.* 105, 311–323. <http://dx.doi.org/10.1007/s00704-010-0382-8>.
- Lindberg, F., Grimmond, C.S.B., 2011b. Nature of vegetation and building morphology characteristics across a city: Influence on shadow patterns and mean radiant temperatures in London. *Urban Ecosyst.* 14, 617–634. <http://dx.doi.org/10.1007/s11252-011-0184-5>.
- Lindberg, F., Grimmond, C.S.B., Martilli, A., 2015. Sunlit fractions on urban facets – impact of spatial resolution and approach. *Urban Clim.* 12, 65–84. <http://dx.doi.org/10.1016/j.uclim.2014.11.006>.
- Lindberg, F., Holmer, B., Thorsson, S., 2008. SOLWEIG 1.0 – modelling spatial variations of 3D radiant fluxes and mean radiant temperature in complex urban settings. *Int. J. Biometeorol.* 52, 697–713. <http://dx.doi.org/10.1007/s00484-008-0162-7>.
- Lindberg, F., Holmer, B., Thorsson, S., Rayner, D., 2014. Characteristics of the mean radiant temperature in high latitude cities-implications for sensitive climate planning applications. *Int. J. Biometeorol.* 58, 613–627. <http://dx.doi.org/10.1007/s00484-013-0638-y>.
- Martilli, A., 2007. Current research and future challenges in urban mesoscale modelling. *Int. J. Climatol.* 27, 1909–1918. <http://dx.doi.org/10.1002/joc.1620>.
- Martilli, A., Clappier, A., Rotach, M.W., 2002. An urban surface exchange parameterisation for mesoscale models. *Bound.-Layer Meteorol.* 261–304.
- Matzarakis, A., Rutz, F., Mayer, H., 2007. Modelling radiation fluxes in simple and complex environments – application of the RayMan model. *Int. J. Biometeorol.* 51, 323–334. <http://dx.doi.org/10.1007/s00484-006-0061-8>.
- Mills, G., Cleugh, H., Emmanuel, R., Endlicher, W., Erell, E., McGranahan, G., Ng, E., Nickson, A., Rosenthal, J., Steemer, K., 2010. Climate information for improved planning and management of mega cities (needs perspective). *Proc. Environ. Sci.* 1, 228–246. <http://dx.doi.org/10.1016/j.proenv.2010.09.015>.
- Mishra, V., Ganguly, A.R., Nijssen, B., Lettenmaier, D.P., 2015. Changes in observed climate extremes in global urban areas. *Environ. Res. Lett.* 10, 024005. <http://dx.doi.org/10.1088/1748-9326/10/2/024005>.
- Nastos, P.T., Matzarakis, A., 2012. The effect of air temperature and human thermal indices on mortality in Athens, Greece. *Theor. Appl. Climatol.* 108, 591–599. <http://dx.doi.org/10.1007/s00704-011-0555-0>.
- Noorian, A.M., Moradi, I., Kamali, G.A., 2008. Evaluation of 12 models to estimate hourly diffuse irradiation on inclined surfaces. *Renew. Energy* 33, 1406–1412. <http://dx.doi.org/10.1016/j.renene.2007.06.027>.
- Norton, B.A., Coutts, A.M., Livesley, S.J., Harris, R.J., Hunter, A.M., Williams, N.S.G., 2015. Planning for cooler cities: a framework to prioritise green infrastructure to mitigate high temperatures in urban landscapes. *Landsc. Urban Plan.* 134, 127–138. <http://dx.doi.org/10.1016/j.landurbplan.2014.10.018>.
- Onomura, S., Grimmond, C.S.B., Lindberg, F., Holmer, B., Thorsson, S., 2015. Meteorological forcing data for urban outdoor thermal comfort models from a coupled convective boundary layer and surface energy balance scheme. *Urban Clim.* 11, 1–23. <http://dx.doi.org/10.1016/j.uclim.2014.11.001>.
- Reindl, D.T., Beckman, W.A., Duffie, J.A., 1990. Diffuse fraction correlations. *Sol. Energy* 45, 1–7. [http://dx.doi.org/10.1016/0038-092X\(91\)90123-E](http://dx.doi.org/10.1016/0038-092X(91)90123-E).
- Ritter, B., Geleyn, J., 1992. A comprehensive radiation scheme for numerical weather prediction models with potential applications in climate simulations. *Mon. Weather Rev.* 120, 303–325. [http://dx.doi.org/10.1175/1520-0493\(1992\)120<0303>2](http://dx.doi.org/10.1175/1520-0493(1992)120<0303>2).
- Rockel, B., Will, A., Hense, A., 2008. The regional climate model COSMO-CLM (CCLM). *Meteorol. Zeitschrift* 17, 347–348. <http://dx.doi.org/10.1127/0941-2948/2008/0309>.
- Roessner, S., Segl, K., Bochow, M., Heiden, U., Heldens, W., Kaufmann, H., 2011. Potential of Hyperspectral Remote Sensing for Analyzing the Urban Environment. In: *Urban Remote Sensing*. John Wiley & Sons Ltd. <http://dx.doi.org/10.1002/9780470979563.ch4>, pp. 49–61.
- Scherer, K., Langner, M., Endlicher, W., 2014. Spatial analysis of hospital admissions for respiratory diseases during summer months in Berlin taking bioclimatic and socio-economic aspects into account. *Die Erde* 144, 217–237. <http://dx.doi.org/10.12854/erde-144-16>.
- Scherer, D., Fehrenbach, U., Lakes, T., Lauf, S., Meier, F., Schuster, C., 2014. Quantification of heat-stress related mortality hazard, vulnerability and risk in Berlin, Germany. *Die Erde* 144, 238–259. <http://dx.doi.org/10.12854/erde-144-17>.
- Schlünzen, K.H., Sokhi, R.S., 2008. Overview of tools and methods for meteorological and air pollution mesoscale model evaluation and user training. WMO Jt. Rep. COST Action 728 GURME, WMO Joint Report of COST Action 728 and GURME.
- Schubert, S., Grossman-Clarke, S., 2014. Evaluation of the coupled COSMO-CLM/DCEP model with observations from BUBBLE. *Q. J. R. Meteorol. Soc.* 140, 2465–2483. <http://dx.doi.org/10.1002/qj.2311>.
- Schubert, S., Grossman-Clarke, S., 2013. The Influence of green areas and roof albedos on air temperatures during extreme heat events in Berlin, Germany. *Meteorol. Zeitschrift* 22, 131–143. <http://dx.doi.org/10.1127/0941-2948/2013/0393>.
- Schubert, S., Grossman-Clarke, S., Martilli, A., 2012. A double-canyon radiation scheme for multi-layer urban canopy models. *Bound.-Layer Meteorol.* 145, 439–468. <http://dx.doi.org/10.1007/s10546-012-9728-3>.
- Schuster, C., Burkart, K., Lakes, T., 2014. Heat mortality in Berlin – spatial variability at the neighborhood scale. *Urban Clim.* 10, 134–147. <http://dx.doi.org/10.1016/j.uclim.2014.10.008>.
- Smiatek, G., Rockel, B., Schättler, U., 2008. Time invariant data preprocessor for the climate version of the COSMO model (COSMO-CLM). *Meteorol. Zeitschrift* 17, 395–405.
- Stewart, I.D., Oke, T.R., 2012. Local climate zones for urban temperature studies. *Bull. Am. Meteorol. Soc.* 93, 1879–1900. <http://dx.doi.org/10.1175/BAMS-D-11-00019.1>.
- Stewart, I.D., Oke, T.R., Krayerhoff, E.S., 2014. Evaluation of the “local climate zone” scheme using temperature observations and model simulations. *Int. J. Climatol.* 34, 1062–1080. <http://dx.doi.org/10.1002/joc.3746>.
- Thorsson, S., Lindberg, F., Björklund, J., Holmer, B., Rayner, D., 2011. Potential changes in outdoor thermal comfort conditions in Gothenburg, Sweden due to climate change: the influence of urban geometry. *Int. J. Climatol.* 31, 324–335. <http://dx.doi.org/10.1002/joc.2231>.
- Thorsson, S., Lindberg, F., Eliasson, I., Holmer, B., 2007. Different methods for estimating the mean radiant temperature in an outdoor urban setting. *Int. J. Climatol.* 27, 1983–1993. <http://dx.doi.org/10.1002/joc>.
- Thorsson, S., Rocklöv, J., Konarska, J., Lindberg, F., Holmer, B., Dousset, B., Rayner, D., 2014. Mean radiant temperature – a predictor of heat related mortality. *Urban Clim.* 1–14. <http://dx.doi.org/10.1016/j.uclim.2014.01.004>.
- VDI, 1994. Environmental meteorology, interactions between atmosphere and surface; calculation of short-and long wave radiation. Part I: Climate, VDI 3789, Part 2: VDI/DIN- Handbuch Reinhaltung der Luft, Band 1b, Düsseldorf.
- Verein Berliner Wetterkarte, 2003. Berliner Wetterkarte, Jahrgang 2003, 2. Halbjahr, vol. 52.
- Yi, C., Kim, K.R., An, S.M., Choi, Y.-J., Holtmann, A., Jänicke, B., Fehrenbach, U., Scherer, D., 2015. Estimating spatial patterns of air temperature at building-resolving spatial resolution in. *Int. J. Climatol.* <http://dx.doi.org/10.1002/joc.4363>, n/a–n/a.

## Paper IV

# Urban-rural differences in near-surface air temperature as resolved by the Central Europe Refined analysis (CER): sensitivity to planetary boundary layer schemes and urban canopy models

Jänicke, B., Meier, F., Fenner, D., Fehrenbach, U., Holtmann, A., Scherer, D., 2016. Urban-rural differences in near-surface air temperature as resolved by the Central Europe Refined analysis (CER): sensitivity to planetary boundary layer schemes and urban canopy models. *International Journal of Climatology*, 1-17. <http://dx.doi.org/10.1002/joc.4835>

**Status:** Published (19 June 2016)

**Copyright:** Royal Meteorological Society (RMS)

### Own contribution:

- Refining the research ideas and research design
- Search, review, and summary of literature
- Evaluation of simulations and calculation of metrics
- Performing the analyses
- Interpretation of statistical analyses
- Creating graphics and tables
- Writing the manuscript, visualising the results, and drafting
- Revisions of the manuscript



## Urban–rural differences in near-surface air temperature as resolved by the Central Europe Refined analysis (CER): sensitivity to planetary boundary layer schemes and urban canopy models

Britta Jänicke,\* Fred Meier, Daniel Fenner, Ute Fehrenbach, Achim Holtmann and Dieter Scherer

*Institute of Ecology, Technische Universität Berlin, Germany*

**ABSTRACT:** Model-based studies on urban heat islands can be seriously affected by errors in near-surface air temperature ( $T_2$ ), especially if errors differ between cities and their rural surroundings. Furthermore, errors in  $T_2$  strongly depend on selected parameterisation schemes, in particular on the planetary boundary layer (PBL) scheme and the urban canopy model (UCM). We developed the Central Europe Refined analysis (CER), a dataset generated by dynamically downscaling a global atmospheric reanalysis with the Weather Research and Forecasting (WRF) model for Central Europe (30 km), Germany (10 km), and the region of Berlin-Brandenburg (2 km). CER data were analysed to study urban–rural and intra-urban differences in  $T_2$  for Berlin as well as to test the sensitivity of  $T_2$  against two different PBL schemes, a mosaic approach, and three UCMs with different levels of complexity. Results were evaluated using data from 22 weather stations. All tested configurations simulated  $T_2$  with small deviations from observations. The PBL schemes predominantly control the deviation of  $T_2$ . From the tested PBL schemes, the Bougeault–Lacarrère scheme performed better than the Mellor–Yamada–Janjić scheme. The application of different UCMs and the mosaic approach also influenced the deviations, but not as strongly as the PBL schemes. The performance of the UCMs regarding the representation of intra-urban and urban–rural differences showed that differences were largest when using a complex multi-layer UCM. Overall, the simplest model showed lowest deviations. We conclude that more research on UCMs is required because complex UCMs showed potentials but did not outperform the simple slab model.

**KEY WORDS** WRF; urban heat island; Berlin; planetary boundary layer schemes; urban canopy models; air temperature; intra-urban differences; mosaic approach

Received 25 February 2016; Revised 14 June 2016; Accepted 19 June 2016

### 1. Introduction

Increased air temperature in cities compared with their rural surroundings, known as urban heat islands (UHIs), and intra-urban differences of temperatures associated with different urban structures are frequently investigated components of urban climate (e.g. Arnfield, 2003; Souch and Grimmond, 2006; Barlow, 2014; Zhao *et al.*, 2014). Model-based studies on UHIs need to reproduce these differences and can seriously be affected by errors in simulations of near-surface air temperature (air temperature at 2 m above ground,  $T_2$ ). Several studies address and summarise the current state of the art and unresolved problems in meso-scale urban climate models (e.g., Martilli, 2007; Hidalgo *et al.*, 2008; Chen *et al.*, 2011; Grimmond *et al.*, 2011; Ng *et al.*, 2012; Best and Grimmond, 2015). A frequently observed problem in model-based studies are cold biases in  $T_2$  (e.g., Hu *et al.*, 2010; Xie *et al.*, 2012; Garcia-Diez *et al.*, 2013; Dasari *et al.*, 2014;

Kleczeck *et al.*, 2014). Cold biases can seriously affect, for example, the detection of heat waves and could lead to fewer identified heat events as studied for Europe by Dasari *et al.* (2014). As long as errors are independent of land cover, assessments of modelled urban–rural and intra-urban differences in  $T_2$  would still be possible. However, errors depending on land cover would hamper UHI analyses or make them impossible at all.

In studies with numerical weather prediction models (NWP), numerous options and configurations can be selected. Some of these options show little effects on  $T_2$  bias such as domain size (Kleczeck *et al.*, 2014), the selected microphysics scheme (Argüeso *et al.*, 2011; Mooney *et al.*, 2013), or initial and boundary conditions (e.g. the selected reanalysis dataset) (Steenneveld *et al.*, 2011). Other options, in particular, the parameterisation of the planetary boundary layer (PBL) and the selected urban canopy model (UCM), have frequently been related to  $T_2$  biases (e.g. Argüeso *et al.*, 2011; Kim *et al.*, 2013).

Processes within the PBL, such as vertical and horizontal mixing, are of major importance for correctly simulating  $T_2$  (Zhang and Zheng, 2004; Hu *et al.*, 2010;

\* Correspondence to: B. Jänicke, Technische Universität Berlin, Institute of Ecology, Chair of Climatology, Rothenburgstraße 12, Berlin 12165, Germany. E-mail: britta.jaenicke@tu-berlin.de



Argüeso *et al.*, 2011; Xie *et al.*, 2012; Garcia-Diez *et al.*, 2013; Mooney *et al.*, 2013; Kleczek *et al.*, 2014; Li and Bou-Zeid, 2014; Shaffer *et al.*, 2014). Turbulent flows in the PBL cannot directly be resolved but have to be parameterised by a PBL scheme with the present grid spacing in NWP (1–5 km).

In urban analyses, the UCM additionally affects errors in  $T_2$  because urban modifications of  $T_2$  by buildings and vegetation are parameterised by the UCM. In general, three different model types can be distinguished: slab models, single-layer and multi-layer UCMs. The simplest slab (or bulk) approach is actually a land surface model (LSM), in which several parameters are modified to describe urban surfaces. Urban land cover is depicted with the same equations as any other land cover category. Therefore, the three-dimensional structure of the city is not resolved. Single-layer UCMs parameterise three-dimensional urban structures as infinitely-long street canyons, and are able to distinguish different facets, namely walls, roofs and ground (Chen *et al.*, 2011). Thus, they can parameterise simple energy fluxes within a street canyon including radiation trapping, shadowing and reflection. However, only multi-layer UCMs allow direct exchanges of energy, momentum and moisture between urban roughness sub-layer and PBL (Chen *et al.*, 2011). In multi-layer UCMs, three-dimensional city structures are represented by roof, wall and ground, and sources and sinks of moisture, heat and momentum are parameterised in horizontal and vertical planes (Chen *et al.*, 2011). In addition, considering sub-grid land cover fractions (mosaic approach) was found to improve model performance as compared to using the dominant land cover category only (dominant approach) in particular in heterogeneous urban areas (Avisar and Pielke, 1989; Pielke, 2002; Li *et al.*, 2013).

Although several studies have analysed the sensitivity of  $T_2$  to PBL and/or UCM, no consensus regarding suitable schemes and models have been found, because biases depend on season (Garcia-Diez *et al.*, 2013), region (Dasari *et al.*, 2014) and target variable (e.g. air temperature, wind speed, PBL height) (Kim *et al.*, 2013). Therefore, individual solutions for each study type must be found according to the ‘fitness-for-purpose’ guidance (Baklanov *et al.*, 2009).

While several studies have analysed the effects of different PBL schemes and UCMs on  $T_2$  based on individual weather stations, the objective here is to focus on the representation of intra-urban as well as urban–rural differences. Such differences in urban model-based studies have rarely been considered in evaluations, although they are essential for many questions in urban climatology. Our overall goal is to develop a gridded meteorological data set at high spatial and high temporal resolutions, called the Central Europe Refined analysis (CER), that provides past atmospheric conditions also suitable for urban climate studies for Berlin. In this study, we limited evaluations of the CER to  $T_2$  and intra-urban and urban–rural differences of  $T_2$ . With the focus on a single variable, we are not able to assess the overall quality regarding other variables, but we can assess the usability of the CER for

UHI analyses. Furthermore, we complement other studies that have applied land surface temperature (e.g. Li and Bou-Zeid, 2014; Monaghan *et al.*, 2014; Ramamurthy *et al.*, 2015) or vertical temperature profiles (e.g. Hu *et al.*, 2010; Garcia-Diez *et al.*, 2013; Trusilova *et al.*, 2016) for evaluating PBL schemes and UCMs.

For a better understanding of the sensitivity of  $T_2$  to different PBL schemes, mosaicking and UCMs, we performed different experiments. We examined the model performance compared to ground-based observations of  $T_2$  in Berlin and its rural surroundings to answer the following questions: (1) How large are the deviations between observations and the CER with different PBL schemes, mosaicking and UCMs? (2) How are urban–rural and intra-urban differences represented in the CER in summer?

## 2. Materials and methods

### 2.1. Model configuration

We used the Weather Research and Forecasting (WRF) model (Skamarock and Klemp, 2008) (version WRF-ARW 3.6.1) to dynamically downscale ERA-Interim data (Dee *et al.*, 2011). We performed a series of short-term integrations using a daily re-initialisation strategy. This means that we executed individual runs for each day by re-initialising the runs every 24 h. Each run consists of 36 h with the first 12 h of spin-up time being removed. The main advantages of this strategy are the close connection to the weather situation and the possibility of parallel computation. Daily re-initialisation strategies have shown to provide robust and reliable results, e.g. for the Tibetan Plateau by Maussion *et al.* (2014).

We followed a cascaded two-way nesting approach (30, 10, 2 km) (Figure 1), with the smallest domain covering Berlin and the federal state Brandenburg. Settings and physical options besides PBL scheme, mosaicking, and UCM were the same in all experiments and mostly adopted from Maussion *et al.* (2014) (Table 1).

We used land cover data from the Coordination of Information on the Environment (CORINE) provided by the European Environment Agency (CLC2006, Version 13, 100 m). Only for areas beyond the CORINE coverage (mostly beyond the European Union), we used coarser land cover data from the U.S. Geological Survey (USGS). We kept the USGS categories in WRF and therefore transformed CORINE categories to USGS categories following the approach as described by Pineda *et al.* (2004) and in Table S1, Supporting Information. We used ‘crop-land/woodland mosaic’ as the natural class representing non-urban fractions within urban land cover categories in the UCMs. We chose this category to represent the mixture of parks and forests in Berlin.

### 2.2. Experiment setup

The experiments included three complete months, January, April and July 2015, for considering atmospheric conditions in winter, a transitional season and summer. We set up experiments with different combinations of UCMs

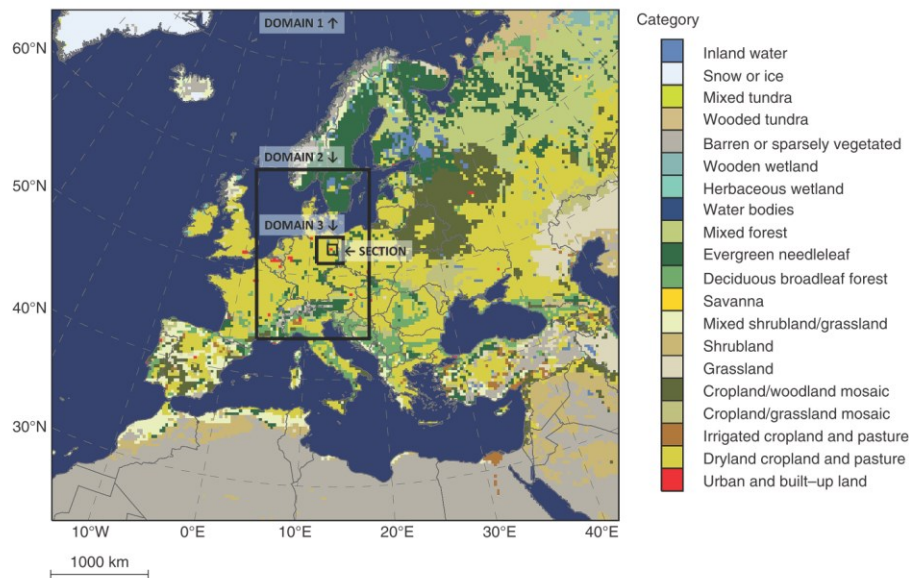


Figure 1. Model domains (marked by boxes) of the CER with dominant land cover categories. The innermost box shows a section of domain 3, which is visualised in Figures 2 and 5.

Table 1. Overview of model settings used in CER.

Model	WRF-ARW 3.6.1
Horizontal grid spacing	2 km (/10 km/30 km)
Vertical grid spacing	28 levels
Temporal resolution	1 h
Analysis periods	January, April, July 2015
Integration strategy	Daily re-initialisation
Initial and boundary conditions	ERA-Interim (6 h)
Land cover	Corine (USGS)
Land surface scheme	Noah land surface model
Microphysics scheme	Modified Thompson scheme
Long-wave radiation scheme	Rapid Radiative Transfer Model
Short-wave radiation scheme	Dudhia scheme
Cumulus scheme	New Grell-Devenyi 3 scheme for D1 and D2

Table 2. Overview of experiments conducted with CER with different planetary boundary layer (PBL) schemes, urban canopy models (UCMs) and with or without mosaicking for January, April and July 2015.

Name	PBL scheme	UCM	Mosaic
MYJ_SLAB	MYJ	Slab	
MYJ_SLAB_mos	MYJ	Slab	×
MYJ_SLUCM	MYJ	SLUCM	
MYJ_SLUCM_mos	MYJ	SLUCM	×
MYJ_BEP	MYJ	BEP	
BOU_SLAB	BOU	Slab	
BOU_SLAB_mos	BOU	Slab	×
BOU_SLUCM	BOU	SLUCM	
BOU_SLUCM_mos	BOU	SLUCM	×
BOU_BEP	BOU	BEP	

and PBL schemes (Table 2). Additionally, we assessed the influence of the mosaic approach developed by Li *et al.* (2013).

We tested the two PBL schemes that can be combined with all three types of UCMs in the WRF model: Mellor–Yamada–Janjić (MYJ) (Janjić, 1990) and Bougeault–Lacarrère (BOU) (Bougeault and Lacarrère, 1989). Both are frequently used in WRF, e.g. MYJ was applied by Fallmann *et al.* (2014) or Kim *et al.* (2013) and BOU by Kleczek *et al.* (2014) or Xie *et al.* (2012). They differ mainly in the definitions of the mixing length and a coefficient used for computing diffusivity (Shin and Hong, 2011).

We combined the selected PBL schemes with three different types of UCMs that differ in their complexity (Table 2): the slab model within the Noah LSM (Chen and Dudhia, 2001), the single-layer UCM (SLUCM) (Kusaka *et al.*, 2001) and the building effect parameterisation (BEP) (Martilli *et al.*, 2002), which is a multi-layer UCM. Anthropogenic heat was excluded for better comparability between the different schemes because slab in the Noah LSM cannot consider it.

In addition, we applied the recently implemented mosaic approach (Li *et al.*, 2013) to account for sub-grid land surface heterogeneity. Thus, different land cover categories relevant for a grid cell are considered in

contrast to the dominant approach, which uses only the dominant land cover category. The underlying idea is that land surface characteristics are often heterogeneous within grid cells (Avissar and Pielke, 1989; Pielke, 2002), particularly in urban areas. We used the mosaic approach with three tiles to include the three most frequent land cover categories within a grid cell. These three tiles are simulated individually and area-averaged according to their fraction of occurrence (flux averaging) (Figure 2). Fractions of occurrence of the respective land cover categories are visualized in Figure S1. Until now, the mosaic approach is only implemented for slab and SLUCM in the WRF code, but not for BEP (Table 2).

Land cover categories also differ between slab, which uses only one urban category, and SLUCM and BEP, in which this category was separated into three urban sub-categories (Table S1). The different urban land cover categories caused changes in fractions for non-urban land cover categories as well. For example, the dominant land cover category of the grid cell referring to the observation site Tempelhof (No. 13) is 'urban and built-up land' in slab with a fraction of 55%. When mosaicking is used, the second and third dominant land cover categories are also considered, which are 'dryland cropland and pasture' (36%) and 'cropland/woodland mosaic' (1%) in SLAB\_mos. In SLUCM and BEP, however, the respective fractions are different due to the splitting into three urban categories.

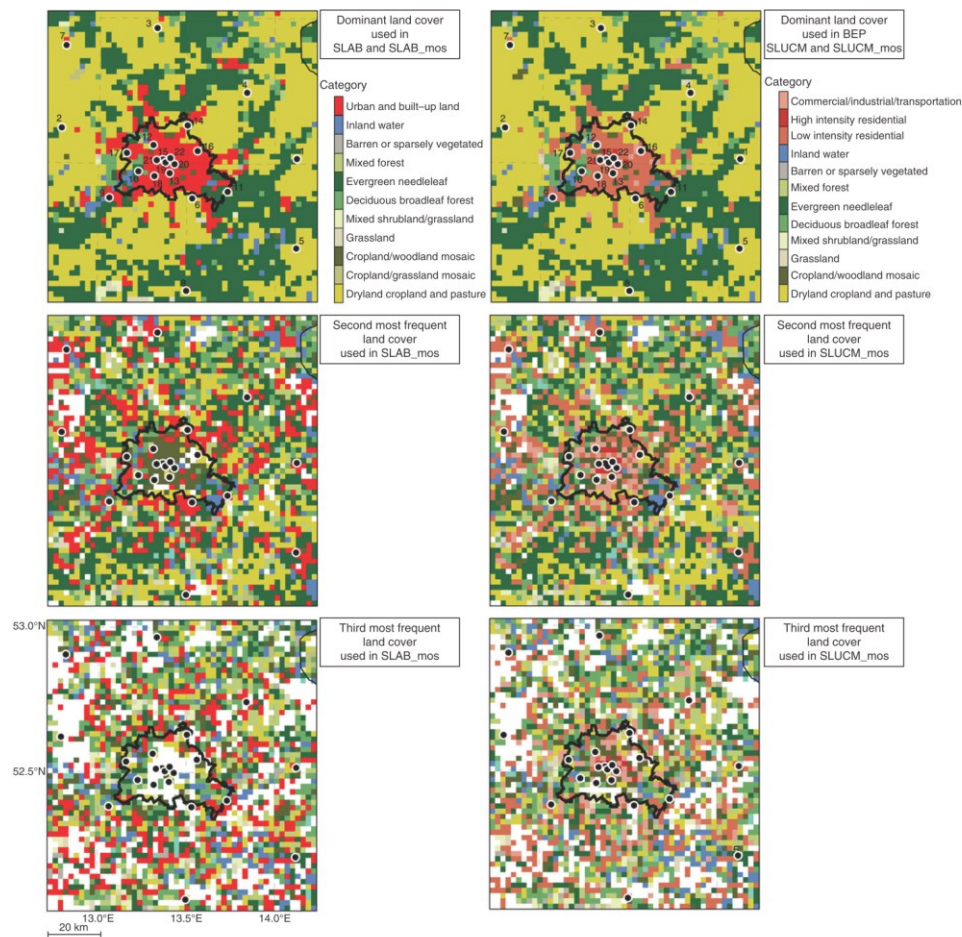


Figure 2. Section of domain 3 with land cover categories and locations of weather stations. Numbers refer to sites as described in Table 5. Land cover categories are visualised for the dominant category as used in slab, SLUCM and BEP, and for the second and third most frequent category as used within the mosaic approach in SLAB\_mos and SLUCM\_mos. White colour indicates that no second or third most frequent land cover exists.



Table 3. Overview of urban canopy parameters in SLUCM and BEP applied for the three urban land cover categories commercial, low intensity residential and high intensity residential.

Urban parameter	Commercial	High density	Low density	SLUCM	BEP
Roof level (m) <sup>c</sup>	9.1	19.3	10	×	
Standard deviation of roof height (m) <sup>c</sup>	5.9	2.3	5.6	×	
Roof width (m) <sup>c</sup>	20	15	10	×	
Road width (m) <sup>c</sup>	30	20	20	×	×
Street direction (%) <sup>a</sup>	0/90	0/90	0/90		×
Building height 5 m (%) <sup>b</sup>	3	3	17		×
Building height 10 m (%) <sup>b</sup>	2	2	45		×
Building height 15 m (%) <sup>b</sup>	19	4	25		×
Building height 20 m (%) <sup>b</sup>	26	19	13		×
Building height 25 m (%) <sup>b</sup>	30	41	0		×
Building height 30 m (%) <sup>b</sup>	20	26	0		×
Building height 35 m (%) <sup>b</sup>	0	5	0		×
Urban fraction (-) <sup>c</sup>	0.6	0.8	0.6	×	×
Heat capacity of roof, wall, ground (J m <sup>3</sup> K <sup>-1</sup> ) <sup>b</sup>	2.30E + 06	2.30E + 06	2.30E + 06	×	×
Thermal conductivity of roof, wall (J m <sup>-1</sup> s K) <sup>d</sup>	1.54	1.54	1.54	×	×
Thermal conductivity of ground (J m <sup>-1</sup> s K) <sup>d</sup>	0.67	0.67	0.67	×	×
Surface albedo of roof (-) <sup>b</sup>	0.163	0.163	0.163	×	×
Surface albedo of ground, wall (-) <sup>b</sup>	0.162	0.162	0.162	×	×
Surface emissivity roof, wall (-) <sup>a</sup>	0.9	0.9	0.9	×	×
Surface emissivity ground (-) <sup>a</sup>	0.95	0.95	0.95	×	×
Roughness length over roof (m) <sup>a</sup>	0.01	0.01	0.01		×
Coefficient modifying the Kanda approach (-) <sup>a</sup>	1.29	1.29	1.29	×	
Lower boundary temperature for building roof, wall (K) <sup>a</sup>	293	293	293	×	×
Lower boundary temperature for ground (K) <sup>c</sup>	283	283	283	×	×
Thickness of each roof/wall layer (m) <sup>d</sup>	0.05/0.05/0.10/0.20			×	
Thickness of each ground layer (m) <sup>a</sup>	0.05/0.25/0.5/0.75			×	
Surface and layer temperature <sup>a</sup>	4-layer model			×	
Anthropogenic heating <sup>a</sup>	No anthropogenic heating			×	×
Lower boundary condition for roof/wall/ground temperature <sup>a</sup>	Zero-Flux			×	

Superscripted letters show the references to the applied values, which are either default (a), Berlin-specific values from Schubert and Grossman-Clarke (2013) (b), from the three-dimensional building model provided by the Berlin Senate Department for Economics, Technology and Research (c), former research results of the authors (unpublished) (d) or approximated from annual mean air temperature in Berlin (e). × indicates the usage of parameters in SLUCM and BEP.

Table 4. Overview of parameters in slab applied for the land cover category 'urban and built-up land'.

Parameter	Urban and built-up land
Fraction of vegetation (-)	0.05
Emissivity (-)	0.88
Albedo (-)	0.15
Roughness length (m)	0.8
Heat capacity (J m <sup>3</sup> K <sup>-1</sup> )	3.0
Thermal conductivity (J m <sup>-1</sup> s K)	3.24

Default values by Liu *et al.* (2006) are used.

This leads to a non-urban dominant land use category at the grid cell referring to Tempelhof (No. 13), namely 'dryland cropland and pasture' with 42%. When using mosaicking in SLUCM\_mos, the second and third land cover categories are 'low intensity residential' (38%) and 'commercial/industrial/transportation' (21%).

Parameters used in the UCMs are not comparable to each other due to different complexities in computations. For instance, in slab, urban parameters need to effectively parametrise, e.g. the three-dimensional city structure that is explicitly resolved in SLUCM and BEP. In SLUCM and BEP, we used as far as possible Berlin-specific parameter

values as indicated in Table 3. In particular, in slab, parameters serve as effective parameters rather than as realistic physical descriptions (Pielke, 2002; Liu *et al.*, 2006). Thus, parameter values in slab cannot be easily derived from measurements. In addition, city-specific parameter tuning would impede transferability. For these reasons, we applied the default parameters in slab (Liu *et al.*, 2006) (Table 4).

### 2.3. Observations

For the evaluation of the CER, we selected 22 weather stations in Berlin and surroundings (Figure 2). These include stations of the Urban Climate Observation Network (UCON) maintained by Technische Universität Berlin (TUB) (described and analysed in Fenner *et al.* (2014)), and all available stations within Berlin and nearest stations in the surroundings maintained by the German Weather Service (DWD) (Table 5). We assured sufficient data quality by searching for unrealistic values, i.e. values 3 K below or above long-term minima and maxima within the respective months in Berlin-Tempelhof (1948–2014) and Potsdam (1900–2014), but almost all values were plausible. T2 from weather stations was hourly averaged whereas CER data are instantaneous hourly values.

Table 5. Overview of weather stations and allocated land cover (in slab, SLUCM and BEP).

	No	Station	Affiliation	Lon.	Lat.	Dominant land cover in slab	Dominant land cover in SLUCM and BEP
Rural (RUR)	1	Müncheberg	DWD	14.1232	52.5176	Dryland cropland and pasture	
	2	Berge	DWD	12.787	52.6192	Dryland cropland and pasture	
	3	Zehdenick	DWD	13.3264	52.9664	Dryland cropland and pasture	
	4	Heckelberg	DWD	13.8403	52.7444	Dryland cropland and pasture	
	5	Lindenberg	DWD	14.118	52.2085	Dryland cropland and pasture	
	6	Schönefeld	DWD	13.5306	52.3807	Dryland cropland and pasture	
	7	Neuruppin	DWD	12.8069	52.9036	Lakes	
	8	Baruth	DWD	13.4996	52.0614	Urban and built-up land	Evergreen needleleaf forest
Urban greened (UGR)	9	Potsdam	DWD	13.0622	52.3813	Deciduous broadleaf forest	
	10	Jagen91	TUB	13.2251	52.4732	Evergreen needleleaf forest	
	11	Kaniswall	DWD	13.7309	52.404	Dryland cropland and pasture	
	12	Tegel	DWD	13.3088	52.5644	Dryland cropland and pasture	
	13	Tempelhof	DWD	13.4021	52.4675	Urban and built-up land	Dryland cropland and pasture
Urban built-up (UBU)	14	Buch	DWD	13.5022	52.6309	Urban and built-up land	Low intensity residential
	15	Tiergarten	TUB	13.3636	52.5145	Urban and built-up land	Low intensity residential
	16	Marzahn	DWD	13.5598	52.5447	Urban and built-up land	Low intensity residential
	17	Spandauer Strasse	TUB	13.1584	52.5364	Urban and built-up land	Low intensity residential
	18	Rothenburg strasse	TUB	13.3158	52.4572	Urban and built-up land	Low intensity residential
	19	Dessauer Strasse	TUB	13.3783	52.5045	Urban and built-up land	Low intensity residential
	20	Wiener Strasse	TUB	13.4291	52.4987	Urban and built-up land	Low intensity residential
	21	TUB main building	TUB	13.328	52.5123	Urban and built-up land	High intensity residential
	22	Alexanderplatz	TUB	13.4057	52.5198	Urban and built-up land	High intensity residential

Stations are grouped into rural sites with vegetated land surfaces (1–9) (RUR), urban sites with greened surfaces (10–15) (UGR) and urban sites with mainly built-up surfaces (16–22) (UBU).

We applied a lapse-rate adjustment to account for minor differences in weather station elevations. The average elevation of the weather stations is 50 m with deviations below  $\pm 40$  m. Therefore, we corrected measured and simulated air temperatures by the dry adiabatic lapse rate ( $-9.8 \times 10^{-3} \text{ K m}^{-1}$ ) to a reference height of 50 m a.s.l.

We grouped these 22 weather stations into rural (RUR), urban greened (UGR) (e.g. airports, parks, forest within the borders of Berlin) and urban built-up (UBU) sites (Table 5). The grouping was based on the surrounding land cover of the weather stations, where sites dominated by buildings were assigned as UBU and sites within the city's border dominated by vegetation were assigned as UGR (see Fenner *et al.*, 2014 for TUB stations). Sites beyond Berlin's border were assigned as RUR. When urban–rural differences are considered, we refer to  $\Delta\text{UBU-RUR}$ , whereas  $\Delta\text{UBU-UGR}$  describes intra-urban differences.

#### 2.4. Model evaluation

We compared data from weather stations with the nearest grid point in the CER. At most sites land cover categories

were similar to the surroundings of the respective weather stations. At some UGR sites (13, 14, 15), however, green spaces were not represented in slab and the dominant class was 'urban and built-up land' (Table 5). We assume that data from weather stations are comparable with simulation data with similar characteristics of land cover representing the stations' footprints, and land cover category representing the model's grid points.

For evaluating the performance of different model configurations in comparison with observations, we calculated the root mean square deviation (RMSD), mean deviation (MD) and skill variance (SKVAR) as described in Schlünzen and Sokhi (2008). In contrast to Schlünzen and Sokhi (2008), we calculated standard deviations in SKVAR from daily amplitudes and not from absolute values. SKVAR describes the representation of the diurnal range, whereas RMSD and MD represent the deviation from observations. For each of the metrics, a threshold-based quality criterion was defined. We used following criteria as desired accuracy:  $\text{RMSD} \leq 2 \text{ K}$  and  $\text{MD} \leq \pm 0.5 \text{ K}$  as suggested by Chemel and Sokhi (2012).

and Schlünzen and Sokhi (2008), which are more strict than results of many current studies (e.g. Flagg and Taylor, 2011; Kim *et al.*, 2013; Dasari *et al.*, 2014). For SKVAR, we used the criterion of  $0.9 \leq \text{SKVAR} \leq 1.1$ .

### 3. Results

#### 3.1. Absolute deviations from observations

Time series of simulated and observed  $T_2$  are shown in Figure 3. We selected the MYJ\_SLUCM and BOU\_SLAB\_mos experiments, showing the worst and the best performance for all sites (see Table 6), respectively. Regardless of the selected parameterisation, all experiments accurately reproduced monthly courses in  $T_2$  over the three months. Table 6 summarises the differences in  $T_2$  between the CER in all experiments and observations. The values of the metrics from each site were averaged for each month and across all sites to the groups RUR, UGR and UBU. The lowest section of Table 6 combines the three metrics for assessing the overall performance.

The overall performance indicated a clear separation between experiments with MYJ and BOU (Table 6).

Experiments with MYJ mostly did not meet our criteria due to underestimated  $T_2$  as documented by negative  $MDs$ , and low daily amplitudes as indicated by  $\text{SKVAR} < 1$ . Experiments with BOU more often fulfilled the criteria. Table 6 also reveals seasonal differences with the best performance of BOU in winter.

Differences between UCMs were not as pronounced as differences between PBL schemes. In terms of the applied criteria, the simple slab model performed best. Using the mosaic approach tended to improve the performance slightly in SLAB\_mos, as well as in SLUCM\_mos. Overall, the combination of BOU and slab with mosaic revealed the best performance. Taken together, however, no individual experiment outperformed the others in each season and site.

After examining the CER with aggregated metrics, we determined the differences between CER data and observations (CER-OBS) in diurnal cycles. Figure 4 shows the hourly mean deviation between the experiments and observations at each site for January and July 2015. April 2015 showed a similar pattern as July (Figure S2).

Again, differences between CER data and observations were lower with BOU than with MYJ (Figure 4). The

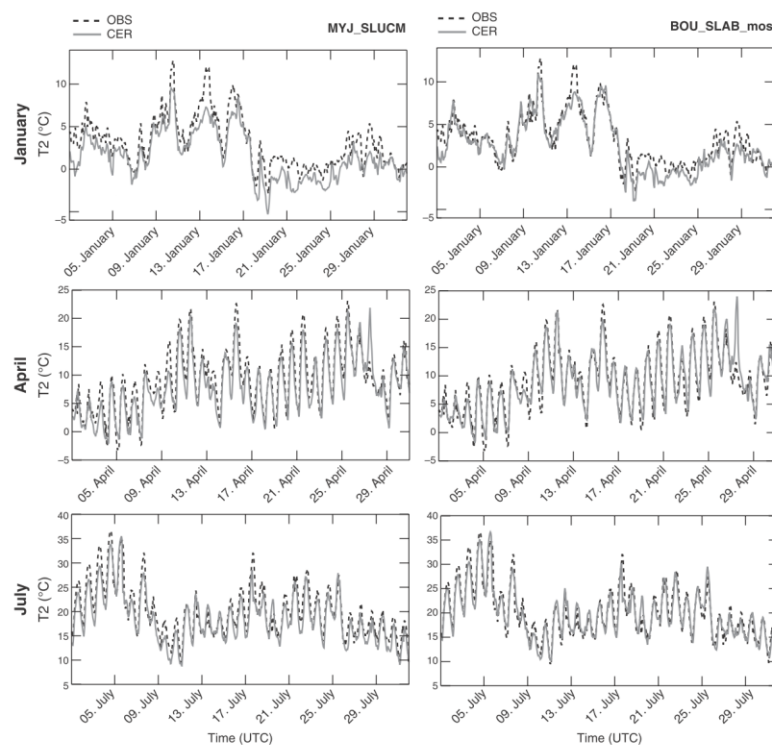


Figure 3. Time series of  $T_2$  as resolved by the CER with the experiments MYJ\_SLUCM and BOU\_SLAB\_mos (solid lines) and observed (dashed line) at an urban greened site (UGR) (Tegel No. 12) during January, April and July 2015. Scaling of axes varies between the months.

Table 6. Metrics for evaluation of the experiments based on  $T_2$  observations averaged across all (ALL), rural (RUR) ( $n=9$ ), urban greened (UGR) ( $n=6$ ) and urban built-up (UBU) ( $n=7$ ) sites for the three months.

		All seasons	January 2015				April 2015				July 2015			
			All	RUR	UGR	UBU	All	RUR	UGR	UBU	All	RUR	UGR	UBU
RMSD (K)														
MYJ_SLAB	1.9	1.6	1.6	1.6	1.7	2.1	2.1	2.2	2.2	2.0	2.0	2.1	2.0	
MYJ_SLAB_mos	1.9	1.6	1.5	1.6	1.7	2.1	2.1	2.2	2.2	2.0	2.0	2.1	2.0	
MYJ_SLUCM	2.2	1.8	1.6	1.8	2.2	2.4	2.1	2.4	2.9	2.3	2.1	2.3	2.7	
MYJ_SLUCM_mos	2.3	1.7	1.5	1.7	2.0	2.5	2.4	2.5	2.8	2.5	2.3	2.5	2.9	
MYJ_BEP	2.0	1.4	1.5	1.4	1.2	2.2	2.1	2.4	2.2	2.2	2.1	2.3	2.5	
BOU_SLAB	1.8	1.3	1.2	1.3	1.4	2.0	2.0	2.2	2.0	2.0	1.9	2.1	1.9	
BOU_SLAB_mos	1.8	1.3	1.2	1.3	1.4	2.0	2.0	2.1	2.0	1.9	1.9	2.0	1.9	
BOU_SLUCM	1.9	1.4	1.3	1.4	1.6	2.1	2.0	2.1	2.3	2.0	1.9	2.1	2.2	
BOU_SLUCM_mos	2.0	1.5	1.3	1.5	1.7	2.2	2.1	2.2	2.4	2.3	2.1	2.3	2.5	
BOU_BEP	1.9	1.3	1.2	1.4	1.4	2.2	2.0	2.5	2.2	2.1	1.9	2.2	2.2	
MD (K)														
MYJ_SLAB	-0.8	-1.1	-1.1	-1.1	-1.3	-0.6	-0.5	-0.4	-1.0	-0.5	-0.6	-0.2	-0.6	
MYJ_SLAB_mos	-0.7	-1.2	-1.1	-1.1	-1.3	-0.6	-0.4	-0.4	-0.9	-0.5	-0.5	-0.3	-0.6	
MYJ_SLUCM	-1.3	-1.4	-1.1	-1.4	-1.9	-1.2	-0.6	-1.1	-2.1	-1.2	-0.8	-1.0	-1.8	
MYJ_SLUCM_mos	-1.2	-1.3	-1.0	-1.2	-1.7	-1.1	-0.4	-1.0	-2.0	-1.2	-0.8	-1.0	-2.0	
MYJ_BEP	-0.7	-0.7	-1.0	-0.6	-0.4	-0.4	-0.4	-0.2	-0.6	-0.9	-0.7	-0.7	-1.4	
BOU_SLAB	-0.1	-0.4	-0.4	-0.3	-0.5	0.0	0.1	0.2	-0.3	0.0	-0.1	0.3	-0.1	
BOU_SLAB_mos	-0.1	-0.4	-0.4	-0.4	-0.5	0.0	0.2	0.2	-0.3	0.1	0.0	0.3	0.0	
BOU_SLUCM	-0.6	-0.6	-0.4	-0.6	-0.9	-0.4	0.0	-0.3	-1.2	-0.5	-0.3	-0.3	-1.1	
BOU_SLUCM_mos	-0.5	-0.4	-0.2	-0.3	-0.8	-0.5	0.1	-0.3	-1.3	-0.6	-0.2	-0.4	-1.3	
BOU_BEP	0.0	0.1	-0.3	0.2	0.5	0.3	0.2	0.5	0.2	-0.3	-0.2	-0.1	-0.7	
SKVAR (-)														
MYJ_SLAB	0.8	0.7	0.7	0.7	0.8	0.9	0.8	0.8	1.0	0.8	0.8	0.7	0.8	
MYJ_SLAB_mos	0.8	0.7	0.7	0.7	0.8	0.9	0.8	0.8	1.0	0.8	0.8	0.7	0.8	
MYJ_SLUCM	0.8	0.8	0.8	0.8	0.9	0.9	0.8	0.9	1.1	0.8	0.8	0.8	0.9	
MYJ_SLUCM_mos	0.8	0.8	0.8	0.8	0.9	0.8	0.7	0.8	1.0	0.8	0.8	0.8	0.8	
MYJ_BEP	0.8	0.8	0.8	0.7	0.8	0.8	0.8	0.8	0.9	0.7	0.8	0.7	0.8	
BOU_SLAB	0.9	0.9	0.9	0.8	0.9	0.9	0.8	0.9	1.1	0.8	0.8	0.8	0.9	
BOU_SLAB_mos	0.9	0.9	0.9	0.8	0.9	1.0	0.8	0.9	1.1	0.8	0.8	0.8	0.9	
BOU_SLUCM	0.9	0.9	0.9	0.9	1.0	0.9	0.8	0.9	1.1	0.8	0.8	0.8	0.9	
BOU_SLUCM_mos	1.0	1.0	1.0	1.0	1.1	1.0	0.9	1.0	1.1	0.9	0.8	0.8	0.9	
BOU_BEP	0.8	0.9	0.9	0.8	0.9	0.8	0.8	0.8	0.9	0.8	0.8	0.8	0.8	
Performance														
MYJ_SLAB	×	×	×	×	×	×	×	×	×	-	×	×	×	
MYJ_SLAB_mos	×	×	×	×	×	×	×	×	×	-	-	×	×	
MYJ_SLUCM	×	×	×	×	×	×	×	×	×	×	×	×	×	
MYJ_SLUCM_mos	×	×	×	×	-	×	×	×	×	×	×	×	×	
MYJ_BEP	×	×	×	×	-	×	×	×	×	×	×	×	×	
BOU_SLAB	✓	✓	✓	-	✓	✓	-	-	✓	-	-	×	✓	
BOU_SLAB_mos	✓	✓	✓	-	✓	✓	-	-	✓	-	-	-	✓	
BOU_SLUCM	-	-	✓	-	-	-	-	-	×	×	-	×	×	
BOU_SLUCM_mos	✓	✓	✓	✓	-	-	-	-	×	×	×	×	×	
BOU_BEP	-	✓	✓	-	✓	×	-	×	-	×	-	×	×	

Desirable values of root mean square deviation (RMSD), mean deviation (MD) and skill variance (SKVAR) ( $\text{RMSD} \leq 2 \text{ K}$ ,  $|\text{MD}| \leq 0.5 \text{ K}$  and  $0.9 \leq \text{SKVAR} \leq 1.1$ ) are indicated by bold font. Overall performance is assessed as desirable (✓) when all three criteria are fulfilled, as acceptable (—) when at least two criteria are fulfilled and as failed (×) when one or no criterion is met.

pattern and the mean diurnal cycle, however, were similar for both PBL schemes, but with larger cold biases in MYJ. In January, most experiments underestimated  $T_2$  during the whole day, with the cold bias tending to be larger during midday. In July, also an underestimation of midday  $T_2$  was visible, while at night-time  $T_2$  was overestimated at most sites. For some UBU sites,  $T_2$  was underestimated during the whole day. At these sites, differences between UCMs were more distinct than at other sites, whereas SLAB and SLAB\_mos showed lower deviations than SLUCM, SLUCM\_mos and BEP.

### 3.2. Urban–rural and intra-urban differences

We focused on the UCMs for analysing the experiments regarding the representation of urban–rural and intra-urban differences. Thus, we considered only the experiments with BOU, which have shown better performance than the ones with MYJ. Furthermore, we concentrated on July, because during summer and especially during night-time, intra-urban differences and the UHI is most pronounced in Berlin as earlier studies have revealed (e.g. Fenner *et al.*, 2014).



# URBAN–RURAL DIFFERENCES IN AIR TEMPERATURE AS RESOLVED BY THE CER

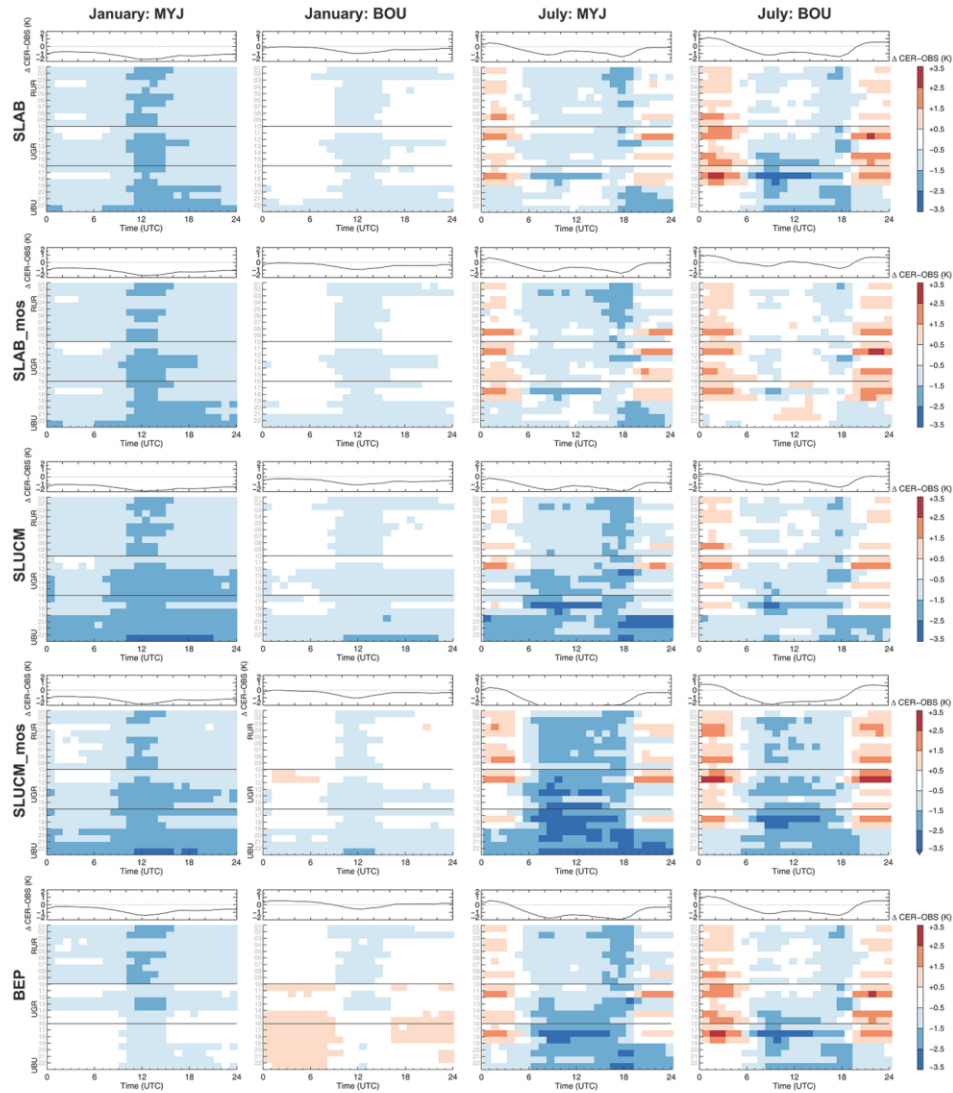


Figure 4. Mean diurnal cycle of  $T_2$  differences (CER–OBS) between experiments (CER) and observations (OBS) across all sites (y-axis) in January and July 2015. Sites 1–9 are rural (RUR), 10–15 are urban greened (UGR) and 16–22 are urban built-up (UBU). (For April refer to Figure S1). The black line in the small plot above each coloured figure shows diurnal deviations averaged over all sites.

First, we analysed urban–rural differences by inspecting the plausibility of spatial patterns of  $T_2$  (Figure 5). Averaged  $T_2$  for day (1300–1500 UTC) and night (2200–0300 UTC) for the five experiments with BOU showed different patterns both within the city and beyond. Mosaicking also influenced spatial patterns of  $T_2$  within and beyond the city (Figure 5). At rural areas, changes in  $T_2$  with mosaicking

were larger in SLUCM\_mos than in SLAB\_mos (Figures 5 and S3). In Berlin, nocturnal urban–rural differences decreased in SLAB\_mos (Figure 5).

Regarding urban–rural differences during daytime, SLAB and SLAB\_mos produced UHIs, while BEP created an urban cold island, i.e. lower  $T_2$  within the city than in the rural surrounding. In SLUCM and SLUCM\_mos,



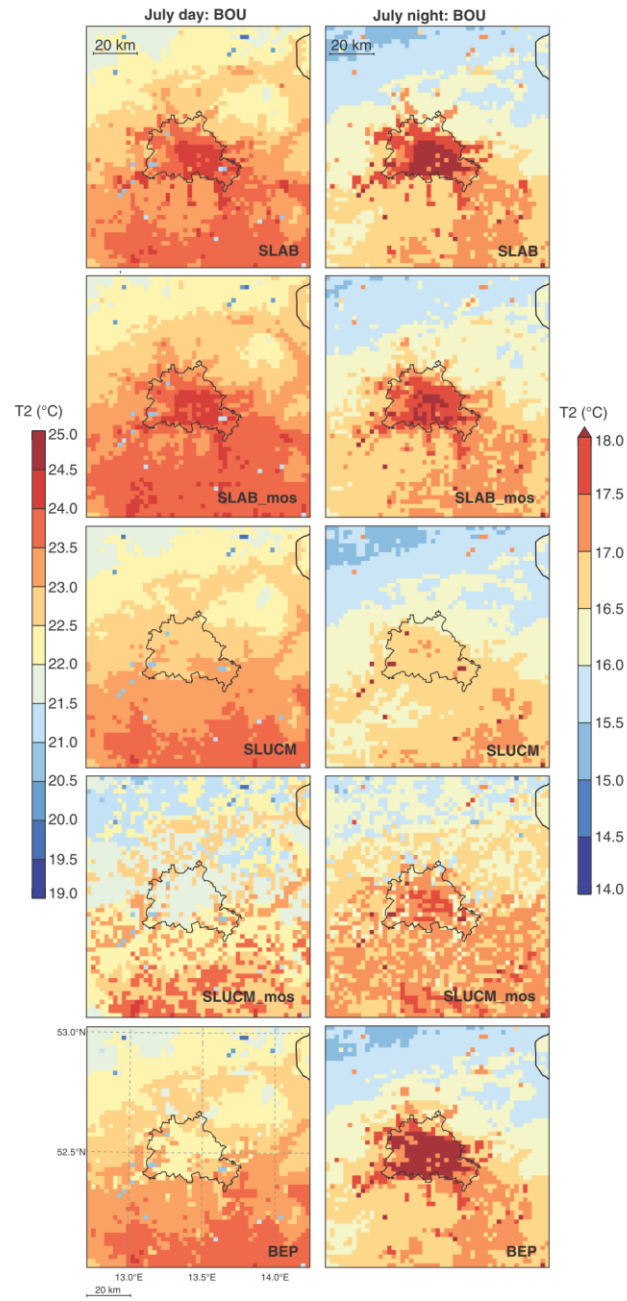


Figure 5. Mean T2 in July 2015 for the experiments with BOU and different UCMs during day (1000–1500 UTC, left) and night (2200–0300 UTC, right). Colour bars vary between day and night.

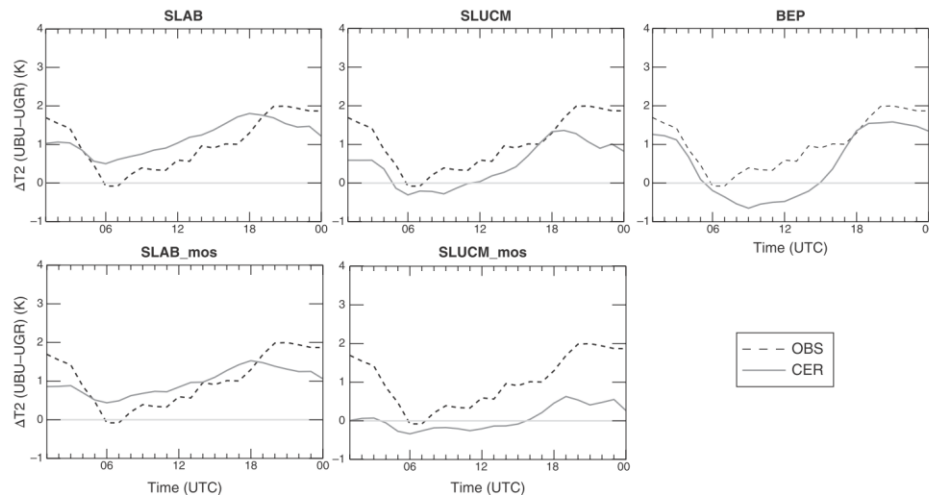


Figure 6. Mean diurnal cycle of differences between an urban built-up (UBU) (Alexanderplatz, No. 22) and an urban greened (UGR) site (Tegel, No. 12) as resolved by the CER using BOU with different UCMs and by observations (OBS) in July 2015.

no clear differences between Berlin and the surroundings were visible at day, and only a small nocturnal UHI in SLUCM\_mos. In contrast, SLAB, SLAB\_mos and BEP exhibited nocturnal UHIs.

By an exemplary pair of one UBU (Alexanderplatz, No. 22) and one UGR (Tegel, No. 12) site (Figure 6), we started examining the intra-urban differences. Figure 6 reveals that during night-time, differences in observations are mostly larger than in CER data. Daytime UBU-UGR is overestimated by SLAB and SLAB\_mos whereas it is underestimated by SLUCM, SLUCM\_mos and BEP. Night-time differences were nearest to the observation in BEP, followed by SLAB and SLAB\_mos. Mosaicking tended to decrease the UBU-UGR differences.

To understand the performance of the UCMs for other sites as well, we aggregated the urban–rural (UBU–RUR and UGR–RUR) and the intra-urban (UBU–UGR) differences in a cross table for day and night (Table 7). The first rows present the observed intra-urban and urban–rural differences. During night, UBU sites were on average 1.8 K warmer than RUR sites and 1.5 K warmer than UGR sites. Differences decreased during day, but UBU sites remained warmer than RUR (0.5 K) and UGR (0.3 K).

In Table 7, the left column shows the simulated differences in the CER, and the right column quantifies the deviations of intra-urban and urban–rural differences between the CER and observations. All experiments underestimated intra-urban and urban–rural differences during night, while some experiments captured the patterns more precisely than others. SLAB, SLAB\_mos and BEP represented the pattern similar to observations, whereas SLUCM and SLUCM\_mos exhibited lower variability. The general pattern of warmer UBU and UGR

sites during night as compared to rural sites, however, was captured by each UCM. During daytime, SLAB and SLAB\_mos overestimated the differences between UBU and RUR, but with correct sign of higher temperatures at UBU sites. SLUCM, SLUCM\_mos and BEP, however, simulated UBU cooler than RUR sites. The effect of mosaicking on the representation of urban–rural and intra-urban differences was low as compared to the effects of the selected UCM.

#### 4. Discussion

##### 4.1. Absolute deviations from observations

We confirmed that the general approach of the CER including dynamical downscaling with a re-initialisation strategy (Mausson *et al.*, 2014) is also justified in the context of urban climate as shown by the representation of the weather changes and the overall low deviations from observations.

Another indicator for reasonable results of  $T_2$  is the good performance regarding the evaluation criteria (Table 6). All experiments, even the one with worst performance, can be considered as state-of-the-art with an RMSD below 2.3 K and an absolute value of MD below 1.3 K, which is an often-reported range in NWP (e.g. Zhang and Zheng, 2004; Flagg and Taylor, 2011; Kusaka *et al.*, 2012b; Kim *et al.*, 2013; Dasari *et al.*, 2014; Liao *et al.*, 2014). We, however, applied more rigorous criteria to assess overall performance and sensitivity to PBL schemes and UCMs, which left few experiments in a desirable range.

In accordance with former studies, we could not detect a single experiment performing best in all seasons (Best and Grimmond, 2013a; Garcia-Diez *et al.*, 2013). Deviations

Table 7. Cross table of urban–rural (UBU–RUR, UGR–RUR) and intra-urban (UBU–UGR) differences in observations (OBS) and the CER (left), and deviations between OBS and the CER in urban–rural (UBU–RUR, UGR–RUR) and intra-urban (UBU–UGR) differences.

		$\Delta T_2$ (K)					
		Absolute			CER–OBS		
OBS		RUR	UGR	UBU	RUR	UGR	UBU
		Night			Night		
RUR			0.3	1.8			
UGR		0.3		1.5			
UBU		0.5	0.3				
		Day			Day		
BOU_SLAB		RUR	UGR	UBU	RUR	UGR	UBU
		Night			Night		
RUR			0.9	1.5		0.6	-0.3
UGR		0.5		0.6	0.2		-0.9
UBU		0.9	0.4		0.4	0.1	
		Day			Day		
BOU_SLAB_mos		RUR	UGR	UBU	RUR	UGR	UBU
		Night			Night		
RUR			0.6	1.3		0.4	-0.5
UGR		0.4		0.7	0.1		-0.9
UBU		0.8	0.5		0.3	0.2	
		Day			Day		
BOU_SLUCM		RUR	UGR	UBU	RUR	UGR	UBU
		Night			Night		
RUR			0.4	0.6		0.1	-1.2
UGR		0.0		0.2	-0.3		-1.3
UBU		-0.1	-0.1		-0.7	-0.4	
		Day			Day		
BOU_SLUCM_mos		RUR	UGR	UBU	RUR	UGR	UBU
		Night			Night		
RUR			0.3	0.6		0.0	-1.3
UGR		-0.1		0.2	-0.4		-1.3
UBU		-0.5	-0.4		-1.0	-0.6	
		Day			Day		
BOU_BEP		RUR	UGR	UBU	RUR	UGR	UBU
		Night			Night		
RUR			0.9	1.7		0.6	-0.1
UGR		-0.1		0.9	-0.4		-0.7
UBU		-0.6	-0.5		-1.1	-0.7	
		Day			Day		

Experiments with BOU are shown during day (1000–1500 UTC) and night (2200–0300 UTC) in July 2015.

were smaller in winter than in summer in our study like in Best and Grimmond (2013a). The smaller deviations in winter might be explained by dependencies of biases to absolute temperature as Garcia-Diez *et al.* (2013) and Best and Grimmond (2013a) detected. Underestimations of  $T_2$  in winter might be related to neglecting anthropogenic heat fluxes (Table 6). According to Best and Grimmond (2013a), anthropogenic heat influences seasonal-varying model performance. Temperature inversions not reproduced have also been discussed as a cause of wintertime deviations (Garcia-Diez *et al.*, 2013; Karsisto *et al.*, 2016). Other factors discussed by Karsisto *et al.* (2016), such as snow cover, were of minor importance because January 2015 was nearly snow-free in Berlin.

Regarding the performance of different schemes, the results suggest that mainly the choice of the PBL scheme controlled the performance of the CER by influencing bias levels. UCMs can refine the simulations concerning the diurnal cycle whereas the choice of mosaicking showed the lowest influence on  $T_2$  accuracy from the three tested options.

The major influence of the PBL scheme on  $T_2$  has been reported before (Shin and Hong, 2011; Li and Bou-Zeid, 2014). The cold bias in MYJ and the better performance of BOU were the main findings. Cold biases have often been reported for BOU and MYJ over different regions (e.g. Texas, Netherlands, Hong Kong, Great Britain) (Zhang and Zheng, 2004; Shin and Hong, 2011; Xie *et al.*, 2012; Kleczek *et al.*, 2014), but MYJ tends to produce stronger cold biases (Zhang and Zheng, 2004; Hu *et al.*, 2010; Xie *et al.*, 2012; Loridan *et al.*, 2013; Kleczek *et al.*, 2014). When directly comparing MYJ and BOU, Kleczek *et al.* (2014) also detected that cold biases were more pronounced in MYJ than in BOU. This may be related to an underestimated PBL height or an underestimated vertical mixing under convective conditions as Hu *et al.* (2010) showed.

We only tested the two PBL schemes that can be used with all three selected UCMs. BOU and MYJ are local PBL schemes that consider only vertical exchange with directly adjacent grid points (Shin and Hong, 2011; Cohen *et al.*, 2015). Non-local schemes, in contrast, consider exchanges with multiple vertical points and horizontal flows as well (Shin and Hong, 2011; Cohen *et al.*, 2015). Local schemes have been found to perform not as good as non-local ones (Shin and Hong, 2011; Xie *et al.*, 2012; Kleczek *et al.*, 2014). Local schemes are reported to produce better results only under weakly stable conditions (Shin and Hong, 2011), and partly during night (Kleczek *et al.*, 2014). Testing non-local schemes with slab and SLUCM and/or developing a connection with BEP would be interesting, for example with the Yonsei University (YSU) scheme, which showed good performances in other studies (e.g. Loridan *et al.*, 2013).

Differences between the UCMs were not as pronounced as between the PBL schemes, but still identifiable as already detected in former studies (Shaffer *et al.*, 2014). Enhanced model performance with increasing complexity of the models, however, was not detected. The simplest UCM (slab) showed the best overall performance, although we used default parameters in contrast to Berlin-specific parameters as used in BEP/SLUCM. The main benefit of applying default parameter values is an easy transfer of the CER to other cities. Wouters *et al.* (2016) also detected that the sensitivity of  $T_2$  and surface temperature to parameter values is lower than the sensitivity to different UCMs when using the COSMO-CLM model. While some former studies (Kim *et al.*, 2013; Fallmann *et al.*, 2014; Shaffer *et al.*, 2014) also revealed no improvements with increasing complexity, other studies (Kusaka *et al.*, 2012a; Kim *et al.*, 2013; Li and Bou-Zeid, 2014) detected that more complex schemes (SLUCMs or multi-layer UCMs) perform better

than slab models. Also, a comprehensive model intercomparison study by Best and Grimmond (2015) showed that simple models performed best, but the authors pointed out that this result does not hold for all applications. Thus, it remains unclear which level of complexity should be incorporated in LSMs depending on the purpose of the simulation (Chen *et al.*, 2011).

It is also important to remember that we evaluated only  $T_2$  without considering other atmospheric variables. Thus, small errors in  $T_2$  might be accompanied by larger errors in other variables. Regarding PBL schemes, for instance, Kleczek *et al.* (2014) detected lowest  $T_2$  deviations using BOU as compared to other PBL schemes, but substantial errors in simulated PBL heights. Errors in PBL height might cause significant errors in wind speed (Zhang and Zheng, 2004; Kleczek *et al.*, 2014). Regarding UCMs, Kim *et al.* (2013) and Liao *et al.* (2014) detected that  $T_2$  was not improved by a more complex UCM (SLUCM/BEP) compared to a simple (slab) while errors in wind speed and PBL height decreased with a more complex UCM.

Regarding the representation of the diurnal cycle, the mainly too low amplitude in  $T_2$  as indicated by  $SKVARs < 1$  (Table 6) was the main finding, which has been detected before in NWP by, e.g. Steeneveld *et al.* (2011) and Zhang and Zheng (2004). At many sites, underestimation of the diurnal amplitude is characterised by an underestimation of  $T_2$  during day and an overestimation during night (Figure 4). A possible explanation for this, which might be neither related to PBL schemes nor to UCMs, would be an overestimation of ground heat flux. In this case, more energy would be stored in the soil at daytime and released again at night, leading to underestimated daytime  $T_2$  and overestimated night-time  $T_2$ . This might be also the case in other studies, such as in Li *et al.* (2013), who detected an overestimated ground heat flux during night and underestimated surface temperature during day. An overestimated ground heat flux can be caused by unsuitable soil parameters or by too high soil moisture producing errors in heat capacity. Soil moisture is a crucial element because it influences many near-surface atmospheric processes (Seneviratne *et al.*, 2010) and urban climate model performance in multiple ways (Best and Grimmond, 2013b). Further research in this direction would be helpful for clarification, in particular with our daily re-initialisation approach that does not allow spin-up times of months to years, which are usually required before soil moisture is adjusted (Best and Grimmond, 2013b). Accuracy of re-initialisation depends on the accuracy of soil moisture used as input data for downscaling. Improvements in data acquisition and assimilation of soil moisture would thus probably lead to better downscaling results. Future studies may also test if deviations in  $T_2$  are reduced by applying the newly developed schemes for parameterisation of urban hydrological processes by Wang *et al.* (2013) and Yang *et al.* (2015), which are available for SLUCM in WRF 3.7. Yang *et al.* (2015, 2016) detected that the representation of

dew point temperature and latent heat flux was improved with the new scheme.

In addition, an underestimation of night-time  $T_2$  was visible at some UBU sites. This was also detected by Loridan *et al.* (2013). They explained this effect by shortcomings in long-wave emitted radiation with overestimation during daytime and underestimation during night-time.

#### 4.2. Urban–rural and intra-urban differences

Former studies (e.g. Fenner *et al.*, 2014; Trusilova *et al.*, 2016) and our observations (Table 7) showed nocturnal UHIs in Berlin during summer with pronounced urban–rural differences, but also intra-urban differences. During day, urban–rural differences and intra-urban differences were lower in these observations, but the city tended to remain warmer than its rural surroundings. In the CER (Figures 5 and 6 and Table 7), this pattern was only represented by SLAB and SLAB\_mos, but with an overestimation during day and an underestimation during night. It is important to note, that observed intra-urban variability at daytime was small in Berlin and thus, changed signs and colours should not be overinterpreted (Table 7). At night-time, urban–rural and intra-urban differences were best represented by the simple slab and the most complex BEP model. BEP produced the nocturnal pattern similar to observation but failed during day, whereas SLUCM and SLUCM\_mos clearly underestimated nocturnal UHI, and produced an urban cool island at daytime that is not observed. Such underestimations of urban–rural differences in UCMs have been detected earlier (Salamanca *et al.*, 2012; Trusilova *et al.*, 2013, 2016; Wouters *et al.*, 2016). Detailed analyses of energy and radiation fluxes would be helpful to understand the underlying reasons for discrepancies between the CER and the observations.

UCMs not only affected spatial variability of  $T_2$  in Berlin but also in its rural surroundings (Figure 5). Differences in rural grid points can be explained by influences of adjacent urban grid cells. Moreover, urban land cover categories used by the CER varied between slab and SLUCM/BEP, which could lead to different dominant land cover categories in rural areas as well (Figure 2). An interesting side-effect is that using a more detailed description of urban land cover in SLUCM/BEP (i.e. three instead of one urban land cover categories) tended to reduce the amount of dominantly urban grid cells (Figure 7, Table 5).

Mosaicking in SLUCM\_mos and SLAB\_mos influenced spatial variability of  $T_2$  in rural and urban areas (Figures 5 and S3) because it is applied to all and not only urban grid cells. Land cover fractions changed due to mosaicking as presented in Figure 7 for the example of urban fractions per grid point ( $f_{urb}$ ).  $f_{urb}$  have been found to largely influence  $T_2$  in Shaffer *et al.* (2014), who tested the sensitivity of  $f_{urb}$  within SLUCM. While mosaicking increased the performance as also detected by Li *et al.* (2013) in slab and SLUCM, the spatial impacts were different between both UCMs. Mosaicking decreased nocturnal urban–rural and intra-urban differences in SLAB\_mos, but produced little impacts on these differences in SLUCM (Figures 5 and 6 and Table 7).



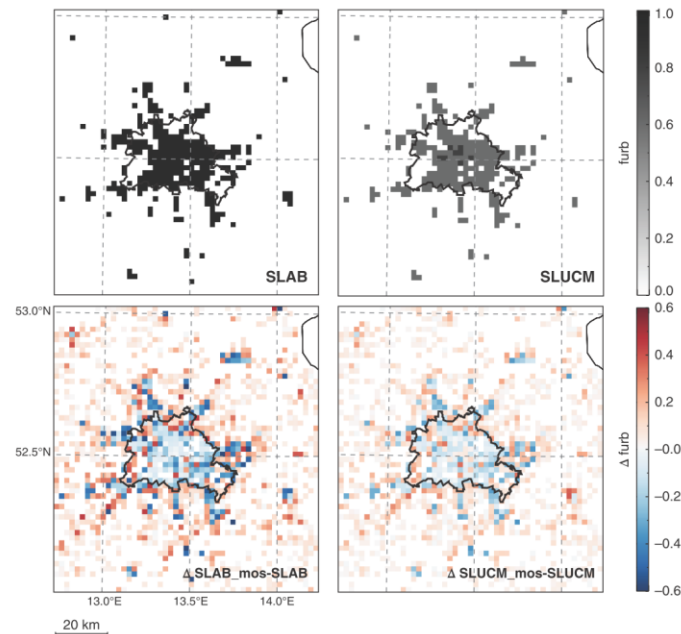


Figure 7. Urban fractions ( $f_{\text{urb}}$ ) used in slab and SLUCM and differences in urban mosaic and dominant approach. Values are derived from the dominant (SLAB, SLUCM) and the three most frequent land cover categories (SLAB\_mos, SLUCM\_mos).

In both UCMs,  $f_{\text{urb}}$  tended to decrease in urban areas (i.e. dominantly urban grid cells) and to increase in rural areas (i.e. dominantly non-urban grid cells) with mosaicking (Figure 7). The modified values of  $f_{\text{urb}}$  explain the differences in  $T_2$  between SLAB and SLAB\_mos and the smaller urban–rural differences (Figures 5 and S3). Urban–rural differences were reduced by mosaicking due to flux averaging with non-urban land cover categories. The differences between SLUCM and SLUCM\_mos, however, are not adequately explained by modified  $f_{\text{urb}}$ , because small differences in  $T_2$  occurred in the city but larger ones in rural sites (Figures 5 and S3).

Causes for the modified  $f_{\text{urb}}$  values vary between both experiments in dominantly urban grid cells. In slab,  $f_{\text{urb}}$  cannot increase but only decrease in dominantly urban cells, because only non-urban land cover categories are added with mosaicking. In SLUCM, both increase and decrease of  $f_{\text{urb}}$  in dominantly urban cells might occur, depending on whether an urban land cover category with a higher  $f_{\text{urb}}$  is added or a category with lower or zero  $f_{\text{urb}}$ . In rural sites,  $f_{\text{urb}}$  increased frequently in SLUCM\_mos and SLAB\_mos, when urban land cover is added as second or third dominant category (Figure 7,  $\Delta\text{SLUCM\_mos-SLUCM}$ ,  $\Delta\text{SLAB\_mos-SLAB}$ ).

Possible causes of the stronger differences in SLUCM\_mos than in SLAB\_mos could be that SLUCM responds differently to the number of considered tiles.

We employed three tiles (dominant, second and third dominant), which is the default setting. Thus, we did not exploit the entire heterogeneity of land cover categories for each grid cell (see Figure 2). Li *et al.* (2013), however, applied eight tiles and detected high sensitivity of  $T_2$  to the number of tiles. Disadvantage of using more tiles are increased computational costs (Li *et al.*, 2013). Further investigations seem to be necessary for understanding the difference in mosaicking between the UCMs.

Overall, the more complex UCMs did not outperform the simple slab model in our experiments with respect to representation of intra-urban and urban–rural differences of  $T_2$ . Complex UCMs require more information, and are thus not easily transferable to other regions. Furthermore, they tend to increase integration time. Therefore, usage of complex UCMs is only advisable if they can add significant profit (Best and Grimmond, 2015). Recently, Wouters *et al.* (2016) presented a new urban parametrisation for bridging the gap between simple slab and complex UCMs. This new approach, implemented in COSMO-CLM, allows faster computations and improves the performance as compared to a slab approach.

For the BEP, too coarse vertical grid spacing could be a reason for the low performance, since Chen *et al.* (2011) recommended to use fine vertical grid spacing with several layers within the urban canopy. Some other studies applied the BEP with more eta levels (up to 51) as compared to

our setup (28) (e.g. Salamanca *et al.*, 2011, 2012; Gutierrez *et al.*, 2015; Heaviside *et al.*, 2015). Comparisons between model performances with different numbers of eta levels are to our knowledge not published. Hence, we conducted an additional experiment using BOU, BEP and 40 vertical layers in order to detect if our results were adversely affected by too few vertical layers. The additional experiment, however, revealed no considerable changes as compared to BOU, BEP, MD and RMSD did not change by more than  $\pm 0.1$  K; the representation of intra-urban and urban–rural differences was also not improved (maximum changes of  $\pm 0.1$  K). Our results demonstrated that within our setup more vertical layers were not beneficial, because they did not enhance model performance but considerably increased computation time (+20–30%) and required memory space (+30%).

Horizontal grid spacing might be another possible reason for the relatively poor performance of SLUCM and BEP. With finer horizontal grid spacing (e.g. 1 or 0.5 km), the more complex UCMs may be more beneficial. This is also supported by results from Trusilova *et al.* (2016).

Other sources of the lower spatial variability in the CER as compared with observations might be related to the general problem in meso-scale model evaluation regarding the comparability of ground-based observations with meso-scale model results (Argüeso *et al.*, 2011). Owing to local-scale to micro-scale influences, particular in heterogeneous urban areas, in contrast to the still coarse grid spacing of 2 km, representation errors may occur (Argüeso *et al.*, 2011). Such errors might contribute to the lower intra-urban differences in the CER as local characteristics are not necessarily represented if heterogeneities exist. This might also be related to the relatively poor representation of intra-urban differences. From studies in Berlin (Fenner *et al.*, 2014) and various other studies (review by Bowler *et al.* (2010)), it is well known that night-time  $T_2$  during summer at greened sites is often much lower than at built-up sites. Studies using finer grid spacing of 0.5 km were able to detect associated effects such as park cool islands (Papangelis *et al.*, 2012). In this study, none of the tested UCMs was able to represent such local effects.

## 5. Conclusions

The main goals of this study were to test the sensitivity of simulated  $T_2$  to UCMs and PBL schemes, and to assess the CER regarding representation of urban–rural and intra-urban differences. In total, the CER simulated  $T_2$  with very small deviations from the observations and captured the weather changes in each season.

We detected that  $T_2$  is mainly sensitive to PBL schemes, and to a lesser extend to UCMs. No single tested combination served best for all sites and seasons. All tested UCMs underestimated intra-urban and urban–rural differences as compared to observations. Overall, however, a combination of the PBL scheme BOU with the simple slab UCM showed the best performance. The moderately complex UCM (SLUCM) and the complex UCM (BEP) also

did not represent intra-urban and urban–rural differences more accurate than the simple slab scheme. Observed deficiencies in simulating intra-urban differences, in particular at greened sites, are important to consider when using the model results, especially because potential local cool areas (i.e., park cool islands) are often in focus in urban climate studies.

Therefore, further research on and development of UCMs is needed with focus on intra-urban differences, because our study revealed that UCMs with low absolute errors are not necessarily the ones that reproduce urban–rural differences and intra-urban differences best and vice versa. Future research should concentrate on improving complex UCMs because these multi-layer UCMs-like BEP offer more opportunities and more flexible usage for different purposes (Grimmond *et al.*, 2011).

This study was limited to evaluation of the CER regarding  $T_2$  and thus, conclusions only refer to this variable. For future studies, it is planned that the CER will be comprehensively evaluated for other variables as well. Despite the current deficiencies of models used in urban climatology, the CER reproduced the spatio-temporal patterns of  $T_2$  with small deviations from observations. Thus, we conclude that the CER approach is highly valuable for urban climate investigations.

## Acknowledgments

We thank our colleagues, who helped with technical issues and maintained the weather stations from TUB. For the provision of meteorological observation data, we thank the German Weather Service (DWD). The study is part of the Research Unit 1736 ‘Urban Climate and Heat Stress in Mid-Latitude Cities in View of Climate Change (UCaHS)’ (<http://www.UCaHS.org>) funded by the Deutsche Forschungsgemeinschaft (DFG) under the codes SCHE 750/8-1 and SCHE 750/9-1.

## Supporting Information

The following supporting information is available as part of the online article:

**Appendix S1.** Supporting Information.

## References

- Argüeso D, Hidalgo-Muñoz JM, Gámiz-Fortis SR, Esteban-Parra MJ, Dudhia J, Castro-Díez Y. 2011. Evaluation of WRF parameterizations for climate studies over southern Spain using a multistep regionalization. *J. Clim.* **24**(21): 5633–5651, doi: 10.1175/JCLI-D-11-00073.1.
- Arnfield AJ. 2003. Two decades of urban climate research: a review of turbulence, exchanges of energy and water, and the urban heat island. *Int. J. Climatol.* **23**(1): 1–26, doi: 10.1002/joc.859.
- Avissar R, Pielke R. 1989. A parameterization of heterogeneous land surfaces for atmospheric numerical models and its impact on regional meteorology. *Mon. Weather Rev.* **117**(10): 2113–2136, doi: 10.1175/1520-0493(1989)117<2113:APOHLS>2.0.CO;2.
- Baklanov A, Ching J, Grimmond CSB, Martilli A. 2009. Model urbanization strategy: summaries, recommendations and requirements. In *Meteorological and Air Quality Models for Urban Areas*. Springer: Berlin Heidelberg, Germany, 151–162.

- Barlow JF. 2014. Progress in observing and modelling the urban boundary layer. *Urban Clim.* **10**(2): 216–240, doi: 10.1016/j.uclim.2014.03.011.
- Best MJ, Grimmond CSB. 2013a. Analysis of the seasonal cycle within the first international urban land-surface model comparison. *Bound.-Layer Meteorol.* **146**(3): 421–446, doi: 10.1007/s10546-012-9769-7.
- Best MJ, Grimmond CSB. 2013b. Importance of initial state and atmospheric conditions for urban land surface models' performance. *Urban Clim.* **10**: 387–406, doi: 10.1016/j.uclim.2013.10.006.
- Best MJ, Grimmond CSB. 2015. Key conclusions of the first international urban land surface model comparison project. *Bull. Am. Meteorol. Soc.* **96**(5): 805–819, doi: 10.1175/BAMS-D-14-00122.1.
- Bougeault P, Lacarrère P. 1989. Parameterization of orography-induced turbulence in a mesobeta-scale model. *Mon. Weather Rev.* **117**: 1872–1890.
- Bowler DE, Buyung-Ali L, Knight TM, Pullin AS. 2010. Urban greening to cool towns and cities: a systematic review of the empirical evidence. *Landsc. Urban Plan.* **97**(3): 147–155, doi: 10.1016/j.landurbplan.2010.05.006.
- Chemel C, Sokhi RS. 2012. Response of London's urban heat island to a marine air intrusion in an easterly wind regime. *Bound.-Layer Meteorol.* **144**(1): 65–81, doi: 10.1007/s10546-012-9705-x.
- Chen F, Dudhia J. 2001. Coupling an advanced land surface-hydrology model with the Penn State – NCAR MM5 modeling system. Part I: model implementation and sensitivity. *Mon. Weather Rev.* **129**(4): 569–585, doi: 10.1175/1520-0493(2001)129<0569:CAALSH>2.0.CO;2.
- Chen F, Kusaka H, Bornstein R, Ching J, Grimmond CSB, Grossman-Clarke S, Loridan T, Manning KW, Martilli A, Miao S, Sailor D, Salamanca FP, Taha H, Tewari M, Wang X, Wyszogrodzki A, Zhang C. 2011. The integrated WRF/urban modelling system: development, evaluation, and applications to urban environmental problems. *Int. J. Climatol.* **31**(2): 273–288, doi: 10.1002/joc.2158.
- Cohen AE, Cavallo SM, Coniglio MC, Brooks HE, Hu XM, Nielsen-Gammon JW, Zhang F, Keene K, NCAR, Stoelinga MT, Xie B, Fung JCH, Chan A, Lau A. 2015. A review of planetary boundary layer parameterization schemes and their sensitivity in simulating a Southeast U.S. cold season severe weather environment. *Weather Forecast.* **117**(12): 591–612, doi: 10.1175/WAF-D-14-00105.1.
- Dasari HP, Salgado R, Perdigao J, Challa VS. 2014. A regional climate simulation study using WRF-ARW model over Europe and evaluation for extreme temperature weather events. *Int. J. Atmos. Sci.* **22**: 704079, doi: 10.1155/2014/704079.
- Dee DP, Uppala SM, Simmons AJ, Berrisford P, Poli P, Kobayashi S, Andrae U, Balmaseda MA, Balsamo G, Bauer P, Bechtold P, Beljaars ACM, van de Berg L, Bidlot J, Bormann N, Delsol C, Dragani R, Fuentes M, Geer AJ, Haimberger L, Healy SB, Hersbach H, Hólm EV, Isaksen I, Kållberg P, Köhler M, Matricardi M, McNally AP, Monge-Sanz BM, Morcrette J-J, Park B-K, Peubey C, de Rosnay P, Tavolato C, Thépaut J-N, Vitart F. 2011. The ERA-Interim reanalysis: configuration and performance of the data assimilation system. *Q. J. R. Meteorol. Soc.* **137**(656): 553–597, doi: 10.1002/qj.828.
- Fallmann J, Emeis S, Suppan P. 2014. Mitigation of urban heat stress – a modelling case study for the area of Stuttgart. *DIE ERDE* **144**(3): 202–216, doi: 10.12854/erde-144-15.
- Fenner D, Meier F, Scherer D, Polze A. 2014. Spatial and temporal air temperature variability in Berlin, Germany, during the years 2001–2010. *Urban Clim.* **10**(2): 308–331, doi: 10.1016/j.uclim.2014.02.004.
- Flagg DD, Taylor P a. 2011. Sensitivity of mesoscale model urban boundary layer meteorology to the scale of urban representation. *Atmos. Chem. Phys.* **11**(6): 2951–2972, doi: 10.5194/acp-11-2951-2011.
- García-Díez M, Fernández J, Fita L, Yagüe C. 2013. Seasonal dependence of WRF model biases and sensitivity to PBL schemes over Europe. *Q. J. R. Meteorol. Soc.* **139**(671): 501–514, doi: 10.1002/qj.1976.
- Grimmond CSB, Blackett M, Best MJ, Baik J-J, Belcher SE, Beringer J, Bohnenstengel SI, Calmet I, Chen F, Coutts A, Dandou A, Fortuniak K, Gouveia ML, Hamdi R, Hendry M, Kanda M, Kawai T, Kawamoto Y, Kondo H, Krayerhoff ES, Lee S-H, Loridan T, Martilli A, Masson V, Miao S, Oleson K, Ooka R, Pigeon G, Porson A, Ryu Y-H, Salamanca F, Steeneveld GJ, Tombrou M, Voogt J, Young DT, Zhang N. 2011. Initial results from phase 2 of the international urban energy balance model comparison. *Int. J. Climatol.* **31**(2): 244–272, doi: 10.1002/joc.2227.
- Gutiérrez E, González JE, Martilli A, Bornstein R, Arend M. 2015. Simulations of a heat-wave event in New York City using a multilayer urban parameterization. *J. Appl. Meteorol. Climatol.* **54**(2): 283–301, doi: 10.1175/JAMC-D-14-0028.1.
- Heaviside C, Cai X-M, Vardoulakis S. 2015. The effects of horizontal advection on the urban heat island in Birmingham and the West Midlands, United Kingdom during a heatwave. *Q. J. R. Meteorol. Soc.* **141**(689): 1429–1441, doi: 10.1002/qj.2452.
- Hidalgo J, Masson V, Baklanov A, Pigeon G, Gimeno L. 2008. Advances in urban climate modeling. *Ann. N. Y. Acad. Sci.* **1146**(2008): 354–374, doi: 10.1196/annals.1446.015.
- Hu X-M, Nielsen-Gammon JW, Zhang F. 2010. Evaluation of three planetary boundary layer schemes in the WRF model. *J. Appl. Meteorol. Climatol.* **49**(9): 1831–1844, doi: 10.1175/2010JAMC2432.1.
- Janjić ZI. 1990. The step-mountain coordinate: physical package. *Mon. Weather Rev.* **118**: 1429–1443.
- Karsisto P, Fortelius C, Demuzere M, Grimmond CSB, Oleson KW, Kouznetsov R, Masson V, Järvi L. 2016. Seasonal surface urban energy balance and wintertime stability simulated using three land-surface models in the high-latitude city Helsinki. *Q. J. R. Meteorol. Soc.* **142**: 401–417, doi: 10.1002/qj.2659.
- Kim Y, Sartelet K, Raut J-C, Chazette P. 2013. Evaluation of the weather research and forecast/urban model over greater Paris. *Bound.-Layer Meteorol.* **149**(1): 105–132, doi: 10.1007/s10546-013-9838-6.
- Kleczeck M, Steeneveld GJ, Holtslag AM. 2014. Evaluation of the weather research and forecasting mesoscale model for GABLS3: impact of boundary-layer schemes, boundary conditions and spin-up. *Bound.-Layer Meteorol.* **152**(2): 213–243, doi: 10.1007/s10546-014-9925-3.
- Kusaka H, Kondo H, Kikigawa Y, Kimura F. 2001. A simple single-layer urban canopy model for atmospheric models: comparison with multi-layer and slab models. *Bound.-Layer Meteorol.* **101**(3): 329–358, doi: 10.1023/A:1019207923078.
- Kusaka H, Chen F, Tewari M, Dudhia J, Gill DO, Duda MG, Wang W, Miya Y. 2012a. Numerical simulation of urban heat island effect by the WRF model with 4-km Grid increment: an inter-comparison study between the urban canopy model and slab model. *J. Meteorol. Soc. Jpn. Ser. II* **90B**: 33–45, doi: 10.2151/jmsj.2012-B03.
- Kusaka H, Hara M, Takane Y. 2012b. Urban climate projection by the WRF Model at 3-km horizontal grid increment: dynamical downscaling and predicting heat stress in the 2070's August for Tokyo, Osaka, and Nagoya Metropolises. *J. Meteorol. Soc. Jpn. Ser. II* **90B**: 47–63, doi: 10.2151/jmsj.2012-B04.
- Li D, Bou-Zeid E. 2014. Quality and sensitivity of high-resolution numerical simulation of urban heat islands. *Environ. Res. Lett.* **9**(5): 55001, doi: 10.1088/1748-9326/9/5/055001.
- Li D, Bou-Zeid E, Barlage M, Chen F, Smith J. 2013. Development and evaluation of a mosaic approach in the WRF-Noah framework. *J. Geophys. Res.* **118**(21): 11918–11935, doi: 10.1002/2013JD020657.
- Liao J, Wang T, Wang X, Xie M, Jiang Z, Huang X, Zhu J. 2014. Impacts of different urban canopy schemes in WRF/Chem on regional climate and air quality in Yangtze River Delta, China. *Atmos. Res.* **145**–**146**: 226–243, doi: 10.1016/j.atmosres.2014.04.005.
- Liu Y, Chen F, Warner T, Basara J. 2006. Verification of a mesoscale data-assimilation and forecasting system for the Oklahoma City area during the joint urban 2003 field project. *J. Appl. Meteorol. Climatol.* **45**(7): 912–929, doi: 10.1175/JAM2383.1.
- Loridan T, Lindberg F, Jorba O, Kotthaus S, Grossman-Clarke S, Grimmond CSB. 2013. High resolution simulation of the variability of surface energy balance fluxes across central London with urban zones for energy partitioning. *Bound.-Layer Meteorol.* **147**(3): 493–523, doi: 10.1007/s10546-013-9797-y.
- Martilli A. 2007. Current research and future challenges in urban mesoscale modelling. *Int. J. Climatol.* **27**(14): 1909–1918, doi: 10.1002/joc.1620.
- Martilli A, Clappier A, Rotach MW. 2002. An urban surface exchange parameterisation for mesoscale models. *Bound.-Layer Meteorol.* **104**(3): 261–304, doi: 10.1023/A:1016099921195.
- Maussion F, Scherer D, Mölg T, Collier E, Curio J, Finkelnburg R. 2014. Precipitation seasonality and variability over the Tibetan Plateau as resolved by the high Asia reanalysis. *J. Clim.* **27**(5): 1910–1927, doi: 10.1175/JCLI-D-13-00282.1.
- Monaghan AJ, Hu L, Brunzell NA, Barlage M, Wilhelm OV. 2014. Evaluating the impact of urban morphology configurations on the accuracy of urban canopy model temperature simulations with MODIS. *J. Geophys. Res.* **119**(11): 6376–6392, doi: 10.1002/2013JD021227.
- Mooney P, Mulligan FJ, Fealy R. 2013. Evaluation of the sensitivity of the weather research and forecasting model to parameterization schemes for regional climates of Europe over the period 1990–95. *J. Clim.* **26**(3): 1002–1017, doi: 10.1175/JCLI-D-11-00676.1.



- Ng E, Chen L, Wang Y, Yuan C. 2012. A study on the cooling effects of greening in a high-density city: an experience from Hong Kong. *Build. Environ.* **47**: 256–271, doi: 10.1016/j.buildenv.2011.07.014.
- Papangelis G, Tombrou M, Dandou A, Kontos T. 2012. An urban “green planning” approach utilizing the Weather Research and Forecasting (WRF) modeling system. A case study of Athens, Greece. *Landsc. Urban Plann.* **105**(1–2): 174–183, doi: 10.1016/j.landurbplan.2011.12.014.
- Pielke R. 2002. *Mesoscale Meteorological Modeling*. Academic Press: San Diego, San Francisco, New York, Boston, United States of America, London, Great Britain, Sydney, Australia, Tokyo, Japan.
- Pineda N, Jorba O, Jorge J, Baldasano JM. 2004. Using NOAA AVHRR and SPOT VGT data to estimate surface parameters: application to a mesoscale meteorological model. *Int. J. Remote Sens.* **25**(1): 129–143, doi: 10.1080/0143116031000115201.
- Ramamurthy P, Li D, Bou-Zeid E. 2015. High-resolution simulation of heatwave events in New York City. *Theor. Appl. Climatol.* 1–14, doi: 10.1007/s00704-015-1703-8.
- Salamanca F, Martilli A, Tewari M, Chen F. 2011. A study of the urban boundary layer using different urban parameterizations and high-resolution urban canopy parameters with WRF. *J. Appl. Meteorol. Climatol.* **50**(5): 1107–1128, doi: 10.1175/2010JAMC2538.1.
- Salamanca F, Martilli A, Yagüe C. 2012. A numerical study of the urban heat island over Madrid during the DESIREX (2008) campaign with WRF and an evaluation of simple mitigation strategies. *Int. J. Climatol.* **32**(15): 2372–2386, doi: 10.1002/joc.3398.
- Schlünzen KH, Sokhi RS. 2008. Overview of tools and methods for meteorological and air pollution mesoscale model evaluation and user training. WMO Jt. Rep. COST Action 728 GURME. World Meteorological Organization (WMO): Geneva, Switzerland.
- Seneviratne SI, Corti T, Davin EL, Hirschi M, Jaeger EB, Lehner I, Orlowsky B, Teuling AJ. 2010. Investigating soil moisture–climate interactions in a changing climate: a review. *Earth Sci. Rev.* **99**(3–4): 125–161, doi: 10.1016/j.earscirev.2010.02.004.
- Shaffer SR, Chow WTL, Georgescu M, Hyde P, Jenerette GD, Mahalov A, Moustaoi A, Ruddell BL. 2014. Multiscale modeling and evaluation of urban surface energy balance in the Phoenix metropolitan area. *J. Appl. Meteorol. Climatol.* **54**: 322–338, doi: 10.1175/JAMC-D-14-0051.1.
- Shin HH, Hong S-Y. 2011. Intercomparison of planetary boundary-layer parameterizations in the WRF Model for a single day from CASES-99. *Bound.-Layer Meteorol.* **139**(2): 261–281, doi: 10.1007/s10546-010-9583-z.
- Skamarock WC, Klemp JB. 2008. A time-split nonhydrostatic atmospheric model for weather research and forecasting applications. *J. Comput. Phys.* **227**(7): 3465–3485, doi: 10.1016/j.jcp.2007.01.037.
- Souch C, Grimmond S. 2006. Applied climatology: urban climate. *Prog. Phys. Geogr.* **30**(2): 270–279, doi: 10.1191/0309133306pp484pr.
- Steenneveld GJ, Tolk LF, Moene F, Hartogensis OK, Peters W, Holt-slag M. 2011. Confronting the WRF and RAMS mesoscale models with innovative observations in the Netherlands: evaluating the boundary layer heat budget. *J. Geophys. Res.* **116**(23): 1–16, doi: 10.1029/2011JD016303.
- Trusilova K, Früh B, Brienen S, Walter A, Masson V, Pigeon G, Becker P. 2013. Implementation of an urban parameterization scheme into the regional climate model COSMO-CLM. *J. Appl. Meteorol. Climatol.* **52**(10): 2296–2311, doi: 10.1175/JAMC-D-12-0209.1.
- Trusilova K, Schubert S, Wouters H, Früh B, Demuzere M, Becker P. 2016. The urban land use in the COSMO-CLM model: a comparison of three parameterizations for Berlin. *Meteorol. Z.* **25**(2): 231–244, doi: 10.1127/metz/2015/0587.
- Wang ZH, Bou-Zeid E, Smith J. 2013. A coupled energy transport and hydrological model for urban canopies evaluated using a wireless sensor network. *Q. J. R. Meteorol. Soc.* **139**(675): 1643–1657, doi: 10.1002/qj.2032.
- Wouters H, Demuzere M, Blahak U, Fortuniak K, Maiheu B, Camps J, Tielemans D, van Lipzig NPM. 2016. Efficient urban canopy parameterization for atmospheric modelling: description and application with the COSMO-CLM model (version 5.0\_clm6) for a Belgian summer. *Geosci. Model Dev. Discuss.* 0–40, doi: 10.5194/gmd-2016-58.
- Xie B, Fung JCH, Chan A, Lau A. 2012. Evaluation of nonlocal and local planetary boundary layer schemes in the WRF model. *J. Geophys. Res.* **117**(D12): 1–26, doi: 10.1029/2011JD017080.
- Yang J, Wang ZH, Chen F, Miao S, Tewari M, Voogt JA, Myint S. 2015. Enhancing hydrologic modelling in the coupled Weather Research and Forecasting-urban modelling system. *Bound.-Layer Meteorol.* **155**: 87–109, doi: 10.1007/s10546-014-9991-6.
- Yang J, Wang Z-H, Georgescu M, Chen F, Tewari M. 2016. Assessing the impact of enhanced hydrological processes on urban hydrometeorology with application to two cities in contrasting climates. *J. Hydrometeorol.* **17**(4): 1031–1047, doi: 10.1175/JHM-D-15-0112.1.
- Zhang D-L, Zheng W-Z. 2004. Diurnal cycles of surface winds and temperatures as simulated by five boundary layer parameterizations. *J. Appl. Meteorol.* **43**(1): 157–169, doi: 10.1175/1520-0450(2004)043<0157:DCOSWA>2.0.CO;2.
- Zhao L, Lee X, Smith RB, Oleson K. 2014. Strong contributions of local background climate to urban heat islands. *Nature* **511**(7508): 216–219, doi: 10.1038/nature13462.





## Danksagung

Die drei Jahre meiner Promotion waren für mich eine spannende und schöne Zeit. Rückblickend fällt mir aber vor allem eines auf: Ohne die vielfältige Unterstützung und die hervorragenden Randbedingungen würde mein Fazit sicherlich ganz anderes aussehen. Daher möchte ich an dieser Stelle allen, die mich während der Zeit unterstützt haben, meinen Dank ausdrücken.

Besonders möchte ich mich bei den Gutachtern und beim Promotionsvorsitz bedanken: bei Prof. Dr. Dieter Scherer, Prof. Dr. Christoph Schneider und Prof. Dr. Johann Kaupenjohann. Mein besonderer Dank gilt Dieter, der meine Arbeit betreut und bereits im Studium mein Interesse an Stadtklimatologie geweckt und gefördert hat. Auch Fred Meier gehört mein größter Dank, der mich durch unzählige wertvolle Hinweise und anregende Diskussionen unterstützt hat. Ebenso danke ich allen anderen am Fachgebiet Klimatologie herzlichst für fachlichen Austausch, Hilfe beim Messen, Modellieren und Korrekturlesen, aber vor allem für das hervorragende und produktive Arbeitsumfeld.

Den Mitgliedern der Forschergruppe UCaHs danke ich für den interdisziplinären Austausch und für die fruchtbare Zusammenarbeit ebenso wie der Deutschen Forschungsgemeinschaft für die Finanzierung meiner Stelle.

Nicht zuletzt gilt mein Dank meiner Familie, meinen Freunden und natürlich Eric, die mich während der gesamten Zeit meiner Promotion auf verschiedenste Weise unterstützt und für die nötige Ablenkung und Abwechslung gesorgt haben.